

Hydrochemistry and Isotope Hydrogeology in the Jericho Area/ Palestine

By

Saed Kuzeed Khayat

From Nablus, Palestine

**A thesis for the degree of Doctor of Natural Sciences
submitted**

to the

**Faculty of Civil Engineering, Geosciences and
Environmental Sciences**

University of Karlsruhe, Germany

Date of thesis defence: 14. 12. 2005

Main Supervisor:

Prof. Dr. Heinz Hötzl, AGK- Angewandete Geologie/ Uni- Karlsruhe

Co-advisors:

Prof. Dr. Eng. Olaf Kolditz, University of Tübingen

ABSTRACT

In the arid to semiarid region of the Middle East, with its water scarcity problems salinisation together with other anthropogenic contaminants is considered as the main threat to fresh groundwater resources now days. Due to this matter of fact the possible sources of salinisation and driving mechanisms should be identified, to take a suitable action to mitigate this phenomenon.

In this study, the natural and anthropogenic salinisation of groundwater in the area of Jericho (north of the Dead Sea) is investigated to describe the possible main causes of the groundwater deterioration in this agricultural area, and highlighting a clear basis for stakeholders to take suitable actions to manage the water resources in more efficient way.

Chloride and TDS concentrations in the shallow Pleistocene aquifer systems in the Jericho area indicate a general trend of increasing salinity eastward and southward. There are some notable exceptions to this trend depending on the wells location and surrounding activities.

The groundwater quality varies from fresh carbonate groundwater in the springs in the west with depleted $\delta^{13}\text{C}$ of -12 to -13‰, to Ca-Cl and Na-Cl brackish water with more enriched signature that bearing this signatures of $\delta^{13}\text{C}$, $\delta^{34}\text{S}$ of evaporate salts Leachate. The analyses of major ions, hydrogen and oxygen isotopes as well as carbons, and sulfur isotopes indicate that primary sources of the salinity are: (1) the leachate of salts included in the Pleistocene sediments, leading mainly to a brackish formation, (2) the mixing with seawater, which result from sea ingression in the Pliocene and partly remaining in the of the terrigenous sediments deposited in that sea, (3) mixing with ascending brines from the depth, which are mainly the result from the dissolution of salt bodies. This brackish or salty water arises up under the lowering of the water pressure in the shallow aquifer by heavy abstraction, through conduits and capillaries in the Lisan formation. The leaching processes in the Pleistocene Lisan formation are supported by the low Tritium units and the $\delta^{34}\text{S}_{\text{Sulphate}}$ signatures that bearing this of the Lisan solid samples. In the eastern part of the study area, where the more finer and silty formation is predominant, deep saline water in the aquitard interface with the upper fresh water forming mixing of brackish water with mixed isotopes signatures. It is unclear, whether this saline water is residual water from former Pleistocene Pliocene sea ingression or recent saltwater migration that was formed due to dissolution of salty rocks in the depth. However, the permeability of the

Lisan formation is very low and can be considered as an aquitard which retained water for long time in contact with salty rocks and forming this brackish water in situ.

An evidence of agricultural backflow was detected in some wells which were not highly affected by saline water. The presence of the brine water input with high TDS may overlap the tracer elements that can indicate the agricultural influence in other wells, which might also be subjected to such kind of anthropogenic pollution. The isotope signatures of nitrogen and oxygen in nitrate confirm that the aquifer is highly influenced by leakage of sewage and manure from the septic tanks, which are widely used in the study area.

Some wells in the west and in the north west part of the study area, adjacent to the springs system and major fault, show the same water type and $\delta^{13}\text{C}$ signatures as the water from the springs with their marine calcareous composition. This can confirm that there is a discharge from the calcareous water of the regional mountains aquifer to the shallow aquifer. These results highly suggest that the previous concept about the major fault barrier between the two aquifers is not definitely correct. The fault system itself serves like a conduit system as it was observed from the ascending brines. Where there is a kind of barrier this is due to the evidence of extreme low permeabilities of the young Plio-Pleistocene sediments bordering the fault and the Cretaceous aquifer on the other side of the fault.

A GIS based model for the study area was constructed using the new developed Geosys program. The model was used to apply several assumptions and scenarios for the mode and mechanism of the contribution of irrigation channels draining water from Sultan spring to the east. It was noticed that the effective infiltration of about 2% from the total discharge of Sultan spring through the irrigation channels has also an effect on the groundwater table in the aquifer. This visualized hydrosystem data can show the different mechanisms of recharge from each contributor, and the flow mode in the system, as well as it can be a good tool to trace the mechanism of salinity after further refining and calibration.

DEDICATION

بِسْمِ اللَّهِ الرَّحْمَنِ الرَّحِيمِ

" قُلْ إِنْ صَلَاتِي وَنُسُكِي وَمَحْيَايَ وَمَمَاتِي لِلَّهِ رَبِّ الْعَالَمِينَ،
لَا شَرِيكَ لَهُ وَبِذَلِكَ أُمِرْتُ وَأَنَا أَوَّلُ الْمُسْلِمِينَ "

صَدَقَ اللَّهُ الْعَظِيمُ

To the Sole of my father "Kuzeed" who formed part of my vision and taught me the good things that really matter in life. The happy memory of my father still provides a persistent inspiration for my journey in this life.

To my mother "Wijdan" who continues to learn, grow and develop,

To my wife "Maysa'a" who has been a source of encouragement, support, and inspiration to me throughout my study,

To my children "Sara and M. Kuzeed",

To my Sisters "Soha and Dua'a",

To my brother "Sari",

With my love to them all,

Saed

ACKNOWLEDGEMENTS

A journey is easier when you travel together. Interdependence is certainly more valuable than independence. This thesis is the result of 3 years of work whereby I have been accompanied and supported by many people. It is a pleasant aspect that I have now the opportunity to express my gratitude for all of them.

The first person I would like to thank is my direct supervisor Prof. Dr. Heinz Hoetzel. I have been in his project since 2003 when I started my PhD assignment. During these years I have known him as a sympathetic and principle-centered person. His overly enthusiasm and integral view on research and his mission for providing 'only high-quality work and not less', has made a deep impression on me. I owe him lots of gratitude for having me shown this way of research. He could not even realize how much I have learned from him.

The other one whom I would like to thank is my co-advisor Stefan Geyer who kept an eye on the progress of my work and always was available when I needed his advises. Besides of being an excellent advisor, Stefan was as close as a relative and a good friend to me. I am really glad that I have come to get know Stefan Geyer in my life.

Also, I would like to express my deepest thanks and gratitude to Prof. Dr. Eng. Olaf Kolditz, who was my entrance to learn the modeling staff, his distinctive personality and the valuable methods in giving information, make me understanding well the hydro-systems modeling principles, It was a pleasure to work with him and the other employees of Center for Applied Geosciences/ Tuebingen.

The Palestinian house that open his arm for me and provide me with all kinds of support was the PHG- Palestinian Hydrology Group, where I found from my friends Dr. Tamimi and Dr. Ghanem all what student need from technical, financial and scientific aid in the field.

Special thanks should go to my best promoter and friend Dr. Wasim Ali for his kindness and almost daily assistance, scientific guidance and support. This man who might forget his right hand but never forget his Palestine. Wasim Ali never forget his people specially the students, thus I was not the only Palestinian student whom Wasim Ali has provided help for him to complete his study in Germany. Thousands regards from Palestine to him.

My deep gratitude to the German Federal Ministry of Science and Research (BMBF) (Dr. S. Kiefer and Dr. H.J. Metzger) for funding and support my work, and for the Country of Germany for their continuous support of the Palestinian people.

My colleagues of the UFZ-Environmental Research Center and AGK- Applied Geology/ University of Karlsruhe and PHG- Palestinian Hydrology Group all gave me the feeling of being at home at work, many thanks for being your colleague. I would also like to thank the other members of my PhD committee who monitored my work and took effort in reading and providing me with valuable comments on earlier versions of this thesis. Finally, I am indebted to everyone who contributed to completing this work whom I have failed to mention.

TABLE OF CONTENTS:

CHAPTER 1: INTRODUCTION: BACKGROUND AND PURPOSE OF STUDY	1
1.1. <i>Aim and Scope</i>	1
1.2. <i>Location and Major Features</i>	2
1.3. <i>Land Use</i>	5
1.4. <i>Population</i>	8
1.5. <i>Soil</i>	8
1.6. <i>Climate</i>	9
1.6.1. <i>Temperature and Wind</i>	9
1.6.2. <i>Precipitation</i>	9
1.7. <i>Previous Investigations</i>	11
CHAPTER 2: GEOLOGY AND HYDROGEOLOGY	13
2.1. <i>General Overview</i>	13
2.2. <i>Stratigraphy and Lithology of the West Bank</i>	15
2.3 <i>Geology and Stratigraphy of the Jericho Area</i>	17
2.3.1 <i>Cretaceous Rocks</i>	17
2.3.1.1. <i>Aptian-Albian-Kobar Formation</i>	17
2.3.1.2. <i>Albian-Lower Beit Kahil</i>	17
2.3.1.3. <i>Albian Upper Beit Kahil Formation</i>	18
2.3.1.4. <i>Cenomanian- Yatta Formation</i>	18
2.3.1.5. <i>Cenomanian- Hebron Formation</i>	18

2.3.1.6. <i>Cenomanian-Bethlehem Formation</i>	19
2.3.1.7. <i>Turonian-Jerusalem Formation</i>	19
2.3.1.4. <i>Senonian- Abu Dis Formation</i>	19
2.3.2. <i>Neogene and Quaternary</i>	19
2.3.2.1. <i>Pleistocene Formation</i>	20
2.3.2.2. <i>Holocene Formation</i>	20
2.4. <i>Structural Settings</i>	23
2.4.1. <i>Faults and Folds</i>	23
2.4.2. <i>Joints</i>	25
2.4.3. <i>Karstification</i>	25
2.5. <i>Hydrogeology</i>	25
2.5.1. <i>Hydrogeology of the West Bank</i>	25
2.5.1.1. <i>North Eastern Basin</i>	26
2.5.1.2. <i>Western Basin</i>	26
2.5.1.3. <i>Eastern Basin</i>	26
2.5.2. <i>Hydrogeology of Jericho Area</i>	29
2.5.2.1. <i>Regional Aquifers</i>	29
2.5.2.1.1. <i>The Upper Cretaceous Aquifer</i>	29
2.5.2.1.2. <i>The Jordan Valley [Dead Sea Group] Aquifer</i>	29
2.5.2.1.3. <i>Hydraulic Separation between the Two Aquifers</i>	31
2.5.2.1.4. <i>Perched Water from the Upper Cretaceous Aquifer</i>	31
2.5.2.1.5. <i>Perched Water from the Pleistocene Aquifer</i>	31

2.5.2.5. Wells	31
2.5.2.6. Springs	32
2.6. History of the Hydrogeochemistry in the Study Area	34
2.6.1. The History of Saline Formation in the Rift Valley	34
2.6.2. Previous Hydrochemistry data from Jericho Area	36
2.6.2.1. Springs	36
2.6.2.2. Wells	38
2.5.3. Groundwater Quality Deterioration in the Study Area	39
2.5.3.1. Salinity	39
2.5.3.2. Anthropogenic Pollution	42
Chapter 3: METHODOLOGY	44
3.1. Sampling Time and Site	44
3.2 Detection of Chemical Parameters	44
3.3 Stable Isotopes	47
3.3.1 Nitrogen Isotopes	48
3.3.2 Sulphur Isotopes	50
3.3.3 Carbon Isotopes	51
3.3.4 Tritium Deuterium and Oxygen Isotopes	52
Chapter4: RESULTS AND DISCUSSION	55
4.1 General Hydrochemistry and Tritium	55
4.1.1. Springs and Fresh Water End Member	58
4.1.2. Wells of Wadi Qilt West	61

4.1.3. Wells of Wadi Qilt East	61
4.1.4. Wells of Wadi Nuwe'meh North	61
4.1.5. East Arab Project Wells	63
4.1.6. Overall Hydrochemical Conditions	63
4.1.7. Salinisation	64
4.1.7.1. Brackish Water Source	64
4.1.7.2. Evaporates and Rock Weathering	65
4.1.8. Anthropogenic Influences	66
4.2. Deuterium and Oxygen Isotopes	68
4.3. Nitrate and Nitrogen Isotopes	74
4.4. Sulphate and Sulphur Isotopes	80
4.5. Carbon Isotopes	86
4.6. Seasonal Variation	94
Chapter 5: GIS BASED HYDRSYSTEM MODEL	96
5.1 Introduction	96
5.1.1 <i>GeoLib</i>	98
5.1.2 <i>MshLib</i>	98
5.1.3 <i>FEMLib</i>	98
5.2 <i>Model Setting</i>	99
5.2.1 <i>Aim of the model</i>	99
5.2.2 <i>GIS Project</i>	100
5.2.2.1 <i>The Layer Formation</i>	101

<i>5.2.2.2 Wadis</i>	102
<i>5.2.2.3 Faults</i>	102
<i>5.2.2.4 Boreholes for Lithological Cross Section</i>	103
<i>5.2.2.5 Water Level</i>	103
<i>5.2.2.6 City Area</i>	103
<i>5.2.2.7 Abstraction Rate</i>	103
<i>5.2.2.8 Wells for Surface Topography</i>	103
<i>5.2.2.9 Sultan Irrigation Network</i>	103
<i>5.2.2.10 Study Area Surfaces</i>	104
<i>5.2.2.11 Interpolated Raster Map</i>	105
<i>5.3 Project Construction</i>	107
<i>5.3.1 Project Elements</i>	107
<i>5.3.1.1 Boundary Conditions</i>	107
<i>5.4 Creating GeoSys Project</i>	111
<i>5.5 Program Processing</i>	114
<i>5.6 First Simulation Results and Discussion</i>	115
<i>5.7 Visualising of Seasonal Variation Effect on Water Level</i>	118
Chapter 6: SUMMARY, CONCLUSIONS AND RECOMMENDATIONS	123
<i>References</i>	130
<i>Appendices</i>	

LIST OF FIGURES

Figure-1 Location map of the study area	3
Figure-2 Agricultural land near Jericho	4
Figure-3 Wadi Qilt general view	4
Figure-4 Eastern part of Wadi Nuwe'meh	5
Figure-5 Satellite image for the study area showing major land use	7
Figure-6 Monthly rainfall and evaporation in the study area	10
Figure-7 Average annual precipitation rate in Jordan Valley	11
Figure-8 General Geological map of the West Bank	14
Figure-9 Geological map of Jericho area	21
Figure-10 Generalized columnar geological section	22
Figure-11 Structural map for the study area	24
Figure-12 Groundwater basin and exposed aquifers in the West Bank	27
Figure-13 Schematic Hydrogeological cross section in the study area	30
Figure-14 Groundwater level of the Plio-Pleistocene Aquifer	32
Figure-15 Location map of the springs and wells in the study area	33
Figure-16 Chloride concentrations for Dyouk and Sultan Springs(1968-2004)	37
Figure-17 Nitrate concentrations for Dyouk and Sultan Springs (1968-2004)	37
Figure-18 Chloride concentrations data from Jericho wells (1968-2004)	38
Figure-19 Nitrate concentrations data from Jericho wells (1968-2004)	39
Figure- 20 Major components of Lisan	41
Figure- 21 Hydrogeological setting of Jericho Aquifer	41
Figure- 22 Possible contaminant sources and surrounding activities	42
Figure- 23 Sampled wells and springs within different geological formations	45
Figure- 24 Collection of Nitrate in the field using resin column	49
Figure-25 Durov Plot diagram	58
Figure-26 Major anions and cations vs. TDS	59
Figure-27 Ions molar ratios	60
Figure-28 Saturation indices	62
Figure-29 K vs. Nitrate	66
Figure-30 Seasonal comparative trends for Deuterium and oxygen isotopes	71
Figure-31 Seasonal variation for Deuterium and oxygen isotopes	71
Figure-32 Isotopic signature of Deuterium and oxygen in dry season	72
Figure-33 Sr/Ca molar ration vs. O-18	73
Figure-34 O-18 vs. NO ₃ /Cl molar ratio	73
Figure-35 N-15 vs. O-18 of Nitrate seasonal variation	77
Figure-36 Groundwater pollution by nitrate sources in Jericho	77

Figure-37 N-15 vs. O-18 isotopic composition of major nitrate sources	78
Figure-38 N-15 vs. O-18 for the groundwater samples	78
Figure-39a, b 1/ [NO ₃] in mg/l vs. N-15 and O-18	79
Figure-40 Seasonal variation of the S-34 signatures	80
Figure-41 Seasonal variation of O-18 signature of SO ₄	80
Figure-42 The isotopic signature of sulphate in the groundwater samples	82
Figure-43 Chloride vs. SO ₄ in mg/l	84
Figure-44 S-34 vs. SO ₄ in mg/l	85
Figure-45 The main two sources of sulphate in the Jericho aquifer	86
Figure-46 Distribution of cations and anions from different sampling sites	88
Figure-47 The relative increase in HCO ₃ vs. SI- Calcite	90
Figure-48 SI- Calcite vs. pH	91
Figure-49 The increase of HCO ₃ vs. slight increase in dolomite	91
Figure-50 C-13 vs. HCO ₃ in mmol	92
Figure-51 Sr/CO ₃ vs Rb/CO ₃ molar ratios	94
Figure-52 C-13 vs. NO ₃ /Ca molar ratio	94
Figure-53 .GIS project for the study area	101
Figure-54 Model assumption based on the real lithological profile	102
Figure-55 Wells for the surface topography	104
Figure-56 Study area surfaces	105
Figure-57 Interpolation: raster map for the layers	106
Figure-58 Volumetric model showing initial heads in meters	108
Figure-59 Well data import from EXCEL	109
Figure-60 Digital elevation model of the top surface	110
Figure-61 Display volumes in Tecplot	112
Figure-62 Display prisms and triangulation result	113
Figure-63 Mapping result in Tecplot	114
Figure-64 Wells as geometric data	115
Figure-65 3D view for the hydraulic distribution of the first aquifer layer	116
Figure-66 Haydraulic head distribution at different situations	117
Figure-67 Monthly pumping rates from wells in Jericho	119
Figure-68 First visualized 3D water level under the normal conditions	119
Figure-69 Pumping effect after wet season	120
Figure-70 Pumping effect after dry season	120

LIST OF TABLES	Page
Table-1 Generalized stratigraphic column of the West Bank	16
Table-2 Generalized Geological columnar section for the Aquifers	28
Table-3 Analytical methods and detection limits for major ions	46
Table-4 Hydrochemical data from sampled Wells and spring in wet season	56
Table-5 Hydrochemical data from Wells and spring in dry season	57
Table-6 Deuterium and O-18 for the groundwater samples	69
Table-7 Nitrate concentration and isotopic signatures of Nitrate	75
Table-8 Sulphate concentrations and the isotopic signatures of sulphate	81
Table-9 Bicarbonate concentration and isotopic signatures of carbonate	87
Table-10 Estimated material Properties for Jericho aquifer	108

CHAPTER 1: INTRODUCTION, BACKGROUND AND PURPOSE OF THE STUDY

1.1. Aims and Scope

The Dead Sea is one of the world's unique geomorphologic features, and is located within another of the world's great landforms: the Jordan Rift Valley. Unfortunately, the Dead Sea is suffering from unsustainable exploitation of water and mineral resources, which cause a dropping of the sea level at a rate of 80 cm to 1 m per year (Salameh, 2000). In addition, sewage from urbanized areas, especially through land use and touristic developments, is entering the Dead Sea via the Jordan River and wadis. Collaborative approaches between the surrounded countries will be critical if the continuing degradation of the Dead Sea and loss of its unique value is to be halted. The implications of the Dead Sea on the whole Jordan valley resources and environment were discussed in many meetings and conferences for the shared countries. The groundwater resources in the surrounding area were deteriorated noticeably in the last 50 years. Salts and TDS concentrations in the aquifer systems along Jordan valley which was covered by Lake Lisan, the ancestor of the Dead Sea, indicate a general trend of increasing salinity which reach its maximum in the lower part of Jordan rift valley and threaten the groundwater resources and consequently the stability of the whole system in the area. The Research Program for Water Resources Evaluation in the Jordan Rift Basin is a project supported by the German Ministry of Education and Research (BMBF). More than 12 institutions participate in the joint research program and work together on one of the main issues in the Middle East region: water resources.

This work is a part of a joint working group in the mentioned project and aims at using different new chemical and isotopic techniques for tracing water quality and possible contaminants at Jericho area catchments area in the lower part of the Jordan rift valley, considering previous studies and explanations of the salinisation mechanisms. The final expected output is to understand the sources and the mechanism of salinity and its rout of entrance in the groundwater system. This concept will help in constructing an integrative conceptual model for all the regional aquifer into the rift valley, thus a further comprehensive idea about the salinisation problem along the edges of the regional aquifers will be a good input tool in any flow model that might be developed in the future.

This research was held by UFZ-Environmental Research Centre in cooperation with Karlsruhe University and the help of PHG-Palestine Hydrology Group.

1.2. Location and Major Features

Jericho, town in Palestine is located in the Jordan Valley, north of the Dead Sea and west of the Jordan River (Fig. 1). From 1967-1996 Jericho was occupied and administered by Israel. Since 1996 the Jericho become under the civil administration of the Palestinian, but kept under the military control of the Israel.

The site of ancient Jericho is half a kilometre away from modern Jericho at a depth of 250 metres below sea level. It lies at latitude 31 52 degrees north and longitude 35 39 degrees east.

The climate of the area is hot and dry in summer and mild in winter, supporting the growth of such crops as dates, bananas, and citrus fruits. Most of Jericho's agricultural land is irrigated by small private wells that provide water throughout the year; the city draws its water for domestic use from an irrigation system originating at the Ayn as Sultan Spring, which has supplied Jericho with water since ancient times. In addition to agricultural activities, Jericho has a long-standing tourist industry.

Road traffic from Jerusalem and other cities in northern West Bank converges in Jericho, and roads continue south to the Dead Sea and the Negev. Also traffic from the Allenby Bridge crossing on the Jordanian border passes through Jericho as well.

Jericho is the site of the oldest settlement yet to be discovered, with significant archaeological remains dating back as far as 8000BC. Located about 2 km (about 1 mi) from today's city centre, the settlement included a walled community and a high tower. Additional findings from the period indicate that there was irrigated agriculture, revealing the prehistoric shift from nomadic to settled forms of life.

The area of Jericho is considered as semi-arid , however, the area surrounded Jericho contain several surface water flow that drained from the upper mountains of Jerusalem and Ramallah through two main wadis, (Wadi Nuwe'meh and Wadi Qilt). The last wadi (Fig. 3) is a natural protectorate, which has fantastic characteristics, it also has historical characteristics, its environmental system represents the desert and depression, it is considered as wetland region and filled of towering mountains and it is full of springs which cover this region.

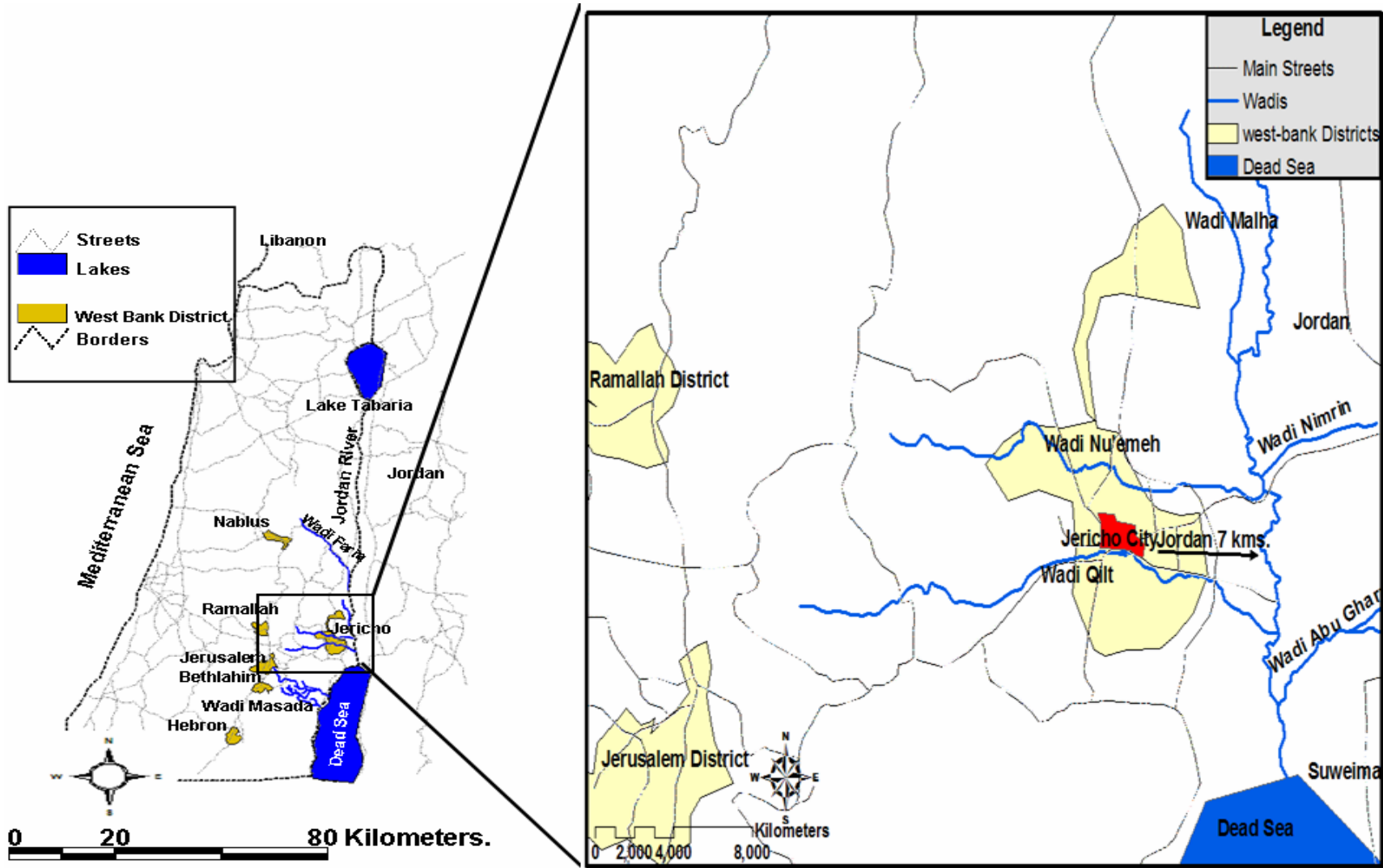


Fig. 1: Location map of the Study Area

Thus the region considered as one of the most beautiful regions in Palestine at which the water flows from the rocks and form small or large waterfalls that feed the life aspects in Jerusalem wild region.



Fig. 2: Agricultural land near Jericho (photo by Stefan Geyer).



Fig. 3: Wadi Qilt general view.

Wadi Nuwe'meh (Fig. 4) is located to the north western side of Jericho city. Wadi region considered as wetland region and, it is also a protected and agricultural grassland region. This wadi is featured by the existence of several springs in the eastern part of it



Fig. 4: Eastern part of Wadi Nuwe'meh

The study area will be described in further details in the next chapters.

1.3. Land Use

Jericho district has a total area of 35,330 hectares (353,300 dunums). Five major land use classes can be distinguished in the district. These are Palestinian built-up areas, Israeli settlements, closed military areas and bases, nature reserves and cultivated areas (Fig. 5). Of the total area, the Palestinian and Israeli built up areas occupy approximately 1.7% and 1.5% respectively.

1.3.1. Palestinian built-up areas

There are seven Palestinian built-up areas in the district. The Jericho city is the only municipality in the district, while Dyouk El-Tahta, Dyouk El-Fuka, Nuwe'meh, Al-Auja are classified as villages. In addition there are Aqbat Jaber and Ein Al-Sultan refugee camps (Fig. 5). These areas collectively account for approximately 591

hectares. The Palestinian built-up areas are located on either alluvial and brown soils, which are considered to be the most suitable soil for agricultural purposes in the district, or loessial serozems soils which are covered with pasture plants.

1.3.2. Israeli settlements

There are 14 Israeli settlements in the district. These are Gilgal, Netiv Hagedud, Niran, Yitav, Zori, Na'ma, Elisha', En Hogla, Bet Ha'erava, Lido Yehude, Atrazia, Mizpe Yeriho, Vered Yeriho and Almog. These settlements occupy approximately 517.4 hectares of land, and are located on different soil associations. Elisha', for example, is found on alluvial arid brown soils, while Atrazia is found on Solonchaks, which is used for agricultural purposes if intensively managed.

1.3.3. Closed military areas and bases

Closed military areas take up approximately 5,844 hectares in the district. The Israeli army claims these areas are of security importance and are used for military training purposes. In addition, there are six military bases with a total area of approximately 265 hectares.

1.3.4. Nature Reserves

Currently, there are four declared nature reserves in the Jericho district with a total area of about 1,965 hectares, mostly located within the declared closed military area in the district (Fig. 5). Because of the Israeli government's history of confiscating land through declaring an area a nature reserve, there is suspicion about the true Israeli intentions and the environmental importance of the areas currently declared.

1.3.5. Cultivated Areas

The cultivated areas in the Jericho district cover approximately 2419.4 hectares. Due to the limited rainfall combined with the hot weather, irrigated agriculture is dominant in the district. The cultivated areas are concentrated in Jericho city, Dyouk, Nuwe'meh and Al-Auja including the following major types of cultivation (Jericho Agricultural Station, 1994):

1. Fruit trees: The cultivated fruit trees occupy an area of 771.1 hectares. Most dominant are bananas and citrus covering an area of 560 and 136.9 hectares respectively.

2. Field crops and Forages: The total area of the cultivated field crops and forages occupy approximately 144.5 hectares and include barley, wheat and sudan grass.

3. Vegetables: The total cultivated area amounts approximately to 1,504 hectares, with 1,026 of the total area located at Jericho city and the rest distributed in Dyouk, Nuwe'meh and Al-Auja villages. For more information about cultivated areas see chapter five.

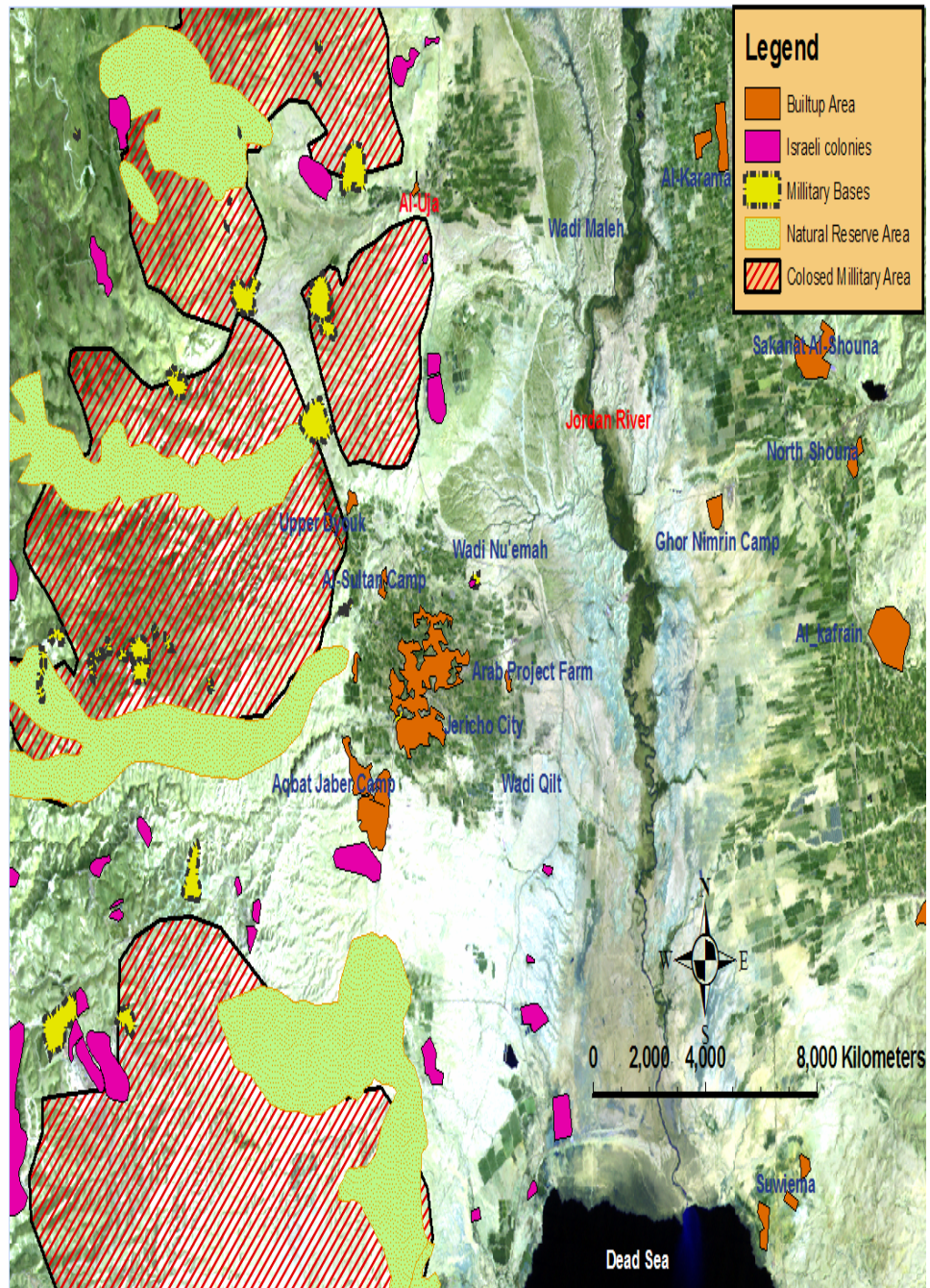


Fig. 5: Satellite image for the study area showing major land use.

1.4. Population

The population of the Jericho district is estimated at around 25,500, representing approximately 1% of the total population of Palestine. This number includes the two refugee camps of Ein Al-Sultan and Aqbat Jaber. Jericho city is the only urban area in the Jericho district and its population represents around 64.2% of the population. The inhabitants of the refugee camps represent 22.5% while the inhabitants of the villages represent 13.3% of the total population in the district (PBS, 1994). Population figures for the year 2002 indicate that around 60% of Jericho city residents were between the ages of 0-19, 22% are between 20-34 and 10% are between 35-54 (PBS, 2002). These figures indicate that over than half of the population is dependent and lack self reliance.

Infant mortality rates have been increasing since 1990, reaching in the West Bank 21 deaths per 1000 live births. Moreover, the life expectancy is approximately 72 years, and the birth rate was estimated at 44 births per 1000 in 1992 (Abu-Libdeh, 1993).

Approximately 68% of the working age population (16-59) in the district has jobs. Out of this number, 46% is permanently employed, 49% has seasonal employment and 5% has part time employment (PARC & Arab Thought Forum, no. 5, 1994).

1.5. Soil

Despite the small size of West Bank, a variety of soils can be found. The major causes of this variety are the extreme conditions which form these soils: climate, arid in the east and wet in the mountainous ridge; variable geology: sedimentary rocks, sand dunes, alluvium, etc., and different topographic circumstances: topography varying from 400 masl at the western edge to 1000 masl at the mountain ridge to 410 masl at the Dead Sea area. Also, physical weathering from both water and wind modifies the soils.

According to ARIJ (1995), the main soil associations that cover Jericho area is alluvial arid brown soil which is covers an area of about 6,470 hectares. It is exists of alluvial fans and plains, formed as a result of erosion of calcareous silty and clayey materials.

1.6. Climate**1.6.1 Temperature and Wind**

In general the climate of the whole Jordan valley is characterized by a hot dry summer and warm low rain winter. Jericho area can be classified as an arid area, its location along the feet of the mountains accompanying the Jordan Valley in the west protect it from the cooler north western Mediterranean wind.

The temperature of the area varies from high temperature in the south that slightly decreases further to the north. Typically, the temperature reaches its maximum in August with an average of 38C°, while January considered as the coldest month in the year with an average of 19C°. The total incoming radiation at the area is extremely high, which make it a very suitable environment for irrigated and greenhouses agriculture (ARIJ, 1995).

The area is affected by 2 winds directions all over the day, one that is mainly coming from the Dead Sea in the morning hours with an average speed of 3 m/sec. Then it turns gradually to a north west wind with an average speed of 5m/sec. The maximum wind speed in the area is measured by ARIJ team, 1995 at 15m/sec in spring time by this northwest winds.

1.6.2 Precipitation

The wet season in the area is starting by the end of October reaching its climax in January and February. The precipitation in the area is characterized by the short duration and the low amount.

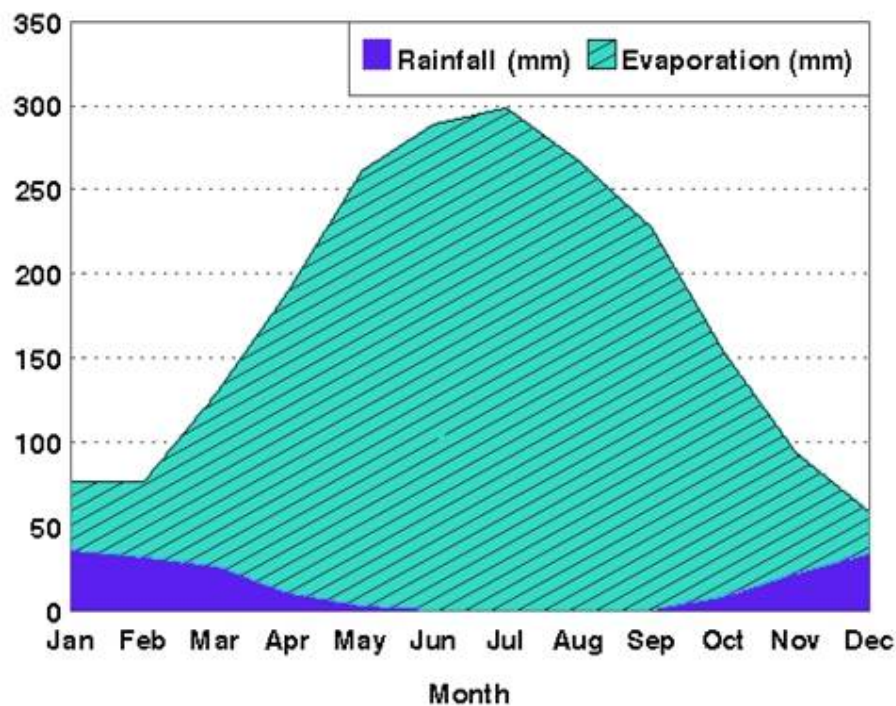


Fig. 6: Monthly rainfall and evaporation in the Jericho district for 1969-1992

According to the Jericho weather station, the mean annual precipitation in the study area is approximately 120 mm/yr, of which approximately 60% falls in the three months of December, January and February (Fig. 6). In general, the Jericho district has the lowest rain in the region (Fig. 7) and short rainy season ranging between 20-25 rainy days per year (Israeli meteorological service, 1994).

The mean annual relative humidity reach about 50%, with the highest rates in winter time that reach 75% and the lowest rate in summer that reach 5% when the temperature is very high.

Accordingly, the evapotranspiration rate in the area is very high that reach 298 mm in July when solar radiation reach its highest point. Normally, this highly evaporation exceeds the precipitation during the year (Fig. 6), thus the agriculture in the area is totally depending on the irrigation (ARIJ, 1995).

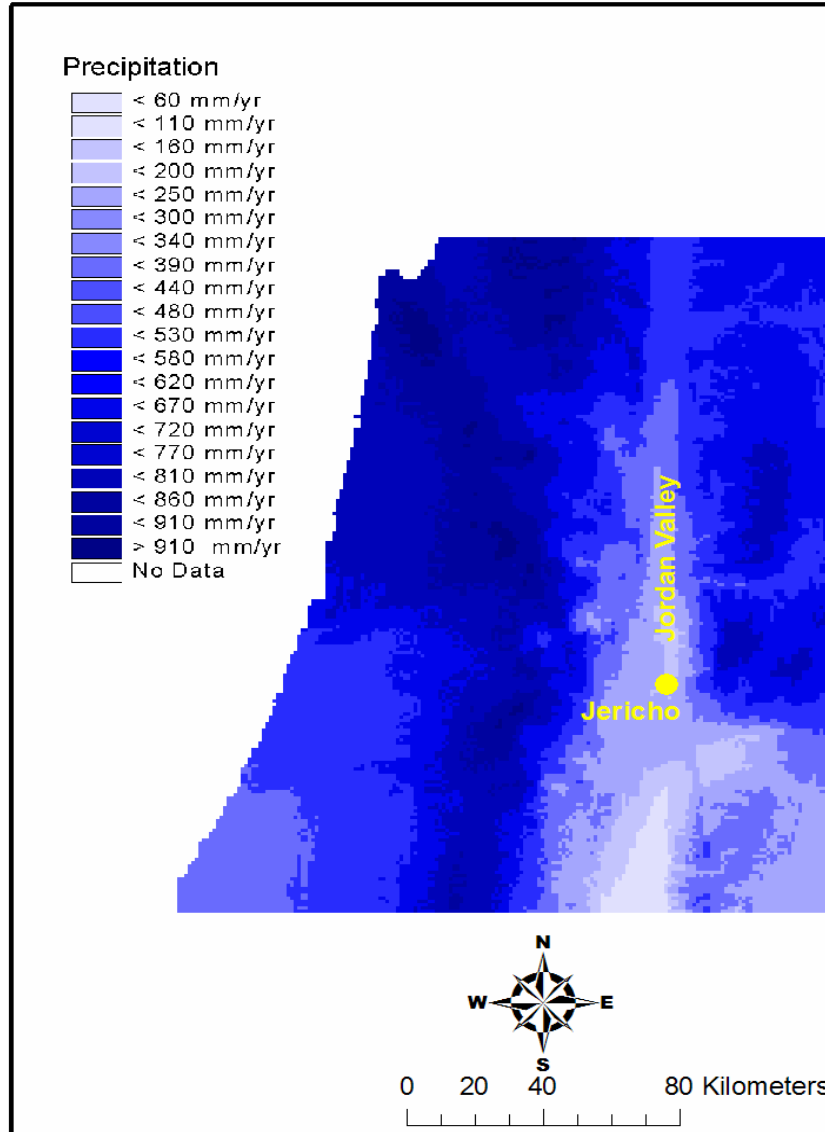


Fig. 7: Average annual precipitation rate in mm in the Jordan valley Area (Fifth RTD Framework Program, Dead Sea Project, 2004).

1.7. Previous Investigations

Many previous studies identified the common sources of salinity and groundwater deterioration in Jericho and vicinity. The common sources of this high salinity rate was reported by Marie & Vengosh (2001), where they identified the in situ dissolution of salts within the well from Lisan formation, the apprising of deep brackish water and anthropogenic effluent as the 3 sources for this phenomenon.

Many other studies referred to the high Ca-Cl and Na-Cl water to the upconning of deep-seated brine water along the fractures of the Rift Valley or to a current

Mediterranean seawater Flux to the topographically low Rift Valley (Kafri & Arad, 1979).

Vengosh & Rosenthal, 1994 described two main type of the brine water as the main cause of salinity in the region these are: Ca-chloride brine waters encountered in the Jordan Dead Sea Rift Valley, in various parts of the Negev and of the Coastal Plain, and Na-chloride saline water identified in the subsurface of the Negev and in the southern part of the Coastal Plain. They found that the intensive exploitation of groundwater in the area has disturbed the natural equilibrium which prevailed between fresh and saline water. The newly established groundwater flow regimes have facilitated the migration of saline water bodies, their participation in the active hydrological cycle and the progressive contamination of fresh groundwater. These processes which were not anticipated by planners and water resources managers emphasize that large-scale groundwater exploitation was undertaken without giving sufficient consideration to the occurrence and subsurface migration of saline water and brines.

Geophysical surveys of groundwater in the Jericho area (Gropius & Klingbeil, 1999) have suggested that brine occupies the deepest part of the Pleistocene sediments at a depth of ~80 m, and is overlain by less-saline groundwater. The chemistry of groundwater in the Jericho area indeed reflects a mixture of these two water sources (Marie & Vengosh, 2001). However up to now, no fixed data regarding the origin or driving mechanisms of the saline water in many areas along the valley has been identified. Also, Farber et al. (2003) conclude that the extensive irrigation over the flood plains of the Jordan River enhances dissolution and leaching of sediments that together with underlying brackish waters control the salt content of shallow groundwater. However up to now, no fixed data regarding the origin, the share of different sources, or driving mechanisms of the saline water in different areas along the valley has been identified. Further details about the problem of Salinity and groundwater deterioration with other anthropogenic contaminants as well as detailed description of the study area will be described in the coming chapters.

Chapter 2: GEOLOGY AND HYDROGEOLOGY

2.1. General Overview

It forms an active part of the African-Syrian Rift, which extends for about 6000km, from east Africa through the Red Sea, Wadi Araba, and Dead Sea, Jordan Valley to south Turkey. Long time before the formation of the Dead Sea Rift, the movement of the African plate including the Arabian plate to the north caused the formation of the Syrian Arc Fold Belt, which was named by Krenkel (1924). The Syrian Arc formed in two stages: the first in the Turonian-Maestrichtian and the second in the Oligocene (Burdon, 1959; Bandel & Mikbel, 1985; Abed, 2000). It extends in S shape, from Sinai through Palestine, Jordan to Syria. Two major tectonic events have shaped the area of the West Bank. The Syrian Arc System folded up the shelf deposits at the end of the Cretaceous Period and the Red Sea-Aqaba transform fault formed the Dead Sea Graben from the Miocene (Krenkel, 1924; Rofe & Raffety, 1963 and Andrew, 2000).

The Afro-Arabian tectonic plate remained relatively stable from Precambrian to the early Cretaceous. The Cretaceous period began with extensional faulting and volcanism over part of the Levant countries and eastern Mediterranean, and terminated in compression, inversion, folding and faulting processes, expressed in Israel and the West Bank by the anticlines of the Syrian Arc (Krenkel 1924) and fault structures, discerned by lateral thickness variations of the sedimentary section between nil and a few hundred meters. The formation of the Syrian Arc, manifested in the reactivation of the pre-existing faults, resulted in the inversion of the late Paleozoic-Turonian lows and highs (Flexer et al. 1989).

From the late Eocene to Pliocene and recent times two stages of movement between the African and Arabian plates took place (Girdler, 1983). The first stage detached the Arabian Shield from the great African Shield in form of an extensional rift system, and thus initiated the opening of the Red Sea. The second stage was caused by Ocean spreading in the Gulf of Aden (Quennell, 1956; Gass, 1979; Bayer et al. 1988; Purser & Hoetzl, 1988). It creates a northward movement of the Arabian plate along a left lateral transform fault along Aqaba- Dead Sea- Jordan Valley, now called Dead Sea-Jordan Rift system with pull- apart-basins and transpression zones. It was continued more or less continuously the last 12 million years with a movement of about 9mm/year. The West Bank is thus located on the Sinai sub-plate to the west of the

fault. This fault system has a vertical, stepped component, forming the rhomb structure pull-apart- basins in which the Dead Sea is located. This led to the lowering of the base level of drainage and deposition of the runoff load (Rofe & Raffety 1963)

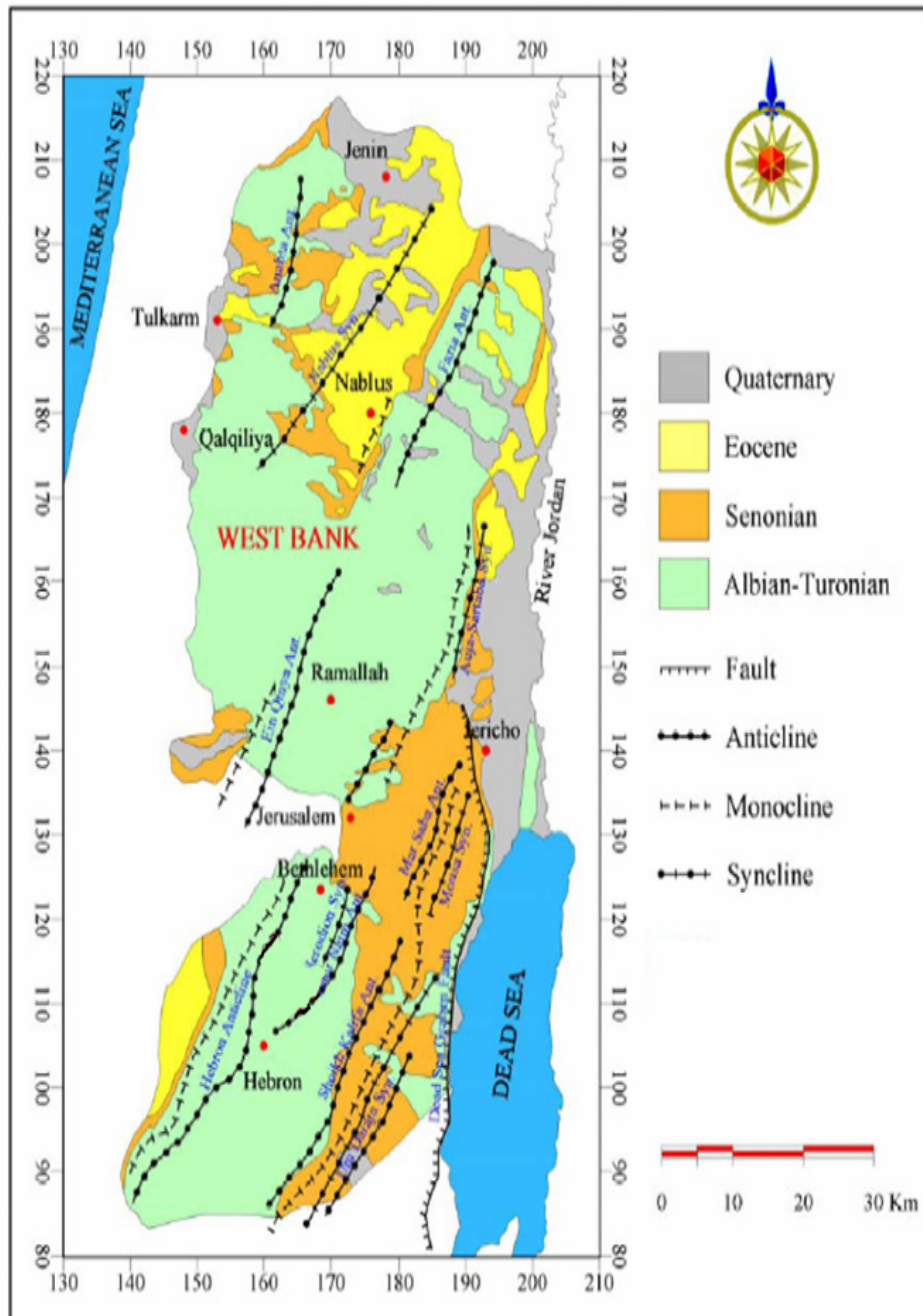


Fig. 8: General geological and structural map of the West Bank (modified after Abed Rabbo et al., 1999; Guttman & Zuckerman, 1995; and Qannam, 2000).

The Jordan Rift, the SSW-NNE Jerusalem (Judean) Anticline, and Nablus Syncline dominate the structure of the West Bank, where Jerusalem Anticline expresses both Surif (Hebron) and Ein Qiniya Anticlines. On the limbs of the Jerusalem anticline there are a number of minor parallel or sub-parallel folds so that the structure can be considered as an anticlinorium (Fig. 8). The Jerusalem Anticline is asymmetrical, with a steeply dipping west limb (mean 30°) and a more gently dipping east limb (mean 15°), (Rofe & Raffety 1963).

2.2. Stratigraphy and lithology of the West Bank

Within the West Bank, the outcrops are predominantly carbonate sediments and rocks of Tertiary and Cretaceous ages. Older rocks cannot be found at the surface though they are known from the boreholes. The oldest exposed rocks belong to the Albian, overlain by younger strata of the Cenomanian, Turonian, Senonian and Eocene, exposed on both flanks of the anticlinal axis in the West Bank.

The exposed rocks (Fig. 8) of the West Bank are:

1. Albian - Lower Cretaceous formations comprising the regional West Bank groundwater system (Beit Kahil, Yatta formations). The thickness of the groundwater system in this area ranges from 500-970 meters.
2. Upper Cretaceous formations comprising the regional West Bank groundwater system (Hebron, Bethlehem and Jerusalem formations). The thickness of the groundwater system in this area ranges from 190-490 meters
3. Senonian age rocks (Abu Dis formation) are composed mainly of chalks and marls. The thickness ranges between 0-450m
4. Pleistocene to Eocene rocks overlay the Senonian rocks in the Northern and Northeastern area of the West Bank, the rocks are composed mainly of limestone, chalky limestone, chalks, marls, and siltstone, which are of limited
5. extent and thickness
6. Unconsolidated, Quaternary alluvial sediments overlie the major rock formations

The general stratigraphy of the West Bank and the Israeli and the Palestinian names of the different geological formations in the West Bank as well as their lithology, thickness and aquifer potentiality are described and illustrated in Table 1.

Table 1: Generalized stratigraphic column of the West Bank (modified after Braun & Hirsch, 1994; Millennium Engineering Group et al., 2000; Guttman, 2000; Guttman & Zuckerman, 1995; Bartov et al., 1988; and Qannam, 2000)

Geological Time Scale			Group		Formation		Lithology	Thickness (m)	Hydrostratigraphy							
Era	System	Epoch	Palestinian	Israeli	Palestinian	Israeli										
CENOZOIC	Quaternary	Holocene	Recent	Kurkar	Alluvium	Alluvium	Marl, alluvium, gravel	Variable	Aquifer							
					Gravel	River gravel			Aquifer							
		Pleistocene	Lisan	Dead Sea	Lisan	Lisan	Thinly laminated marl with gypsum bands	200+								
	Tertiary	Neogene	Pliocene-Miocene	Beida	Jenin Sub Series	Saqia	Beida	Bit Nir and Ziglag	conglomerate	0-200	Aquifer					
						Avidat	Reef nummulitic limestone				Zor'a	Reef limestone, bedded limestone, chalk with limestone undifferentiated	100-500	Aquifer in limestone and aquiclude in chalk		
		Paleogene	Eocene	Belqa	Mount Scopus	Nummulitic limestone	Taqiya	Marl, chalk and clay		Aquiclude						
						Khan Al Ahmar and Zerga	Ghareb			Yellowish chalk	Aquiclude					
	MESOZOIC	Senonian	Mastrichtian								Aquiclude					
											Amman and Abu Dis	Mishash	Chalk with back chert	Aquiclude		
			Campanian	Santonian									Aquiclude			
Menuha													Chalk	Aquiclude		
Cretaceous		Turonian	Cenomanian	Ajlun	Judea	Jerusalem	Bina	Limestone and dolomite (karstic).	90-120	Aquifer						
						Bethlehem	Weradim	Hard gray porous dolomite	90-100	Aquifer						
							Kfar Shaul	Chalky limestone, chalk and marl	30-40	Aquitard						
						Hebron	Aminadav	Karstic limestone and dolomite	110-140	Aquifer						
						Yatta	Moza	Marl, clay and marly limestone	10-20	Aquiclude						
							Beit Meir	Limestone, chalky limestone and dolomite	120-140	Aquifer						
		Albian										Aquiclude				
												Upper Beit Kahil	Kesalon	Limestone inter-bedded with marl	30-50	Aquifer
													Soreq	Dolomite inter-bedded with marl	110-170	Aquifer
												Lower Beit Kahil	Giva't Yearim	Limestone, dolomite	20-70	Aquifer
													Kefira	Limestone, dolomite and marly limestone	120-180	Aquifer
												Kurnub				
Kobar		Qatana	Marl and clay	50	Aquitard											
		Ein Qinyia	Marl and marly limestone	60-70	Aquitard											
		Tammun	Caly and marl	80-150	Aquitard											
		Ein Al Asad	Limestone		Aquifer											
Aptian					Limestone			Aquifer								
Neocomian			Kurnub						Aquifer							
Jurassic	Callovian-Bajocian	Zerqa	'Arad	Upper Malih	Upper Malih	Marl interbedded with chalky limestone	190	Aquitard								
				Lower Malih	Lower Malih	Dolomitic limestone, jointed and karstic	55	Aquifer								

2.3. Geology and Stratigraphy of the Jericho Study Area

The Rift Valley faults are the major structure that affects the geology and hydrology of the whole Rift Valley. The stratigraphy consists of carbonates, chert, chalk, gravels, and sandstones and evaporates which range in age from the Triassic to Holocene age in the east near the rift. The ancient Jurassic and Lower Cretaceous formations are composed mainly of limestone, sandstones and marl layers. The youngest formations are of Pleistocene to Holocene age (ARIJ, 1997). The following is a description of the stratigraphy and the characteristics of the geological formations exposed in the study area, it is based mainly on the studies of Guttman (2006), Guttman (2000), Qannam (2000), Millennium Engineering Group et al. (2000), and Braun & Hirsch (1994) as well as the generalized stratigraphic sequence of the West Bank that is shown in Table 1 and the geological map of the Geological Survey of Israel in Fig. 9 and 10.

2.3.1 Cretaceous Rocks

2.3.1.1 Aptian-Albian – Kobar Formation

According to the Israeli nomenclature, this formation is made-up of five sub formations (Table 1): the Nabi Said, Ein Al Asad, Tammun, Ein Qiniya and Qatana. In the area of study this formations of are not exposed. Ein Qiniya Formation is made-up of layers of thin gray to brown, thin to middle grained limestone's which contains iron concretions and thin calcite veins. The limestone layers are inter-bedded with horizons of marl, rich in fossils (Shakhnai 1969 and Millennium Engineering Group et al. 2000). On the other hand the Qatana Formation is composed of yellowish-brown-gray limestone alternating with layers of yellow marls. The thickness of Ein Qiniya in these outcrops is about 15 m according to Hirsch (1983), whereas Qatana reaches a thickness of about 40 m (Hirsch, 1983; and Millennium Engineering Group et al., 2000). The two formations are part of regional aquiclude, including the Tammun Formation below them.

2.3.1.2 Albian - Lower Beit Kahil Formation

This formation represents the lower part of the upper Albian (Braun & Hirsch 1994). It is also not exposed in the study area. It is built of two sub formations, Kefira and Giva't Yearim. Kefira, the lower part of this formation, is made-up of limestone with

thin layers of porous dolomite interchanging with marly limestone. Gray limestone layers alternating with layers of shale and marl, are typical for the lower part of the Kefira Formation. On the other hand, Giv'at Yearim, the upper part of the Lower Beit Kahil Formation, is made-up of gray to brown dolomite with clayey and marly limestone. The marly uppermost part of Ein Yorqe'am is equivalent to Moza marl (Picard 1938). Generally, the Lower Beit Kahil is considered to be a moderate to good aquifer, forming the lower part of the Albian aquifer.

2.3.1.3 Albian Upper Beit Kahil Formation

This formation is regarded as the upper part of the upper Albian. It has two sub formations that are; Soreq and Kesalon (**Kuke**). The lower part of this formation (Soreq) consists of porous dolomite, marly dolomite, marl and at times some chert. The occurrence of the marl in this formation reduces its water bearing capability. On the other hand, the upper part of this formation (Kesalon) mainly consists of brittle dolomite and brittle limestone rich in fossils.

2.3.1.4 Cenomanian - Yatta Formation

The Lower Cenomanian Yatta Formation (Beit Meir (**Kubm**), En yorqe'am (**Kuey**) and Moza formations in Israeli literature) overlies the Upper Beit Kahil Formation. Beit Meir, 50-110 m thick, is composed of limestone, chalky limestone, dolomite, marl and greenish clay at the bottom. Moza, 10-20 m thick, is composed of yellowish marly limestone with traces of greenish marl at the bottom. The dolomite of the upper part of Beit Meir shows some water bearing nature. Sometimes the limestone near the top, officiates as a local perched aquifer, which explains why a few springs emerge 20 m below the contact of the Yatta Formation with the Hebron Formation (Rofe & Raffety 1963).

2.3.1.5 Cenomanian - Hebron Formation

The Middle Cenomanian Hebron Formation, Aminadav (**Kua**) in the Israeli terminology. This formation is exposed in a very small area to the west of Ein Sultan.

It is composed of brittle karistified gray dolomite, dolomitic limestone and gray limestone. At its base it is formed of hard dolomite and dolomitic limestone with some silicification. The lithology is uniform since dolomite and dolomitic limestone are found throughout the sequence of Hebron Formation. The porosity of this Formation is

mainly secondary because the rocks are well jointed and karstified. The Hebron Formation without doubt is the most important aquifer within the West Bank.

2.3.1.6 Cenomanian – Bethlehem Formation

The Upper Cenomanian Bethlehem Formation. This formation exposed in a small part to the north western of the Jericho area, by the mountains foot. It is built of two formations: Weradim (**Kuw**) as its upper part and Avnon (**Kuav**) as its lower part. Avnon is made-up of limestone, chalky limestone and marl that act as a confining aquiclude for the Hebron Formation beneath. The Weradim Formation is made-up of hard dolomite with some limestone. Bethlehem Formation is frequently highly jointed and fractured making this formation a good aquifer.

2.3.1.7 Turonian - Jerusalem Formation

This formation is of Turonian age. It is built of three formations (Derorim (**Kua**), Shivta (**Kush**), and Nezer (**Kun**) formation according to Israeli terminology). In the western and north western part of the study area only the formations of its upper part Nezer and Shivta are exposed. Its lithology is characterized by karstified limestone and dolomite with marl and clay mainly near the bottom. Sometimes occurrence of chalk is evident on the top of this formation.

2.3.1.8 Senonian – Abu Dis Formation

This formation is part of Senonian age. It composed of Menuha (**Kum**), Mishash (**Kumi**) and Ghareb (**Kug**) formations (Israeli nomenclatures). This Meshash formation is mainly exposed in the western part of the Jericho district, near the Sultan area. It consists of chalk and chert, the chalk usually white but in some areas dark colored due to the presence of bituminous materials. In general chalk often appears to be a fracture flow aquifer but because of its clayey nature it is considered as an aquiclude. The formation is structurally cut by minor faults. According to ARIJ (1995) the thickness of this formation ranges between 40 and 150 m.

2.3.2 Neogene and Quaternary

The Neogene and Quaternary successions are built mainly of marine and continental clastic formations, marine and limnic chalk, evaporates and magmatic rocks (Schulman, 1959). Alluvial formations are of Pleistocene, Holocene to Recent age. These formations are limited mostly to the Jordan Rift Valley itself. The thickness

varies between a few hundreds of meters on the rift shoulders to a few thousands in the deep depo-centers. The sequence is divided into two Groups: the Tiberias Group of Neogene age at the base and the Dead Sea Group (or the Jordan Valley Group in Jordan) of Plio-Pleistocene - Holocene age, at the top. The study area as a part of lower Jordan valley is belonging to the second group. The main formations in this group are:

2.3.2.1. Plio-Pleistocene formation

This formation composed of 3 sub-formations, these are:

1-Samra Formation: crops out along the western part of the Jordan Valley floor, at the base of the marly cliffs lining the Jordan River. It was deposited as marginal sediments along the Jordan Valley. The formation consists of conglomerates, sandstones and silts and is subdivided into two members:

a) Coarse Clastic member (**NQs (b)**): which is form as a result of wadis fan deposits and dominated in the western part of the study area, it consists of gravel and conglomerate with a thickness that reach 35 meter.

b) Silt member (**Qs (a)**): this member exists further to east of the coarse clastic member, it covers a large part of the study area and within Jericho city. It consist of more fine particle of silt and clay with a thickness that reach 20 meter

The two members show interfingering relationships and both interfinger with the Lisan Formation this formation cover the major part of the Jericho area west and inside Jericho city. It includes three local faults of up to 3 kms. long with 35 m thickness layer in certain unconformity.

2- Lisan formation (Qli): this formation is exposed in the eastern part of the study area as well as the whole Jordan valley rift and the wadis. It consists mainly of laminated aragonite-chalk, gypsum and clay with some sandstone and pebble beds. The section contains hypersaline and brackish fauna. The Lisan formation acts as an aquiclude.

2.3.2.2. Holocene formation

These formations comprise recent alluvial deposits in the wadis and associated flood plains of ephemeral streams. These sediments found in the eastern part of the study area lining and surrounding the Jordan River. In the study area this formation have five members that varied in its lithology from one location to

another (Fig. 9 and 10), these members are consist of: conglomerate (Q1), Gravel (Q2), Stream (Q3), Soil (Q4) and Sabha soil (Q5).

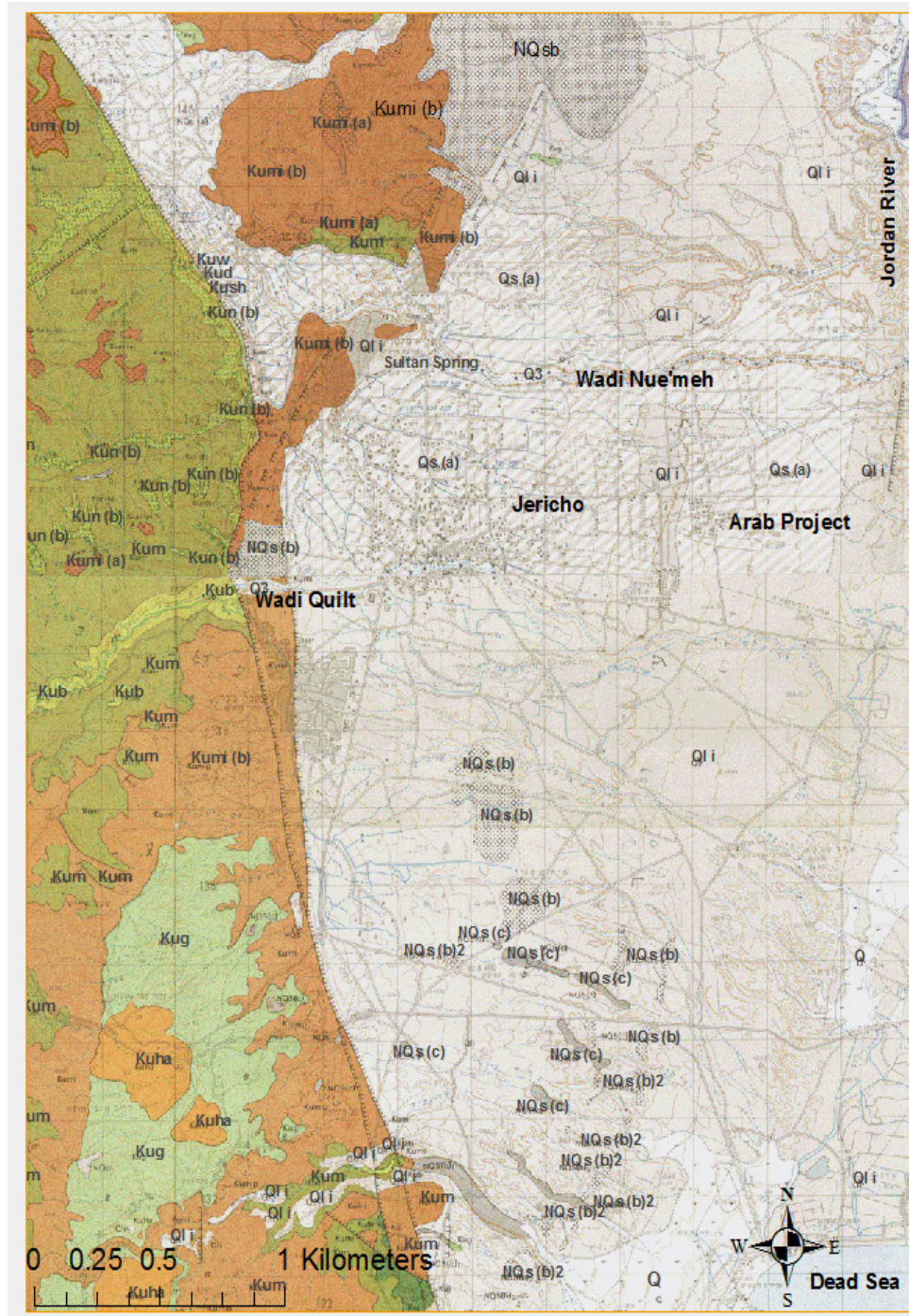


Fig. 9: A geological and structural map of Jericho Area -see legend in figure 10- (modified after the Geological Survey of Israel 1973; Hirsch 1983; and Rofe & Raffety 1963).

STRATIGRAPHY

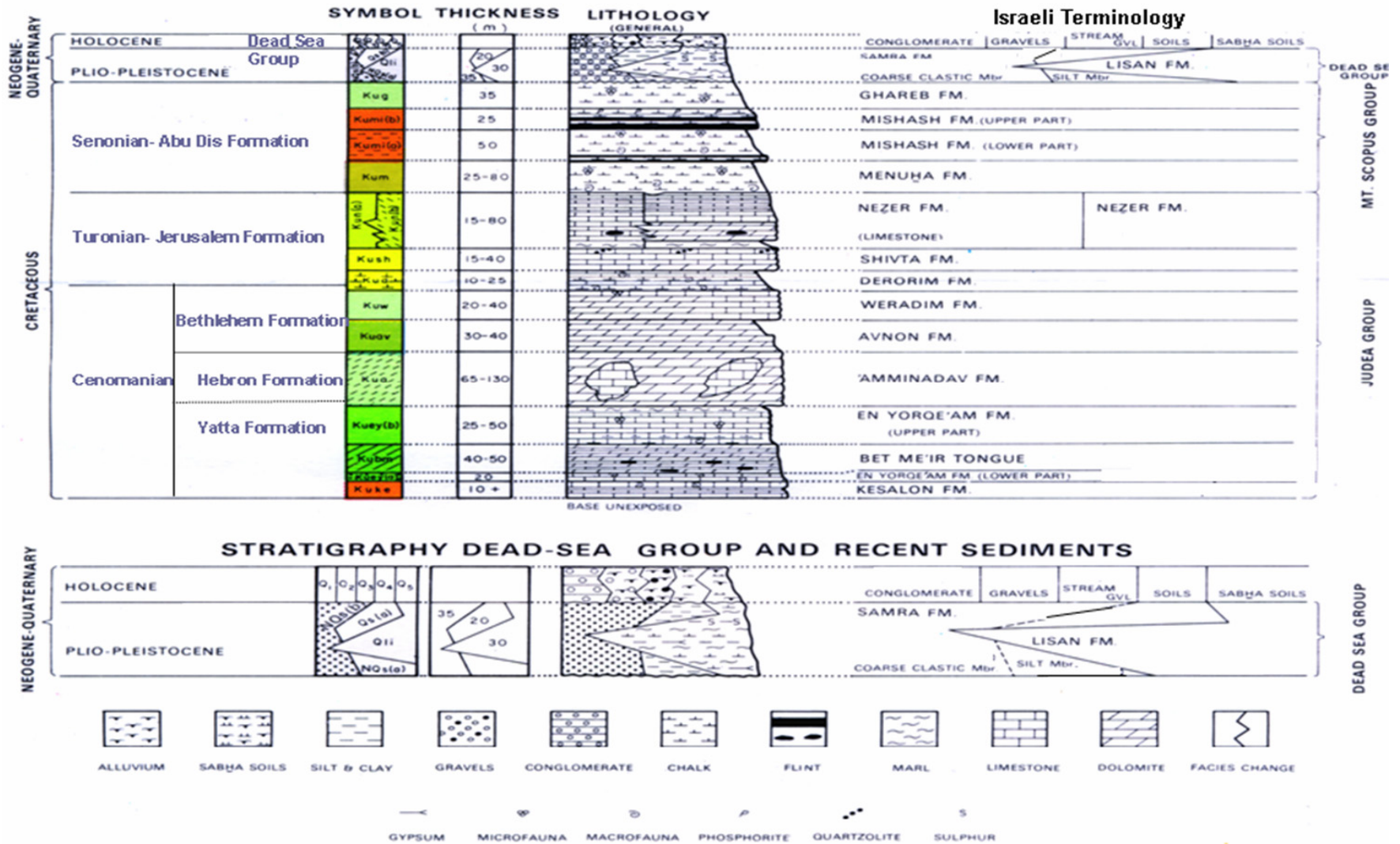


Fig. 10: Generalized columnar geological Section indicating various formations in the study area. (Modified from Geological Survey of Isreal, 1973)

2.4 Structural setting

2.4.1. Faults and Folds

The major structural element of the study area is the Jordan Dead Sea – Jordan Rift system structure that was formed since the Miocene age during the last 12 mill. years (section 2.1). There are evidences of younger faulting from the Pleistocene to the present age. In upper crustal levels longitudinal strike-slip and normal faults are the most prominent elements controlling the whole Dead Sea basin structure, but transverse faults that extend across the basin are also important. This significant fault in the study area is of SE NW trend, formed by a large pull-apart that formed between the left stepping the study area of Jericho and Arava strike-slip faults that extend north and south of the whole lower Jordan Rift, (Figs. 9 and 11, Quennell, 1958, 1959; Neev & Hall, 1979; Garfunkel et al., 1981; Garfunkel, 1981; Kashai & Crocker, 1987; Purser & Hoetzl, 1988; Ten Brink & Ben- Avraham, 1989). The pull-apart forms a deep trough, mostly some 8 km wide, between the extensions of these major strike-slip faults. These structures are embedded in a wider depression which comprises the entire width of the transform valley, 13 to 17 km, and whose marginal zones, on the two sides of the pull-apart, were shaped by gravitation normal faulting.

The western marginal zone, 4-5 km wide, extends from near the study area to the Wadi Araba in the south and comprises several blocks down-faulted few kilometers. Mesozoic sections drilled in these blocks confirm the pattern of facies changes and erosive unconformities of the adjacent area on the west (which trend obliquely to the transform). This proves that the marginal blocks were not displaced laterally, so that transform motion took place east of them. The marginal zone east of the pull-apart is quite narrow, often less than 2 km wide. Thus in cross section the whole Dead Sea basin including the study area has an overall asymmetric structure, with its deepest portion, comprising the pull-apart, being closer to the eastern border fault (Ben-Avraham, 1992). This asymmetry is present all along the basin, and it is expressed in the bathymetry of the Dead Sea.

A number of minor faults cut across the Rift, resulting in the separation between the southern and northern basins. A step-fault structure can be identified mainly on the western side of the study area . There are sets of faults facing away from the Rift to the west and northwest of the area. The fault on the western side is normal and cuts some

structures surrounding the area such as the Buqei'a Syncline, the Auja Monocline, the Mousa Syncline, Mar Saba Anticline, Hebron Anticline and Al Far'a Anticline. The beds of the western side dip strongly towards the Rift. The mountainous region of the West Bank (west of the study area) constitutes a relatively large symmetrical anticline, on which secondary structures of different ages are formed. The principal fold structures in this block are the Anabta, Al Far'a, Ramallah, Mar Saba, Hebron and Bani Na'im Monoclines (Fig. 8). The axes of these structures trending north-northeast, south southeast. Between these anticline structures, there are wide synclines such as the Nablus-Beit Qad and Buqei'a Synclines. Fault structures are concentrated in the area between Ramallah and the Hebron Monoclines. They trend east-west. On the western margins of the Dead Sea, faults trend north-northwest, while the faults of the Al Far'a and Malih Grabens trend northwest-southeast.

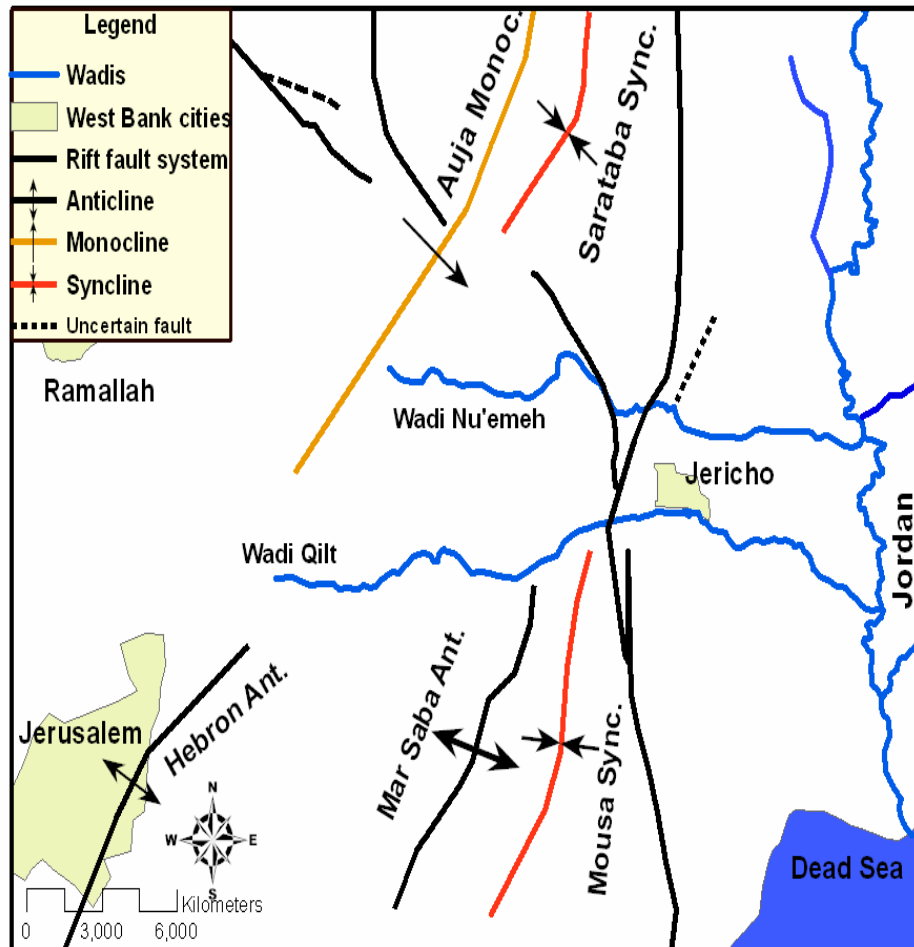


Fig. 11: Structural map for study area showing major faults, anticlines and synclines.

2.4.2 Joints

According to Rofe & Raffety (1963), the joints in the West Bank, part of which is the Jericho lower Jordan valley area, are either a result of shrinking or the varying competency of individual beds within a formation. The shrinking joints are supposed to originate from the dolomitization of limestone, reduces the volume by about 12 % (Pettijohn, 1957 & Schlumberger, 2002), that assist the occurrence of the fairly well develop joints in the dolomite limestone of the Lower Beit Kahil, Hebron and Jerusalem formations, all of which are wholly or partially dolomitic. On the other hand, brittle beds of Yatta, Bethlehem and Jerusalem formations are highly jointed, perhaps due to their brittleness, whereas the marly and chalky beds of these formations are less affected.

2.4.3. Karstification

Generally, limestone's and other soluble rocks at or near the surface that have been modified by corrosive solution of limestone characterize karst regions. Surface sinks; sparse streams, subsurface caverns and deep water tables are typical features in such areas (Legrand & Stringfield 1973). Karstification is a result of the widening of the joints and fractures, through the dissolution of the carbonate rocks, by CO₂- rich percolating water. As the solubility of the dolomite is less and slower than that of the limestone, karst is less developed in the dolomite than in limestone and only minorly developed in marl (Milanovic 1981). The dominance of the jointed and fractured carbonates rocks, limestone and dolomite, in the West Bank suggests the possible existence of karst caves. According to Arkin (1980), fractures and Karstification are common features of the West Bank. In The study area there are several karst features to be seen. Caves are common in the mountains, particularly in the Hebron-Cenomanian formation to the west of the study area. The caves are also common among the houses and they are used for animal keeping.

2.5. Hydrogeology

2.5.1. Hydrogeology of the West Bank

The Following description of hydrogeology of the West Bank is based mainly on (Qannam, 2000; PHG, 2003; and Guttman, 2006). Groundwater, derived from the shallow and deep water bearing formations of the Mountain Aquifer, represents the main source of domestic water in the entire West Bank. Based on the direction of

hydraulic drainage of the Mountain Aquifer, it was divided and named to three main groundwater basins; Western, North-Eastern and Eastern Basin. The approximate boundaries between the three basins are shown in Fig. 1.2. Only the Eastern Basin lies entirely in the West Bank while the other two basins are shared with Israel. About 80-90 % of the recharge areas for the North-Eastern and Western basins lie within the West Bank (WWS, 2002 and Libiszewski, 1995), but the groundwater flows westwards towards the Mediterranean and northwards towards Bisan and Marj Ibn Amer.

2.5.1.1. North-Eastern Basin

There are several estimates for the recharge and storage capacity of this basin. According to Sturm et al. (1996) this basin has a total area of 700 km² out of which 650 km² are within the boundaries of the West Bank, while Elmusa (1996) estimated 500-590 km². The dominant direction of water movement is northeastwards along the plunge of Nablus-syncline. Different estimations for the safe yield of this basin are assumed to be 130 Mill. m³/yr (Schwarz 1982), 140 Mill m³/yr (Gvirtzman 1994 and Wolf 1995), and 145 Mill. m³/yr according to Oslo 2 Accords (1995). Out of this yield the Palestinians use 25 Mill. m³/yr around Jenin and 17 Mill. m³/yr from east Nablus springs, the rest is being utilized by the Israelis (Oslo 2 Accords 1995).

2.5.1.2. Western Basin (Yarkon-Taninim in Israel)

This basin has a recharge area of 1800 km² of which 1400 km² are in the West Bank, whereas its storage area, about 2500 km², lies almost completely in Israel (Sturm et al. 1996). Gvirtzman (1994) and Oslo 2 Accords (1995) estimated the potential yield of this basin to be 360 Mill. m³/yr, while Wolf (1995) estimated it by 320 Mill. m³/yr. According to Oslo 2 Accord (1995), the Palestinians use 20 Mill. m³/yr from wells in addition to 2 Mill. m³/yr from springs near Nablus, while the rest is utilized by the Israelis. The flow direction in this basin is westward towards the Mediterranean Sea. Groundwater from this basin is discharged by the springs of Ras Al-Ayin (Rosh Ha'ayen), which feeds Al-Auja (Yarqun) River and AlTimsah (Tanninim) springs.

2.5.1.3. Eastern Basin

The direction of the water flow of this basin is eastwards toward the Jordan River and the Dead Sea. Naturally this basin is drained by several groups of springs in the West Bank, whereas a small fraction of its water discharges into the Jordan River and the Dead Sea and a negligible amount leaks to Israel. The recharge area of this basin

encompasses over 2200 km² and the storage area over 2000 km² (Gvirtzman, 1994). This basin lies almost entirely in the West Bank. Estimates of the safe yield (or extraction potential) of this basin are not well determined; 100 Mill. m³/yr (Elmusa 1996 and Gvirtzman 1994), 125 Mill. m³/yr (Wolf 1995) and 172 Mill. m³/yr (Oslo 2 Accords 1995). According to Oslo 2 Accords (1995), the 172 Mill. m³/yr is shared as follows: 24 Mill. m³/yr utilized by the Palestinians from wells, 30 Mill. m³/yr utilized by the Palestinians from springs, 40 Mill. m³/yr used by the Israelis and 78 Mill. m³/yr to be developed in the future. According to the surface and subsurface hydrological divisions of the West Bank, Jericho area is part of the Jerusalem Ramallah sub-basin and accordingly part of the Eastern Basin (Fig. 1 2).

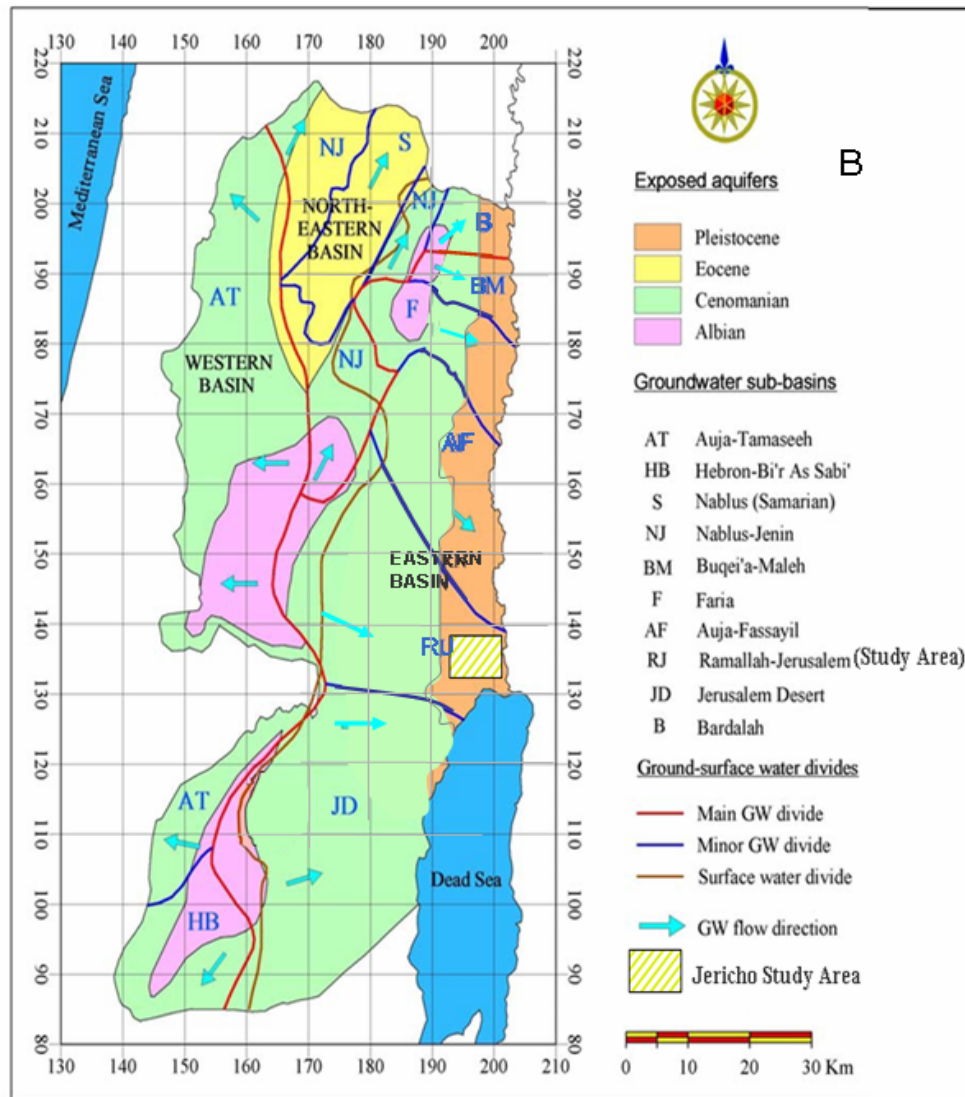


Fig. 12: Groundwater basins and exposed aquifers in the West Bank / Palestine (modified after ARIJ 1995 and Husary et al. 1996).

Table 2: Generalized Geological coulomnar section indicating the aquifere characteristics of various formation in the study area (modified after Marie, 2001)

Period	Age		Group	Formation name		Thickness (m)	Simplified Lithology	classification					
Quaternary	Pliocene-Plietocene		Dead Sea	Palestinian	Israeli	200-300	Conglomeates	Aquifer/ Aquiclude					
				Lisan	Lisan		sandstone						
				Samra	Samra		and clay						
Upper Cretaceous	Senonian-Paleocene		Mt. Scopus	Abu Dis	Taqiye	100-300	Chalk	Aquiclude					
					Ghareb								
					Mishash								
					Menuha								
	Turonian			Judea	Jerusalem	Nezer	200-300	Limestone	Aquifer				
						Shivta		Limestone					
						Derorim		Marl					
						Weradim		Dolomite					
					Betlehem	Kefar Shaul		Limestone					
					Hebron	Amendav		Dolomite					
					Cenomanian	Upper		Yatta		Moza/Ein Yorqe'am, Beit Meir	200-270	Marl	Aquicluse
						Lower				Upper Biet Kahil		Kisalon	Dolomite
					Soreq			Dolomie and Marl					
					Lower Biet Kahil	Givat Ye'arim		200-270		Dolomite			
Kefira	Marly Limestone												
Lower Cretaceous	Albian		Judea	Qatana		Marl	AquiclcludeAquitard						
				Ein Qinya		Ein Qinya		Marly Limestone					
				Tamun		Tamun		Marl					

2.5.2. Hydrogeology of Jericho Area

2.5.2.1 Regional Aquifers

The aquifer potentiality of the geological formations of the Jericho area as well as Jerusalem Ramallah sub-basin is represented in Table 2. The whole sub-basin is mainly fed by inflows of excess water from the surface runoff across the wadis and the neighboring aquifers, namely the lower Cretaceous Kurnub sandstone aquifer and the Albian to Turonian limestone and dolomite aquifer, also known as the lower and upper aquifer. The annual precipitation amount in the main recharge zones for the aquifer in Jerusalem and Ramallah mountains is about 540mm (Marie, 2001). The main local aquifer systems in the study area are (Fig. 13):

2.5.2.1.1. *The upper Cretaceous carbonate aquifer:* this aquifer is of Cenomanian to Turonian age. Composed of karstified rocks, and characteristic of the aquifer system and represent one of the most important water resources in the region. The thickness of the upper Cretaceous aquifer ranges between 170m in the western part of the study area and 200m in the upper Jerusalem area. The aquifer is divided into two sub-aquifers. A lower confined sub-aquifer includes the Kefira and the Givat Yearim Formations [Lower Beit Kahil Fm.] and an upper sub-aquifer that includes the Aminadav [Hebron Fm.], Veradim [Bet-Lehem Fm.] and Bina Formations [Jerusalem Fm.] (Table2). The outlets of this sub-aquifer are in the Jericho springs and Wadi Qilt Springs and Wadi Nuwe'meh Springs in the lower part of Wadi Makuk, close to the Jericho Fault.

2.5.2.1.2. *The Jordan Valley deposits [Dead Sea Group:]* Two Dead Sea group aquifers are located in the Jericho area these are:

a) The Holocene or sub-recent Alluvial aquifer: is distributed mainly in the Jordan Valley and neighboring areas. It is built up of sub-recent terrigenous deposits formed along the outlets of major wadis. These alluvial fans are still under accumulation after large floods and consist of debris from all neighboring lithologies and are deposited according to their transport energy. The transport normally takes place along alternating channels. Thus permeable horizons alternate with impermeable lithologies within the deposits. The total thickness is maximum near the rift margins can reach up to high values, thinning out towards the centre of

the rift basin. The alluvial aquifer often directly overlies the Pleistocene gravel aquifer and by that is hydraulically interconnected with this aquifer.

- b) Pleistocene Lisan Samra aquifer: This includes three members [Samra coarse clastic, Samra silt and Lisan] of the Pleistocene Samra aquifer are a lateral facies succession from terrestrial/fluviol, to deltaic/limnic and limnic/brackish lake environments. They reflect the Pleistocene depositional conditions of the Lisan Lake. Lisan, the marl, gypsum and silt lacustrine unit is generally considered an aquiclude, void of exploitable water. It is distributed mainly towards the middle of the graben. Samra formation consists of two members: A silt member underlying or interfingering with Lisan and a coarse clastic member further to the West that predominantly consists of gravel, interbedded with clay, sand and marl horizons. The natural recharge by rain is almost negligible. Therefore, the aquifer is mainly fed by inflows of excess water from neighboring aquifers, namely the lower Cretaceous Kurnub sandstone aquifer and the Albian to Turonian limestone and dolomite aquifer, also know as the lower and upper aquifer and from runoff in the wadis on the Eastern slopes of the West Bank. The aquifer supplies agriculture in the Jordan Valley between Jericho and Fari'a Graben.

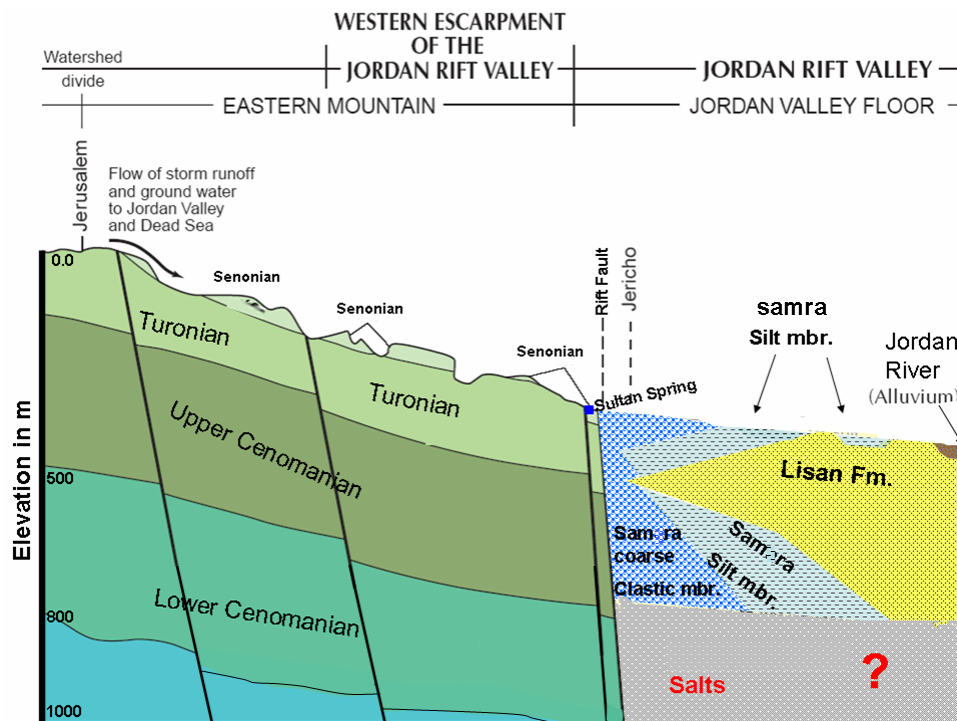


Fig. 13: Schematic hydrogeological cross section in the study area. Modified from (Exact, 2000 and Rosenthal, 1978).

2.5.2.1.3. Hydraulic separation between the two aquifers

In the west of the Jericho , faulted blocks of the impermeable Senonian chalk (Mt. Scopus group in Israeli literature) prevent lateral flow of groundwater from the Upper Cretaceous aquifer to the Plio-Pleistocene shallow aquifer system (Golani, 1972). However, the water from the Upper Cretaceous aquifer leak into the Plio-Pleistocene aquifer along the Dead Sea (Yechieli et al. 1995).

2.5.2.1.4. Perched water tables of the Cenomanian-Turonian aquifer

The water level along Ramallah anticlinal axes is about +450 m and declines eastward in the direction of the Jericho area to level about -300 and -350 in the lower and upper sub-aquifer. This large decline is a result of the long distance between the recharge area and the wells, the gradient and the permeability. These wells also react to fluctuation of replenishment. The water levels raised 2 - 2.5 years after the very rainy year 1992.

2.5.2.1.5. Perched water table of Pleistocene aquifer

The Plio-Pleistocene aquifer shows piezometric level variation between -300 to -337 (Fig. 1 4, Marie, 1997). The groundwater flow from west to east and also toward southeast. Water level show general decrease toward east. The changes in aquifer hydraulic properties from west to east, as well as the high abstraction rate are the main results for the decline in the groundwater level.

2.5.2.5. Wells

A large number of active boreholes have been drilled in the study area (Fig. 15), mostly at two locations. The first location is located along the foothills and on the mountain tops exploit water from the Regional upper Cretaceous Aquifers. The wells tap water from the calcareous aquifers and are characterized by low to moderate discharge [100-300 m³/h] and by deep static water levels (Guttman, 2006). These wells are located close to the recharge area and suffer from large water level fluctuation that sometimes [especially during drought periods] influence their discharge. The water is characterized by low salinity. The second group of wells is located in the Jordan Valley abstract water from the Jordan Valley deposits. The wells are shallower than the first group. The average depth is around 100 meter. Their discharge is also smaller than the discharge of the first group and is only some tens of cubic meters /hr (ARIJ, 1995). The Jordan Valley deposits receive water from

different sources such as lateral flows from the surrounding mountainous aquifers, infiltration of precipitation and flood water, irrigation return flows and ascending of saline water from deep aquifers. Therefore, the groundwater in the Jordan Valley deposit contains saline water. As mentioned in previous section, the water level dropped and these saline water flows towards the pumped wells raising the salinity of the water (Guttman, 2006).

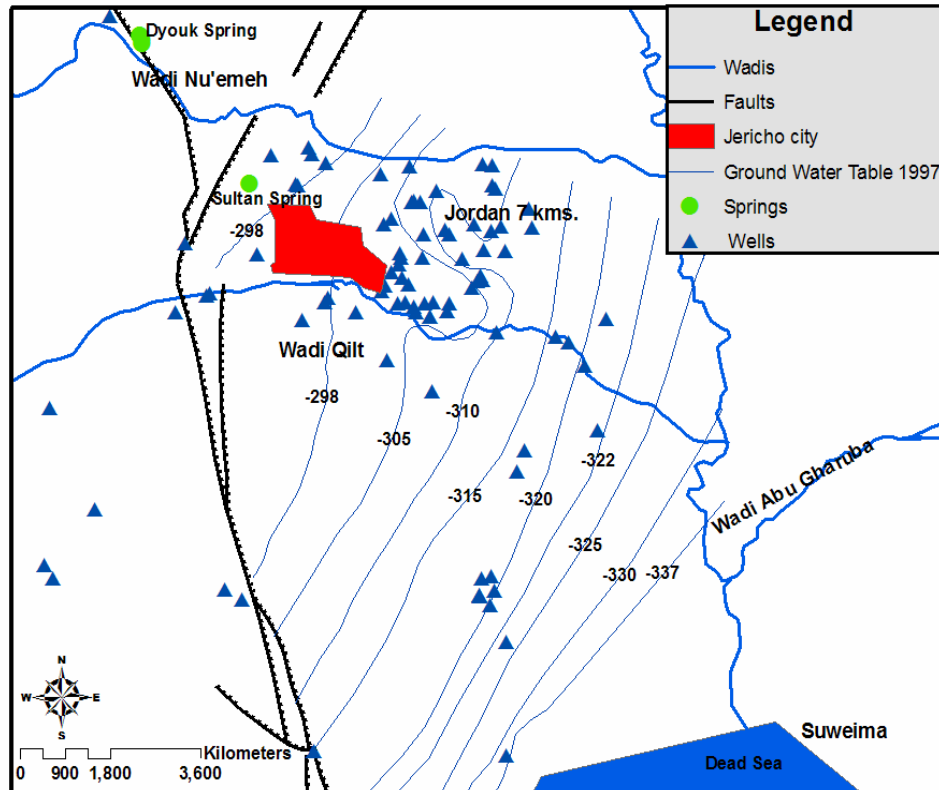


Fig. 14: Groundwater level of the Plio-Pleistocene Aquifer (Marie, 1997).

2.5.2.6 Springs

The springs in the study area (Fig. 15) are discharges from the upper Cretaceous aquifer. The springs are strongly related to the Auja Monocline, NW-SE trending rift faults and joints, where the faults and joints may represent a zone of higher permeability and consequently preferred flow of the groundwater which is tapped by an old caustic shaft in the wadi bottom, which now forms the spring outlet (WOLFER 1998). All of the springs discharge fresh water with 8 to 14meq/l total dissolved ions.

According to their geographic distribution and discharge behavior, the springs in the study area can be divided into two groups:

- 1- The Eastern Slope springs of Wadi Qilt (Ein Qilt, Ein Fawwar, Ein Fara,): this group of springs is located in Wadi Qilt and its tributaries. These wadis are deeply incised canyons and only here the Turonian aquifer is exposed and spring outflow occurs. The springs discharging in this area are characterized by an immediate response to precipitation and a highly fluctuating discharge pattern.

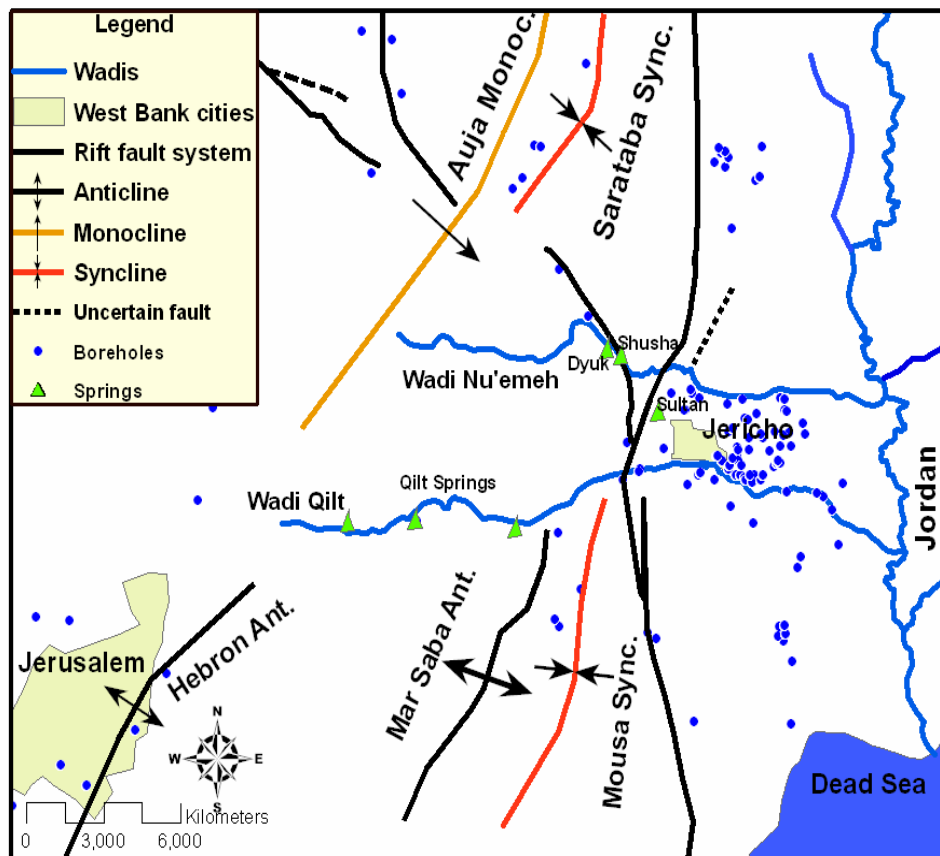


Fig. 15: Location map of springs and wells in the study area. The Cenomanian mountain aquifer wells are located to the west of the Jericho fault whereas the Pleistocene well further to the east inside Jericho plain.

- 2- Jordan Valley springs: The springs located in the Jordan Valley are related to the Samia Fault (Duyuk Spring, Nuwe'meh Spring and Shosha Spring) or to a NW-SE trending Rift faults (Ein El Sultan). Due to various step faults close to the Jordan Valley the base of the Uppermost Aquifer is exposed. These springs discharge at a constant rate. The fluctuations in the discharge pattern

depend on the precipitation rate in the recharge zone (WOLFER 1998). The main springs of this group are described as follow:

- a) Sultan Spring: Sultan is located 2km NW of Jericho and discharges at an elevation of -215m a.s.l. The spring was used for 10,000 years for domestic water supply of Jericho. The outflow of the spring is structurally controlled by a large SW-NE trending normal fault postulated by WOLFER (1998) and the spring can be classified as a fault spring. The mean annual discharge of Ein El Sultan is ca. 5,600,000m³/year (ARIJ 1995, Israeli Hydrological Survey data base).
- b) Duyuk Spring, Nuwe'meh Spring and Shosha Spring: discharges at the margin of the Eastern Slopes 3.7km NW of Ein Sultan. The system consists of three springs emerging at -110m a.s.l (Toll et al., 2006). The outflow of these is collected in a concrete channel and water is used by farmers for irrigation purposes. The average annual discharge of Duyuk spring is 5,000,000 m³/year, while the average annual discharge for Nuwe'meh spring is ca. 2,700,000 m³/year and for Shosha is about 668,000 m³/year (Israeli Hydrological Survey).

2.6. History of Hydrogeochemistry in the Study Area

2.6.1. The history saline waters formation in the Jordan Rift Valley

In the study area, during several major phases of the geological history, brines were formed which endanger all groundwater reservoirs of the Dead Sea-Jordan Rift system. During the Late Proterozoic-Early Cambrian, a major evaporative phase occurred in the Middle East (Stoecklin 1968). Later, the Triassic was characterized by large-scale marine oscillations and due to alternations of normal shelf and intertidal hypersaline to brackish environments; thick layers of Upper Triassic gypsum [and locally of halite] were laid down both west- and east of the present-day Jordan River (Zak, 1963; Bandel and Khoury, 1981). During the Mio-Pliocene, brines were mainly generated by the post-Messinian ingression of seawater which dissolved evaporites previously deposited on the dried-up Mediterranean Sea bed and in the erosive channels incised into the adjoining coastal areas (Rosenthal et al., 1999). During the

Pleistocene, fluvio-lacustrine conditions prevailed in the Jordan Valley and the fresh water Samra Lake developed. This lake became progressively saline, probably as the result of dissolution and flushing of salts from the previous hypersaline Sdom Sea (Picard, 1943) resulting in the saline Lisan Lake. From the Pleistocene onwards, the Lisan Lake became more and more saline by evaporation and by subsequent flushing of evaporites. At present, the remnant of this period is the Dead Sea. Thus, during four major periods, the rock sequences were flushed of previously formed brines and evaporites and were made ready for the following generations of liquids.

The following major scenarios of brine formation and of salinisation of groundwater's are considered (Rosenthal, 2006):

1. Seawater penetrated from the Mediterranean Sea into the Rift, and was subsequently confined (Mazor and Mero, 1969; Kafri and Arad, 1979; Gat et al., 1969). The later up flow of brines was assumed to be controlled by the movement of blocks as a result of tectonic processes. Bergelson et al. (1999) outlined a schematic hydrochemical evolution of the saline springs in the region of Lake Tiberias according to which seawater was evaporated to generate an "original brine", which was later diluted to yield the "Sea of Galilee brine". It was suggested that the "original brine" is represented by the thermo saline springs of Tiberias. The groundwater's emerging in the springs of Fuliya and Tabgha were assumed to be dilution products of the "Sea of Galilee brine".
2. The Mg-rich brines, emerging from the springs along the western shore of the Dead Sea were thought to represent residual brines derived from evaporated Pliocene seawater which was trapped in the primordial Sdom depression within the Rift (Rosenthal, 1988; Starinsky, 1974). The Ca-chloride composition of these brines was attained by subsequent dolomitization of limestone and became confined and pressurized in an unexplained manner. Ca-chloride brine is known from a thick sequence of evaporites in wildcat well Zemah 1 located close to the southern shores of the Lake (Simon and Mero, 1992). Based on $\delta^{11}\text{B}$ studies, Vengosh et al. (1994) considered these Rift brines as the main source of salts in the contemporary Dead Sea water.
3. Ablation of post-halite evaporites which were identified in the rock-sequence penetrated by borehole Zemah 1 (Flexer et al., 2000). There is geological and geophysical evidence for the existence of similar evaporite bodies at other places

along the Rift. Considering evidence as to the presence of bittern salts (Bender, 1974; Raab, 1998), ablation of such bodies creates Mg-rich brines such as encountered along the eastern and southern shore of Lake Tiberias. The Ca-rich brines encountered along the western littoral of Lake Tiberias and elsewhere in the Rift, could be the result of Mg removal by dolomitization.

4. Mixing of two different evaporation brines of seawater was proposed by Klein-Ben David et al. (2004). In their dual-mode evaporation scenario, the salinity of one end member was controlled by the rates of inflow and outflow of seawater. The second end member was generated, when evaporative loss exceeded the inflow of seawater. When the total evaporation rate from the surface of the shrinking water body equalled seawater supply, the mixing process came to a halt.

2.6.2. Hydrochemical data from Jericho area in the previous three decades.

Along the last three decades, the main significant groundwater quality problems in the area were the increase of salinity and nitrate. These two problems vary according to the aquifer type and the activities surrounding the pumping well. The springs to the west still have relatively higher quality than the groundwater from the wells in the east. Although, along the past years until these days these wells and springs were subjected to various fluctuated content of pollutants, this fluctuation depend on several factors like the annual precipitation rate for each year, the annual pumping rate, the season of the groundwater sampling and the activities surround the well.

2.6.2.1. Springs:

The springs show relatively steady fluctuated trends of chloride (Fig. 1 6). In the last three years these trends show a slight increase in salinity. The springs show also an increase in nitrate trend which show the high significant values in the last five years (Fig. 1 7). Dyouk spring locate within a populated area of Bedouins with their animals and agricultural activities, while Sultan spring is locate directly in between populated area, tourism and agricultural activities.

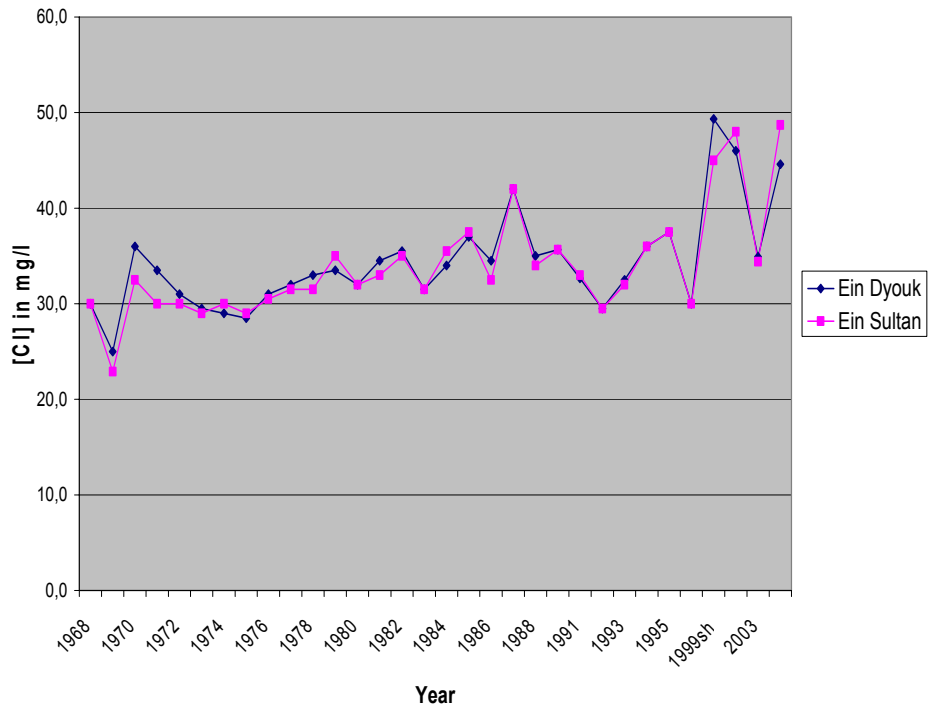


Fig. 16: Chloride concentration for the Dyouk and Sultan springs during the period 1968 to 2004 (PWA, 2004).

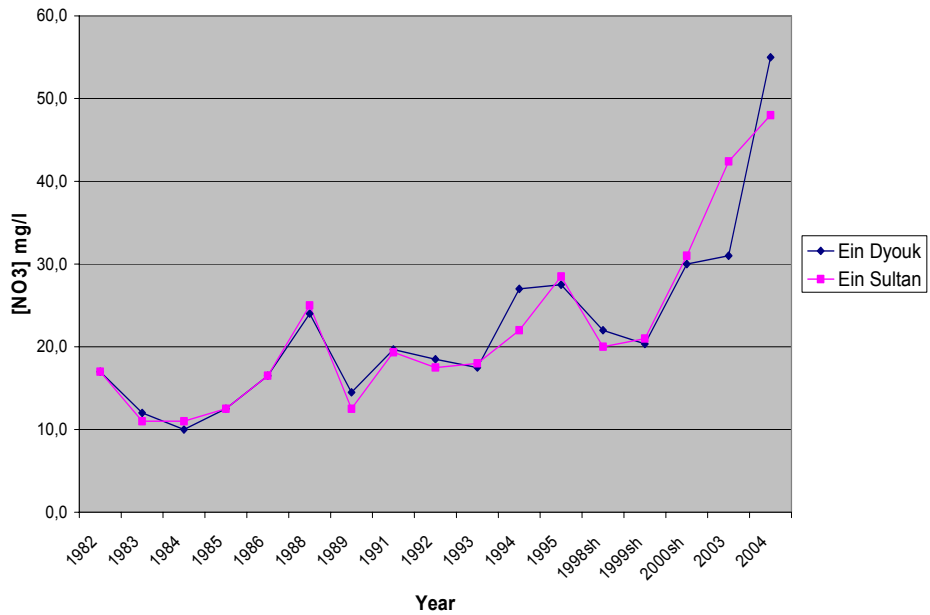


Fig. 17: Nitrate concentration for the Dyouk and Sultan springs during the period 1968 to 2004 (PWA, 2004).

2.6.2.2. Wells:

There are nearly 61 shallow borehole distributed within Jericho plan area. These wells are undergoes various salinisation processes which will be discussed later on. The salinity increased in the area significantly within the last years especially in the wells of Arab Project (Musa Alami) in the east (Fig. 1 8) where salinity reach it maximum values. The nitrate also shows such significant increase for nearly most of the wells (Fig. 19). This increase was varied according to well location and has no trend like in chloride content. The sources and mechanisms of salinisation and pollution by nitrate will be discussed later in this report.

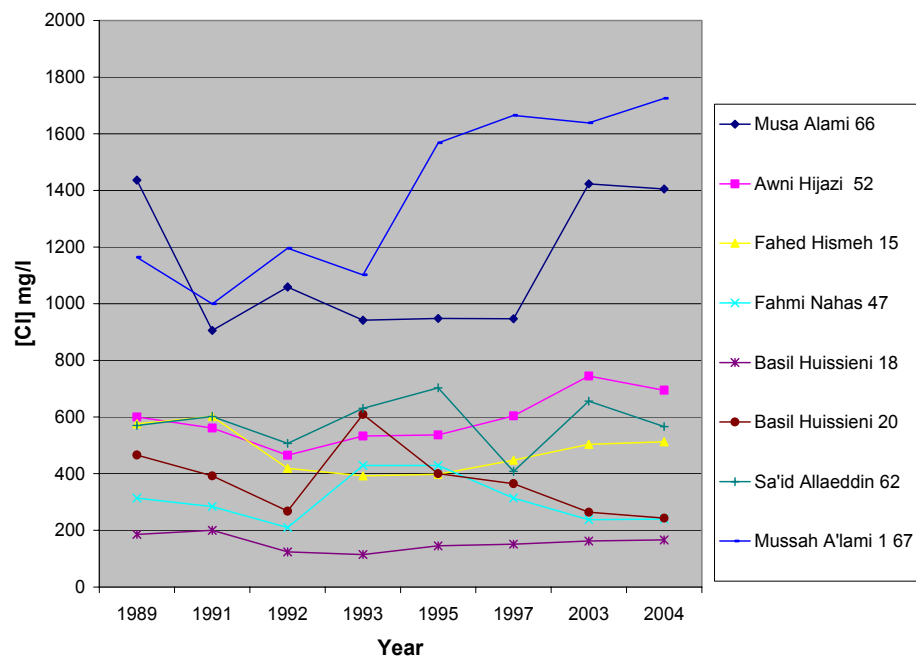


Fig. 18: Chloride concentration in the groundwater samples from some wells in Jericho area during the period 1989 to 2004 (PWA, 2004).

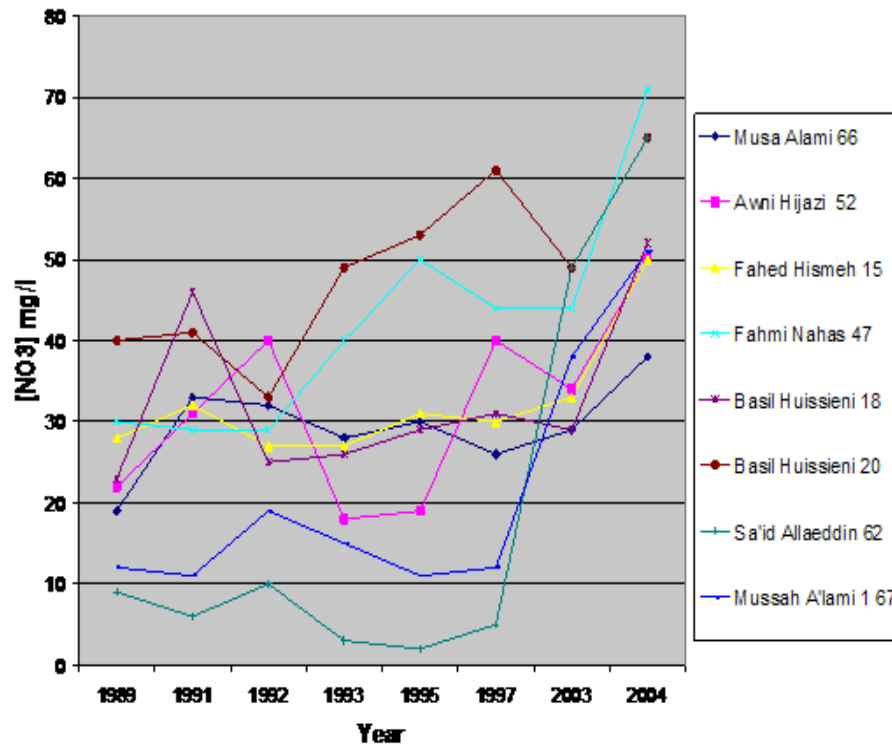


Fig. 19: Nitrate concentration in the groundwater samples from some wells in Jericho area during the period 1989 to 2004 (PWA, 2004).

2.6.3 Description for the groundwater quality deterioration problem in Jericho area

2.6.3.1. Salinity

In general, the Lisan formation is a major source of soil and water salinity in the Jordan Valley. The permeability of the Lisan formation is in general very low and considered as an aquiclude. However, because of a laminated structure of alternative marl and gravel layers, of embedded sand and silt beds up to 30 cm, and of evaporitic materials as gypsum and other salts (Fig. 20), an extended network of pathways for water has been formed resulting in higher porosity and permeability (Salameh, 2002). Moreover, the Lisan and Samra formation is horizontally interfingering along the Jericho aquifer system.

The transmission properties show that the aquifer varies from low potential (less than $10\text{m}^2/\text{day}$) to fair potential (between 10 and $50\text{m}^2/\text{day}$) (Aliewi et al., 2001). The shallow aquifer consisting of alternating marl and gravel layers and in direct contact

with the Lisan layers, receives Lisan leachate water which leads to increase in their salinity. The steep dip of the aquifers along the Jordan Valley has caused deep circulation of the recharging groundwater bringing it into contact with the salty formations at depth. Some water confined with the thin compact lime stones lenses which surrounded with the layers of tiny valved marl and shales, this water keep in contact with gypsum and halite salts for long period of time and finally resulting in high saline and relatively old water or (Evolved Connate Water). Recent drilling in the Pleistocene aquifer has shown that salinity increases with depth in which finer formation of Samra are present. Salinity data obtained from one well in Jericho shows that the chloride content increases from 380mg/l at 30m depth to over 2000mg/l at 162m depth.

The other possible sources of the salinity may originate from flushing of soluble salts from the soil zone by excess of irrigation water (Eliewi et al., 2001).

Fig. 21 shows the fresh water/saline water interaction in Jericho eastern wells. The water quality in the aquifer becomes deteriorated due to the encroachment of saline water which welled up from the previous mentioned confined fringes and lenses of the alluvial fans into the heavily pumped areas and this has led eventually to the abandonment of several wells in the Jordan Valley. Owing to the heavy pumping in the Jordan Valley a considerable decline of water table levels has been observed. The principle result is an increase of groundwater salinity (Marie, 2001). It has been observed that high chloride concentrations prevail in the heavy pumping areas (1000–2000 mg/l), whereas sulphate shows values between (200->300 mg/l).

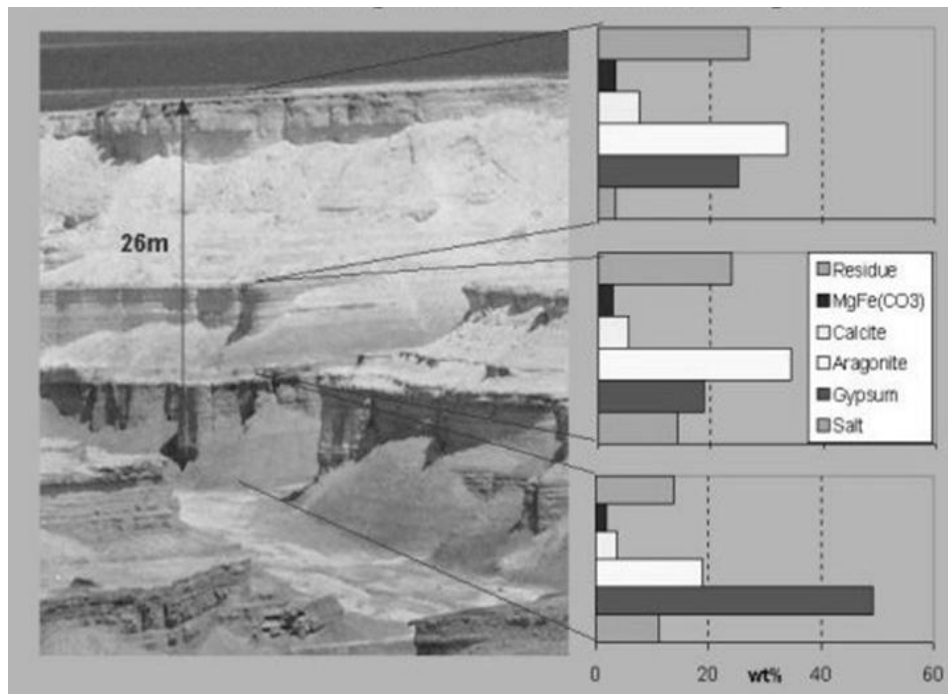


Fig. 20: Major component of Lisan formation (Landmann, 2001).

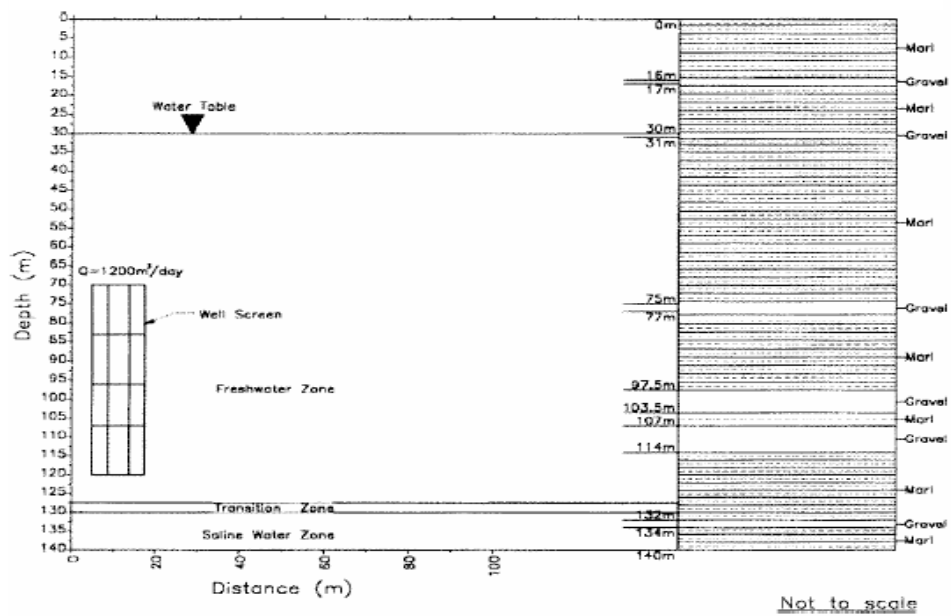


Fig. 21: Hydrogeological setting of Jericho Aquifer (Eliewi et al., 2001).

Much lower concentrations are seen in the areas near the wadis. At distance from the heavy pumping areas the salinity was measured at 500–1000 mg/l.

In this study, sulphur and oxygen isotope analyses of dissolved sulphates are used to assess the role of Lisan evaporates in the salinisation process by tracing the groundwater sulphate sources according to their isotopic composition.

2.6.3.2. Anthropogenic pollutants

The shallow Pleistocene aquifer in the area is subjected to many potential hazardous pollutants, which are mainly, of anthropogenic origins.

Often water pollution is associated with images of point source pollution like oil spills or raw sewage and toxic chemicals spewing from pipes at industrial facilities and sewage systems. Although point source discharges still produce some pollution, most of them are controlled by imposing specific permit conditions. The lack of such rules in the area make it an open yard to all kind of hazardous and anthropogenic pollutants, where open dumping sites, illegal waste water collection facilities and septic tanks are widely distributed within an area (Fig. 2).

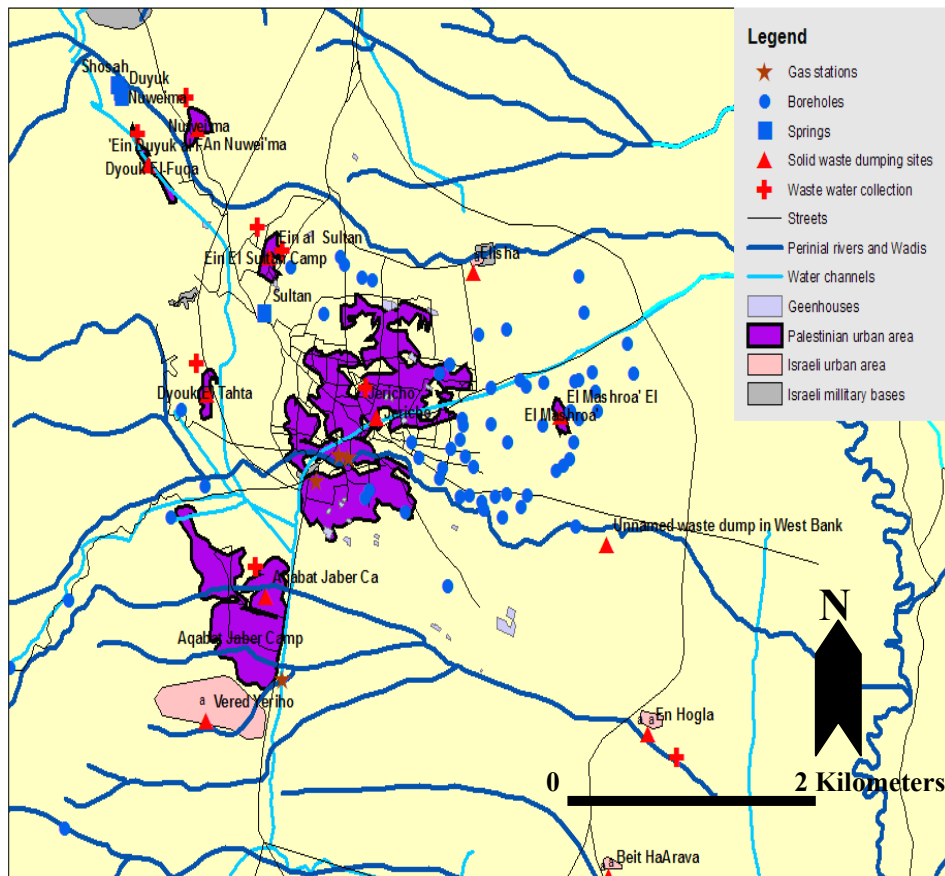


Fig. 22: The study area and possible sources of contamination from the surrounding activities.

Non-point sources deliver pollutants to water-bodies in a dispersed manner rather than from a discrete pipe or other conveyance. Non-point sources include atmospheric deposition, contaminated sediments, and many land activities that generate polluted runoff and leaching, such as agriculture (pesticides and fertilisers), logging, and onsite sewage disposal. Less frequently cited sources include atmospheric deposition, in-place contaminants, and natural sources. In Jericho area a lot of polluted activities are noticed. The used of huge and unaccountable amount of fertilizers in agriculture is widely common in the area. No restrictions or monitoring system is adopted in these chemical uses. The other main type of pollution in the study area is this of septic origin. Jericho populated area is suffering from lack of good sanitary system and most of the houses in the area still using a septic tank for sewage disposal. The raising in nitrate level in the groundwater from the study area might be an indication of such pollution to be occurring.

In this study, these potential sources and the other point and non-point sources in the area will be traced using different isotopic and Hydrochemical tracers.

CHAPTER 3: METHODOLOGY

3.1. Sampling time and site

The plan of groundwater sampling and selection of the samples sites was based on providing a supplement analyses for tracers which had not been previously used in the study area to characterize chemical and isotopic signature of both fresh and saline groundwater and its variation with location.

Two times sampling of 21 water samples from springs and wells were collected, the first time at the end of October/2003 (dry season) and the second time at the end of March/2004 (wet season). Two water samples are belonging to the Sultan and Dyouk springs in the western and north western side of the study area, in addition to one closed well. Two wells are located to the north of the study area within alluvial Samra formation of Wadi Nuwe'meh, 10 wells are distributed along Wadi Qilt (5 west of the wadi and 5 east of the wadi), while the rest of the wells locate more to the east of the area. Sampling localities are shown in Fig. 23.

3.2. Determination of Chemical Parameters

Onsite measurements for physicochemical parameters (pH, temperature, m-value and redox potential) were done. All the samples were tested for the Cations and Anions as well as for some trace elements. The samples were filtered with 0, 45+0, 2 μm Cellulose-Acetate-Filters and filled in 2x 60 ml HDPE bottles (cations and anions). In order to stabilizing the anion and cations were acidified using HgCl_2 for prolonged preservation of nitrate. The Mercury Chloride is highly dissolve in water, the chemical formula for the reaction of Mercury Chloride in water is given as:



The Hydrochloric acid, keep the water sample in acidic media, thus prevent any bacterial growth. Moreover, the resulted inorganic mercury has been reported to have effects at concentrations of the metal in the bacterial culture medium of 5 $\mu\text{g/liter}$. Therefore, Mercuric chloride is used as a topical antiseptic or disinfectant agent. Mercury is bound to the cell walls or cell membranes of microorganisms, apparently to a limited number of binding sites. This means that effects are related to cell density as well as to the concentration of mercury in the substrate.

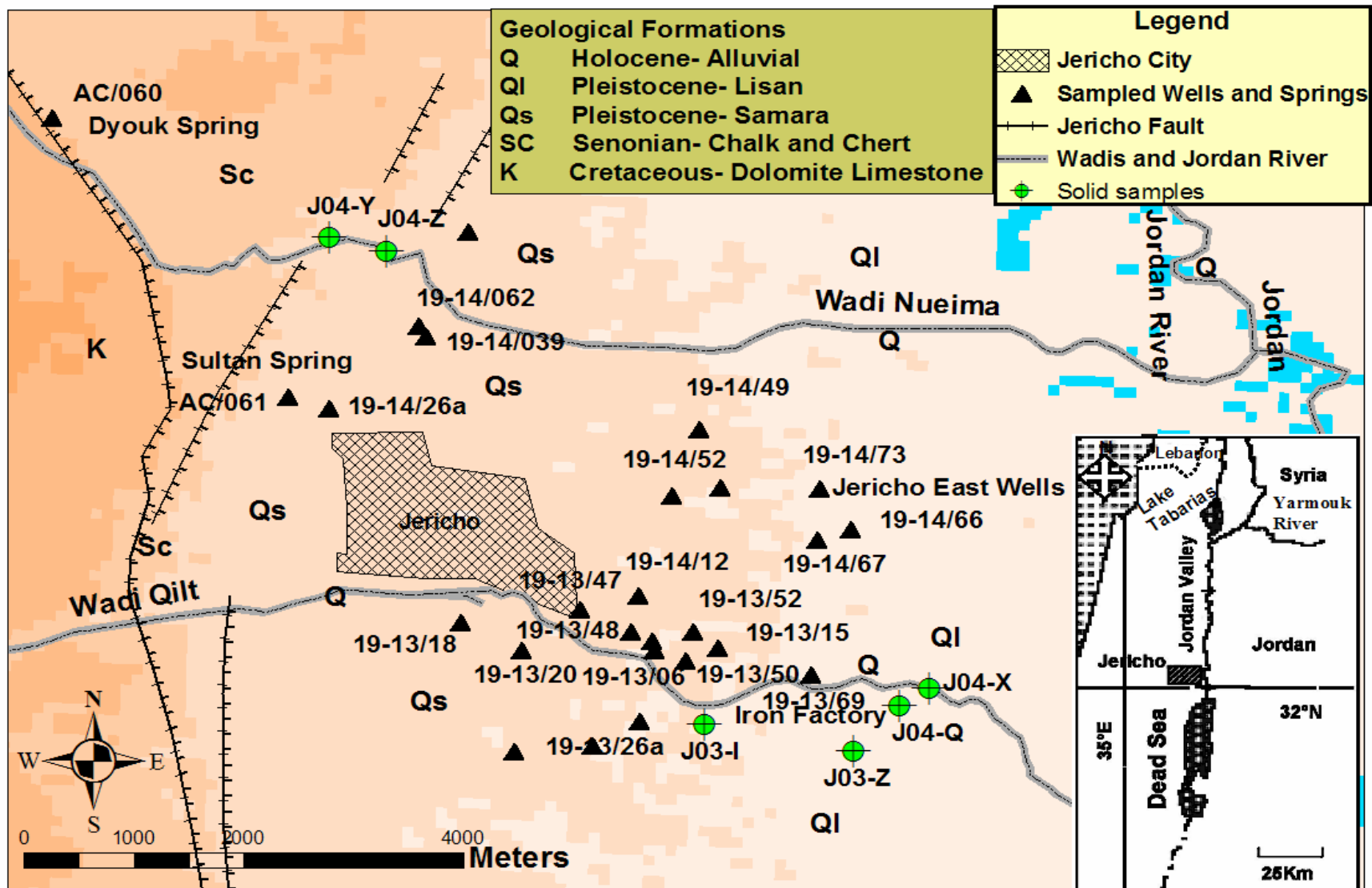


Fig. 23: Map of the study area in Jericho and its vicinity, shown are the sampled wells and springs within different geological formations.

Table 3: Illustration for the analytical methods, and detection limits.

Messgröße	Methode/Technik	RSA* [%]	Detection limits [mg/l]
Ca ²⁺	ICP-AES ⁺	≤1	0,03
Mg ²⁺	ICP-AES	≤1	0,04
K ⁺	ICP-AES	≤1	0,3
Na ⁺	ICP-AES	≤1	0,4
Mn	ICP-MS [#]	≤5	0,05
(II,IV,VI,VII)			
Fe (II,III)	ICP-AES	≤5	0,05
B ³⁺	ICP-AES	≤1	0,04
NH ₄ ⁺	Photometrie	≤2	0,01
Ba ²⁺	ICP-AES	≤1	0,01
Sr ²⁺	ICP-AES	≤1	0,01
Si ⁴⁺	ICP-AES	≤1	0,09
Cl ⁻	IC [§]	≤1	0,07
SO ₄ ²⁻	IC	≤1	0,12
HCO ₃ ⁻	Titration		
Br ⁻	IC	≤1	0,18
NO ₃ ⁻	IC	≤1	0,12
NO ₂ ⁻	IC	≤1	0,05
PO ₄ ²⁻ (P ₂ O ₅)	Photometrie	≤1	0,05
Rb ⁺	ICP-MS	≤4	6

⁺ICP-AES: Inuctive-Coupled-Atom Emission spectroscopy

[#]ICP-MS: Inuctive-Coupled-Mass spectroscopy

[§]IC: Ions chromatography

*RSA: relative Standardabweichung (Die RSA ist abhängig von der spezifischen Elementkonzentration in der Wasserprobe. Mit zunehmender Annäherung an die Elementspezifische Nachweisgrenze (RSA>33%) wird die RSA geräteunabhängig mit <10% angegeben.)

ICP-AES: Insofern die Konzentration der Einzelemente oberhalb des mittleren Konzentrationsbereiches der ICP-AES liegt, wird die Probe soweit verdünnt, dass die Konzentration sich innerhalb dieses Bereiches befindet. Die RSA beträgt 0,5-1%.

ICP-MS:

IC: Bei IC-Messungen beträgt die RSA ≤2%.

[Quelle: persönliche Kommunikation mit Dr. Wennrich (2005): Departmentleiter Analytik UFZ Leipzig-Halle GmbH]

These effects are often irreversible, and mercury at low concentrations represents a major hazard to microorganisms (Komura et al., 1971).

Because samples were collected in the agricultural seasons all the sampled wells were in operation for a long period, thus no further water purging was necessary before sampling, and the samples were collected immediately. The collected samples then were kept and cooled until measurement. The concentration of cations were measured using Inductive Coupled Plasma – Atom adsorption spectrometry (ICP-AES) and for Anions using Ions chromatography (IC) at the UFZ Department for Analysis in Leipzig (Table 1).

3.3. Stable Isotopes

Isotopes of an element have the same number of protons but a different number of neutrons. Elements have predominant isotopes and less abundant isotopes. The standard notation for identifying different isotopes is to write the sum number of protons and neutrons in the upper left corner of the symbol of the element. The term stable isotopes simply refer to isotopes that are no radioactive forms of an element.

The ratio of the heavier isotopes to that of the lighter isotopes in a substance can provide useful information because the slight differences in the mass of the isotopes cause slight differences in their behaviors.

Stable isotopes are measured as the ratio compared with the most abundant isotope of a given element. Isotope ratios are quantified as δ values in which

$$\delta = [(R_{\text{SAMPLE}} - R_{\text{STANDARD}}) / R_{\text{STANDARD}}] 1000\text{‰} \quad (2)$$

R is defined as D/H for δ D values and $^{18}\text{O}/^{16}\text{O}$ for δ ^{18}O values. These δ values are relative in nature and represent the positive or negative deviation from the reference standard material for each element, each of the elements has its own reference standard, which in this study was as follow (Clark and Fritz, 1997):

- Stable isotopes of ($^{18}\text{O}/^{16}\text{O}$) Vienna Standard Mean Ocean Water (VSMOW).
- Stable isotopes ($^{13}\text{C}/^{12}\text{C}$) Pee Dee Belemnite (VPDB).
- Stable isotopes of nitrogen ($^{15}\text{N}/^{14}\text{N}$) atmospheric nitrogen.
- Stable isotopes of sulphur ($^{34}\text{S}/^{32}\text{S}$) Canyon Diablo Troilite standard (VCDT).

Values are expressed as δ -value as part per thousand or per mil (‰) difference from the standard reference.

For example, if δ X value of +10 per mil means that it has 10 parts per thousand (one percent) more δ X than the standard reference. Positive δ values are said to be “enriched” or “heavy”, while a negative δ values are said to be “depleted” or “light”.

Several steps in the element cycle and transfer actions of the element in nature can modify the stable isotope composition in different chemical compounds. These changes, called fractionation, occur as a result of physical and chemical reactions.

Isotopic effects (caused by slight differences in the mass of two isotopes) in any chemical reaction tend to keep the same isotopic signature of the starting material. These isotopes effect mean that, depending on its origin, the same compound may have different isotopic compositions depending on the starting material of the reaction. Therefore, stable isotopes provide a useful tool in identifying the sources of groundwater contamination. The isotopic composition of the potential contaminant sources must be distinguishable. Thus the major potential sources of groundwater contamination in the hydrosphere can be assigned using isotopic ratios as a tracing tool.

3.3.1. Nitrogen Isotopes

The nitrogen stable isotope ratio analysis was conducted on water samples to identify the possible sources of nitrate in the groundwater. The nitrogen test provides a measurement of the ratio of the two most abundant isotopes of nitrogen ^{14}N and ^{15}N .

The nitrogen isotopes ^{15}N and ^{14}N constitute an isotope pair. The lighter isotope ^{14}N is significantly more abundant in the environment than ^{15}N . In the atmosphere there is one atom of ^{15}N per 273 atoms of ^{14}N (Drever, 1997). The ratio of the heavier isotope to that of the lighter isotope in a substance provide useful information because the slight difference in the mass of the isotopes are caused by special processes. Denitrification of nitrogen compounds, for example, causes the nitrate of the starting material to become isotopically heavier. Volatilization of ammonia results in the loss of lighter isotope to the atmosphere, and ammonia that remains behind become isotopically heavier (Mook, 2001).

In the study area many sources can cause a rising in the nitrate values in the groundwater, these sources including the sewage and manure, fertilizers and pesticides, where many related anthropogenic activities were recorded . The nitrogen as well as the oxygen isotopes in the nitrate compound is a useful tool to differentiate between each possible source.

For this purpose, bottles of 1.5 l of water were taken for isotope analyses; samples with high nitrate were collected using ion exchange resins (Fig. 24).



Fig. 24: Collection of nitrate in the field using ion exchange resins column (right side of the picture over the carton box)

This alternate method concentrates the NO_3^- or NH_4^+ on anion or cation exchange resins. Collection of nitrate on anion exchange resins eliminates the need to send large quantities of chilled water back to the laboratory, eliminates the need for hazardous preservatives, makes it easier to archive samples, and allows analysis of extremely low concentrations. Anion resin has the capacity of 1.2 meq/L so 5 mL can hold 6 meq or 6,000 M of NO_3 . The cation resin, 50WX has the capacity of 1.7 meq/mL, so 5 mL will retain 8.5 meq. The anion column will also fill up with other anions besides NO_3 . The relative selectivity for SO_4 and Cl and NO_3 is 15, 2.3, and 8 (higher number means greater selectivity). But when trying to determine which anions will fill the column first, so the concentration also has been taken into account. There is no specific formula that allowed predicting the exact behavior of the column with low-nitrate waters. The resin is washed using silver oxide until there is < 0.5 ppm of nitrate in rinse water. Silver nitrate was rinsed with distilled water to remove nitrate. About 500 grams of resulted silver oxide was put in a 4 L flask. Stir and shacked the silver in distilled water. The residual silver was removed by pouring the rinse water through

large paper filters and captures the water in a flask. NaCl was added to the rinse water to precipitate the silver as silver chloride. This water was filtered through 0.45 micron filters and then discarded. It takes about 30 rinses for the silver to be "nitrate free". Initially, the nitrate concentration of the rinsed water was high. Gradually, after many rinses, the nitrate concentrations become equilibrate around 2 ppm.

Sample-size requirements are in the range of 10-100 μM of N; however sample size requirements also vary between laboratories. In addition to measuring the d^{15}N value of nitrate, a few labs are able to measure the d^{18}O value as well. Samples were measured using isotope ratio mass spectrometry (IRMS). IRMS separates the ions of the element ($^{14}\text{N}/^{15}\text{N}$) on the basis of their differing mass/charge ratio. Sample preparation consists of converting solid or liquid material to a gas (N_2) and isolating the particular gas that must be analyzed.

3.3.2. Sulphur isotopes

Sulphur isotopes are used in hydrology to trace natural and anthropogenic sources of sulphur in particular, to study the cycling of sulphur in agricultural watersheds, the sources of salinity in coastal aquifers or sedimentary strata, groundwater contamination by landfill leachate plumes, and acid mine drainage. It provides a measurement for the ratio of the two most abundant Sulphur isotopes ^{34}S and ^{32}S where the last one is lighter and more abundant in the environment (Kendall et al., 1992).

To assess the importance of the possible influence of the lithological formation from Lisan and Samra on the isotope composition of dissolved sulphate in the studied aquifer, the sulphur isotope composition of two solid samples from Samra in Wadi Nuwe'meh north (J04-Y and J04-Z), and 4 solid samples from Lisan in Wadi Qilt east and south (J04-X, J04-I, J03-Z, and J04-Q) were also analyzed. For that, samples were eluted with distilled water (100g/500ml) at room temperature, and then filtered with a Millipore's filter of 0.45 μm pore size. Major anions of elutes and water samples were analyzed by HP liquid chromatography. Concentrations of the major cations of these solutions were determined by ICP-OES, and the trace elements were analyzed by ICP-MS. For sulphur isotope analysis the dissolved sulphate was precipitated as BaSO_4 by the addition of barium chloride, the sulphate precipitate was then filtered, washed and

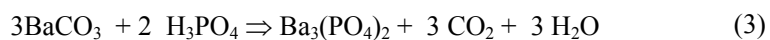
dried. The sulphur isotopic composition was determined with a mass spectrometer (Finningan Mat delta C) coupled with an elemental analyzer (Carlo Erba 1108). δ -Notation is expressed in terms of $\delta^{34}\text{S}$ per mil (‰) relative to the Vienna Canyon Diablo Troilite (VCDT) standard. The isotope ratios were calculated using NBS-127, IAEA-S1, IAEA-S2, IAEA-S3 and internal laboratory standards for calibration. Reproducibility of the samples calculated from standards systematically interspersed in the analytical batches is 70.2%; the error of a double measurement is 0.4%.

3.3.3. Carbon isotopes

$\delta^{13}\text{C}$ values are used to understand the biogeochemical reactions controlling alkalinity in watersheds.

The primary reactions that produce DIC (Dissolved Inorganic Carbon) are commonly related to the dissolution of biogenic soil CO_2 by infiltrating rain water forming carbon acid, where the carbonic acid causes a weathering of carbonate minerals and silicate minerals in the soil and rocks. The reactions produce DIC identical in $\delta^{13}\text{C}$ to the composition of the reacting carbonate, carbonic acid or an intermediate signature between them. Consequently, without further information, DIC produced solely by the reaction of weathering of carbonate minerals is identical to DIC produced in equal amounts from the soil weathering reactions (Kendall et al., 1992). Because $\delta^{13}\text{C}$ analysis provides information on the origins of dissolved inorganic carbon in the groundwater it can also be used to aid in discriminating the sources of recharge to a groundwater System, depending in the aquifer composition, particularly the carbonate sediment of a specific aquifer. Carbon isotopes are also useful tracers of seasonal and discharge related contributions of different hydrological flow paths to stream flow (shallow vs. deep flow-paths).

The carbonate from water samples was transferred to BaCO_3 in an alkalic $\text{pH} > 12$, as in the same sample which was used for sulphur isotopes. In the lab the amount in carbonate materials are measured by reacting 100% water-free phosphoric acid (H_3PO_4) at 25°C with BaCO_3 , to convert it to free CO_2 . according the reaction:



As long as all the CO₂ is recovered, there is no fractionation of ¹³C. The ¹³C/¹²C –ratio of the gas is the same as in the sample. The CO₂ gas then runs through the IRMS and measured.

3. 3.4. Tritium Deuterium and Oxygen isotopes

Oxygen has three stable isotopes, ¹⁶O, ¹⁷O, and ¹⁸O; hydrogen has two stable isotopes, ¹H and ²H (deuterium), and one radioactive isotope, ³H (tritium). Oxygen and hydrogen are found in many forms in the earth's hydrosphere, biosphere, and geosphere. Oxygen is the most abundant element in the earth's crust. Hydrogen also is common in the biosphere and is a constituent of many minerals found in the geosphere. Oxygen and hydrogen combine to form water, thus making their isotopic composition a powerful tracer for the hydrosphere.

There are nine isotopic configurations for water molecule, which are distinguished by their mass numbers as well as their characteristics. However, because of the low abundance of the heavier isotopes, almost all water molecules are of three isotopic combinations.

Characteristics of three types of water molecules (Hoefs, 1997):

	¹ H ₂ ¹⁶ O	² H ₂ ¹⁸ O	¹ H ₂ ¹⁸ O
density @ 20°C	0.997	1.1051	1.1106
boiling point	100.00	101.42	100.14
vapour pressure @100°C	760	721.60	?
temperatory density max	3.98	11.24	4.30

Stable isotopes in water (¹⁸O and ²H) are affected mainly by meteorological processes that provide a characteristic fingerprint of their origin (Clark and Fritz, 1997). The isotopes O and H are partitioned among different freshwater reservoirs by various hydrologic processes such as evaporation from the oceans, rainout, re-evaporation from terrestrial basins, snow and ice accumulation, and runoff. As water evaporates, the lighter isotopes, ¹⁶O and ¹H are preferentially removed and the remaining reservoir becomes enriched in the heavier isotopes, ¹⁸O and ²H. Condensation of water vapor causes the reverse effect. The heavier molecules condense more efficiently leaving the residual vapor in the cloud depleted in ¹⁸O and

²H. Because of their dose relationship and the abundance and importance of water on the planet, O and H and their isotopic fractionation characteristics are usually considered together. As a result of fractionation, waters develop unique isotopic compositions that can be indicative of their source or the processes that formed them. Isotopic composition differs for sea water, polar ice, atmospheric water vapor, and meteoric water.

Models of oxygen/hydrogen isotopic fractionation have been developed and refined over the last 50 years. Models of isotopic variability take into account vapor pressure, humidity, temperature, altitude, rainout and moisture content, evaporation and solute concentration, and combinations of them. Craig (1961) showed that ¹⁸O and ²H behave predictably and that ¹⁸O and ²H in fresh waters correlate on a global scale. He developed a “global meteoric water line” that defines the worldwide fresh surface water relationship between ¹⁸O and ²H by the equation:

$$\delta^2\text{H}=8 \delta^{18}\text{O}+10\text{‰ SMOW} \quad (4)$$

Craig’s (1961) observation only has application globally because it represents an average of many local and regional meteoric water lines, which are individually affected by varying climate and geographic factors. A local meteoric water line, based on analyses of surface water samples from the recharge area of Jerusalem and Ramallah mountains (Abu Dees meteorological station) which done by the UFZ isotopic hydrogeology department in cooperation with Al-Quds University, is represented by the equation:

$$\delta^2\text{H}=8 \delta^{18}\text{O}+19.5\text{‰ SMOW} \quad (5)$$

Tritium, ³H, the radioactive isotope of Hydrogen, is a short-lived isotope of hydrogen with a half-life of 12.32 years. Tritium concentrations are represented in tritium units (TU). One tritium unit is equal to one molecule of ³H per 10¹⁸ molecules of ¹H and has an activity of 0.118 Bq/kg (3.19pCi/kg). The large pulse of tritium, that entered the hydrologic cycle from the middle of 1950 to early 1960’s during atomic bomb test in the atmosphere, could be used to establish the age of groundwater recharge. High levels of tritium (>~30 TU) indicate water that was recharged during the late 1950s or early 1960’s; moderate concentrations indicate modern recharge; levels close to detection (~1 TU) are likely submodern or paleo-groundwaters that have mixed with shallow modern groundwater’s (Clark and Fritz, 1997). Rough general guidelines are:

<0.8 TU	submodern (prior to 1950's)
0.8 - 4 TU	m of submodern and modern
5 - 15 TU	modern (<5 to 10 years)
15 - 30 TU	some bomb tritium
>30 TU	recharge in the 1960's to 1970's
>50 TU	recharge in the 1960's (Bomb Tritium)

Samples were collected in 60 ml polyethylene bottles. Gas Source Isotope Ratio Mass Spectrometry (IRMS) was used to determine the hydrogen and oxygen isotope ratios of collected groundwater samples. Oxygen isotope ratios were measured by the Carbon Dioxide Equilibration Syringe method proposed by Matsui (1980), in which carbon dioxide is equilibrated with CO₂ (Epstein & Mayeda, 1953) (to GI-M2: H₂¹⁸O + C¹⁶O₂ ↔ H₂¹⁶O + C¹⁸O₂) and then isolated from water vapor and other trace gases prior to injection into the mass spectrometer. Gehre et al. (1996) method was used to prepare samples for deuterium analysis in the mass spectrometer. This method involves reducing sample water into elemental hydrogen through use of a Heated Chromium Furnace packed with oxidizable material at 850°C. The resulted H₂ was measured in Isotope Ratio Mass Spectrometer (IRMS) of delta S type (Fa. Finnigan MAT, USA). Data quality was checked through an internal laboratory calibration of standards (Coplen et al., 1991).

Samples for tritium were collected in 500ml bottles. Distillation of samples under N₂-atmosphere, then NaO₂ in electrolysis cells was added as batch process electrolytically decomposes: Enrichment (T for instance 15-18-fach) heavy H₂-Isotope in the arrears (D, T) (Taylor, 1983; Rozanski & Groening, 2004). PbCl₂ was added on the produced NaOH. A distillation process was adopted until drying, water after addition of Ultima gold radiometric detection over 1000 min in liquid scintillation spectrometer Quantulus 1220 Canberra luggage pool of broadcasting corporations 2770 TR/SL (EG&G Wallac, Finland). By this method, Tritium emits beta decay electrons, which excites the solvent. The solvent transfers its energy to the solute, which emits light photon pulses which are detected and counted.

CHAPTER 4: RESULTS AND DISCUSSION

4.1 General Hydrochemistry and Tritium

The hydro-chemical data for both wet and dry seasons are shown in tables 4 and 5. The major cations and anions concentrations of the groundwater from springs and wells in the region are plotted on a Durov diagram in Figure 25.

There are no significant differences in ions concentrations between wet and dry seasons. However, the groundwater samples in the period of wet season shows slight increase in TDS, which might refer to the wash out effect of the older water stored in the aquifer during the dry season.

In both seasons all the major anions and cations show an increasing trend with water path from west to east (Fig. 26). Mg, K, Na, and Br show a good linear correlation with the TDS and all follow the west-east pattern, while Ca, Sr, B, SO₄, HCO₃ show a relatively low correlation, and nitrate shows very poor correlation (Fig. 26g) which indicates a source different from all the other elements.

In general the data reflect distinctive end-members of fresh water to west and saline water further to the east.

Table 4: Hydrochemical data in mg/l of the wells and springs from Jericho-Palestine in wet season (March, 2004).

Well Name	Well Code	pH	Eh korr [mV]	T [°C]	Cond [mS/cm]	Li	Na	K	Mg	Ca	Fe	NH4	B	Ba	Sr	Ru	Cl	Br	SO4	NO3	HCO3	PO4	Si	TDS
Arab Project66	19-14-66	7.37	580.21256	26.4	5.36	0.1648	559	78.3	198	168.1	0.0333	0	1.023	0.1028	3.173	0.06	1405	11.5	285	38	409.31	0.01	8.51	3165.95
Arab Project67	19-14/067	7.14	472.49219	26.1	6.23	0.1897	668	102.9	219.7	163.2	0.0447	0	1.313	0.1513	2.753	0.07	1725	13.9	221	51	405.04	0	7.94	3582.51
Arab Project73	19-14/073	7	470.49219	26.1	4.11	0.1337	357.6	75.1	158.9	123.9	0.0738	0.001	0.945	0.2113	1.729	0.05	1014	7.1	111	48	386.13	0.01	7.56	2292.55
Fahmi Nahas48	19-13/048	7.15	446.72923	23.7	1.538	0.037	112.7	14.68	66.4	89.8	0.0103	0	0.2666	0.0683	1.896	0.01	240	1.6	82.7	61	317.81	0.05	6.89	996.007
Fahmi Nahas47	19-13/047	7.1	450.3817	23	1.483	0.0343	109.5	12.07	63.3	89.7	0	0.018	0.2633	0.0624	2.054	0.01	228	1.2	82.2	71.5	322.69	0.05	7.45	990.155
Sabiru Rantizi	19-13/006	7.01	459.10207	23.3	2.38	0.0334	160.7	7.75	91.1	163	0	0.02	0.32	0.1242	3.415	0.01	452	2	153	100	342.21	0.01	8.8	1484.55
Fahed Hishmi	19-13/015	7.11	433.98355	24.5	2.46	0.0747	212.9	37.34	101	103.9	0.1163	0.02	0.4659	0.0978	1.775	0.03	513	4.5	62.1	50	337.33	0.3	6.77	1431.73
Zuhdi Hashwa	19-13/052	7.1	376.4496	24	2.78	0.0629	216	27.95	115.4	128	0.1531	0	0.527	0.0885	3.358	0.02	556	3.4	194	79	349.53	0.05	7.14	1680.79
Salah Arouri	19-14/012	7.16	485.89034	24.6	1.325	0.0299	89.3	10.86	60.2	87.7	0.0188	0	0.2168	0.0592	1.814	0.01	195	1.1	64.5	70	342.21	0.3	7.32	931.3
Basil Husaini20	19-13/020	7.3	509.4496	24	1.6	0.0363	138.6	14.82	63	82.8	<0.01	0	0.3908	0.0732	1.366	0.01	243	1.6	120	65	317.2	0.06	6.2	1055
Basil Husaini18	19-13/018	7.5	498.5175	25	1.189	0.0249	83.1	9.2	49.72	86.4	<0.01	0	0.2262	0.0414	1.226	0.01	166	0.5	71.4	52	292.8	0.1	6.75	820.514
Ibrahim Daek	NW	7.07	437.35639	24.1	3.3	0.0881	311	39.32	127.3	126.7	0.0303	0.169	0.746	0.1514	2.241	0.03	764	5.9	189	47	369.05	0.05	6.86	1990.26
Ein Sultan	AC/61	7.39	541.15269	21.1	0.678	0	25.79	2.678	27.88	83.9	0.0328	0	0.0486	0.0334	0.1176	0	48.7	0.5	24.1	48	266.57	0.165	4.43	533.46
Ein Dyouk	AC/60	7.33	485.2459	21	0.678	0	26.29	2.688	28.25	85.9	0.0241	0.054	0.0467	0.0314	0.117	0	44.6	0.5	23.8	55	293.41	0.215	4.473	565.88
Awni Hijazi	19-14/052	7.01	489.42429	25.1	3.04	0.0791	285.7	34.12	117.3	115.6	0.3821	0.054	0.4702	0.1657	2.654	0.03	695	6.5	76.5	50	417.85	0.08	8.16	1810.79
Saeed Aladeen	19-14/062	6.96	391.05145	25.5	2.57	0.0492	208.1	21.16	94.8	125.8	<0.01	0.01	0.2717	0.0739	1.032	0.02	566	5.6	43.5	20	393.45	0.2	6.36	1486.9
Mohammed Masri	19-14/38	6.95	375.95824	25.6	2.42	0.0538	201.8	19.04	97.5	140.1	0.0591	0	0.3059	0.1054	1.116	0.02	527	6.2	44	10.5	403.21	0.06	6.87	1458.01
Samed	19-14/26a	7.12	405.4496	24	1.222	0.0102	58.3	5.56	58.5	116.9	0.0117	0	0.1042	0.0641	0.4578	0.01	130	0.9	20.9	41	412.97	0.03	6.48	852.339
Arab Project69	19-13/069	6.99	395.39898	26.2	4.12	0.1292	508	75	148.9	112.1	0.0148	0	0.786	0.1561	1.809	0.05	1054	11	109	43	415.41	0.012	7.39	2486.86
Awn Hijazi	19-14/37	6.91	499.77182	25.8	3.67	0.0934	355.2	47.14	157.4	157.2	0.0185	0	0.595	0.1432	1.867	0.04	916	8.4	117	49.5	383.69	0.01	8.22	2202.54
Saleem Nimmari	19-13/49	7.29	507.4496	24	1.89	0.0776	183.8	50.1	76.2	71.9	<0.01	0	0.519	0.126	1.126	0.03	335	1.8	66.2	75	385.52	0.12	7.49	1255.27
Qasir Hisham	19-13/003	7.05	393.5854	26	3.43	0.0636	306.3	27.63	123.7	163.6	0.0219	0	0.3349	0.0355	1.42	0.02	890	11.9	52.6	23.5	349.53	0	9.31	1960.08
Bail Hussaini22	19-13/22	6.97	349.42429	25.1	3.15	0.0885	266.4	42.26	135.6	133.7	0.0223	0.01	0.648	0.1219	2.178	0.03	693	4.2	222	50	344.65	0.1	7.64	1902.64
Mahmud Akramawi	19-13/50a	6.7	284.54281	23.9	2.18	0.0617	149.7	33.47	92.8	119.5	0.4029	0.17	0.3775	0.1162	1.946	0.03	385	2	109	54	406.26	0.14	8.28	1363.17
Bail Hussaini21	19-13/21	7.14	418.30577	26.3	2.83	0.0789	263.7	36.26	118.2	117.4	<0.01	0.03	0.586	0.1265	1.764	0.03	722	5.7	172	95	349.53	0.023	7.11	1889.69

Table 5: Hydrochemical data in mg/l of the wells and springs from Jericho-Palestine in dry season (October, 2003).

Site	Well Code	pH	Eh korr [mV]	T [°C]	Cond [mS/cm]	Li	Na	K	Mg	Ca	Fe	NH4	B	Ba	Sr	Ru	Cl	Br	SO4	NO3	HCO3	PO4	Si	TDS
Arab Project66	19-14/066	7.04	357.02614	26.6	5.39	0.1744	577	82.6	213.7	186.1	0.084	0.01	1.078	0.099	3.56	ND	1423	15.7	300.9	29.69	439.2	0.035	8.8	3282.01
Arab Project67	19-14/067	6.99	319.21256	26.4	5.84	0.1909	639	104.1	220.8	167.3	0.868	0	1.32	0.1534	2.843	ND	1638	14	183.4	38.86	366.61	0.043	8.36	3385.98
Arab Project73	19-14/073	6.99	328.21256	26.4	3.89	0.1397	359.3	79.6	164.6	128.3	<0.05	0	0.973	0.2205	1.833	ND	1000	7.6	95.9	40.41	405.65	0.016	7.97	2292.6
Fahmi Nahas48	19-13/048	7.18	424.3817	23	1.471	<0.07	113.6	15.38	69.9	91.5	<0.05	0	0.2566	0.0651	2.003	ND	238	2.5	70	41.67	347.7	0	7.3	999.907
Fahmi Nahas47	19-13/047	7.2	421.56812	22.8	1.454	<0.07	116.3	12.42	66.6	93.7	<0.05	0.006	0.2671	0.0673	2.144	ND	225	2.2	77.2	43.73	355.02	0	7.96	1002.67
Sabiru Rantizi	19-13/006	6.88	331.19528	23.2	2.33	<0.07	158.6	7.95	93.5	173.4	<0.05	0	0.3118	0.1269	3.553	ND	414	2.5	117.6	62	376.37	0.301	9.23	1419.22
Fahed Hishmi	19-13/015	7.08	338.89034	24.6	2.35	0.0751	214.4	38.47	101.4	99.5	0	0.002	0.476	0.0893	1.732	ND	504	5.3	60.8	33.24	378.81	0.001	6.99	1445.43
Zuhdi Hashwa	19-13/052	7.15	343.00886	23.4	2.59	<0.07	207.4	28.32	113.9	127.7	<0.05	0.005	0.4956	0.0713	3.579	ND	536	4.1	166	46.55	369.05	0	7.43	1610.67
Salah Arouri	19-14/012	7.14	375.75454	22.6	1.279	<0.07	92.3	11.17	63.3	88.4	<0.05	0.001	0.2083	0.054	1.887	ND	187	1.9	59.2	40.54	417.85	0	7.74	971.603
Basil Husaini20	19-13/020	7.16	425.72923	23.7	1.16	<0.07	148.3	17.01	73.4	92	0.4107	0.007	0.4115	0.0838	1.607	ND	264	2.5	110.1	49.38	349.53	0.005	6.99	1116.02
Basil Husaini18	19-13/018	7.2	409.22059	22.1	1.146	<0.07	81.5	9.63	52.2	87.7	<0.05	0.004	0.216	0.0353	1.3	ND	162	2.2	58.6	29.08	304.39	0	7.05	795.886
Ibrahim Daek	NW	7	371.26318	24.2	3.23	0.0875	315.1	39.52	130	131.7	<0.05	0.008	0.734	0.126	2.259	ND	750	6.2	167.7	29.68	376.37	0	6.98	1956.52
Iron Factory	19-13/26a	7.22	219.79713	24.7	1.939	<0.07	104.8	16.7	97.6	130	<0.05	0.005	0.2302	0.3069	4.308	ND	406	2.5	90	70.13	259.25	0	10.69	1192.54
Ein Sultan	AC/061	7.56	471.96627	21.3	0.637	<0.07	22.83	2.503	30.08	79.1	<0.05	0.005	0.0406	0.0301	0.1253	ND	34.4	1	17.2	42.46	295.24	0.095	4.757	530.125
Ein Dyouk	AC/060	7.14	507.2459	21	0.637	<0.07	23.15	2.471	29.81	81.5	0.1126	0.015	0.0407	0.0342	0.1324	ND	34.9	0.5	16.7	29.07	287.31	0.097	4.785	510.543
Awni Hijazi	19-14/052	6.88	446.23787	25.3	3.11	0.0832	300.2	35.78	124.3	122	<0.05	0.012	0.4954	0.1649	2.853	ND	745	7.2	72.1	34.07	380.03	0	8.17	1832.44
Saeed Aladeen	19-14/062	6.89	465.07676	24.4	2.72	<0.07	230	24.18	109.9	140.7	<0.05	0.016	0.295	0.079	1.19	ND	656	8.7	40.6	5.18	364.17	0.088	6.87	1587.83
Mohammed Masri	19-14/038	6.8	345.05145	25.5	2.27	<0.07	176.6	19.42	102.1	128.1	<0.05	0.031	0.294	0.1076	1.166	ND	499	6.1	39.6	7.5	380.03	0	7.27	1367.18
Samed	19-14/26a	7.2	410.54281	23.9	1.233	<0.07	64.5	6.37	64.2	117.9	<0.05	0.017	0.1239	0.0603	0.525	ND	121	1.7	22.6	15.97	437.37	0	7.04	859.517
Arab Project69	19-13/069	7.02	345.30577	26.3	4.05	0.1371	460.1	79.6	140	116.7	<0.05	0.017	0.818	0.16	1.961	ND	1041	10.9	103.8	24.51	418.46	0.012	7.85	2406.16
Abdallah Araikat	19-14/049	6.68	306.05145	25.5	2.47	<0.07	210	15.34	105.7	131.2	0.1426	0.024	0.2927	0.1571	1.127	ND	528	5.8	92.7	30.58	364.78	0.004	7.12	1492.83

4.1.1 Springs and Fresh Water End Member

Springs in the west are characterized by Ca-Mg-CO₃ water with a low degree of mineralization (~548 mg TDS/l). Tritium units in the groundwater from the springs are 4.5 TU, while for the adjacent Samed well is 1 TU. These springs, which correspond to the fresh end-member, show low Cl content with molar ratios of B/Cl (0.0033-0.0039, Fig. 27b), Na/Cl (~1, Fig. 27c), Br/Cl (0.0065-0.013, Fig. 27d), Mg/Cl (~1.2 Fig. 27a), SO₄/Cl (~0.18 Fig. 27e) and Sr/Ca ($7.2-7.4 \times 10^{-4}$). The groundwater shows an over saturation index with dolomite and calcite, while it shows an under saturation index for gypsum and aragonites (Fig. 28 a, b, c, d).

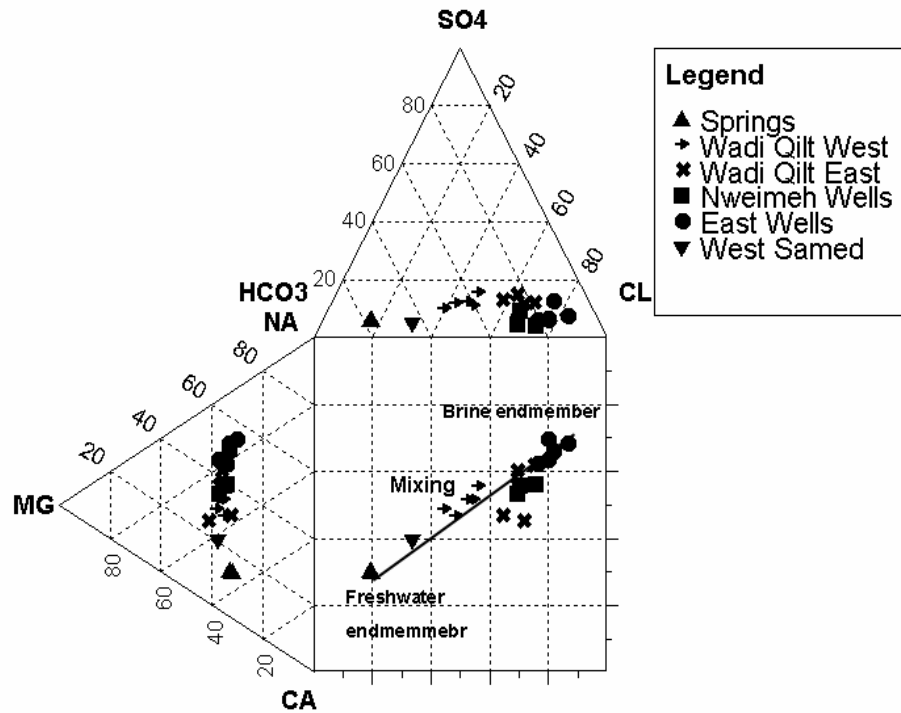


Fig. 25: Durov Plot suggests simple mixing or dissociation, the trend of water from fresh Ca-Mg-CO₃ water in the springs and wells to the west goes to NA-Mg-Cl water to the east.

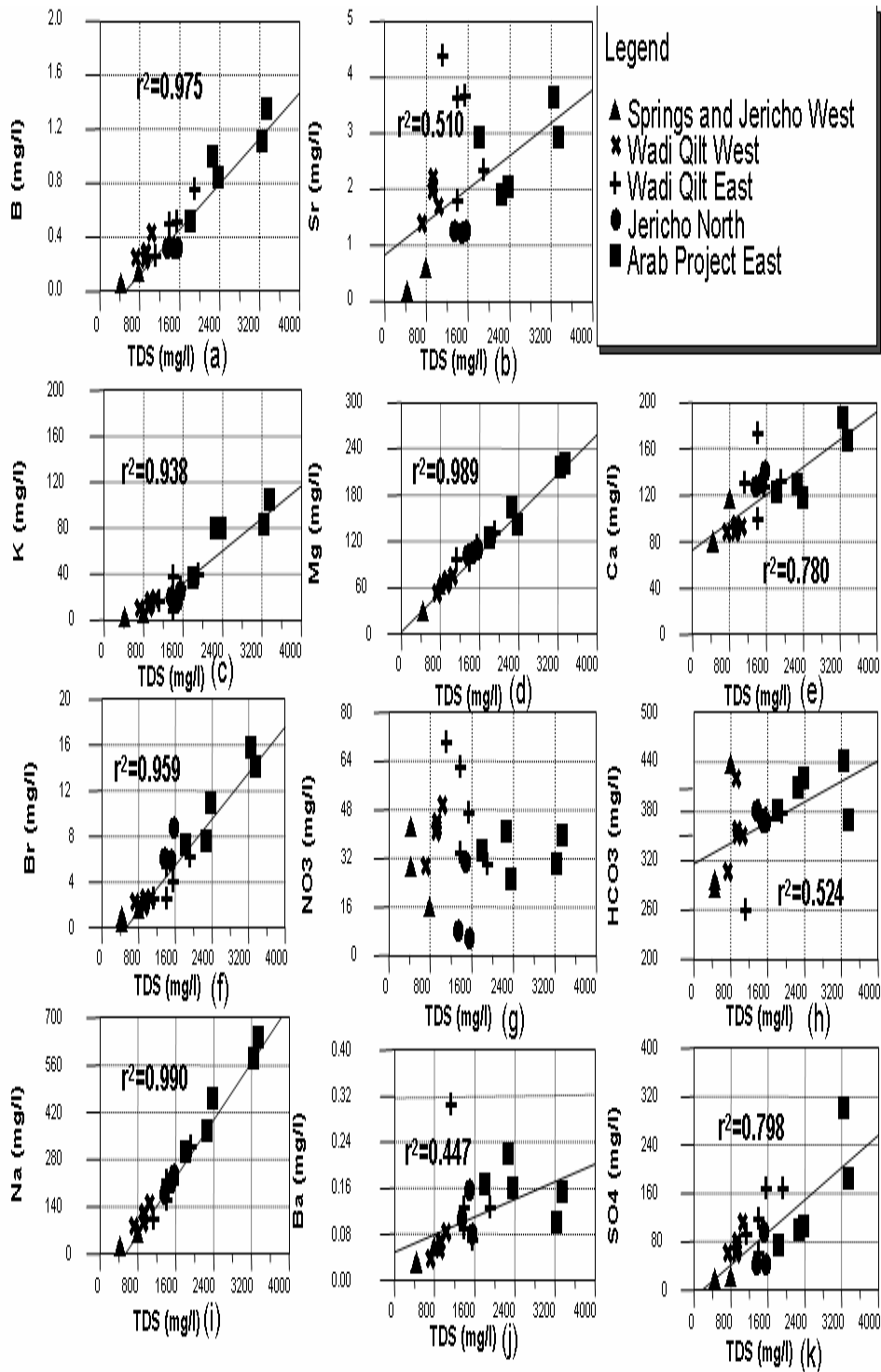


Fig. 26: Major anions and cations vs. TDS in mg/l, for the wells and springs of Jericho area (October, 2004). Salinity increase in one trend from west to east of the area. Mg, K, Na, and Br show a good linear relation, while Ca, Sr, B, SO₄, and HCO₃ show relatively low correlations, and nitrate shows very poor one with scattered nitrate values.

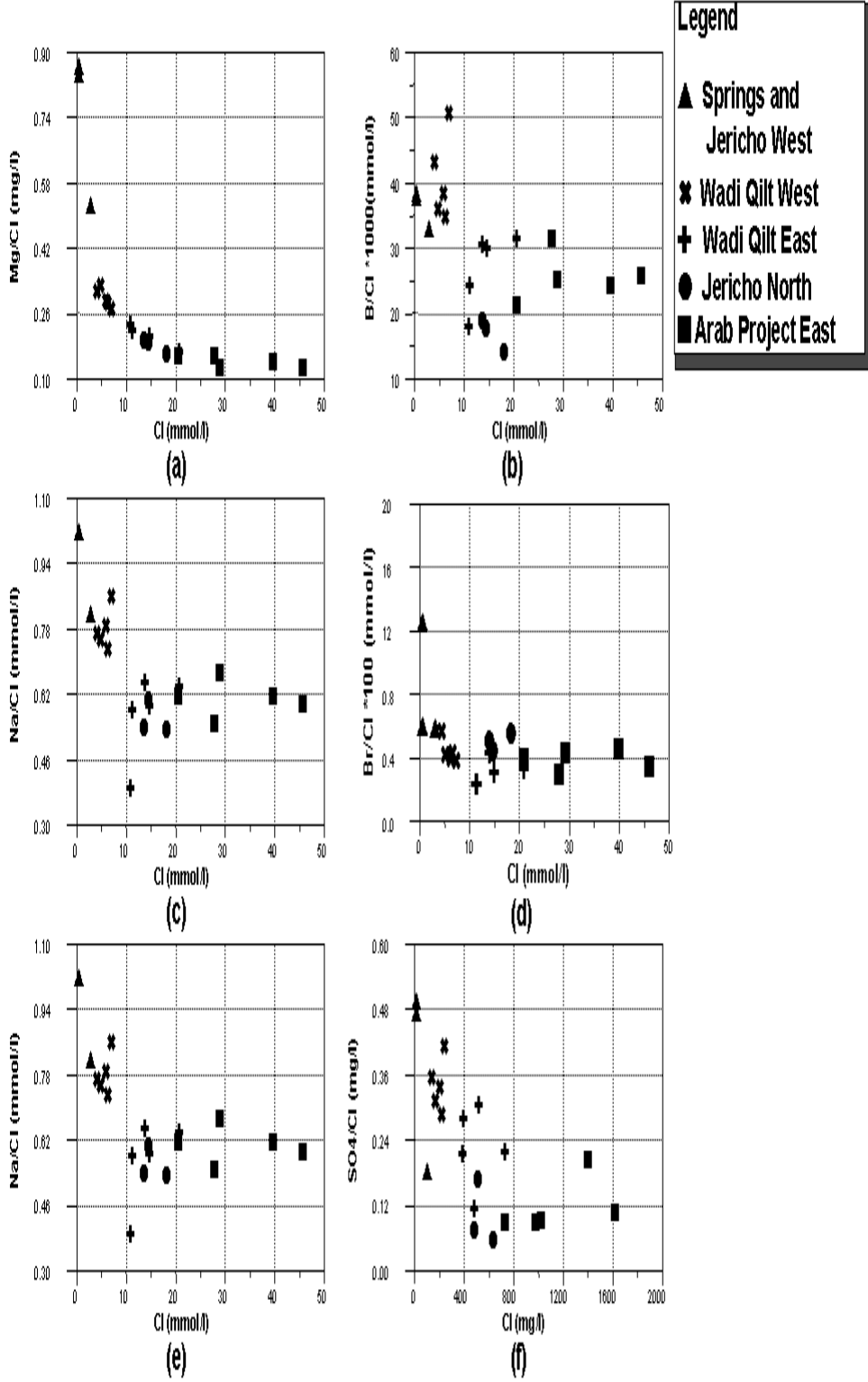


Fig. 27: Ions molar ratios for the wells and springs of Jericho area. The wells in the east have a stable molar ratio for most of the anions and cations.

4.1.2 Wells of Wadi Qilt West

The groundwater from wells in the west of Wadi Qilt show intermediate values between the fresh and saline end members with a water type of (Mg-Na-Ca-Cl-HCO₃). However the ion concentrations, mainly chloride is much lower than the eastern wells, and sometime show values that are close to these in the fresh end-member of the springs. Tritium units in the groundwater from these wells are between 3.3-3.9 TU. The ionic molar ratios for these wells lay between those of the two mentioned end-members. It shows lower saturation indices for dolomite and calcite than those of the springs, while the saturation indices for anhydrite and gypsum were higher. These wells contain relatively high carbonate, boron and nitrate values.

4.1.3 Wells of Wadi Qilt East

The hydrochemistry of the wells further to the east show a close trend to those in the west region, with more TDS as well as major ion concentrations. The area is characterized by overlapping Lisan and Samra layers. Tritium units in the groundwater from these wells are lower than the wells to the west with values between 2-3.5 TU. It has the same saturation indices of dolomite and calcite as the rest of Wadi Qilt wells to the west, and a much higher one for gypsum and anhydrite (Fig. 28). Even though the chloride concentrations for these wells are higher (500-900 mg/l and TDS >2100 mg/l), the molar ratios for ions are much lower. Most of the molar ratios start to take on stable trends when reaching these wells (Fig. 27).

4.1.4 Wadi Nuwe'meh North

The analysis of the wells in this area north of Jericho, show high chloride content (600 -700 mg/l) as well as high concentration of major anions and cations relative to wells in the west and Wadi Qilt west. This area is characterized by the dominance of Samra formation with high hydraulic conductivity. The water type is Mg-Na-Cl-HCO₃ the same as that for wells in the west, where both have surplus Mg which originates from dolomite dissolution that leaching through wadi runoff from the dolomitic limestone formation adjacent to the west. All chemical parameters in the groundwater from these wells are under-saturated with regard to different minerals. The molar ratios for the major ions are close to those in the eastern wells. Tritium units in the groundwater from these wells are around 1.5 TU.

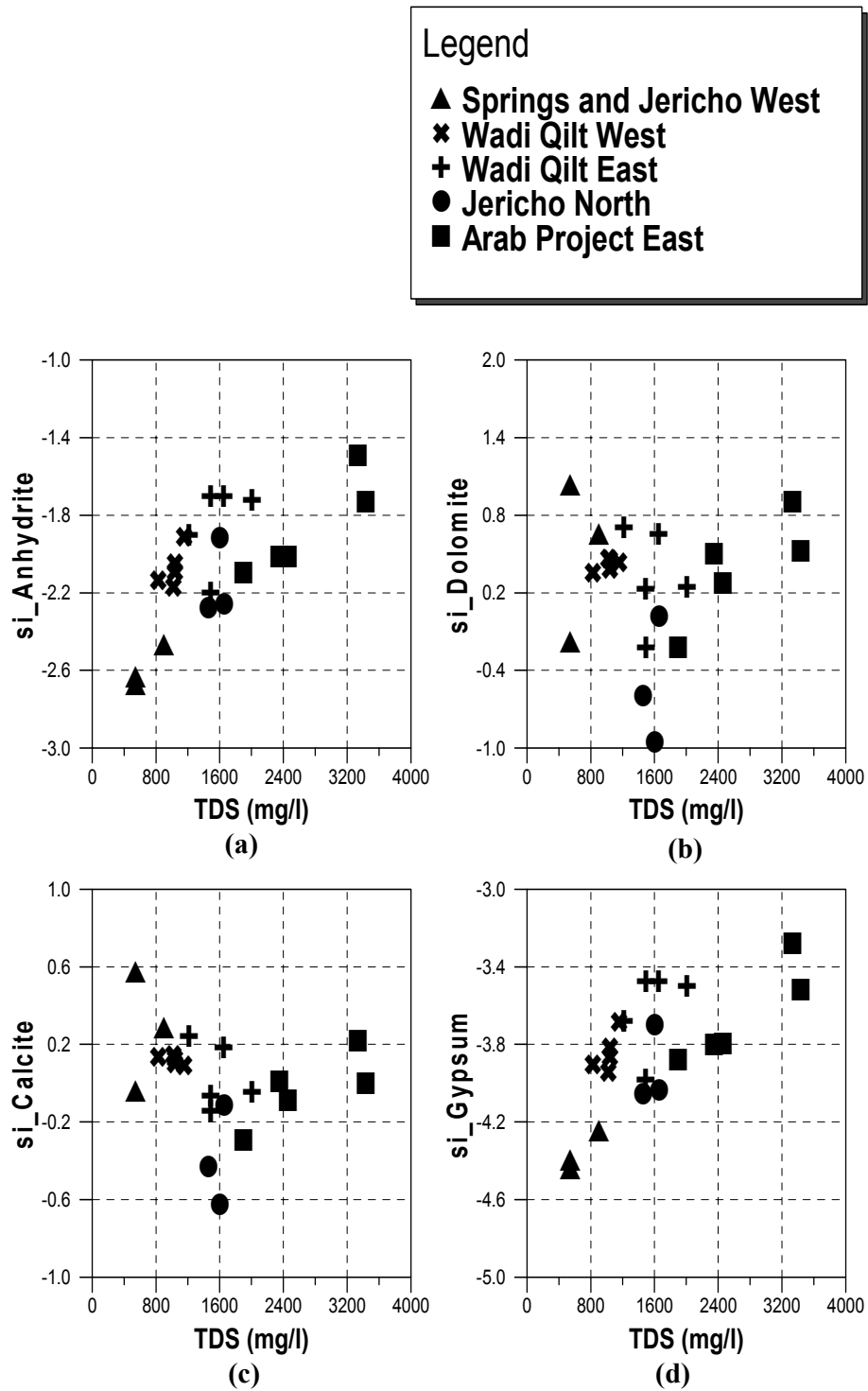


Fig. 28: Saturation indices for dolomite, calcite, gypsum and anhydrite vs. TDS for the groundwater samples from Jericho area. Figures show different trends for each mineral, where the wells to the east show higher SI with respect to TDS.

4.1.5 East Arab Project Wells (brackish end-member)

The groundwater from Arab Project wells in the east of Jericho shows the highest salinity in the area, with a Chloride content of more than 1800 mg/l for well 19-14/067 and a TDS value of 3664 mg/l. This highly saline water is of the Na-Mg-Cl and Mg-Ca-Cl type. The SO_4 concentration is 320 mg/l. The groundwater from these wells is highly saturated with dolomite and relatively saturated with calcite, while the saturation indices for gypsum and anhydrite are relatively higher than the rest of the wells but still undersaturated (Fig. 28). Carbonate concentration of 440 mg/l (Fig. 26h) is relatively high. The groundwater from these wells shows low tritium units which were below detection limit of <0.6 TU for well 19-14/067.

4.1.6. Overall Hydrochemical Conditions

The chemical data for all of the springs and wells shows a gradual increase for the major elements from west of the area to east along the water flow path. The groundwater salinity varies from fresh Ca-Mg- CO_3 water in the west to high saline Na-Mg-Cl and Mg-Ca-Cl water in the east ($\text{EC} > 5000 \mu\text{S}$) differentiating two distinctive end-members. The molar ratios for most of the elements tend to be stable in the east and Wadi Qilt east. Some wells in the Wadi Qilt west which show less chloride content also show high boron and nitrate values. While those wells to the north show less anthropogenic indicators but higher chloride content.

The linear correlation in the Durov diagram (Fig. 25) also suggests a type of dissolution or simple mixing that increases with distance from west to east and to the north. The water type varies along the mentioned paths. It is of Ca-Mg- HCO_3 water in the spring water and Mg-Na-Ca-Cl- HCO_3 water for the pumped wells in the west and middle of the studied area, but the water becomes more saline to the east and the Mg-Ca-Cl and Na-Mg-Cl water type becomes the most dominant. The variability in bromide and nitrate concentrations depend on well location and agricultural/domestic activities around the borehole. The groundwater mineralization do not really reflect the previous spatial trend for the major elements; this is due to variation in the ion input along the water path (Fig. 2 8). The groundwater from wells further to the east (19-14/67) with ^3H below detection must have been recharged prior to 1952 and can be considered as sub-modern or older water. Most of the other groundwater samples show tritium units between 0.8 to ~ 4.5 which reflect a sub-modern and modern recharge (Clark, 1997). These values could reflect a mixing process between two

water of different age, where the tritium units differentiate two different age end-members of old to modern and sub-modern recharged water that represent this mixing. The groundwater in the western springs and wells of an alluvial aquifer comprise mixtures of recharge from the past few years only (less than 5 years), where the data show a TU of 4-6 which are bearing the precipitation value (~ 6 TU) . It seems that the tritium level declines with increased distance along the water path through wadis, and emphasize that the mechanism of recharge is not related to direct infiltration of rainfall but of infiltrated run off along the wadis that drained from the Jerusalem-Ramallah Mountains (the main recharge point). In general, the variation in salinity within Jericho can be one or combinations of multi-sources of salinity and pollutants.

4.1.7. Salinisation

According to hydrochemical analysis salinisation process could be defined as having two main causative factors, as follows:

4.1.7.1. Brackish Water Source:

There is a good evidence of brackish water evolution further to the east of the study area. It is believed that the overexploitation of the wells to the east of the Jericho area has resulted in upwelling from deeper brackish water which confined in aquiclude. This water could be salt leachate brackish water that mainly formed as a result of long contact with the salty rocks, or deep old brine water which derived from residual Lisan lake water that entrapped in the interstices of the sediments in the Pleistocene age. This water coexists deeply in a confined aquiclude chamber within the Lisan formation. However, its source, direction and location are not well identified (section 2.6.1.). The analysis of samples from wells in the east show highly saline Ca-Cl and Na-Cl brackish water. The Na/ (Na+Cl) ratio which is less than 0.5 in combination with a high TDS of >500 suggest a reverse softening and a mixing of brackish water in the east with the discharging and uploading fresh water from the west. Moreover, the trend of a continuous increment of salinity from the west to the middle of the area demonstrated as steady ratios for Na/Cl and B/Cl in the east group with a molar ratio ~0.5 and 0.0026 (Fig. 27b, 27c). The low tritium concentration from the study wells emphasizes the presence of such a mixing process. The lower tritium units between <0.6-1 in the wells to the east might reflect a mixing of recent age water infiltrated from wadis run off with a deep old water characterized by high salinity. This evidence

could be made clearer by further studies of the rare earth elements concentration and isotopic signature analysis.

4.1.7.2. Evaporites and in situ Rock Weathering:

Generally, all the wells and springs show $\text{HCO}_3/\text{SiO}_2$ ratio of >10 and $\text{TDS}>500$ which suggests carbonate weathering along the water path. The $\text{Mg}/(\text{Ca}+\text{Mg})$ ratios, which is over 0.5 in most cases (Fig. 27c), indicates a Mg rich leachate by wadi run off from the dolomitic limestone's formation in the north west and south west of the area. In addition to calcite precipitation, especially for the wells in the east, where the $\text{Ca}/(\text{Ca}+\text{SO}_4)$ ratios were between 0.75 and 0.95, there is surplus calcium from the suggest Ca-Cl brine beside gypsum or carbonate dissolution of the Lisan layer. The Results show two main effects. These are mainly the effect of dissolution of salts from Samra layers and the dolomite limestone formations further to the west and the effect of Lisan layer and its gypsum and calcite to the east and north. Fig. 28 shows that the groundwater in the west is oversaturated with respect to dolomite and calcite and becomes less saturated further to the east of Wadi Qilt and Nuwe'meh north. This trend changes for the wells to the east where another input of Mg-rich salts raising the saturation indices for dolomite and calcite in a trend that increases until it reaches the brackish water end-member at eastern Arab Project wells. The Ca as well as HCO_3 concentrations decrease by precipitation of other minerals such as aragonites. Relatively high SO_4 concentrations in the east, in parallel with low saturation index of gypsum, indicate gypsum dissolution. Moreover, the increase in ion content, mainly Mg from a suggested brackish water source to the east, favored a process of dolomitization of the calcite and aragonite that dominating the entire sequence. Sr/Ca molar ratio which is between 0.0025 and 0.0155 emphasizes the dolomitization process (Sass and Starinsky, 1997).

Except the springs that show relatively fresh water, the ratios of Na/Cl (0.4 east-0.7 west) Mg/Cl (0.18 east-0.5 west) and SO_4/Cl (0,015 east-0.15 west) shows ratios which are even less than the Lisan leaching ratios which have values of (0.54, 0.23, 0.05) respectively (Salameh, 2002) and much lower than sea water ratios (Na/Cl 0.86, SO_4/Cl 0.135). While the Br/ Cl (0.006 east-0.014 west) was higher than that of sea water ratio which is ~ 0.0016 . Although the groundwater from many of the studied wells show different Br/Cl molar ratios that might also be affected by dissolution of salts, the variation between the mentioned value and those from the wells is mainly due to more Br input which suggests that it originated from two sources: 1) Halite

dissolution from the evaporitic Lisan layer with different Br/Cl molar ratio than brine or seawater, 2) the anthropogenic influent of bromide which is used widely in the form of methyl bromide within this agricultural area.

4.1.8. Anthropogenic Influences:

The greatest anthropogenic effect on the groundwater quality in the Jericho area is the agricultural effects which have 4 main agricultural practice indicators. These are: 1) Bromide which is injected as a fumigant to the land as a methyl bromide gas. 2) Pesticides. 3) NO_3 from nitrogen fertilizers and animal manure. 4) Potassium, magnesium and calcium which might appear in surplus amounts due to irrigation back flow through the soil to the groundwater. The wells in the middle and west of Jericho area are susceptible to agricultural influence. This is more clearly present in the east, even though the high Chloride content and the influence of natural evaporites there make this indicator less unambiguous.

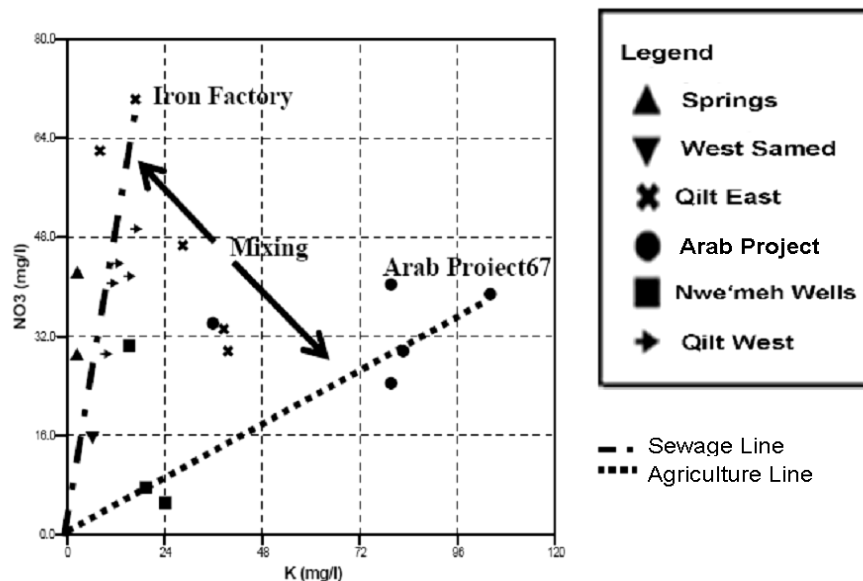


Fig. 29: Potassium versus Nitrate in the groundwater samples from Jericho area: Iron Factory used as sewage indicator end member and Arab Project 67 as agricultural end member. Most of the wells are mainly affected by sewage influences.

Fig. 29 makes this picture clearer. The area Iron Factory was taken as an end-member for the sewage input, because it is a non-agricultural area, and a lot of nitrate salts which is used in the salts path for hardening the iron steal (sodium nitrate), is excreted to the septic tank as well as other human sewage. Moreover, this area is located in the most far south eastern point with flow direction. Therefore, it is expected that the groundwater in this area also received the nitrate flushed out from

the recharge stream along whole area. Moreover, it was noticed that there is some septic tanks from houses and factory distributed surround the area. On the other hand, the Arab projects wells, where there is an extensive agriculture was taken as the other end member. There were two different trend lines for the two end-members. Other groundwater samples show a mixing from the two influences in between. Nitrate values varied with activities and location. The NO_3 values increase significantly in the wells in agricultural and animal farm areas or within the stream of septic tanks (eg. Sabiru Rantizi well 19-14/06). This well is next to an animal farm and in an area that has wide agricultural activities and uses pesticides application. The same values are shown by the Iron factory well which taps the alluvial fans of the Wadi Qilt interfingering with Lisan formation in the east south of Jericho, has no surrounded agricultural activities. The well also as mentioned above received the flushed water out of the whole Wadi stream. The main reason for highly nitrate level is the wide use of septic tanks. Unsuitable location of septic tanks in this area could be hazardous, especially as the area is mainly formed by marls and gypsum layers.

The Lisan formation as an aquiclude has highly consolidated sands and evaporates with a lot of solution conduits in the evaporates, where the pollutants can easily pass through and reach the alluvial aquifer. The continuous input of potassium in the groundwater from wells to the east might reflect an agricultural source. Potassium is added as an element within synthetic fertilizers compounds, where it is elaborated to absorb by the plants, or infiltrate through the soil profile to the groundwater. Another additional source of Potassium can be through the suggested brine water described in the previous section, that up welled from the Arab Project wells in the east of Jericho. The pesticides also might contain a lot of nitrogenous compounds from which an additional amount of nitrate can be infiltrate to the groundwater.

The pollution of groundwater by the nitrate from fertilizers has low evidence in the region, samples for pesticides in groundwater was taken in the same study shows no synthetic fertilizers or pesticides. This might be referred to the complicated structure of these chemicals which make it have long persistence in the upper soil environment without further oxidation reaction or hydrolyses for the chemical particles, more detailed information about the usage of nitrogen chemical and its effect on the groundwater in the study area is described in section 4. 3.

4. 2. Deuterium and Oxygen Isotopes

The local precipitation line ($\delta D = 8.1 \delta^{18}O + 19.5$) (Fig. 30 and 31) from the precipitation of the main recharge area at the Palestine eastern mountains of Jerusalem-Ramallah (Abu Dees Station), shows a nearly closed slope to the Mediterranean Meteoric Water Line $\delta D = 8 \delta^{18}O + 22$ (Gat and Dansgaard, 1972), suggesting nearly the same evaporation trend of the precipitation during the storm events. Although the data (Table 6) show no significant variation in $\delta^{18}O$ signature between 2 sampling times in dry and wet season. However, the isotopic signature for deuterium exhibits a slight shifting toward more enriched signatures (Figs.30 and 31).

In dry season the isotopic signatures of δD and $\delta^{18}O$ for the springs fall nearly on the local precipitation line, indicating no further evaporation of the recharged water and confirm more direct infiltration without any alteration. The values for the Pleistocene wells distributed in Jericho plain have more enriched values. These values are distributed along a mixing line that has been calculated between 'Arab project well 67' as a brackish water end member and 'Samed' well to the west as fresh end member. The heavier (less negative) isotopic signature in the wells of Arab project in the east shows also a high Cl content, where the wells of less saline wells in the west shows more depleted signatures at the same line. There were some scattered values distributed around, most of these values also show low chlorine content. The seasonal variation of enriched deuterium signatures (Fig. 30) put forward two possibilities: One is the variation within rain events but this is not possible in the area because there is no seasonal rain and all the precipitation events occur in winter under the same conditions. The other possibility is related to a fractionation process which only effects on deuterium. Such process was defined by Coplen and Hanshaw (1973) as 'ultrafiltration'. Hoefs (2004) shows that the hydrogen isotopes fractionation is affected by the absorption of water on mineral surfaces due to the tendency for clay and shales to act as semi permeable membranes.

The fractionation of hydrogen isotopes occur during this process in such a way that the residual water will be enriched in deuterium due to the preferential adsorption of lighter hydrogen isotopes, this process has no effect on the oxygen isotopes (Fig. 30). During the continuous recharge in wet season the increasing of hydraulic pressure flush out the residual older water

Table 6: $\delta^2\text{H}$ and $\delta^{18}\text{O}$ values for groundwater samples of the Jericho area in wet and dry seasons (March, 2004 and October, 2003 respectively).

Site	Well Code	Dry Season (October , 2003)			Wet Season (March, 2004)		
		TDS	$\delta^{18}\text{O}$	$\delta^2\text{H}$	TDS	$\delta^{18}\text{O}$	$\delta^2\text{H}$
Arab Project66 (East)	19-14/066	3282.01	-5.39	-26.1	3165.95	-5.4	-23.5
Arab Project67 (East)	19-14/067	3385.98	-5.29	-25.4	3582.51	-5.28	-22.6
Arab Project73 (East)	19-14/073	2292.6	-5.36	-26.7	2292.55	-5.39	-23.2
Fahmi Nahas48 (Qilt West)	19-13/048	999.907	-5.38	-26.2	996.007	-5.39	-23.6
Fahmi Nahas47 (Qilt West)	19-13/047	1002.67	-5.39	-26	990.155	-5.41	-24
Sabiru Rantizi (Qilt East)	19-13/006	1419.22	-5.5	-26.7	1484.55	-5.55	-25.9
Fahed Hishmi (Qilt East)	19-13/015	1445.43	-5.46	-26.3	1431.73	-5.44	-23.8
Zuhdi Hashwa (Qilt East)	19-13/052	1610.67	-5.44	-26.6	1680.79	-5.44	-24.1
Salah Arouri (Qilt West)	19-14/012	971.603	-5.5	-25.9	931.3	-5.51	-24.1
Basil Husaini20 (Qilt West)	19-13/020	1116.02	-5.27	-26.6	1055	-5.28	-23.9
Basil Husaini18 (Qilt West)	19-13/018	795.886	-5.48	-27.7	820.514	-5.44	-23.7
Ibrahim Daek (Qilt East)	NW	1956.52	-5.23	-26.4	1990.26	-5.22	-23.4
Iron Factory (Qilt East)	19-13/26a	1192.54	-5.52	-27	N D	N D	N D
Ein Sultan (West)	AC/061	530.125	-5.87	-28.1	533.46	-5.96	-26.1
Ein Dyook (West)	AC/060	510.543	-5.87	-28.1	565.88	-5.96	-26.2
Awni Hijazi (East)	19-14/052	1832.44	-5.5	-27.7	1810.79	-5.48	-24.8
Saeed Aladeen (North)	19-14/062	1587.83	-5.54	-27.6	1486.9	-5.55	-25.1
Mohammed Masri (North)	19-14/038	1367.18	-5.54	-27.3	1458.01	-5.52	-25.7
Samed (West)	19-14/26a	859.517	-5.56	-27.8	852.339	-5.52	-24.6
Arab Project69 (East)	19-13/069	2406.16	-5.54	-28.3	2486.86	-5.52	-23.6
Abdallah Araikat (North)	19-14/049	1492.83	-5.54	-25.7	N D	N D	N D
Awn Hijazi	19-14/37	N D*	N D	N D	1832.44	-5.27	-22.8
Saleem Nimmari	19-13/49	N D	N D	N D	1587.83	-5.51	-24.1
Qasir Hisham	19-13/003	N D	N D	N D	1367.18	-5.49	-24
Bail Hussaini22	19-13/22	N D	N D	N D	859.517	-5.27	-23.4
Mahmud Akramawi	19-13/50a	N D	N D	N D	2406.16	-5.45	-23.9
Bail Hussaini21	19-13/21	N D	N D	N D	1492.83	-5.22	-23.1

*N D: no data available (no sample was taken).

This water which sampled in the wet season, which is enriched in deuterium by Ultrafiltration process washed out along the aquifer, replaced by the new recharge water in the upper layer. On the other hand, Gat (1998) suggests what is named Isotope Transfer Function (ITF) effect as a main cause for modifying the isotopic composition in arid environment and wet lands with surface runoff. The behaviors of isotopes show that the rain fall in the top of the mountains and along the wadis is partitioned into singular fluxes of surface run off. The water infiltrates through soil and sinkholes at different distances from the main recharge point into the ground.

The isotopic signature is shifted due to such processes as a result of evaporation during runoff and due to the selective utilization of rainfall with different isotopic signatures, which are varying with distance. $\delta^2\text{H}$ and $\delta^{18}\text{O}$ for the springs in the west indicates different recharge and infiltration mechanisms compared to other wells in the lower plain Dead Sea Group. The springs, as described in the section of hydrogeology, are an outcrop of the regional mountain aquifer through rain water that infiltrated to the Upper Cretaceous aquifer, where the shallow Pleistocene aquifer is mainly fed through the infiltrated surface water runoff that drained through wadis from the same recharge area of the springs. Normally the drained water through wadis runoff runs for a long distance and infiltrates in the shallow Samra aquifer or alluvial fan layer in the lower plain of the study area. The shifting from the local meteoric water line for the shallow wells (Fig. 32) caused mainly by the climate of the area which characterized by low humidity and highly evaporation rate in the lower and warmer area of Jericho plain, thus the isotopes undergoes further fractionation through evaporation in the run of path and tends to be more enriched. The signature for the springs fell directly on the LMWL (the same as the precipitation signatures), while wells have shifted signatures that forming a semi-linear trend closed to that of calculated mixing line from fresh water in the west to brackish water in the east. The primary shifting in the wells groundwater signatures can be explained by the Isotope Transfer Function (ITF) according to Gat (1998), due to the high evaporation from drainage draught in the wadis as well as the irrigation channels in this semi-arid area. This ITF effect can be distinguished from the normal evaporation effect, which normally occurs as gradual deviation in the isotopic signatures from the LMWL forming a new slope of ~ 5 . While in the study area the surface run off cut a long distance through wadis, where part of it infiltrated to the upper mountain aquifer, and the remained part (isotopic heavier due to evaporation) feed the shallow aquifer at different distances forming a shifted line.

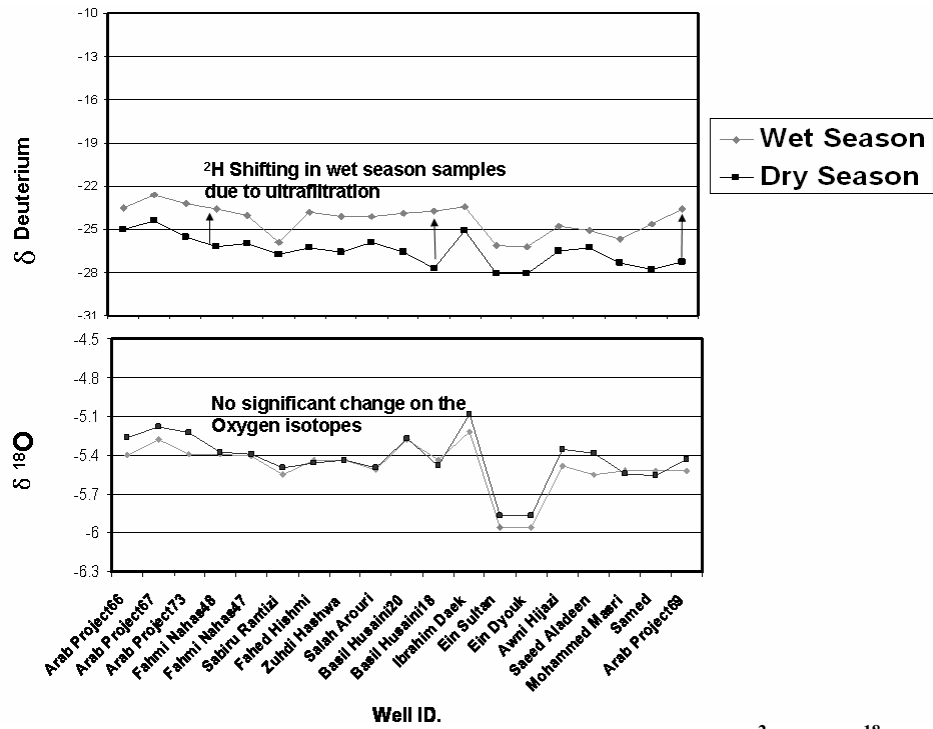


Fig. 30: Seasonal comparative trends for isotopic signatures of $\delta^2\text{H}$ and $\delta^{18}\text{O}$ the trend shows nearly no significant change in $\delta^{18}\text{O}$ and a shifting in $\delta^2\text{H}$ toward more enriched values in the wet season due to the process of ultrafiltration, (Hoefs, 2004).

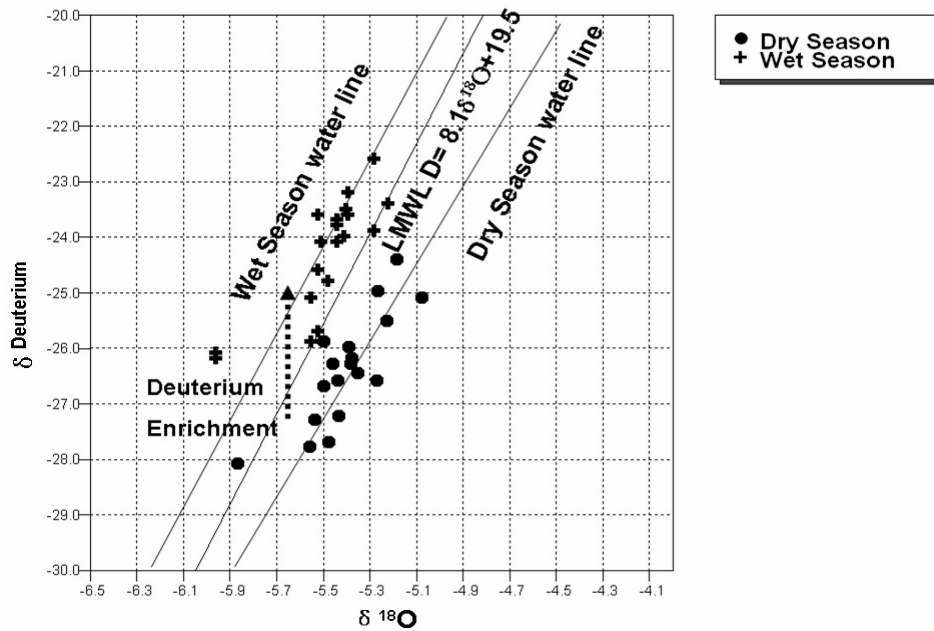


Fig. 31: Seasonal variation of groundwater isotopic signatures around LMWL, the shifted $\delta^2\text{H}$ values located as a parallel line on the left of LMWL, where the dry season samples located in a separate line to the right of the LMWL, this line shifting is depend on the process of ultrafiltration which effect only on the hydrogen but not Oxygen isotopes .

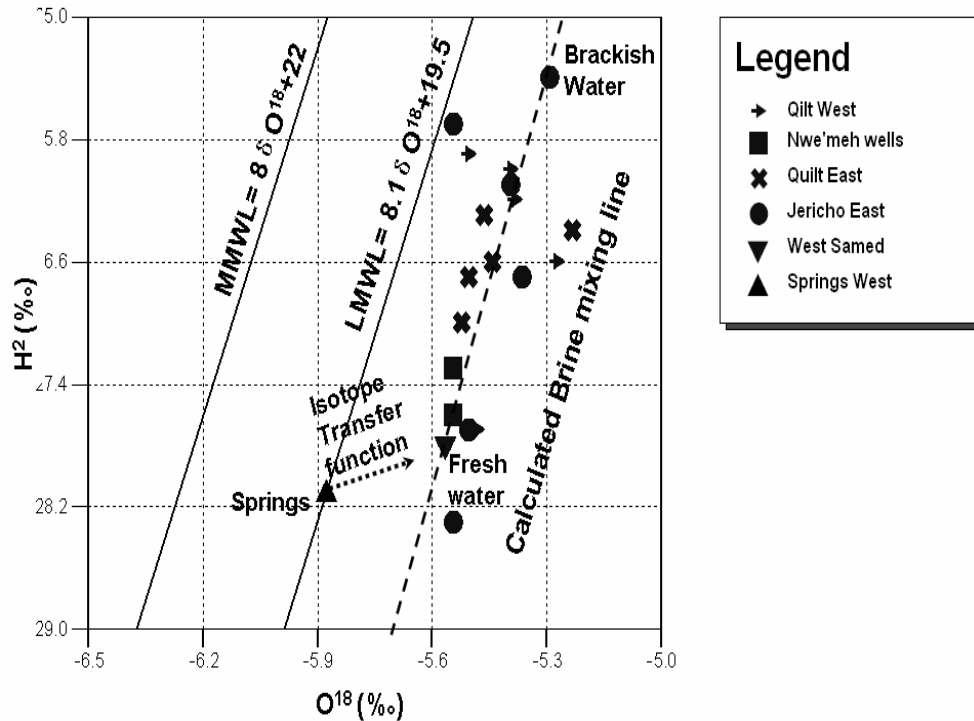


Fig. 32: Isotopic signature of the wells and springs in dry season. The signature for the springs fell directly on the LMWL, while wells have shifted signatures that forming a semi linear trend close to that of calculated mixing line from fresh water in the west to brackish water in the east. The primary shifting in the groundwater signatures of the wells can be explained by the Isotope Transfer Function (ITF) according to Gat (1998), which mean that all the wells are fed by the surface runoff water which was exposed to evaporation along the drainage path (water origin either from precipitation runoff from the upper mountains through wadis or spring discharge through the irrigation channels).

The shifting in isotopic composition of oxygen and hydrogen formed a parallel line to that of meteoric water line. This trend also goes toward more positive isotope ratios in the eastern wells and fitting the calculated brackish water mixing line between the 2 end members, which suggest an effect of salts and brackish water in the east. Even though, the figure shows different scattered values which have more enriched oxygen isotopes signatures. These enriched signatures reflect those wells that coincident within intensive agricultural activities and effected by irrigation backflow that contains heavier water due to further evaporation process and/or the presence of agricultural pollutants.

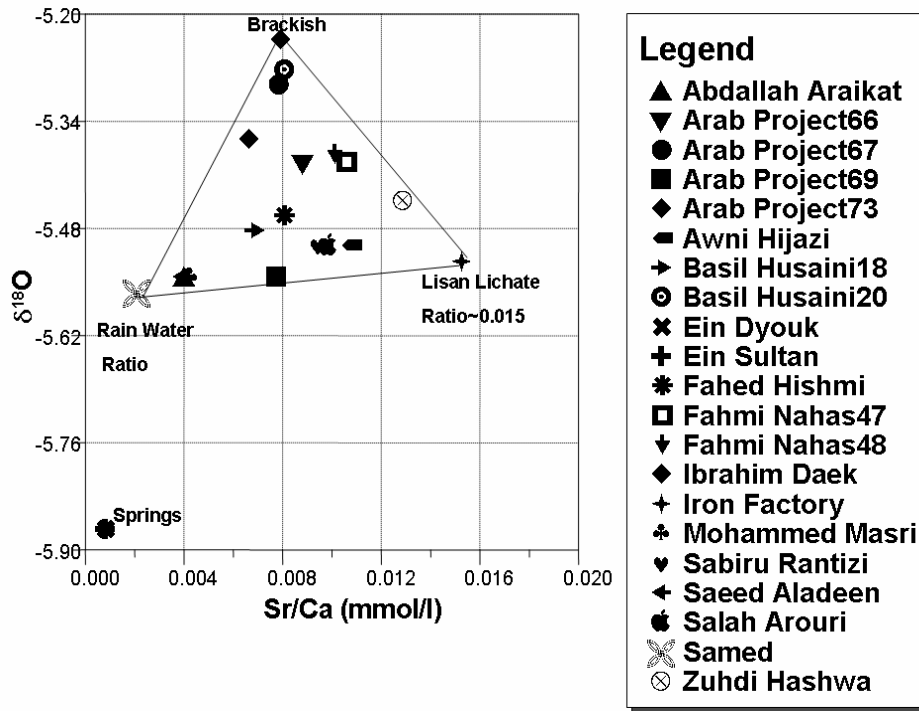


Fig. 33: Sr/Ca molar ratio vs. $\delta^{18}\text{O}$ suggest three inputs to the groundwater, the brackish water cause the main significant effect on $\delta^{18}\text{O}$ signature, most of the wells undergo a mixing between the three end members.

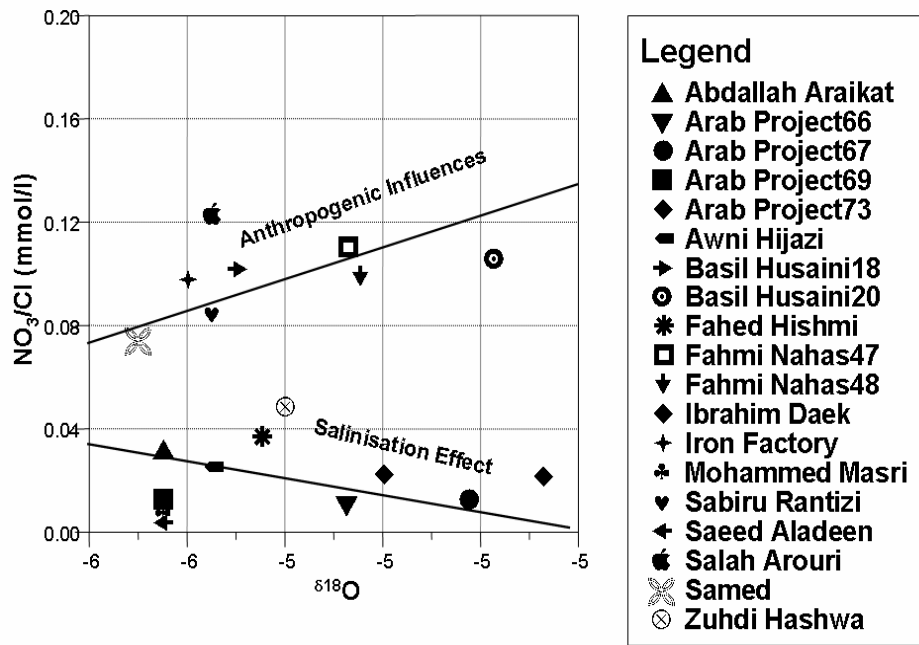


Fig. 34: $\delta^{18}\text{O}$ vs. NO_3/Cl molar ratio shows two separate trends, one is an anthropogenic effect and the other salinisation effect.

Fig. 33 shows the relation between the molar ratios of Sr/Ca versus $\delta^{18}\text{O}$, and the distribution of the groundwater samples between three end members. The figure shows that the $\delta^{18}\text{O}$ values were mainly affected by the brackish water evolution to the east, where the enriched $\delta^{18}\text{O}$ signatures were combined with high Sr/Ca molar ratio close to these of brines which is $\sim 1 \cdot 10^{-2}$, while the fresh water end member of 'Samed' well shows a Sr/Ca ratio of $2.6 \cdot 10^{-3}$ which is close to fresh water ratio of $2\text{--}4 \cdot 10^{-3}$ (Siemann and Schramm, 2002). Even though some other wells show the same signatures between the end members triangular, this can be referred to a mixing from other anthropogenic sources and salts leachate of Lisan layers.

Fig. 34 is emphasizing the anthropogenic effect on the groundwater. It shows two different trends. One trend is bearing the calculated mixing line with brackish water and salts, and the other trend represents the anthropogenic effect with most of the scattered enriched values. The most important characteristic for these scattered wells is the low amount of chloride which means low evidence of brackish water exposure, thus the other minor anthropogenic influences is clearly expressed. These wells also show a highly content of boron, nitrate and bromide. All of these indicators beside the enriched $\delta^{18}\text{O}$ values suggest a different heavy water input from sewage and irrigation backflow.

4.3. Nitrogen Isotopes

Nitrate concentrations, $\delta^{15}\text{N}_{\text{nitrate}}$ and $\delta^{18}\text{O}_{\text{nitrate}}$ for groundwater samples taken in both wet and dry season are shown in Table 7. The nitrate concentrations vary spatially depending on the well location and surrounding activities, ranging between 10 to 100 mg/l in the wet season and from 7 to 72 mg/l in dry season. Both samples series show no significant change in the isotopic signature, where the values scattered nearly around the same trend line and shows the same behavior with the same sources more or less (Fig. 35). The $\delta^{15}\text{N}_{\text{nitrate}}$ values ranged from +3.0 to +15.78 ‰. Oxygen isotope ratios of nitrate were around +3.3 to +8.5 ‰. Two of the samples exceed this range where they show signatures of +13.9 ‰ and +14.7 ‰. These two anomalous signatures belong to the samples which have very low nitrate values. Nitrate in the environment has various sources, including atmospheric deposition, soil organic nitrification, fertilizer, sewage and manure. Nitrate from each of these sources is typically characterized by a distinct isotopic signature.

Table 7: Nitrate concentrations, $\delta^{15}\text{N}_{\text{nitrate}}$ and $\delta^{18}\text{O}_{\text{nitrate}}$ for groundwater samples of the Jericho area.

Location	Well Name	Well Code	Dry Season			Wet Season		
			Nitrate (mg/l)	$\delta^{15}\text{N}_{\text{nitrate}}$	$\delta^{18}\text{O}_{\text{nitrate}}$	Nitrate (mg/l)	$\delta^{15}\text{N}_{\text{nitrate}}$	$\delta^{18}\text{O}_{\text{nitrate}}$
West spring	Ein Dyouk	AC/060	29.07	10.48 ‰	3.9 ‰	55	10.1	3.9
West spring	Ein Sultan	AC/061	42.46	10.08 ‰	3.3 ‰	48	9.8	4
JerichoNorth	Saeed Aladeen	19-14/062	5.18	10.12 ‰	13.9 ‰	20	12.7	10
JerichoNorth	Mohammed Masri	19-14/038	7.5	2.99 ‰	14.7 ‰	10.5	3	13
Jericho West	Samed	19-14/26a	15.97	15.78 ‰	8.5 ‰	41	11.3	6.4
Jericho East	Abdallah Araikat	19-14/049	30.58	8.14 ‰	3.4 ‰	N D	N D	N D
Jericho East	Awni Hijazi	19-14/052	34.07	9.99 ‰	4.9 ‰	50	8.9	4
Qilt West	Basil Husaini	19-13/018	29.08	8.29 ‰	5.2 ‰	52	7.7	4.8
Qilt West	Basil Husaini	19-13/020	49.38	6.89 ‰	3.4 ‰	65	6.8	3.9
Qilt West	Fahmi Nahas	19-13/047	43.73	6.94 ‰	3.8 ‰	71	6.6	3.8
Qilt West	Fahmi Nahas	19-13/048	41.67	7.42 ‰	3.8 ‰	61	7.1	4.3
Qilt West	Salah Arouri	19-14/012	40.54	8.47 ‰	4.3 ‰	70	7.5	4
Qilt West	Sabiru Rantizi	19-13/006	72.71	9.29 ‰	2.3 ‰	100	8.2	2.8
Qilt East	Zuhdi Hashwa	19-13/052	46.55	7.7 ‰	4.3 ‰	79	7.6	6
Qilt East	Fahed Hishmi	19-13/015	33.24	8.5 ‰	4.8 ‰	50	7.5	4
Jericho East	Arab Project	19-13/069	24.51	10.9 ‰	7.3 ‰	43	10.2	7.2
Qilt East	Iron Factory	19-13/26a	70.13	9.64 ‰	5.2 ‰	N D	N D	N D
Qilt East	Ibrahim Daek	NW	29.68	6.59 ‰	4.9 ‰	47	5.9	4.2
Jericho East	Arab Project	19-14/067	38.86	7.42 ‰	4.5 ‰	51	7	6.2
Jericho East	Arab Project	19-14/073	40.41	7.37 ‰	3.9 ‰	48	7.1	4.5
Jericho East	Arab Project	19-14/066	29.69	9.25 ‰	5.7 ‰	38	9	-3.3
Qilt East	Awn Hijazi	19-14/37	N D*	N D	N D	49.5	6.1	2.8
Qilt East	Saleem Nimmari	19-13/49	N D	N D	N D	75	8.1	4.1
JerichoNorth	Qasir Hisham	19-13/003	N D	N D	N D	23.5	8.6	7.8
Qilt East	Bail Hussaini22	19-13/22	N D	N D	N D	50	7.1	4.4
Qilt East	Mahmud Akramawi	19-13/50a	N D	N D	N D	54	7.9	5.1
Qilt East	Bail Hussaini21	19-13/21	N D	N D	N D	95	10.3	4.2

*N D: no data available (no sample was taken)

Typical $\delta^{15}\text{N}_{\text{nitrate}}$ values for chemical fertilizers range from -4 to $+4\%$, for human and animal waste it has a wide range between $+7$ and more than $+30\%$, and from less than -10 to $+4\%$ for soil nitrate. $\delta^{18}\text{O}_{\text{nitrate}}$ values for atmospheric deposition is $> +25\%$. While for chemical fertilizers this is about $+18$ to $+22\%$, and for human and animal waste and soil nitrate it ranges from -10 to $+10\%$ (Fig. 36) (Fritz and Clark, 1997). Hence, the isotopic composition of nitrate constitutes a useful tracer for determining its sources, provided that, no alteration of isotopic ratios by biogeochemical reactions, such as denitrification has occurred.

Except two wells in the north, most of the isotopic signatures for the sampled wells and springs suggest sewage or manure as a main source responsible for the higher nitrate concentrations, with $\delta^{15}\text{N}$ values $> +7\%$, and $\delta^{18}\text{O}_{\text{nitrate}}$ between $+3\%$ and $+6\%$. Samples also show a slight denitrification process where this process was significant in the Samed well (Fig. 37, 38). This was clear for the samples of dry season and mainly might refer to the period of sampling which was held by the end of summer, where there was nearly no recharge and thus the groundwater is stored in the reservoir for the months of the dry season. The values in Fig. 39 a. and b. show a slight increase in $\delta^{15}\text{N}_{\text{nitrate}}$ with decrease of $[\text{NO}_3^-]$, whereas $\delta^{18}\text{O}_{\text{nitrate}}$ also shows the same increment trend with decreasing $[\text{NO}_3^-]$. These combined trends favored the presence of slight denitrification within the aquifer, where the heavy isotopes ^{15}N and ^{18}O are preferentially retained in the remaining nitrate (Böttcher et al., 1991). Sewage is considered as a direct source of nitrate as it contains a high amount of urea and other organic and inorganic nitrogenous compounds. Manure in the presence of aerobic condition in shallow aquifers is also another source of nitrate which originates by oxidation process. The presence of many animal farms especially in Wadi Qilt east and Ein Dyouk area confirm this suggestion, because of using animal manure as natural fertilizers (Fig. 36). The wells in the north show relatively small nitrate concentrations, and much higher $\delta^{18}\text{O}_{\text{nitrate}}$ values (Fig. 38b.). This might indicate a different (non-continuous) nitrate sources, in which nitrate might persist for a long time within the groundwater of these wells. The isotopic signature shown by these wells bearing the signature of chemical fertilizers, even though these signatures become more depleted than this of the fertilizers signatures due to a mixing with other signature of different sources such as sewage. Moreover, the source which yielding lower nitrate concentrations could also represent the residual nitrate from bacterial denitrification of sewage or manure, which give these high $\delta^{18}\text{O}$ values above $+12\%$.

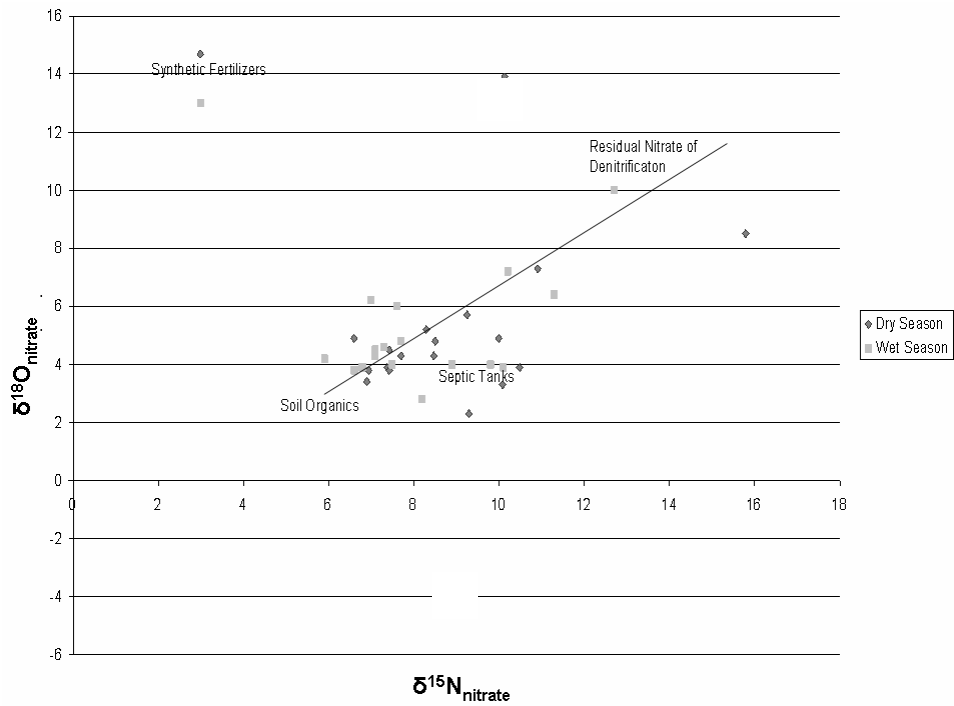


Fig. 35: $\delta^{15}\text{N}_{\text{nitrate}}$ vs. $\delta^{18}\text{O}_{\text{nitrate}}$, from the water samples of dry and wet season show more or less the same trend.

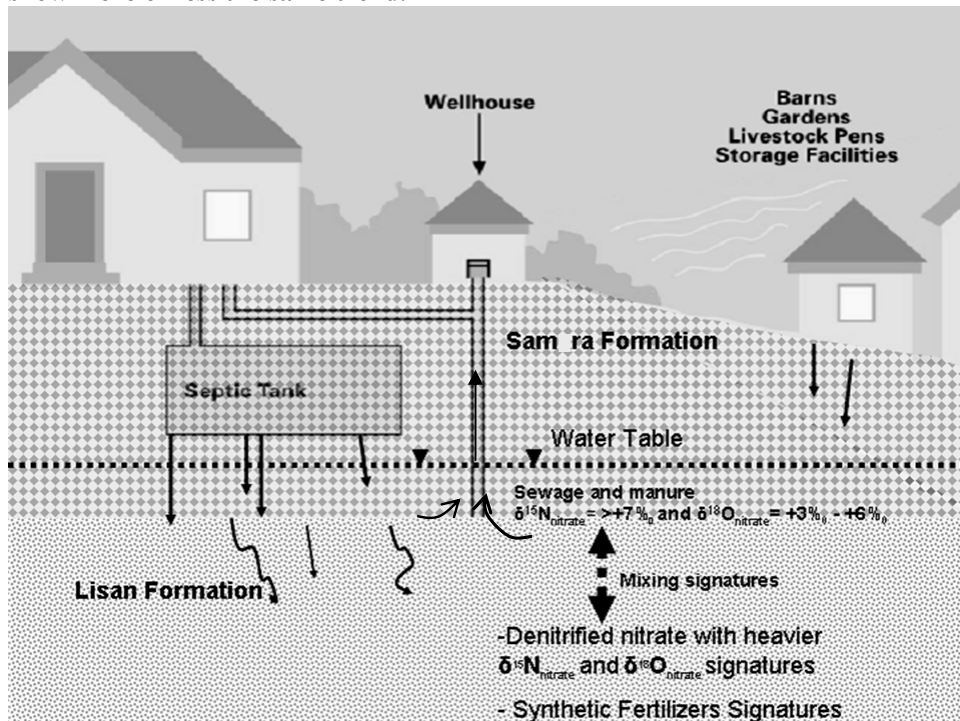


Fig. 36: Groundwater pollution by nitrate sources in Jericho area.

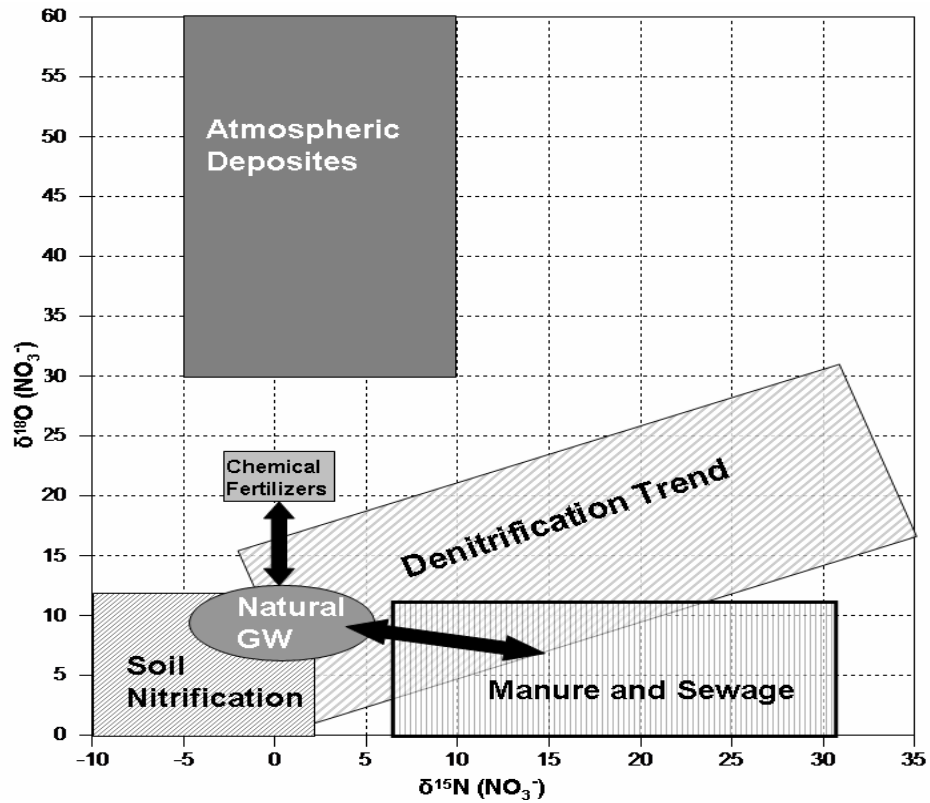


Fig. 37: $\delta^{15}\text{N}_{\text{nitrate}}$ vs. $\delta^{18}\text{O}_{\text{nitrate}}$, isotopic composition of major nitrate sources (Clark, 1997)

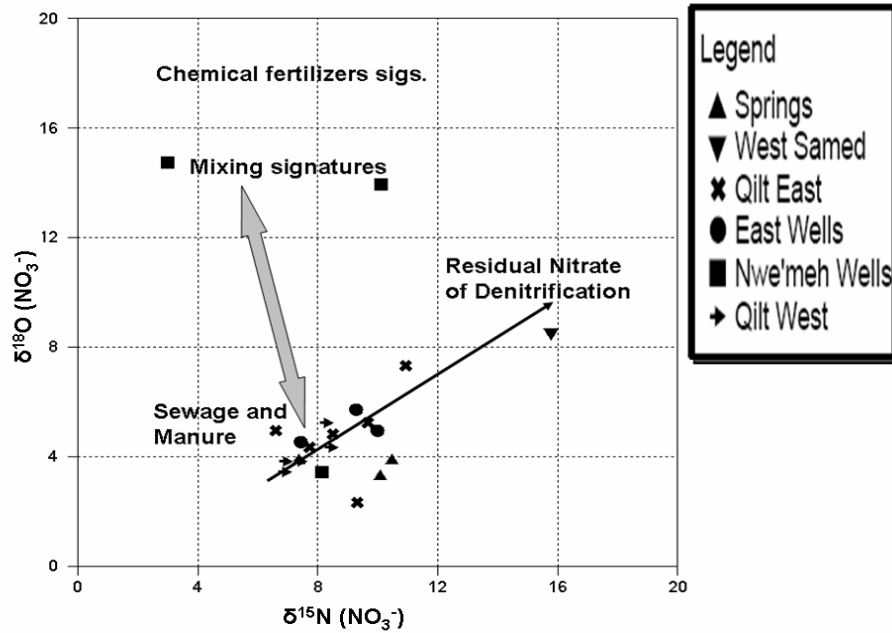


Fig. 38: $\delta^{15}\text{N}_{\text{nitrate}}$ vs. $\delta^{18}\text{O}_{\text{nitrate}}$, most of the isotopic signatures lay within the range of sewage and manure with slight denitrification process. 2 wells show a mixing signature of fertilizers with other sources

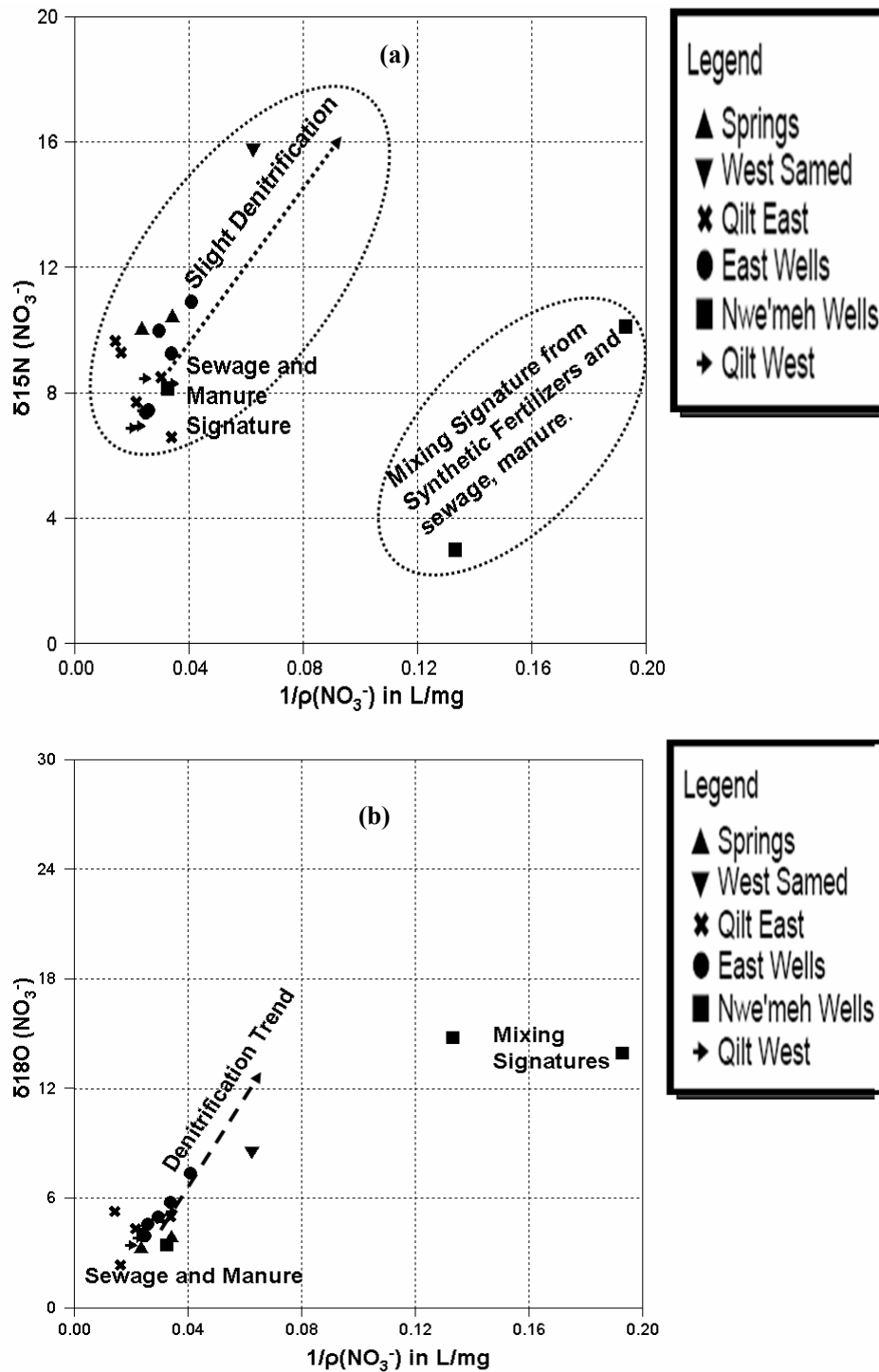


Fig. 39 a, b: $1/\rho[\text{NO}_3^-]$ in L/mg vs. $\delta^{15}\text{N}_{\text{nitrate}}$ and $\delta^{18}\text{O}_{\text{nitrate}}$, most of the wells and springs show no significant differences within the isotopic signature, except in Samed well where it shows low nitrate level with more enriched signature, which reflect a denitrification process. Jericho Nuwe'meh north wells shows low nitrate concentration with a higher $\delta^{18}\text{O}_{\text{nitrate}}$ signatures which reflect a mixing signature from other sources.

4. 4. Sulphur Isotopes

The isotopic components of $\delta^{34}\text{S}$ and $\delta^{18}\text{O}$ in sulphate from both sampling times, as well as the concentrations of sulphate are shown in Table 8. The eastern wells show sulphate concentrations that vary between 100-320 mg/l and chloride concentrations between 800 to 1800 mg/l, while the wells to the west are less mineralized between 20-90mg/l for sulphate and 100-750 mg/l for chloride. The isotopic signatures show the same trend in both sampling periods, where no significant differences have been observed in both period of sampling (Fig. 40 and 41).

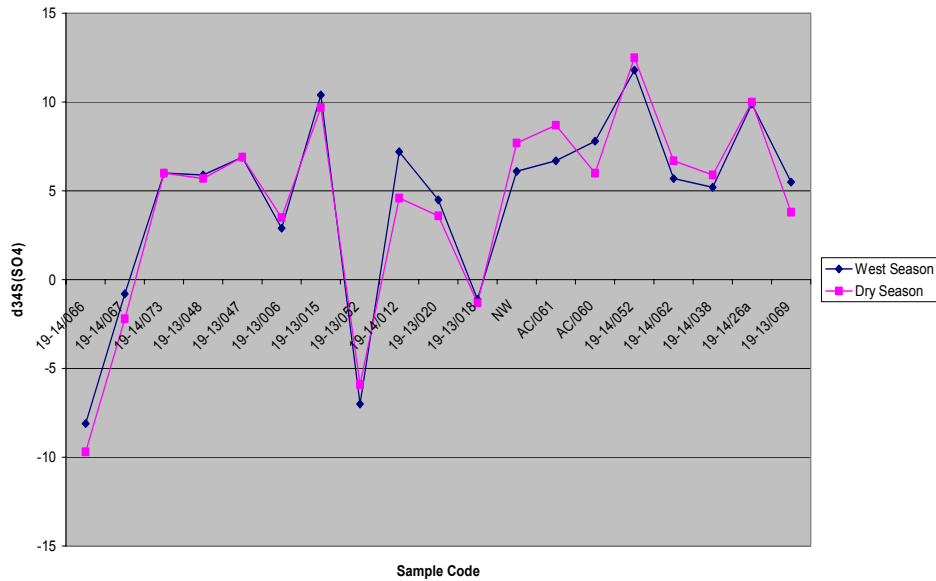


Fig. 40: Variation of $\delta^{34}\text{S}$ in sulphate between wet and dry season.

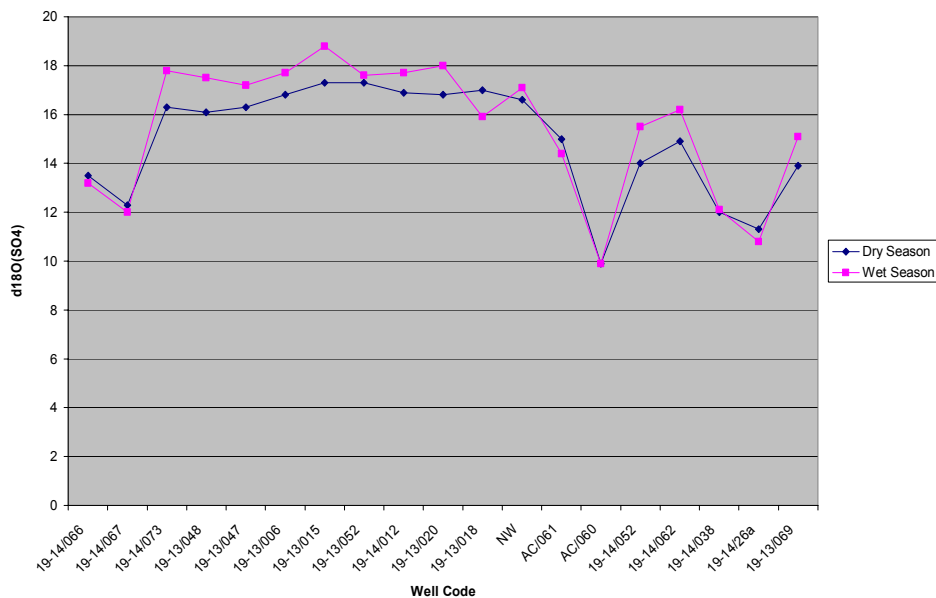


Fig. 41: Variation of $\delta^{18}\text{O}$ in sulphate between wet and dry season.

Table 8: The concentration of sulphate mg/l, and the isotopic signatures of S and O in dissolved sulphate in groundwater in wet and dry seasons.

Site	Well Code	Dry Season			Wet Season		
		SO ₄ ⁻² (mg/l)	δ ³⁴ S _(SO4)	δ ¹⁸ O _(SO4)	SO ₄ ⁻² (mg/l)	δ ³⁴ S _(SO4)	δ ¹⁸ O _(SO4)
Arab Project66 (East)	19-14/066	300.9	-9.7	13.5	285	-8.1	13.2
Arab Project67 (East)	19-14/067	183.4	-2.2	12.3	221	-0.8	12
Arab Project73 (East)	19-14/073	95.9	6.0	16.3	111	6	17.8
Fahmi Nahas48 (Qilt West)	19-13/048	70.0	5.7	16.1	82.7	5.9	17.5
Fahmi Nahas47 (Qilt West)	19-13/047	77.2	6.9	16.3	82.2	6.9	17.2
Sabiru Rantizi (Qilt East)	19-13/006	117.6	3.5	16.8	153	2.9	17.7
Fahed Hishmi (Qilt East)	19-13/015	60.8	9.7	17.3	62.1	10.4	18.8
Zuhdi Hashwa (Qilt East)	19-13/052	166.0	-5.9	17.3	194	-7	17.6
Salah Arouri (Qilt West)	19-14/012	59.2	4.6	16.9	64.5	7.2	17.7
Basil Husaini20 (Qilt West)	19-13/020	110.1	3.6	16.8	120	4.5	18
Basil Husaini18 (Qilt West)	19-13/018	58.6	-1.3	17.0	71.4	-1.1	15.9
Ibrahim Daek (Qilt East)	NW	167.7	7.7	16.6	189	6.1	17.1
Iron Factory (Qilt East)	19-13/26a	90.0	-5.1	3.3	N D	N D	N D
Ein Sultan (West)	AC/061	17.2	8.7	15.0	24.1	6.7	14.4
Ein Dyouk (West)	AC/060	16.7	6.0	9.9	23.8	7.8	9.9
Awni Hijazi (East)	19-14/052	72.1	12.5	14.0	76.5	11.8	15.5
Saeed Aladeen (North)	19-14/062	40.6	6.7	14.9	43.5	5.7	16.2
Mohammed Masri (North)	19-14/038	39.6	5.9	12.0	44	5.2	12.1
Samed (West)	19-14/26a	22.6	10.0	11.3	20.9	9.9	10.8
Arab Project69 (East)	19-13/069	103.8	3.8	13.9	109	5.5	15.1
Abdallah Araikat (North)	19-14/049	92.7	9.5	12.7	N D	N D	N D
Awn Hijazi	19-14/37	N D	N D	N D	117	9.8	18.6
Saleem Nimmari	19-13/49	N D	N D	N D	66.2	10.9	17.8
Qasir Hisham	19-13/003	N D	N D	N D	52.6	9.6	17.3
Bail Hussaini22	19-13/22	N D	N D	N D	222	-1.1	15.4
Mahmud Akramawi	19-13/50a	N D	N D	N D	109	-0.2	-3.8
Bail Hussaini21	19-13/21	N D	N D	N D	172	4.8	17.5

*N D: no data available (no sample was taken)

The δ³⁴S values of sulphate eluted from the Lisan samples J04-X, J03-I, J03-Z and J04-Q range from 9.8‰ to 16.6‰, while δ¹⁸O vary around 16‰. In contrast, the

sulphate for the two Samra samples J04-Y and J04-Z are more depleted with $\delta^{34}\text{S}$ signatures of 6.9 and 9.1 ‰ and 1.4 and 9.1 ‰ for $\delta^{18}\text{O}$. Most of the samples including springs and wells range between -2.2 to +12.5‰ in $\delta^{34}\text{S}$ and +3.3 to +17.3 ‰ in $\delta^{18}\text{O}$ which is close to the eluted sulphate from the Lisan and Samra formation (Fig. 42). However, the wells laying further to the east and south east, particularly the Arab project wells (highly brackish water signatures), show a high depletion in $\delta^{34}\text{S}$ to -10 ‰ in parallel with high sulphate concentrations.

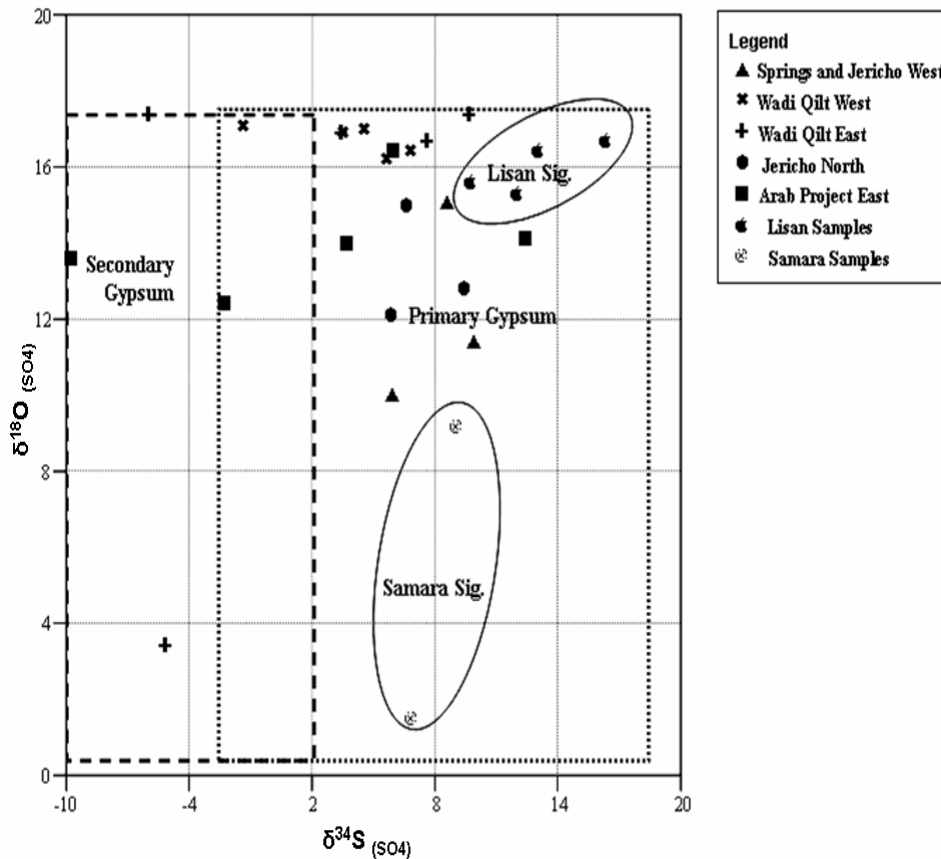


Fig. 42: The isotopic signatures of sulphate in groundwater and in eluates from solid samples. Primary sulphate dissolution from the Lisan and partially Samra formation are enriched in $\delta^{34}\text{S}$ and $\delta^{18}\text{O}$, while disseminated sulphate from secondary gypsum and oxidized pyrite has more depleted signatures.

The isotopic signatures of sulphate from groundwater samples could be signatures of Lisan, Samra and flooding water. High sulphate concentration in the groundwater from the Pleistocene aquifer is mainly a result of Lisan sediment dissolution which contributes to the system in a form of salt leachate (Marie, 2001).

The in situ water rock interaction is considered one of the main contributors in the process of salinisation, where the isotopic signature of $\delta^{34}\text{S}_{\text{SULPHATE}}$ and $\delta^{18}\text{O}_{\text{SULPHATE}}$ for the most of samples are coincident within the range of the solid samples signature (Fig. 42). These reflect dissolution of sulphate from Lisan gypsum and anhydrite. The seepage water from the upper surface runoff and irrigation back flow infiltrates through the Lisan and Samra layers forming a saline leachate (relatively less chloride contents) that contains sulphate with positive $\delta^{34}\text{S}_{\text{SULPHATE}}$ signatures (Fig. 43).

However, some wells in the eastern part of the study area shows more depleted sulphur signatures which reach -10‰. These depleted signatures show an additional sulphate source.

Gavrieli et al. (1998), reported a range between 14-28‰ in $\delta^{34}\text{S}$ signature for the primary gypsum layer in Lisan, and more depleted $\delta^{34}\text{S}$ signature for the disseminated secondary gypsum within the layers of the Lisan, which reach -26 ‰. Thus the obtained depleted values in this study could be mixed signatures between these sulphates from the two gypsum sources. Farber et al. (1989), also suggested a mixing between two different sulphate sources with mixed $\delta^{34}\text{S}$ signatures in the southern Jordan valley, they distinguish between a hypersaline brine with a signature of 6-10‰ and a sulphate rich groundwater of >200 mg/l with depleted signature of -17‰ in Wadi Malih further to the north of Jericho. However, the results from the groundwater in Jericho don't reflect any influence or a mixing between such two sources.

In the west and middle of Jericho data show positive signatures, bearing the signatures of eluted solid samples of Lisan but with relatively low chloride content and high Na/Cl, Br/Cl molar ratios (Khayat et al., 2005), that couldn't reflect the presence of the suggested saline effluent. Moreover, the groundwater which show more depleted $\delta^{34}\text{S}$ signatures in the east contain a relatively high chloride content of more than 1800mg/l and SO₄ concentration reach to 320 mg/l with Br/Cl, Na/Cl molar ratios of .006 and 0.4 respectively (Khayat et al., 2005). These different signatures in the west and the east of the study area and the differences in solutes contents and molar ratios suggest two different inputs of sulphate to the system with a degree of mixing between them (Fig. 43). In such case the isotopic signatures couldn't definitely confirm the sources of any estimated sulphate rich brine.

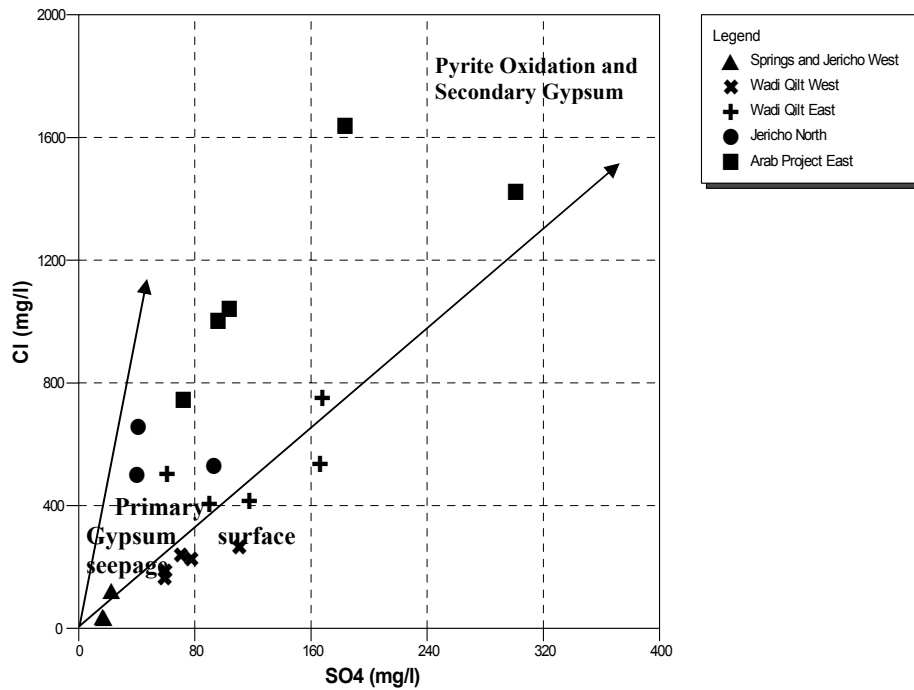


Fig. 43: Chloride vs. SO_4^{-2} in mg/l. The figure shows related to chloride content two different sources for sulphate.

The relation between sulphate and $\delta^{34}\text{S}$ (Fig. 44) can appraise these two inputs, where some of the signatures especially from those wells of Arab project have high depleted values with high sulphate content.

This contradictory relation, in which sulphate values getting higher and are relatively depleted in $\delta^{34}\text{S}$ signatures, reflect a mixing signature of the secondary gypsum and primary gypsum dissolution, which could be leached upward under heavy abstraction, and upper surface leachate of primary gypsum. The previous hydrochemical study shows that the water samples from some of the eastern wells were relatively enriched with iron (Khayat et al., 2005), which can give an indication for additional possible source of sulphate that originate from pyrite oxidation source (Clark, 1997). The groundwater in the wells to the east might interact with deeper pyrite rich water (highly chloride content), which is in contact with the deep salty rocks or in aquiclude chamber for a prolonged period of time. This water is welling up from an anoxic environment holding the sulphide, which is oxidized to sulphate in the shallow environment of the upper aquifer. The given depleted signatures of $\delta^{34}\text{C}_{\text{SULPHATE}}$ and $\delta^{18}\text{O}_{\text{SULPHATE}}$ in some wells to the east, suggest a sulphate that is

derived from disseminated secondary gypsum and/or from other sulphur compounds coning up from a deep anoxic environment and being oxidized in the shallow aquifer.

Both of the above mentioned sources give the indication about an interaction between the upper groundwater layer and a deeper saline layer.

On the other hand, the seepage water from the upper surface runoff and irrigation back flow infiltrate within the Lisan and Samra layers forming a saline leachate (relatively less chloride contents) that contains sulphate with positive $\delta^{34}\text{S}_{\text{SULPHATE}}$ signatures (Fig. 45).

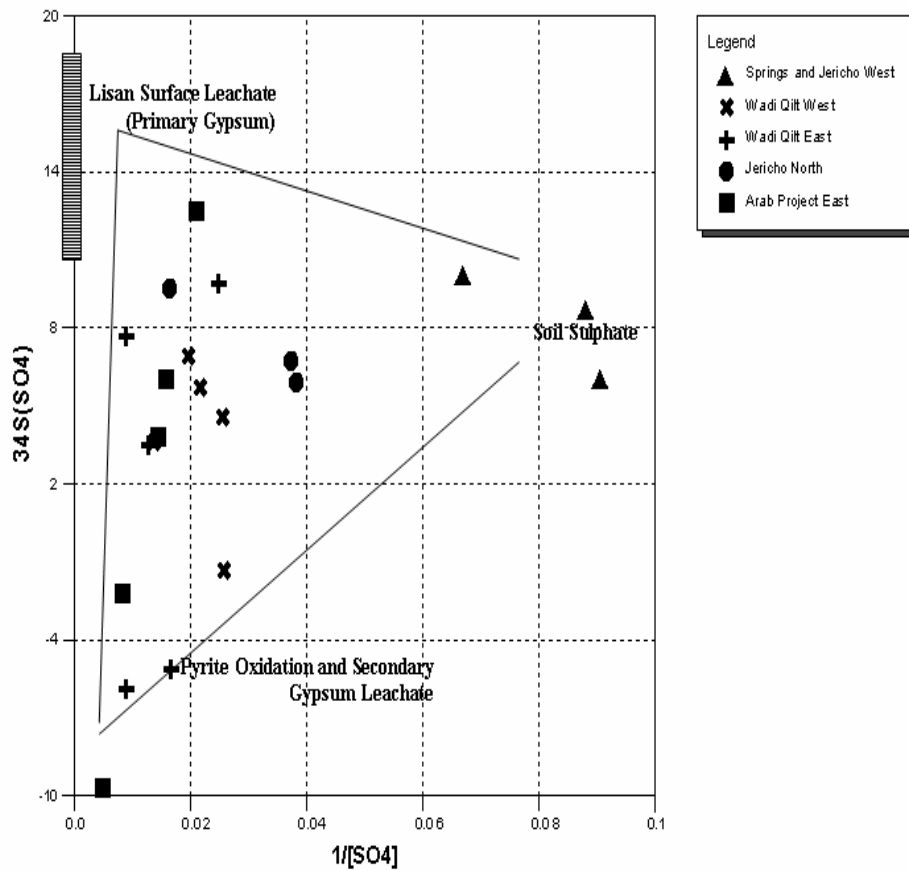


Fig. 44: $\delta^{34}\text{S}_{\text{SULPHATE}}$ vs. $[\text{SO}_4]^{-1}$. The depleted $\delta^{34}\text{S}_{\text{SULPHATE}}$ values indicate pyrite oxidation while the enriched $\delta^{34}\text{S}_{\text{SULPHATE}}$ values indicate sulphate from primary gypsum in Lisan and Samra formations.

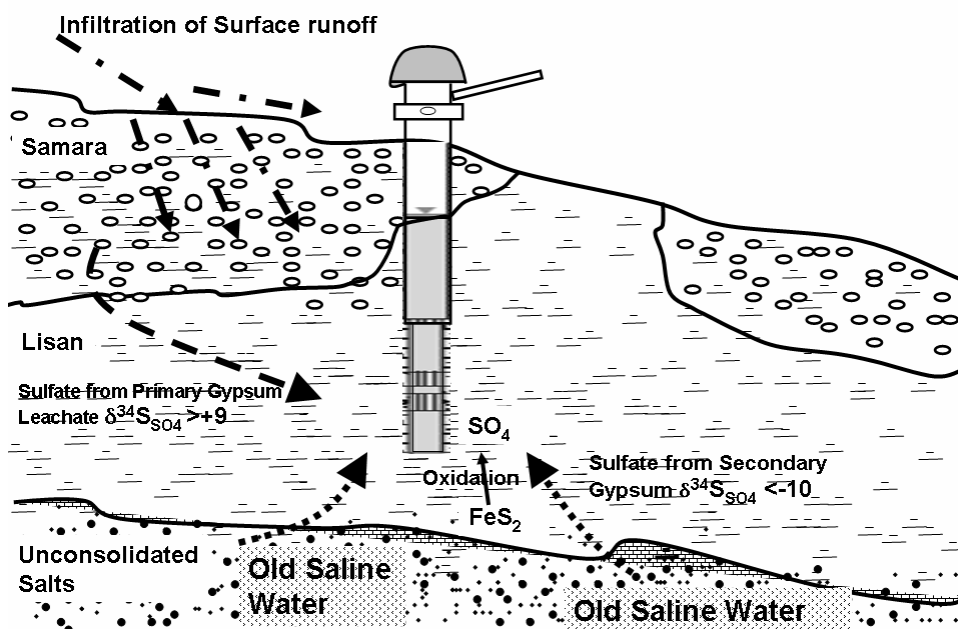


Fig. 45: Illustration for the main two different sources or contribution mechanisms of sulphate into the groundwater from Pleistocene aquifer in Jericho area.

4. 5. Carbon Isotopes ($^{13}\text{C}/^{12}\text{C}$)

The concentrations of bicarbonate, as well as the isotopic signatures of $\delta^{13}\text{C}$ in dissolved inorganic carbonate from groundwater in wet and dry seasons are shown in Table 9. The atmosphere is the smallest global reservoir of carbon. Craige and Keeling (1963), and Friedli et al. (1986), identified the isotopic signature $\delta^{13}\text{C}$ of atmospheric CO_2 about -6.4‰ . This value nowadays has been changed to slightly more negative values due to the burning of fossil fuel.

Normally when water infiltrates to the subsurface it equilibrates with soil CO_2 which produces from the plant root respiration and bacteria oxidation. The soil CO_2 has normally a higher partial pressure than atmospheric CO_2 and gives the CO_2 a significant depleted isotope signature, which follows the photosynthesis of plants and the resulting carbon.

In most cases this signature is around -25‰ because plants with C-4 cycle of photosynthesis is outweighed. In regions where predominantly C-3 plants like grass or maize is growing the CO_2 has a $\delta^{13}\text{C}$ signature of around -16‰ (Kalin, 1996).

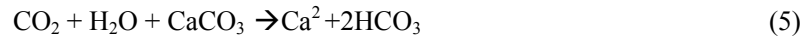
Table 9: The concentration of HCO₃⁻, Sr and Rb in mg/l, and the isotopic signatures of δ¹³C in dissolved inorganic carbonate from groundwater in wet and dry seasons.

Site	Well Code	Dry Season		Wet Season		Sr (mg/l)	Rb (mg/l)
		CO ₃ ⁻² (mg/l)	δ ¹³ C _(CO3)	CO ₃ ⁻² (mg/l)	δ ¹³ C _(CO3)		
Arab Project66 (East)	19-14/066	439,2	-9,56	409,31	-9,3	3,173	0,06
Arab Project67 (East)	19-14/067	366,61	-9,1	405,04	-9,6	2,753	0,07
Arab Project73 (East)	19-14/073	405,65	-10,2	386,13	-10,2	1,729	0,05
Fahmi Nahas48 (Qilt West)	19-13/048	347,7	-10,2	317,81	-11,3	1,896	0,01
Fahmi Nahas47 (Qilt West)	19-13/047	355,02	-10,7	322,69	-10,7	2,054	0,01
Sabiru Rantizi (Qilt East)	19-13/006	376,37	-10,5	342,21	-10,2	3,415	0,01
Fahed Hishmi (Qilt East)	19-13/015	378,81	-9,7	337,33	-10	1,775	0,03
Zuhdi Hashwa (Qilt East)	19-13/052	369,05	-9,84	349,53	-9,4	3,358	0,02
Salah Arouri (Qilt West)	19-14/012	417,85	-10,6	342,21	-10,4	1,814	0,01
Basil Husaini20 (Qilt West)	19-13/020	349,53	-9,3	317,2	-10,8	1,366	0,01
Basil Husaini18 (Qilt West)	19-13/018	304,39	-10,7	292,8	-11,3	1,226	0,01
Ibrahim Daek (Qilt East)	NW	376,37	-9,8	369,05	-10,1	2,241	0,03
Iron Factory (Qilt East)	19-13/26a	259,25	-8,9	N D	N D	4,308	N D
Ein Sultan (West)	AC/061	295,24	-12,4	266,57	-12,8	0,1176	BDL**
Ein Dyouk (West)	AC/060	287,31	-12,7	293,41	-13	0,117	BDL**
Awni Hijazi (East)	19-14/052	380,03	-10,2	417,85	-10,6	2,654	0,03
Saeed Aladeen (North)	19-14/062	364,17	-11,1	393,45	-12,5	1,032	0,02
Mohammed Masri (North)	19-14/038	380,03	-11,6	403,21	-12,1	1,116	0,02
Samed (West)	19-14/26a	437,37	-12,1	412,97	-12,8	0,4578	0,01
Arab Project69 (East)	19-13/069	418,46	-9,57	415,41	-9,2	1,809	0,05
Abdallah Araikat (North)	19-14/049	364,78	-11,9	N D	N D	1,127	ND
Awn Hijazi	19-14/37	N D*	N D	383,69	-10,9	1,867	0,04
Saleem Nimmari	19-13/49	N D	N D	385,52	-9,7	1,126	0,03
Qasir Hisham	19-13/003	N D	N D	349,53	-12,1	1,42	0,02
Bail Hussaini22	19-13/22	N D	N D	344,65	-10	2,178	0,03
Mahmud Akramawi	19-13/50a	N D	N D	406,26	-7,4	1,946	0,03
Bail Hussaini21	19-13/21	N D	N D	349,53	-9,8	1,764	0,03

*N D: no data available (no sample was taken)

**BDL: below detection limit.

Dissolution of soil CO_2 in the infiltrating rain water normally produces carbonic acid, thus lowering the pH, and increases the weathering capacity of the soil water; mainly it dissolves the soil limestone according to the following formulas:



Marine carbonates have $\delta^{13}\text{C}$ content similar to the reference VPDB with a signature of $\sim 0\text{‰}$. The carbonate signature of the infiltrated water within the soil profile will have a $\delta^{13}\text{C}$ signature according to their origin (marine, caliche, soil). The signature of the soil varies as mentioned above according to area condition and the vegetation. The Jerusalem Ramallah mountain area (the Upper Cretaceous formation west of the study area) is considered as fertile area with a lot of precipitation and high soil organics. In such case the carbonate isotopes signature for the infiltrated water in the soil profile from this area is originated from marine ($\sim 0\text{‰}$), caliche ($\sim -7\text{‰}$), organic ($\sim -22\text{‰}$) or an intermediate signature by mixing of these sources ($\sim -12\text{‰}$). This signature can be found in the groundwater samples of the springs freshwater end member.

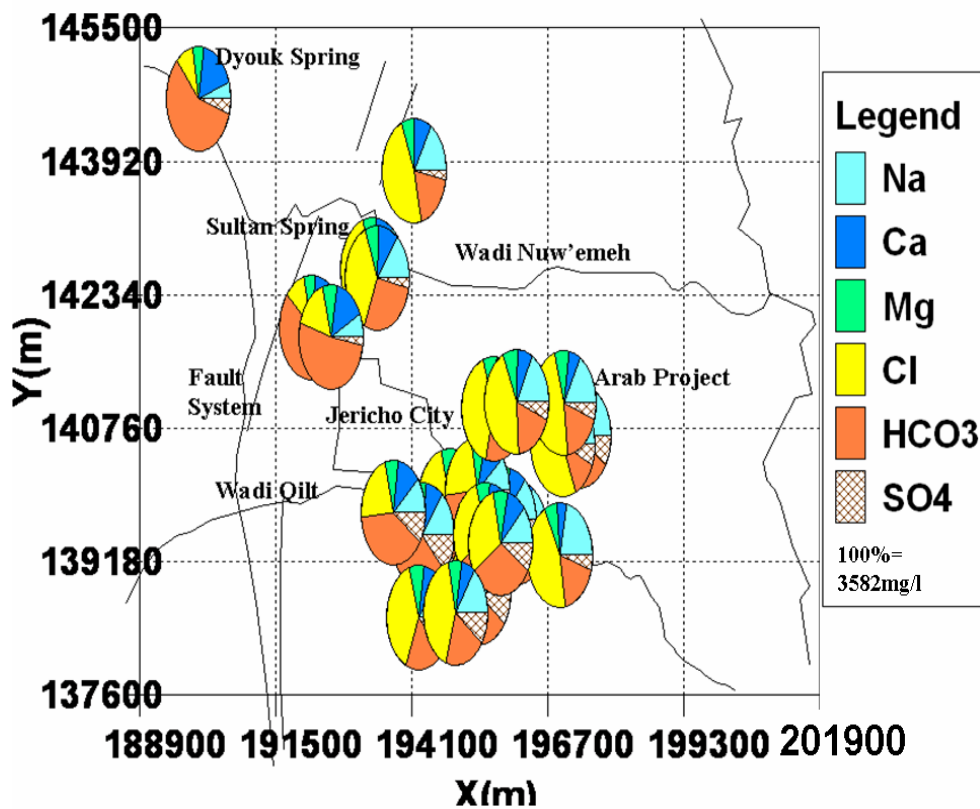


Fig. 46: Distribution of cations and anions from different sampling sites.

Kaline (1996) and El-Naser & Subah (2000) were measuring and investigation the groundwater system on the eastern side of the Jordan River using $\delta^{13}\text{C}$ and $\delta^{14}\text{C}$. They estimated the $\delta^{13}\text{C}$ of soil CO_2 in the Jordan valley area, as a semi-arid region between -12 to -16‰ (Kalin, 1996), while the $\delta^{13}\text{C}$ in the sediments around Dead Sea showed values of ~ 0 to +1 (El-Naser & Subah, 2000). Therefore, the isotopic signature for the infiltrated runoff water that feed the shallow Pleistocene aquifer is a function of (marine carbonate sediments $\sim +1\%$, soil $\text{CO}_2 \sim -16\%$ or an intermediate signature by mixing of these sources ($\sim -8 \pm 1 \%$). This signature reflect the isotopic signature of $\delta^{13}\text{C}$ in the brackish water end member of Arab project wells in the east which was also between -9 to -7‰. The $\delta^{13}\text{C}_{(\text{DIC})}$ signature influenced by various factors according to the system condition where the dissolution of minerals occur. In an open system more exchange of CO_2 between the DIC and the soil atmosphere occurs, whereas if the dissolution take place under closed system, then the $\delta^{13}\text{C}$ will be depleted by DIC from the carbonate mineral source. The combination of Pco_2 , concentration of DIC and $\delta^{13}\text{C}_{(\text{DIC})}$ can provide an indication of recharge conditions (Clarck & Fritz, 1997). In an open system more exchange of CO_2 between the DIC and the soil atmosphere occurs, whereas if the dissolution takes place under closed system, then the $\delta^{13}\text{C}$ will be depleted by DIC from the carbonate mineral source. The combination relation between the Pco_2 , concentration of DIC and $\delta^{13}\text{C}_{(\text{DIC})}$ can provide an indication of recharge conditions (Clarck & Fritz, 1997).

In the study area, the isotopic signatures $\delta^{13}\text{C}_{(\text{DIC})}$ for the springs were about -12‰ which bearing the carbonate mineral signature, whereas the HCO_3 values for these samples were the highest in proportion to other TDS from the same sample with a portion of 75% of TDS (Fig. 46). The recharge for the springs, as shown in section 4.2., has different infiltration mechanism: as a direct outcrop from the upper mountain aquifer, where the groundwater infiltrate directly through the soil and reach the deep saturated zone before it begins desolving calcite, where CO_2 lost occurs, as it needed for the dissolution process) and HCO_3 is produced (Equ. 5). There will be no CO_2 soil replenishment at this deep aquifer as the dessolution proceed, and the ammount of dissolution and the final DIC concentration is lower. This can be shown by the high mineralization of groundwater from the springs and the high pH as well. This process also can confirm the karstification character of the upper mountain aquifer, where the infiltrartion process to the water table is fast.

“Samed” well 19-14/26a and the north Nuwe’meh wells, very adjacent to the springs system in the west, show also the same trend with higher HCO_3^- with $\delta^{13}\text{C}$ signatures close to these from the springs with calcareous effect (Figs.46 and 50), which emphasize that there is a leakage from the calcareous water of the mountains aquifer, that feed the spring, to the shallow aquifer. This suggests strongly the contribution of the irrigation backflow from the channels drained from Sultan spring or means that the method of Golani (1972) about the impervious fault is not definitely correct (See section 2.5.2.2).

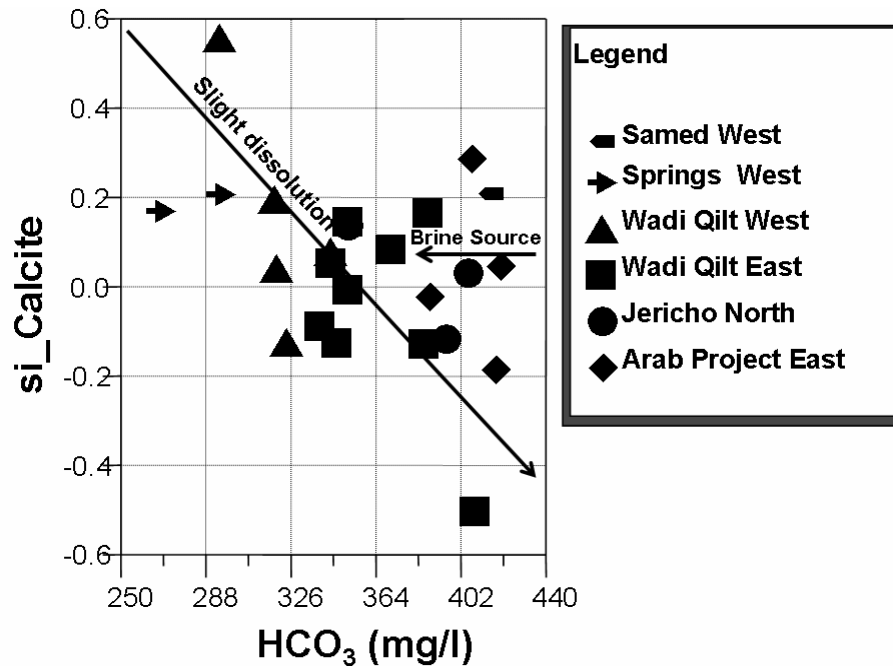


Fig. 47: The relative increase in HCO_3^- vs. the decrease of calcite saturation from west to east, the increase of the HCO_3^- caused mainly by the brine water source in the east in addition to the dissolution of calcite, which act as a buffer for the system.

The samples from the shallow aquifer further to the east show different behavior with regard to carbon system. The shallow nature of the aquifer makes its unsaturated zone typical for gas and aqueous phases to be coexist. Much more calcite can be dissolved due to continuous replenishment of CO_2 and some HCO_3^- released, thus the DIC equilibrium concentration from these wells is much higher. This dissolution continues slightly along the flow path from the wells in the Wadi Qilt West to the Arab Project wells in the east faced by additional HCO_3^- of the brine water source (Fig. 47). The pH gradually gets lower and lower due to CO_2 replenishment (Fig. 48). The additional input of salts which are coming from Lisan Leachate with the $\delta^{13}\text{C}$ signature of -9 to -7‰, and mainly rich in Mg, Na and Cl, initiate other mineralization

forms, mainly dolomitization in which some of the precipitated calcite undergoes a dolomitization process resulting in a surplus Ca release (Khayat et al., 2005).

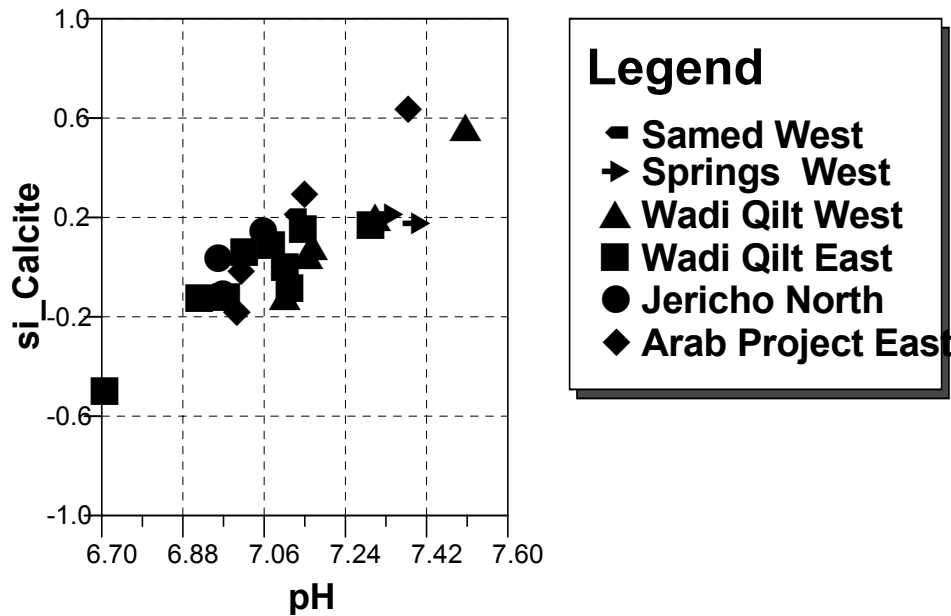


Fig. 48: Decreasing pH due to CO₂ replenishment accompanied with calcite dissolution in the shallow wells from west to east.

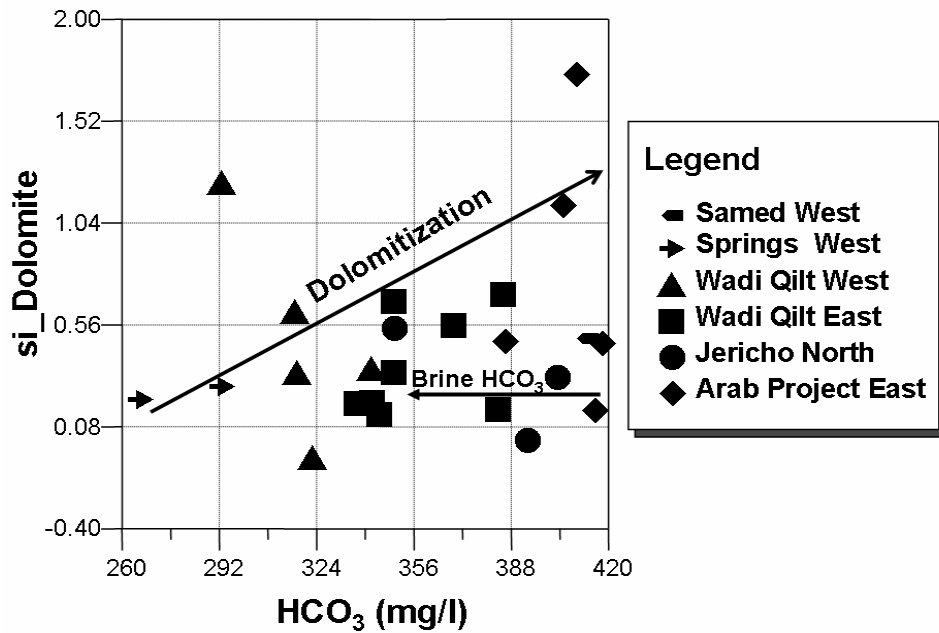
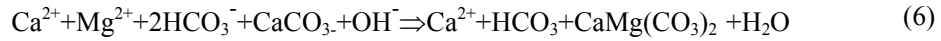


Fig. 49: The increase of bicarbonate vs. slight increase of the dolomite saturation from the west to east of the studied aquifer, in addition to this HCO₃ from up welled deep brine in the east.

The high Mg concentration shown by the shallow aquifer indicates the presence of dolomite and magnesium calcite in the aquifer. The loss of some calcite by

dolomitization (Equ. 6) has a minor effect on the $\delta^{13}\text{C}_{(\text{DIC})}$, the gain of dolomite add carbonate with $\delta^{13}\text{C} \sim 0\text{‰}$ to the DIC pool which is lead to dilution of DIC and give the above this typical $\delta^{13}\text{C}_{(\text{DIC})}$ signature for the infiltrated water in the shallow aquifer (Fig. 49 & 50).



Many factors play a role in the changes of DIC pool; these are mainly related to the suggested sources of salinity described in the previous section, the lithological formation of Lisan and Samra with brackish Leachate, in addition to anthropogenic influences in this agricultural and populated area. However it is difficult to show the importance of the last factor on the carbonate system in the area.

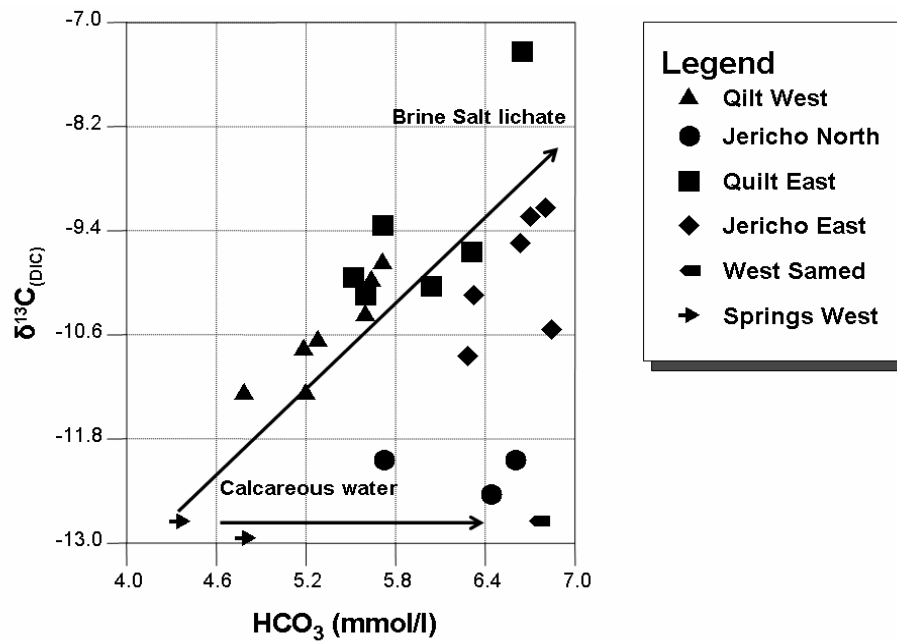


Fig. 50: $\delta^{13}\text{C}$ vs. bicarbonate in mmol/l, the figure shows two main signatures the depleted one which is represented in the calcareous water from the spring and affected the adjacent wells and more enriched signature which is bearing this signature of brine Leachate in sedimentary aquifer.

In this study, trace elements, rubidium and strontium (alkaline earth metals), were also used to differentiate between the effects of carbonate minerals transformations and salt Leachates (Table 9).

The NO_3^- was also used as an indicator for the anthropogenic influences within the aquifer. Rubidium is the twenty-third most abundant element in the Earth's crust. It

occurs in the minerals pollucite, carnallite, leucite and lepidolite, from which it is recovered commercially, as well as potassium minerals and brackish waters which also contain this element.

The Rb normally precipitates in a very late stage of the evaporation sequence forming the above mentioned minerals. The presence of free Rb in the groundwater can give an indication of the dissolution of the salts minerals in the groundwater (Saline Water). On the other hand, strontium comprises about 0.025 percent of the Earth's crust. Although it is widely distributed with calcium, and carbonate minerals, there are only two principal ores of strontium alone, celestite (SrSO_4) and strontianite (SrCO_3).

The presence of high strontium in the groundwater can give an indication of elaborated Sr due to demineralization of carbonate minerals. Rb/ CO_3 and Sr/ CO_3 molar ratios were used to trace the effect of mineral salts Leachates which mainly has a highly Rb/ CO_3 ratio in relative to higher Sr/ CO_3 resulted from carbonate minerals transformations (Fig. 51).

The NO_3/Ca molar ratio vs. $\delta^{13}\text{C}$ was also used to trace the anthropogenic influences on the carbon system of the groundwater (Fig. 52); the elaborating Ca also can give an indication about the carbonate minerals dissolution.

Obviously, 3 main factors affect the carbon system in the Pleistocene aquifer:

- The influence of calcareous rock (Cenomanian formation), which affects mainly the springs and adjacent wells in the west and north. This is characterized by low Sr/ CO_3 molar ratio and depleted $\delta^{13}\text{C} \approx -12\%$ (Fig. 51).

- The anthropogenic influence indicated by the low pH value and high NO_3/Rb molar ratio and $\delta^{13}\text{C}$ between -10 and -11‰ (Figs. 48 and 52).

- The salts leachate influence, mainly in the eastern wells, with a high Rb/ CO_3 molar ratio and $\delta^{13}\text{C} \approx -7\%$ (Fig. 51).

- The mineral transformation influences (dissolution, dolomitization), which is characterized by high Sr/ CO_3 molar ratio and $\delta^{13}\text{C} \approx -9\%$ (Fig. 51).

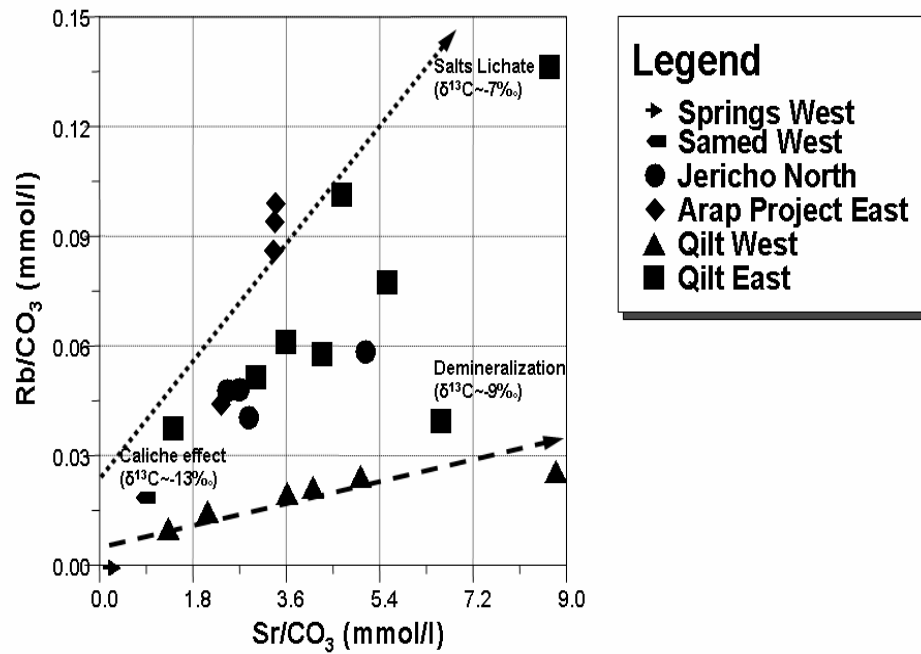


Fig. 51: Sr/CO₃ vs. Rb/CO₃ molar ratios, the figure shows the mixing between three main factors that control the carbon system in the aquifer.

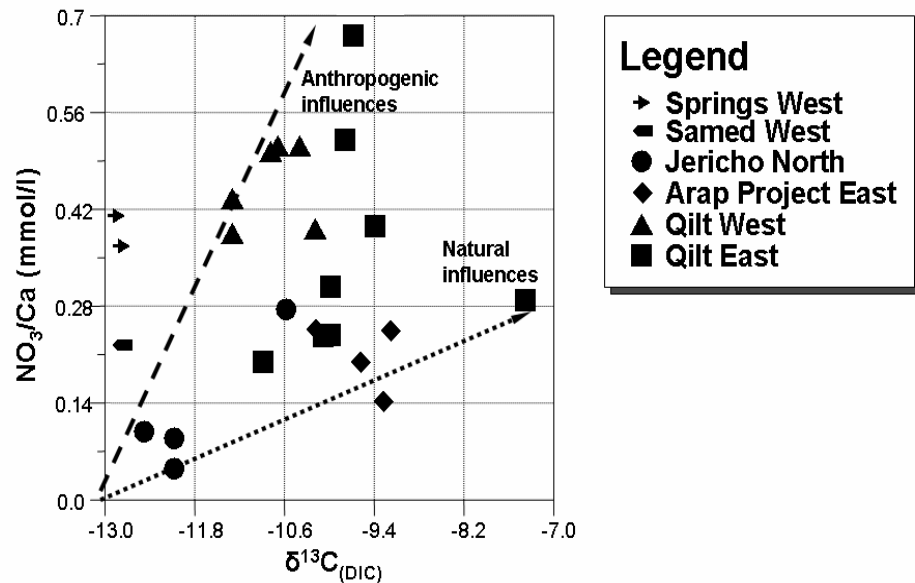


Fig. 52: δ¹³C vs. NO₃/Ca molar ratio, the figure shows two trends with different NO₃ content.

4. 6. Seasonal Variation

The goals of the two seasons sampling study have been to done for measurements quality assurance as well as to evaluate seasonal trends in major minor and trace

element geochemistry in addition to isotopic signatures, with the focus on understanding the behavior of different tracers in the groundwater. The preliminary results shown in this study indicate that the majority of chemical constituents, including parameters such as pH and specific conductivity, remained fairly constant throughout this study. These data suggests that the groundwater has not been influenced by seasonal variations in the local water table heights, and that the “time dependent” oxidation reduction reactions of primary sulphur and nitrogen compounds has no big role in variations in groundwater chemical contents in the sampled groundwater.

The isotopic signatures behave always the same except the signatures of deuterium and the isotopes of nitrate. The seasonal variation of enriched deuterium signatures put forward possibility of a fractionation process which only effects on deuterium. Such process is defined as ‘ultrafiltration’. Hoefs (2004) shows that the hydrogen isotopes fractionation is affected by the absorption of water on mineral surfaces due to the tendency for clay and shales to act as semi permeable membranes. The fractionation of hydrogen isotopes occur during this process in such a way that the residual water will be enriched in deuterium due to its preferential adsorption. During the continuous recharge in wet season the increasing of hydraulic pressure pushing the older water to the zone of the water uptake. This water which is enriched in deuterium by ultrafiltration process drilled out along the aquifer, replaced by the new recharge water.

The isotopic signatures of nitrate show in some wells a slight denitrification process. In the Samed well where this effect could be observed, less than 10% of the total nitrate content was denitrified. This process could clearly be identified by the samples of the dry season samples, where there was nearly no recharge and thus the groundwater is persist in the reservoir for the months of the dry season.

CHAPTER 5: GIS BASED HYDROSYSTEM MODEL

5.1. Introduction

The implementations of analytical and numerical methods involving geometrical description of geo-systems with the application of numerical meshes were used to obtain solutions to a mathematical model of groundwater flow or solute transport. Innovative application of CAD-Systems in combination with computer aided modeling of such systems provides a user friendly powerful tool for the often complex geometrical descriptions necessary for comprehensive modeling of the dominant processes.

Numerical modeling has been the primary tool for analyzing the interaction of groundwater and surface water since the mid-1960s. Most models continue to use a simple Darcy calculation (where discharge = hydraulic conductivity * hydraulic gradient * cross-sectional area) as well as highly idealized stream geometry, to transfer water (seepage) through the stream sediments based on head differences between the surface water and groundwater.

More efficient methods were also developed in the beginning of sixties, where the finite volume was initially applied to the flow of the fluids in petroleum reservoirs. This method was applied then to the groundwater flow and solutes transport in the middle of sixties (Aschroft et al., 1962; Remson et al., 1965).

By the early of 1970's the finite element method was first used to solve groundwater flow and solute transport problem (Zienkiewicz et al., 1966; Price et al., 1968; Zienkiewicz et al., 1971). With finite element method, irregular shape boundary, an-isotropic and heterogeneous aquifer properties can easily incorporated to the numerical model.

Cooley (1983) developed a finite-element code that was used by Winter (1983) to evaluate the dynamic groundwater flow conditions caused by nonuniform areal distribution of recharge directly adjacent to surface-water bodies. Using the model for 2-dimensional vertical sections, the study indicated that recharge is initially focused directly adjacent to the surface water. These near-shore flow paths cause increased flow where groundwater seeps into the surface water, and may cause flow to reverse where surface water seeps out to groundwater prior to recharge. Tracy & Marino (1987) developed a Galerkin finite-element code for simulating the interaction of

surface water with a variably saturated groundwater system. The model solves for the transient position of surface-water stage and the distribution of the phreatic surface (water table) in the porous medium, as well as providing estimates of seepage rates.

Numerical models have been used as routine analytical tools for numerous field studies in virtually every conceivable hydrogeologic setting and for virtually all scales of systems.

The application of Geographical Information Systems (GIS) in combination with computer aided modeling of Hydrosystem becomes more and more important for a detailed process simulation. Hydrosystem in subsurface are very complex systems described by many parameters with spatial data distributions, and their realistic modeling is based on precise calculations, which absolutely need precise located data. The advantage of Geographical Information Systems is that they are able to analyze, edit, and manage such definite geographic located data.

The section for Geohydrology and Hydroinformatics of the Center for Applied Geoscience at the University of Tübingen concerns with the software engineering of ROCKFLOW. This model enables to calculate complex flow and transport processes of one and more fluid phases in subsurface hydrosystems by the use of finite element and finite volume methods.

The finite element program ROCKFLOW has been developed to simulate complex flow and transport processes of one and more fluid phases in subsurface hydrosystems, combining coupled modules with the method of automatic grid adaptation (Kolditz et al., 1998).

The numerical model used for the simulations is the FE Simulator GeoSys/RockFlow (Kolditz et al., 2003) which are programmed in C and C++ according to object oriented software concepts (Beinhorn & Kolditz, 2004 and Kolditz and Bauer, 2003). The numerical approach is based on the Galerkin finite element method using governing equations given above.

Time derivatives are evaluated by a finite difference scheme. The iterative coupling between the discretized flow and transport equations is realized by a Picard iteration scheme, i.e. actual densities of a new iteration step are calculated from the field variables of the previous iteration step. The code has been tested against benchmarks given in (Kolditz et al., 1998).

Basic modules of GeoSys/ RockFlow are the GeoLib, MshLib, and FEMLib, which can be connected via a Graphical User Interface (GUI). These components are described below as:

5.1.1 GeoLib

Geometric objects of the GeoLib are points, polylines, surfaces, volumes which form domains. All these geometric entities are implemented as C++ classes: CGLPoint, CGLPolyline, CGLSurface, CGLVolume, and CGLDomain. Instances of these objects can alternatively be stored in vectors and lists for convenience and specific purposes. A detailed description of the implementation of GeoObjects is given in Kalbacher et al. (2003b).

5.1.2 MshLib

Currently, the following build-in mesh generators can be used: PrisGen (Kalbacher et al., 2003a), TetMesh (Manabe et al., 2003) as well as open and commercial systems such as gmsh (2004) and gOcad (2004).

The resulting mesh geometry can be manipulated using mesh operations like the mapping operation.

Here a surface object (SFCObj) is being used to relate mesh data to a surface data file such as top or bottom of an additional operation of the MshLib is vertical mesh refinement. All these operations of the MshLib are controlled via GUI.

5.1.3 FEMLib

The FEMLib contains independent units necessary to set up and solve the finite element problem.

As a result of the numerical approximation method described, two sets of algebraic equations were derived. The general form of this equation is:

$$\mathbf{A}_i(t, \mathbf{x}, \mathbf{u}_i, \mathbf{u}_j) \mathbf{u}_i = \mathbf{b}_i(t, \mathbf{x}, \mathbf{u}_i, \mathbf{u}_j) \quad (1)$$

where i, j denote different processes, with \mathbf{A}_i system matrix of process i , t time, \mathbf{x} coordinates, \mathbf{u}_i solution vector (primary variable) of process i , \mathbf{b}_i RHS vector of process i . Dependence of process i on process j means coupling, and dependence of system matrix on solution itself means non-linearity.

5.2. Model Setting

5.2. 1. Aim of the model

The study area (Figs. 18 & 53) included in the GIS project was described in further details in chapter 2.

The Deuterium, Oxygen and Carbon isotopes data in a previous study (see chapter 4.) suggest two possible mechanisms of recharge, the first is the direct diffuse surface infiltration and the infiltration of the water run off in wadis. The data also show that there is a leakage from the Upper Cretaceous aquifer to the Pleistocene one. This leakage could be through the major fault system which separate between Cretaceous and Pleistocene formations, or it caused by an infiltration from irrigation network drained from Sultan spring that also fed by the upper cretaceous aquifer system with CaCO₃ rich water to the west of the area. Moreover, the tritium units reflect a recent groundwater age in the west boreholes in relation to old water age (prior to 1956) of the eastern Arab Project wells. The other sampled wells within the area show in between values. However, the mode of this suggested mixing between the two possible recharge points is still not well known.

A modeling routine was carried out in order to suggest alternatives for a better understanding of the mechanism of recharge and the mixing mode between the possible recharge sources in the aquifer as well as, to build different hydrological scenarios to estimate the effects of the pumping rates and water demand on the water level with respect to abstracted quantity and the time of the year, thus to maintain a sustainable exploitation of the groundwater resources in the study area. The model is constructed as a building block for more future studies about the solutes transport and distribution, which allow to visualizing and further understanding for the mechanism of salinisation. For this purposes, the model will still need further calibration and validation.

The geology of the area is part of the Jordan rift valley geology (see chapter 2). The Pleistocene age formation dominates in Jericho area characterized mainly by Lisan and Samra formations. The sedimentary sequences within the Lisan and Samra formations are covering the study area.

Pleistocene formation is grouped into two main lithological alternative heterogeneous sequences of the gravel and marl. The last with low hydraulic

conductivity and considered as an aquiclude layer, while the gravel and sandstones layer have good hydraulic properties and thus forming a good aquifer media. Despite the fact that from the geological point of view, this alternative sequence varied all over the area, which mean that both lithological units coincident in a lenses each cover a limited part in the profile, where each layer forming certain drained filling via which they partially hydraulically connected. Although 7 alternatives hydraulically connected layers of the mentioned formations were assumed. This assumption based mainly on a real lithological profile for 12 wells in the area using the lithological data that obtained from the Palestinian Water Authorities (PWA), (Khayat et al., 2005). Each similar layer was assumed to be connected by a type of aquifer or aquiclude, according to the hydraulic properties of each layer.

GeoSys/RockFlow scientific modeling software (Kolditz et al., 2004) is used in developing a numerical groundwater flow model within the Pleistocene shallow aquifer system. Based on the groundwater model the recharge mechanisms and the mixing mode between different water sources and water types in the study area are considered.

5.2. 2. GIS Project

Based on the groundwater model the recharge mechanisms and the mixing mode between different water sources and water types in the study area are considered. The hydrogeological conceptual model of the study area is converted to (GIS Project) shape files using the ArcGIS software. All required data for modeling, such as aquifer geometry, boundary conditions, material properties, well positions and pumping rates etc. are kept in the GIS project.

These data can be directly imported to GeoSys for modeling purposes (Kalbacher et al., 2003; Chen et al., 2003).

The study area in the GIS project is shown in the Figure 53:

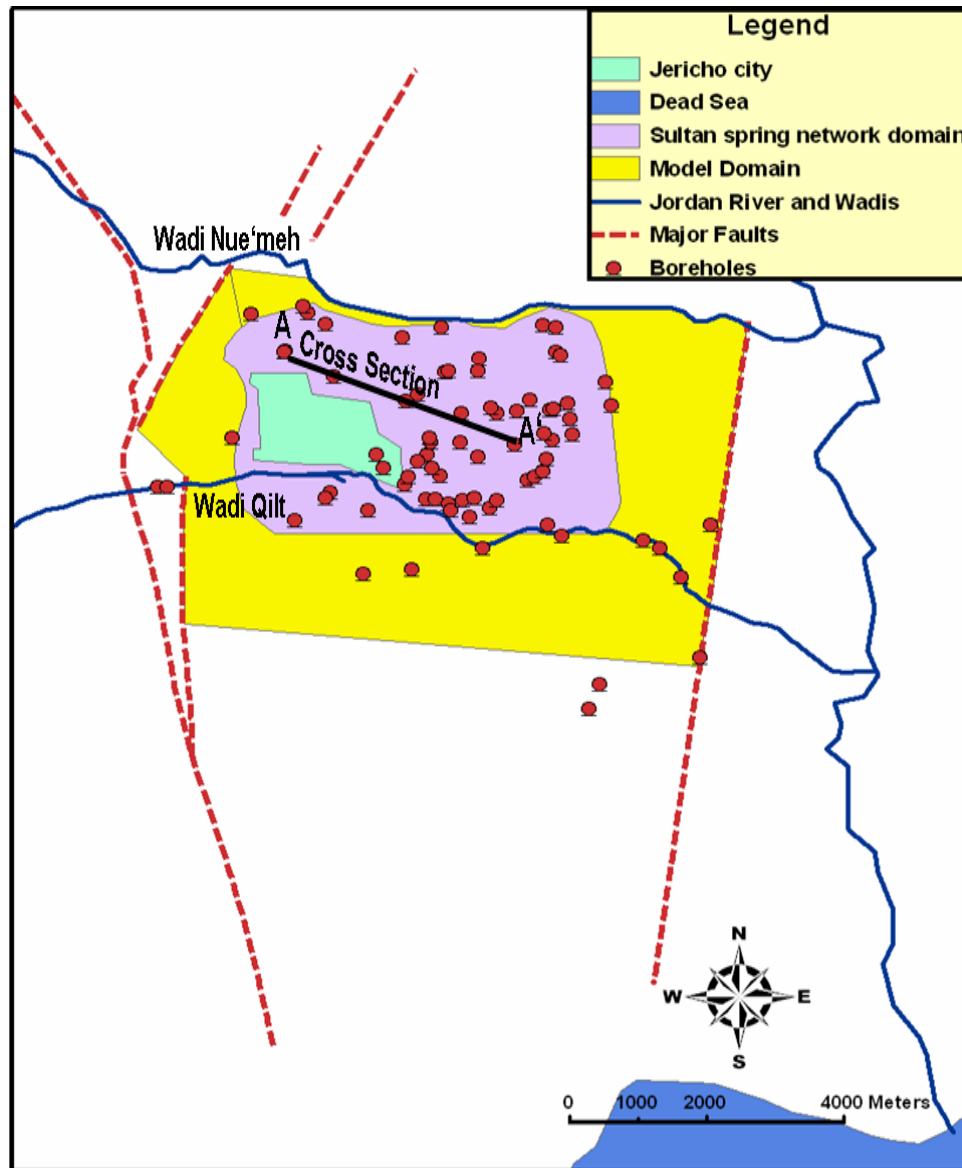


Fig. 53: The modeled area in GIS project, noting the cross section A-A' which shown in Fig. 54.

The GIS project consists of several shape files or layers, these are:

5.2. 2. 1. The layers formations

The alternative layers structure of Marl and Gravel for the first 160 m depth in the Lisan and Samra of the Pleistocene formation were converted to a shape files, where each shape file represent one layer elevation for 12 wells distributed in the area. The minimum layer elevation was set to be 0.5 m especially in the area where the layer forming a closed lenses. (Fig. 54).

5.2. 2. 2. Wadis

The study area is drained eastwards toward Jordan River by two major wadis; Wadi Qilt in the South of the area and Wadi Nuwe'meh in the north. In addition the Sultan Spring irrigation network, which covers a part of the area, has to be considered. These wadis represent the line recharge of the flooding surface runoff. (Fig. 53).

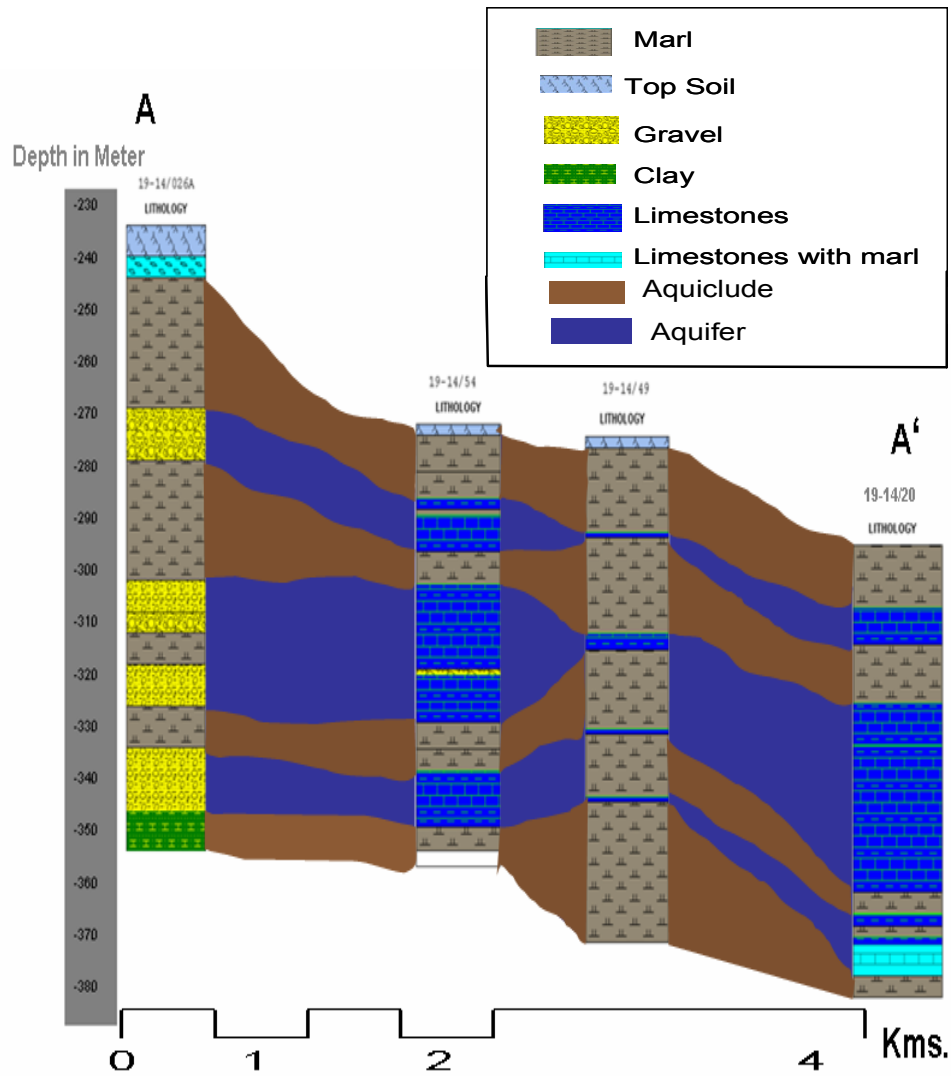


Fig. 54: Hydraulic conceptual model assumption based on the real lithological profile for some wells, the assumed connection layer with brown color represent the marl Aquiclude and with blue represent the gravel and lime stones Aquifer.

5.2. 2. 3. Faults

The study area is highly affected by faults especially in the western part.

These faults to the west are responsible on the spring's system mainly Sultan spring and also act as a barrier between the Upper Cretaceous aquifer and the shallow Pleistocene aquifer. The inferred old fault to the east defined by (Rotstein, 1991) also suggested in the study as a barrier boundary that prevent groundwater seepage to the Jordan River for certain distance (Fig. 53).

5.2. 2. 4. Boreholes for lithological cross section

More than 60 wells were drilled in the Jericho plan area. The majority of these wells are private wells, which have been drilled for agricultural purposes, 12 of these wells were used to describe the lithological formation of the upper most 100-170 meter of the aquifer. (Fig. 53).

5.2. 2. 5. Water Level

Several water level measurements for many previous years were taken and are used in constructing a water level contour map in the shallow aquifer system.

5.2. 2. 6. City Area

The city area is characterized by low agricultural activities and low abstraction rate, relative to the surrounded agricultural lands.

5.2. 2. 7. Abstraction rates

Several abstraction rates measurements were taken from the working wells in the area in m³/hr; the average daily of wells operation is 8 hrs/day, thus long term estimation for the system output in this aspect was also calculated.

5.2. 2. 8. Wells for the surface topography

The surface elevations for the wells were used also for the surface topography all over the whole model area. (Fig. 55)

5.2. 2. 9. Sultan irrigation network

Depending on the irrigation network that drained from sultan spring, a shape file that covers the irrigation channels area was created.

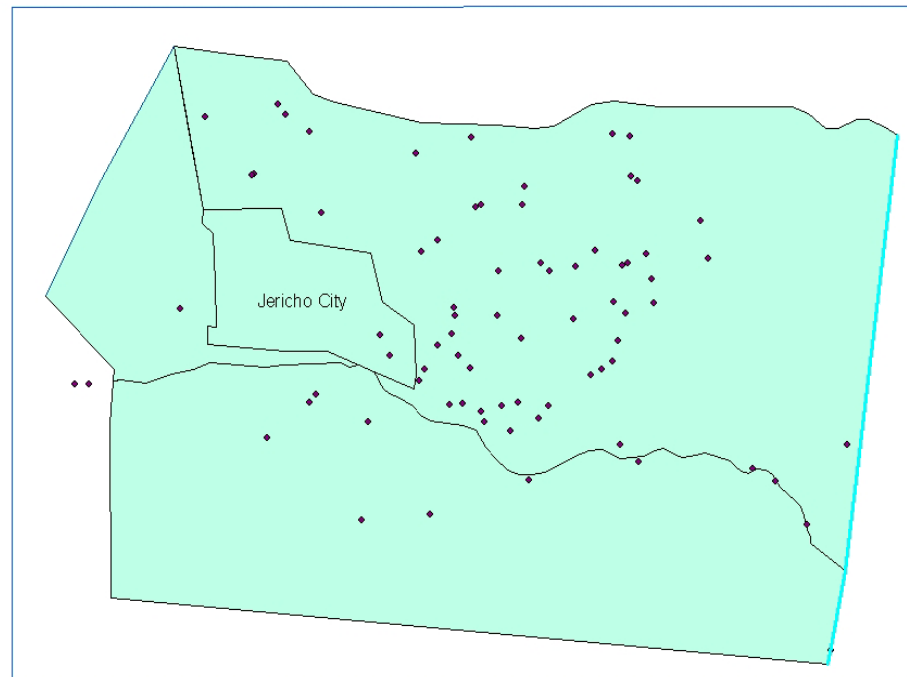


Fig. 55: Wells used for the surface topography, depending on the wells Z-value. These elevations values for the wells help in doing the surface interpolation process using Arc GIS program for surface layer geometry.

5.2. 2. 10. The study area surfaces

Despite the modeled area were divided into 4 surfaces to facilitate the processes of geometric model building (Fig. 56). Although, the surface separation can be used to allow to give each area its specific properties according to the structural material and the surrounding activities which can effect on system input or output, thus it allows for more easier data handling in each surface, in addition this division can help in solving the problem of different spatial conditions and solutes or contaminant distribution, with which a further improvement and studies based in this model can be conducted in the future. The first surface is the city area surface, the second is the north surface that extends from Wadi Nuwe'meh to Wadi Qilt, and the third one is the area further to the south of Wadi Qilt. The area surrounding Sultan spring to the west with coarse Samra was assigned as a fourth area.

For example, the surface no. 1 of the Jericho city is the higher populated area in the model that contains a lot of anthropogenic activities and septic tanks effluent. Where surface no. 2 contain the highest number of pumping wells that effect on the water level and the wells of Arab Project with the higher salinity. The layer further to the south of Wadi Qilt has finer formation of Lisan aquiclude, and so on.

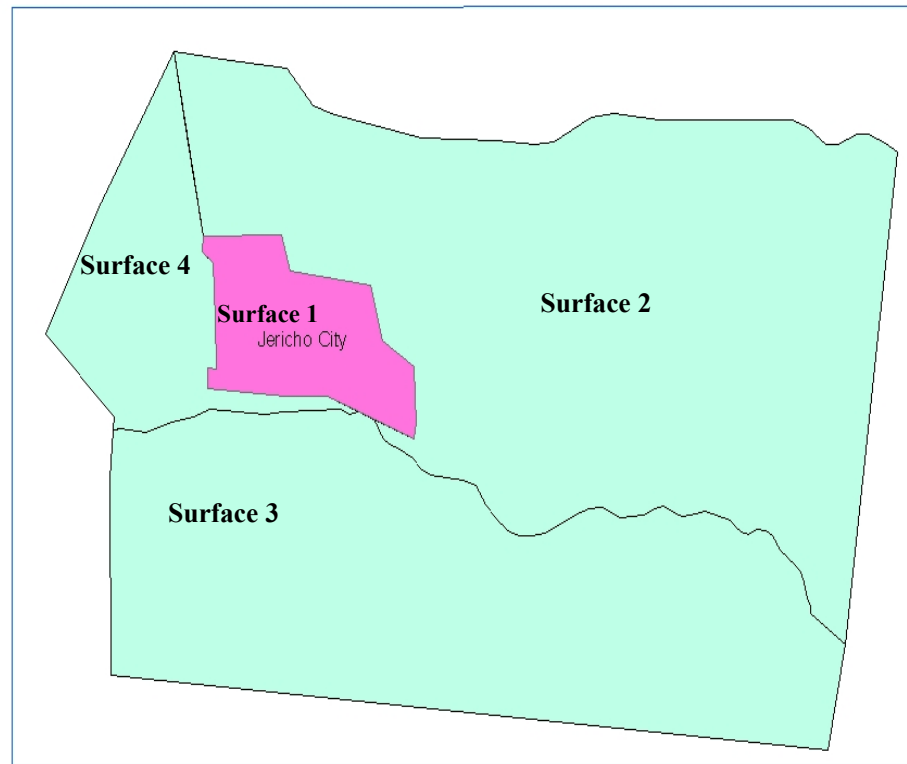


Fig. 56: study area surfaces

5.2. 2. 11. Interpolated Raster map for layers

Interpolation is a mathematical method of creating missing data. An image can be increased from 100 pixels to 200 pixels through interpolation. By this process a computing new intermediate data values between existing data values. In this case the data from the wells and the seven layers elevation were used to create in-between data to build construct a continuous topographical surface, within a defined domain.

The file of assumed layers elevation as well as the wells elevations for surface layer were imported for the process of layers interpolation using ArcGIS program, by which a topographical surface map for each layer were constructed with different elevation. Figure 52 shows the interpolated layers within the interpolation domain of the modeled area.

The colors represent the spatial distribution of the elevation data for each layer surface within the interpolation domain (Fig. 57).

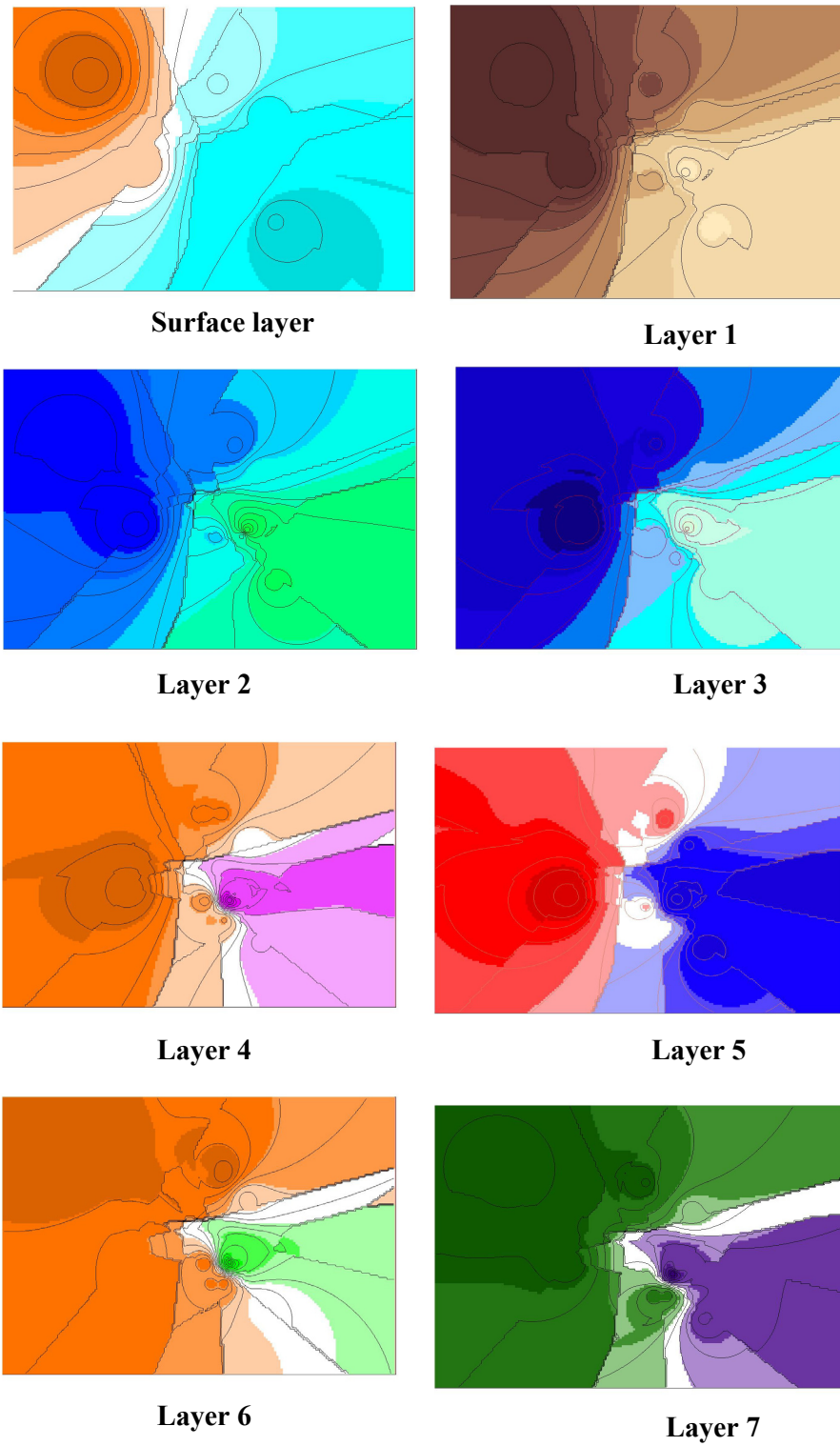


Fig. 57: Interpolated raster map for the seven layers, showing the spatial distribution for the elevation data.

5. 3. Project Construction

5. 3. 1. Project Elements

5. 3. 1. 1. Boundary Condition

The geographical boundaries for the modeled area are set as: Wadi Nuwe'meh in the north; few kilometers from the Wadi Qilt to the south Jericho faults in the west and Hugla fault in the east.

It is assumed that there is no water movement from the north to the south or vice versa, depending on the fact that the water direction in this sub-basin is from west to the east and south east. Therefore the only active model boundaries were assumed to be those in the west and in the east.

- West boundary: No hydraulic connection between the Upper Cretaceous aquifer to the west of the fault and the shallow aquifer to the east of the fault was assumed, except for the recharge generated by Sultan spring and the surface run off of the wadis from the precipitation of the upper mountain.

Fixed head were assigned at the beginning of the wadis entrance to the system.

- East boundary: It was estimated that the eastern fault shown in figure 53 on that extend until reaching Ein Hugla Spring area, act as barrier for groundwater flow toward Jordan River (Rotstein, 1991). The only amount of water that reaches the river is this of the wadis surface runoff. A fixed head were assigned near this boundary.

- **Initial Head**

Water levels measurements from the years 2002-2003 (PWA, 2001) were used as an initial reference head data for comparing eventually with the model results (Fig. 58).

- **Material parameters**

The material properties used for the different layers are shown in Table 10. It was assumed that the hydraulic properties for the western surface near the spring have higher K_x and K_z values than the surfaces further to the east. The data were estimated according to Guttman (1998), and Hobler et al. (1996). An intermediate values were set from different formations for the aquifer and the aquiclude, due to heterogeneous content of the layers (i.e. gravel with small size pebble, gravel with black clay, and marl with sand...etc).

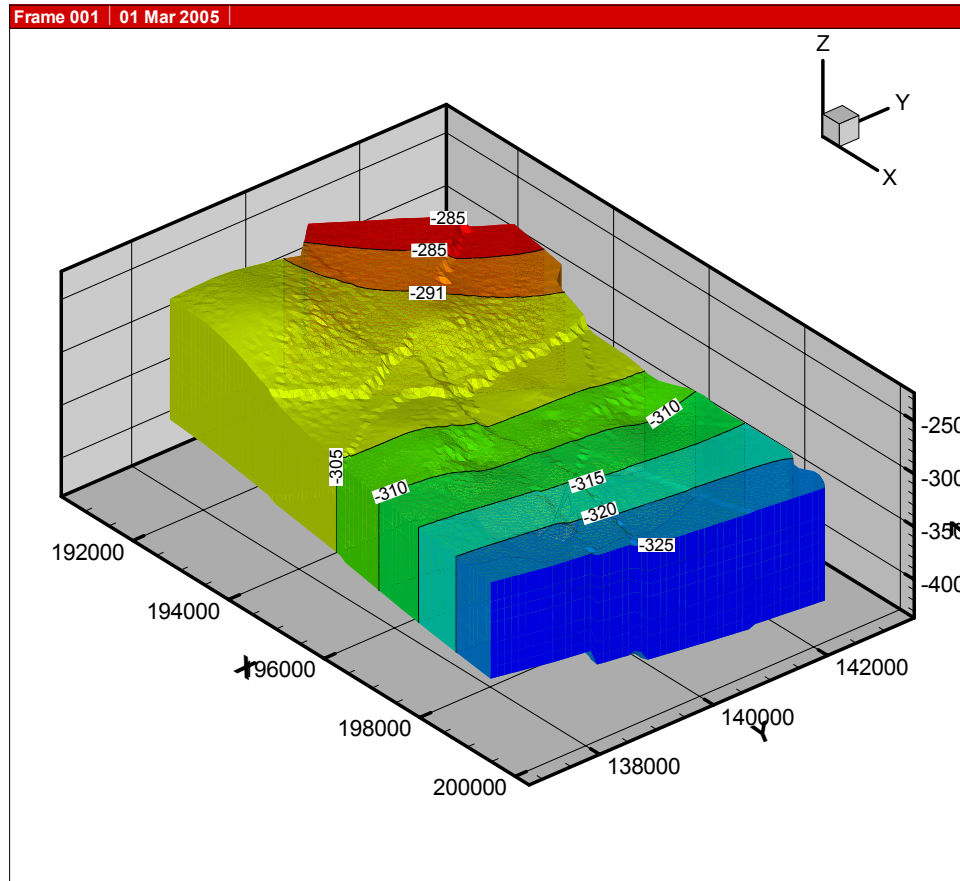


Fig. 58: 3D volumetric model showing the groundwater initial head in meters. Y refer to north direction, X east direction and Z is the elevation according to Palestinian coordinates.

Table 10: Estimated material properties.

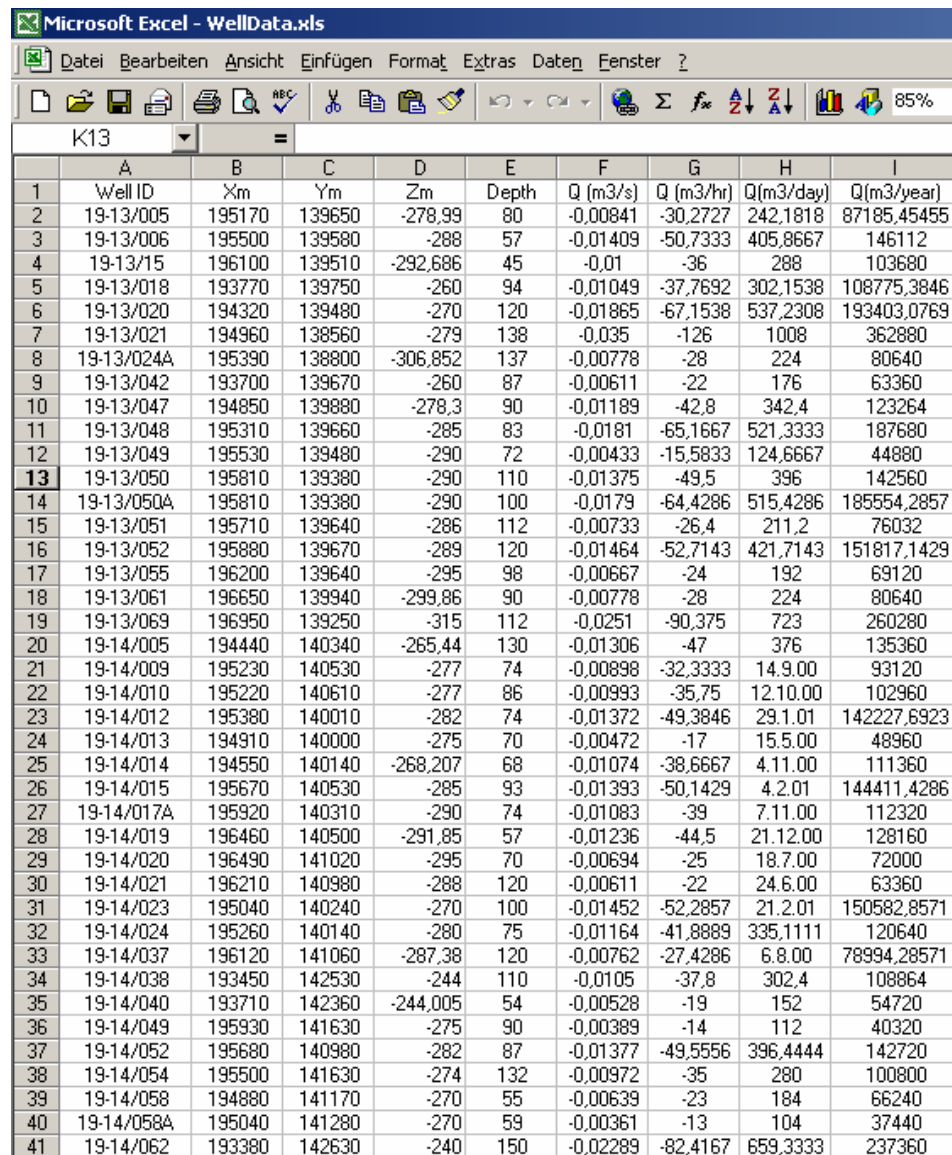
		For Sultan	For the aquifer as a whole	
Hydraulic Conductivities		Surface in the west		
Aquiclude layers		Aquiclude layer	Sy(-)	0.1
Kx	1.0 E-9 m/s	1.0E-6 m/s	Ss(1/m)	1.0E-5
Kz	1.0E-12 m/s	1.0E-9 m/s		
Aquifer layers		Aquifer layers		
Kx	1.0E-4 m/s	1.0E-2 m/s		
Kz	1.0E-6 m/s	1.0E-5 m/s		

- **Source Terms**

In general, source terms are the system input or output within the model domain. These sources can be described as the points, surfaces or lines from which the material such as water, solutes or pollutants can enter and get out from the model area. In the study area, for a simple flow model the source terms are:

- **Pumping wells**

Values of time dependent pumping rate were taken from around 44 wells. Well data can be directly imported e.g. from EXCEL files (Fig. 59).



	A	B	C	D	E	F	G	H	I
1	Well ID	Xm	Ym	Zm	Depth	Q (m3/s)	Q (m3/hr)	Q(m3/day)	Q(m3/year)
2	19-13/005	195170	139650	-278,99	80	-0,00841	-30,2727	242,1818	87185,45455
3	19-13/006	195500	139580	-288	57	-0,01409	-50,7333	405,8667	146112
4	19-13/15	196100	139510	-292,686	45	-0,01	-36	288	103680
5	19-13/018	193770	139750	-260	94	-0,01049	-37,7692	302,1538	108775,3846
6	19-13/020	194320	139480	-270	120	-0,01865	-67,1538	537,2308	193403,0769
7	19-13/021	194960	138560	-279	138	-0,035	-126	1008	362880
8	19-13/024A	195390	138800	-306,852	137	-0,00778	-28	224	80640
9	19-13/042	193700	139670	-260	87	-0,00611	-22	176	63360
10	19-13/047	194850	139880	-278,3	90	-0,01189	-42,8	342,4	123264
11	19-13/048	195310	139660	-285	83	-0,0181	-65,1667	521,3333	187680
12	19-13/049	195530	139480	-290	72	-0,00433	-15,5833	124,6667	44880
13	19-13/050	195810	139380	-290	110	-0,01375	-49,5	396	142560
14	19-13/050A	195810	139380	-290	100	-0,0179	-64,4286	515,4286	185554,2857
15	19-13/051	195710	139640	-286	112	-0,00733	-26,4	211,2	76032
16	19-13/052	195880	139670	-289	120	-0,01464	-52,7143	421,7143	151817,1429
17	19-13/055	196200	139640	-295	98	-0,00667	-24	192	69120
18	19-13/061	196650	139940	-299,86	90	-0,00778	-28	224	80640
19	19-13/069	196950	139250	-315	112	-0,0251	-90,375	723	260280
20	19-14/005	194440	140340	-265,44	130	-0,01306	-47	376	135360
21	19-14/009	195230	140530	-277	74	-0,00898	-32,3333	14,9,00	93120
22	19-14/010	195220	140610	-277	86	-0,00993	-35,75	12,10,00	102960
23	19-14/012	195380	140010	-282	74	-0,01372	-49,3846	29,1,01	142227,6923
24	19-14/013	194910	140000	-275	70	-0,00472	-17	15,5,00	48960
25	19-14/014	194550	140140	-268,207	68	-0,01074	-38,6667	4,11,00	111360
26	19-14/015	195670	140530	-285	93	-0,01393	-50,1429	4,2,01	144411,4286
27	19-14/017A	195920	140310	-290	74	-0,01083	-39	7,11,00	112320
28	19-14/019	196460	140500	-291,85	57	-0,01236	-44,5	21,12,00	128160
29	19-14/020	196490	141020	-295	70	-0,00694	-25	18,7,00	72000
30	19-14/021	196210	140980	-288	120	-0,00611	-22	24,6,00	63360
31	19-14/023	195040	140240	-270	100	-0,01452	-52,2857	21,2,01	150582,8571
32	19-14/024	195260	140140	-280	75	-0,01164	-41,8889	335,1111	120640
33	19-14/037	196120	141060	-287,38	120	-0,00762	-27,4286	6,8,00	78994,28571
34	19-14/038	193450	142530	-244	110	-0,0105	-37,8	302,4	108864
35	19-14/040	193710	142360	-244,005	54	-0,00528	-19	152	54720
36	19-14/049	195930	141630	-275	90	-0,00389	-14	112	40320
37	19-14/052	195680	140980	-282	87	-0,01377	-49,5556	396,4444	142720
38	19-14/054	195500	141630	-274	132	-0,00972	-35	280	100800
39	19-14/058	194880	141170	-270	55	-0,00639	-23	184	66240
40	19-14/058A	195040	141280	-270	59	-0,00361	-13	104	37440
41	19-14/062	193380	142630	-240	150	-0,02289	-82,4167	659,3333	237360

Fig. 59: Well data import from EXCEL tables.

- **Springs irrigation network**

For the spring the discharge is around 4.6 MCM, only 3.2 MCM is assumed to be drained to the open irrigation canals, and the rest is piped for domestic purposes (ARIJ, 1995). The first drained water for irrigation in the open canals exposed to evaporation and infiltration to the groundwater by which it might effect on the water level. Fig. 60 shows a digital elevation model for the top surface of the modeled area where the irrigation network with the identified grid nodes of the finite element meshes is also displayed.

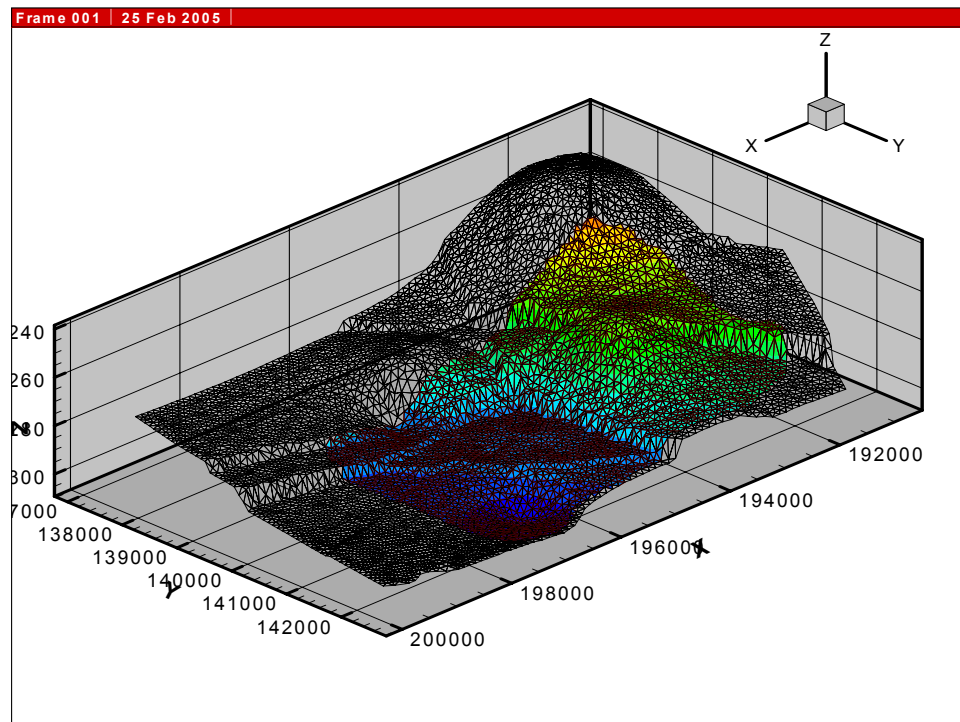


Fig. 60: Digital elevation model of the top surface of the model domain with Sultan spring irrigation area.

- **Line recharge by wadis**

The estimated annual distribution of the recharge for Wadi Nuwe'meh was assumed to be 4 MCM while for Wadi Qilt it assumed to be 5 MCM (section 2.5.2.6.)

- **Area recharge by precipitation**

The annual precipitation rate for the study area is about 166 mm/yr (section 1.6.2.).

- **Area discharge by evaporation**

The annual potential evaporation rate is about 2120 mm/yr (section 1.6.2.).

5.4. Creating a GeoSys Project

This is the first step when we start a new project in GeoSys. All the data reference needed for the model like geometry data, meshing data, processing data, are stored in one project file to keep the connection between the project and its data components.

Import of GIS data (SHP files)

SHP file means ArcGIS data format. It is prepared by using the features of digitizing in ArcGIS. There are three major types for 2D model: point, plotline, and polygon.

Geometry

A separate GEO view was created to view geometry data. This will be the same process for viewing meshing data, material group, processing data, etc. This will be done by simply going to menu 2D View, and click on GEO View to create it directly.

The type of geometry data to be displayed can be switched on, whether it is points, polylines, and point or line components from plotline, surface, TIN from the surface, label from those features could be done depending on the selection. The geometric model was created step by step as follow:

- 1- Creating Point view: where points are the basic element of all other geometry types. It can be used point to define the following 1-D geometry elements: Source term, boundary condition. The red points show that they are double points, and we need to remove those points because of inconsistency based on our setting of tolerance.
- 2- Creating Polylines: Plotline are important geometry object, they can be used to define the following 2-D geometric elements:
 - boundary of a model domain
 - boundary to assign boundary condition
 - Line structures.
- 3- Surfaces: Surfaces are closed plotline, i.e. the last point of plotline is connected to the first one. A surface can be used as a 2-D domain boundary. One surface could be created from one closed plotline (polygon) or from several polylines which form a closed area. In our case, each surface is created from one closed plotline.

- 4- Layer surfaces: Vertical surfaces can be created from two vertical layer polylines. Those surfaces are converted to TINs.
- 5- Creation TINs for Surfaces: TINs (triangulated irregular networks) a surface representation derived from irregularly spaced points and breakline features. Each sample point has an x, y coordinate and a z value or surface value. can be used for a discrete geometric description of surfaces and then for volumes as well.
- 6- Creating layers volumes: this by selecting the two consequent surfaces, then creating the volume which is filling in between. Then using Write TEC function in Geo Sys the prepared volumes are exported and displayed by Tec plot program (Fig. 61)
- 7- Meshing: the general steps for the hybrid meshing procedure in this application are:
 - Create a triangulation based on surfaces (SFC) for the 2-D surface water model. The surfaces must be topologically consistent,
 - Create line elements for the 1-D wadis model based on the triangulation,
 - Create prismatic elements for the 3-D subsurface model,

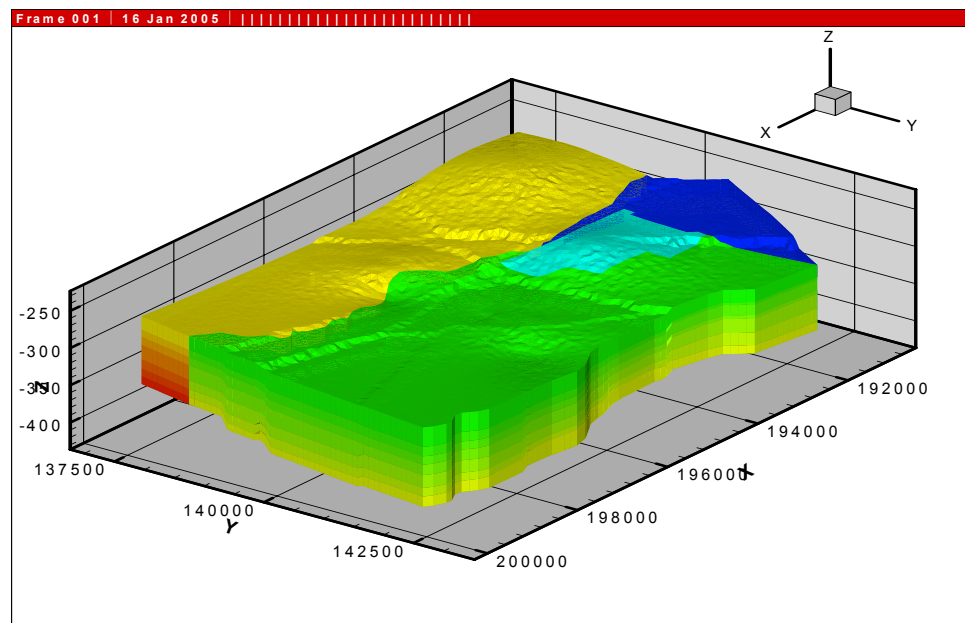


Fig. 61: Display created volumes in Tec plot program, noting the filling between layers (displayed as blocked lateral surfaces).

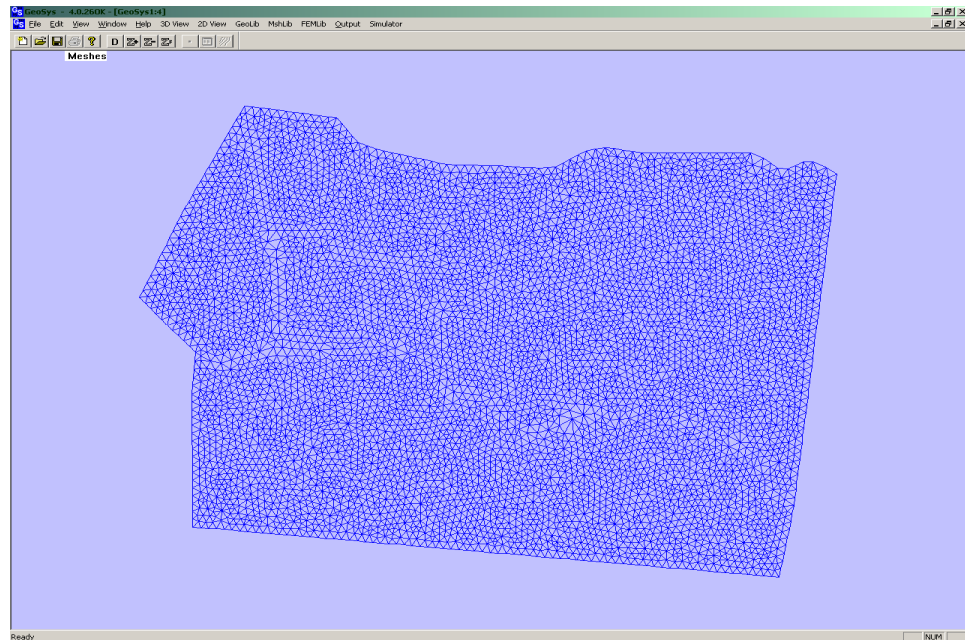


Fig. 62: Display triangulation and prisms result, noting the triangular items all over the surface of the model domain.

- 8- Triangulation: is method of surveying in the location of an object may be calculated from the known locations of two other objects. Creating a triangle from the three items, the angles and sides of the triangle can be measured and the location of the unknown object is calculated algebraically.
- 9- Prisms: Prism elements can be generated from triangles while extending these to the vertical direction. (Fig. 62).
- 10- Lines: Line elements can be created along polylines. To this purpose the edges of triangles along these polylines are used. Therefore, the polylines intended for generating line elements must be parts of the surfaces which were used for the triangulation. Creating polylines for line elements was done by using drawing tool in GeoSys or Import SHP file for wadis
- 11- Mapping: Surface mapping is the process of making the mesh conform to stratigraphic irregularities, i.e. thickness and orientation of the mesh slices can be deformed. Different data types can be used. Mapping result in Tec plot is shown in Figure 63.

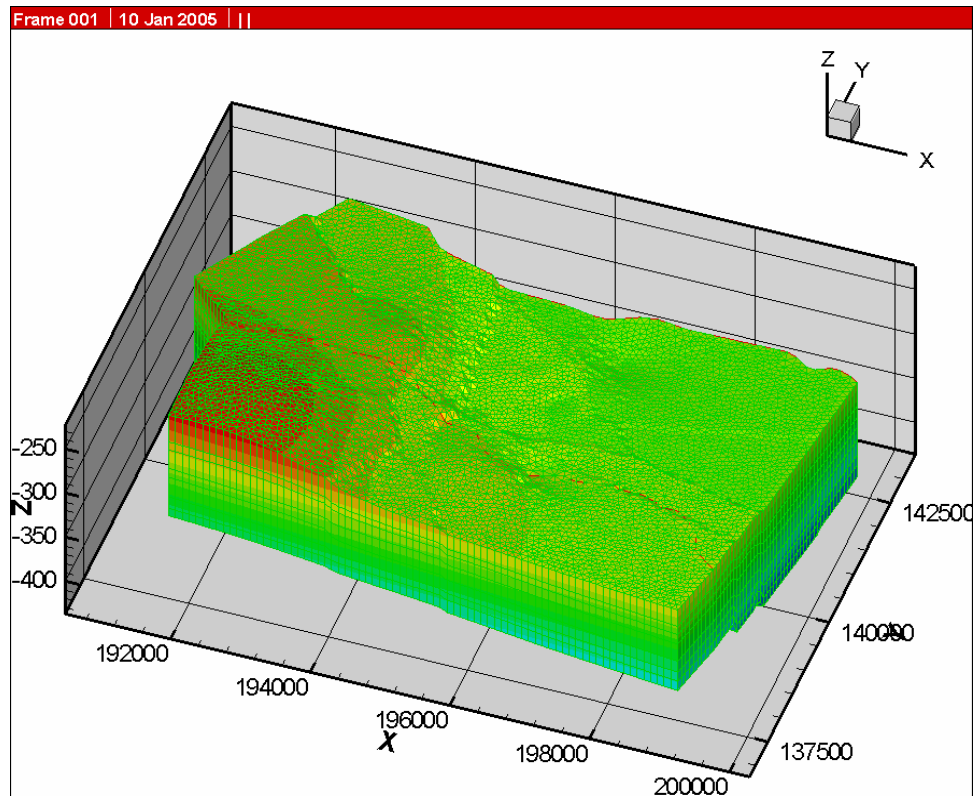


Fig. 63: mapping result in Tec plot, the first map showing the mesh that conforms to the stratigraphic thickness for different layers.

5. 5. Program Processing

This includes:

- Create FEM View
- Create Processes
- Write PCS File
- Defining Boundary Conditions

The surface for boundary condition is created from layer surfaces. One layer surface consists of two layer polylines. TINs are also created inside the surface.

- Defining Material Groups.
- Link MAT groups with MSH data
- Defining Source of Terms: Well data were imported from EXCEL files which converted to CSV files. The imported wells shown in Figure 59. The wells then converted as geometric data using Geosys (Fig. 64).

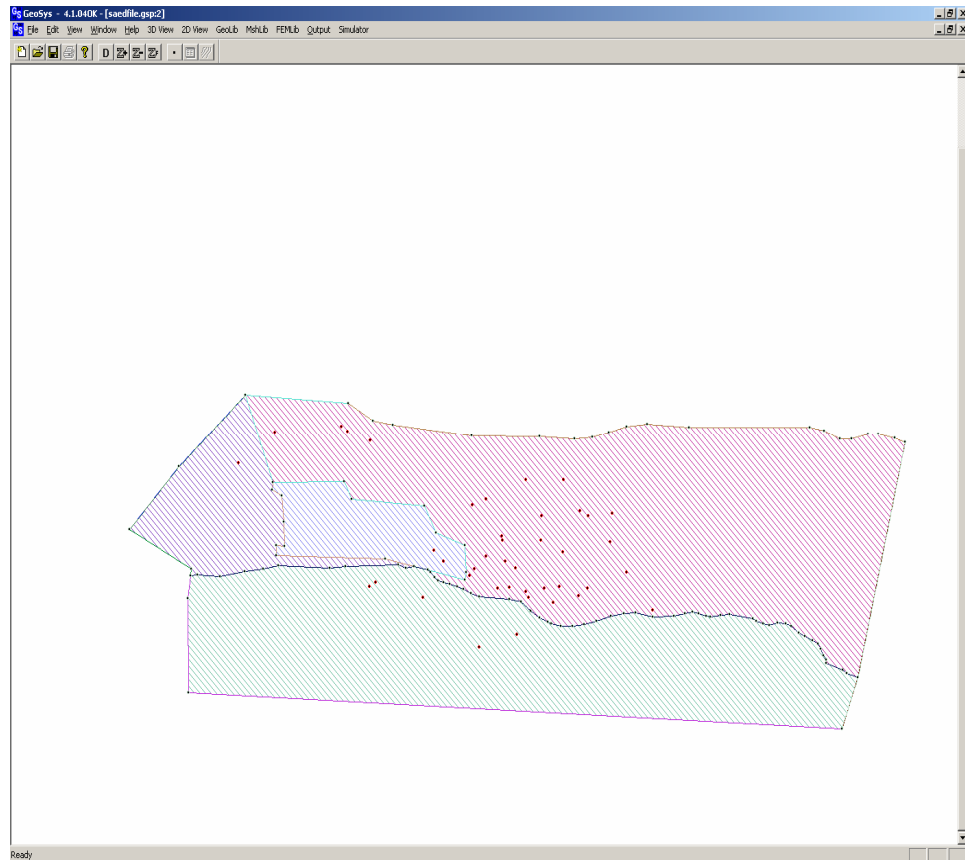


Fig. 64: Wells as geometric data using Geosys, showing the wells distributed in the surfaces.

5. 6. First simulation results and discussion

The numerical simulation is based on the 3D structural and hydraulic model described in previous sections. The simulations started from an undisturbed situation without pumping and irrigation activities taking into account the regional groundwater flow only. Fig. 65 shows the groundwater head distribution in meters of the first (from top) aquifer layer considering the differences in k values for Sultan spring and remaining area. The resulted head are bearing more or less the initial head shown in Fig. 58. In order to assess the rule of the sultan irrigation network and its effect on the groundwater table. The successively data of all pumping wells and irrigation from Sultan spring are included in the simulation. The recharge input from the wadis runoff was switched off, in order to recognize how the infiltration from the Sultan irrigation network only would effect on the groundwater table.

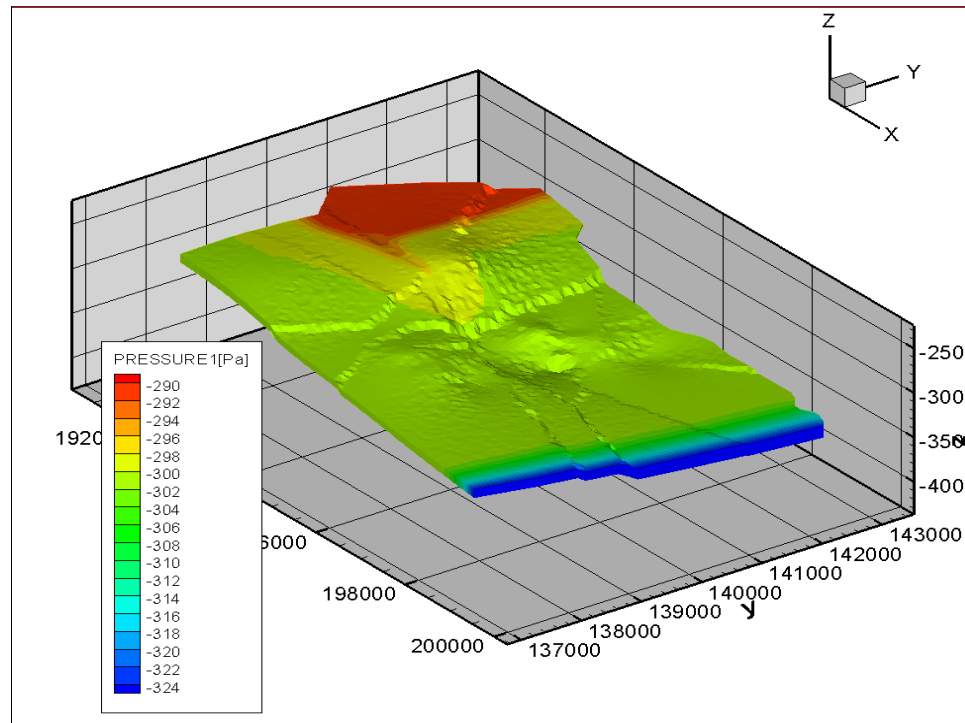


Fig. 65: 3D view of the groundwater head distribution in meters of the first aquifer layer (undisturbed situation without pumping and irrigation), the colors represent elevation of the groundwater level in this layer. Y refer to the north direction, X east direction and Z the elevation in meters.

The overall irrigation from Sultan spring is calculated to 3.024 MCM/year. Irrigation network input was modeled as a homogeneous infiltration rate, and the linear recharge from the wadis were neglected. Different scenarios for the percentage of effective infiltration were tested. Figure 66 shows simulation results for the taken assumptions which assumed to highlight the hydraulic functioning from each contributor.

Figure 66a depicts the groundwater level if pumping only is taken into account. Local hydraulic head lowering is observed. Figure 66b depicts the groundwater level if homogeneous irrigation only is taken into account. A rise of groundwater is resulting from this area water source.

Figures 66c and d, illustrates the hydraulic head distribution for different assumption of infiltration rates (2 and 10% of irrigation rate respectively). Qualitatively, these modeling results fit very well to the measured data. There is a groundwater lowering in the central northern part and a rising in the central southern part of the investigated Jericho area. However the absolute deviations of hydraulic head from the undisturbed situation are overestimated.

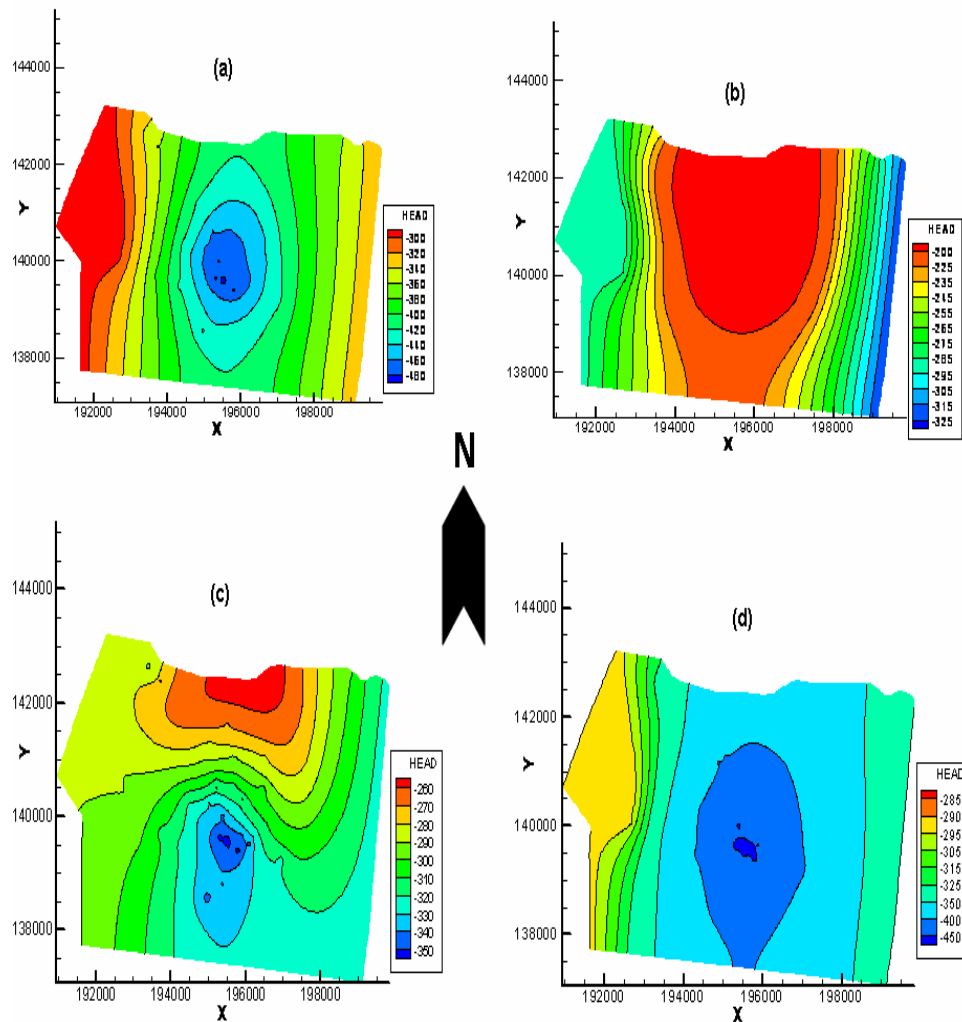


Fig. 66: Hydraulic head distribution in meters, in the upper aquifer taking into account: (a) pumping wells only, (b) irrigation from Sultan spring only, (c) pumping and irrigation (10% infiltration rate) and (d) pumping and irrigation (2% infiltration rate).

The water level as expected have its higher values to the west near the spring recharge and begin to decrease under the heavy abstraction from the wells further to the east. The conceptual model shows that the irrigation backflow from the irrigation network which drained from sultan spring can effected with uncertain limit on the groundwater table. The data of hydrochemistry and isotopes reflect also a possible mixing between the water from the regional mountains aquifer (that the springs drained from) and the shallow aquifer. The assumption shown in Figure 66c shows the effect of 10% infiltration from the irrigation backflow in the presence of well

pumping. This assumption seems to be far from the actual situation if we considered also the other water input from the wadis flood, in which the water level will be over the reference limits. Assumption in Figure 59d can be more closed to real situation if we take into account the additional input from the wadis flood. The water heads in Fig 66d represent by the large depression in the zone of pumping can be replenished to certain extend by the wadis input. Moreover, it seems that the assumption of system closure from the east is not totally correct. It should be taking into account that some of water from the irrigation network is escape by surface runoff to go to the wadis and Jordan River; this can be noticed by the relatively higher water level near the eastern border. At this part the model need further calibration to assume the hydraulic functioning of the wadis and how far exactly the irrigation backflow play a role in the system recharge as well. At this stage, and under the given model parameters, further application on the model were adopted, where the effect of the pumping rates for different seasons on the water level were visualized.

5. 7. Visualizing the seasonal Variation of the water level

There are two major agricultural seasons in Jericho, connected to the beginning of crop irrigation with a large abstraction rate from the agricultural wells. One of this begins by the end of September (dry season) and the second is by the beginning of February (wet season). Figure 67 illustrates the shifting in the pumping rate during the agricultural months in Jericho (figure was drawn using Geosys program).

The groundwater level in Jericho is highly affected by the seasonal pumping rate from the agricultural boreholes. This effect can be located more sharply during the dry season by the end of October after a long period of summer time. Monthly based pumping rate were imported as an excel file to the program (Fig. 59). Then running the simulation according to the data update, the first visualized water level under the normal conditions without extreme pumpage is shown in Figure 68.

The visualized water level after the wet season of February is shown in Figure 69, and the water level after the pumping in the dry season of October is also shown in Figure 70.

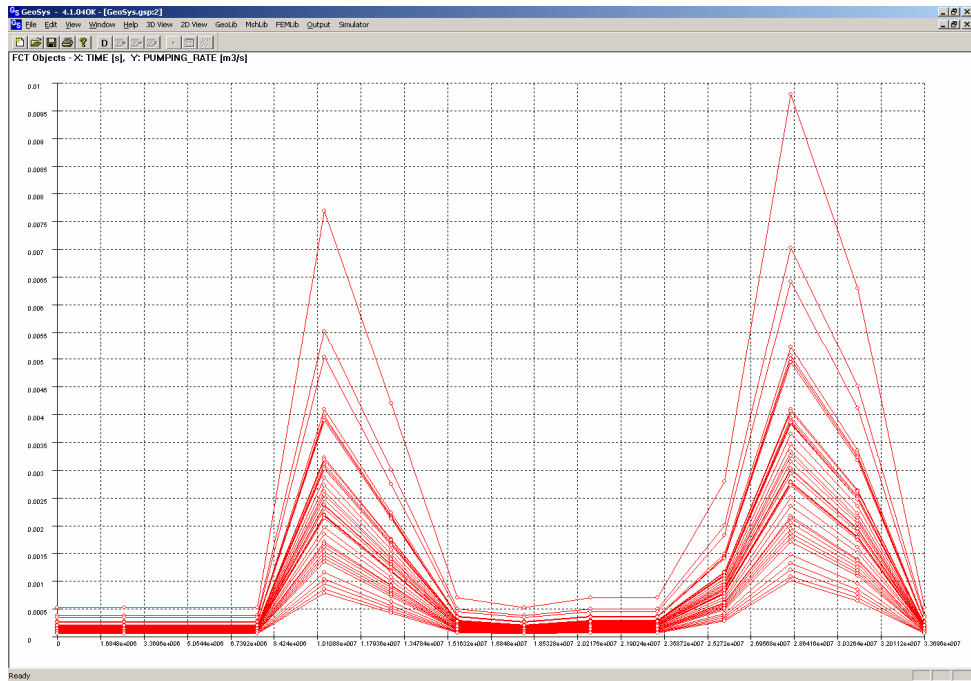


Fig. 67: Monthly pumping rates from the wells in Jericho area. Each red line represents a pumping well, on X-axis the month of the year and on Y-axis the pumping rate in cubic meter/s.

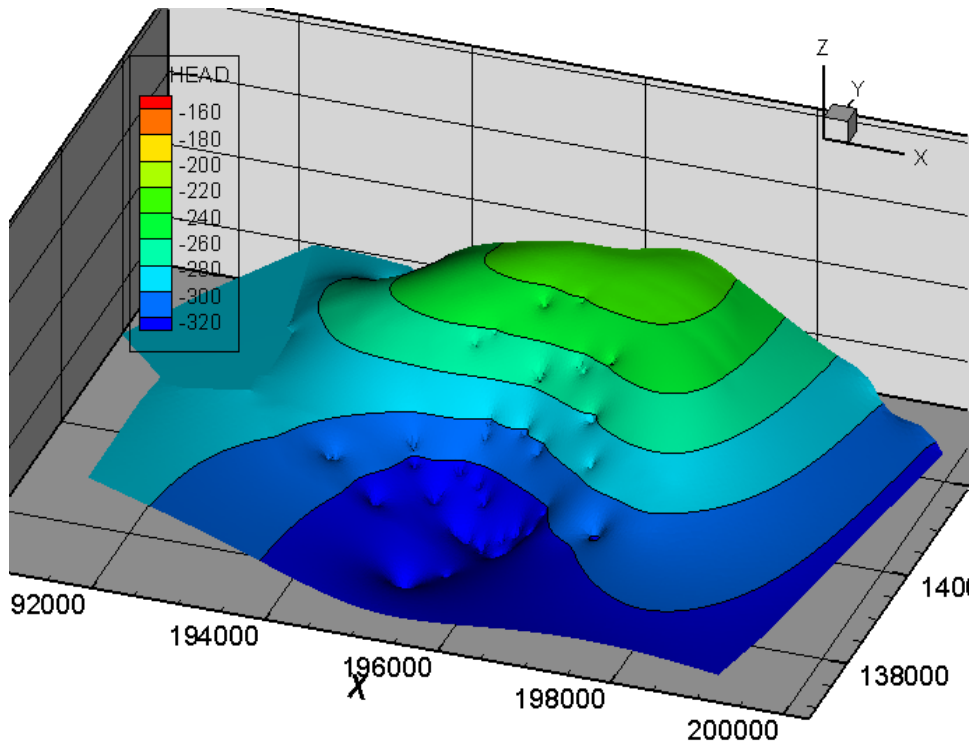


Fig. 68: Visualized water level under the normal conditions without extreme pumpage activity, using Palestinian coordinates. X refers to east direction, Y to north and Z to the elevation the water head on meter.

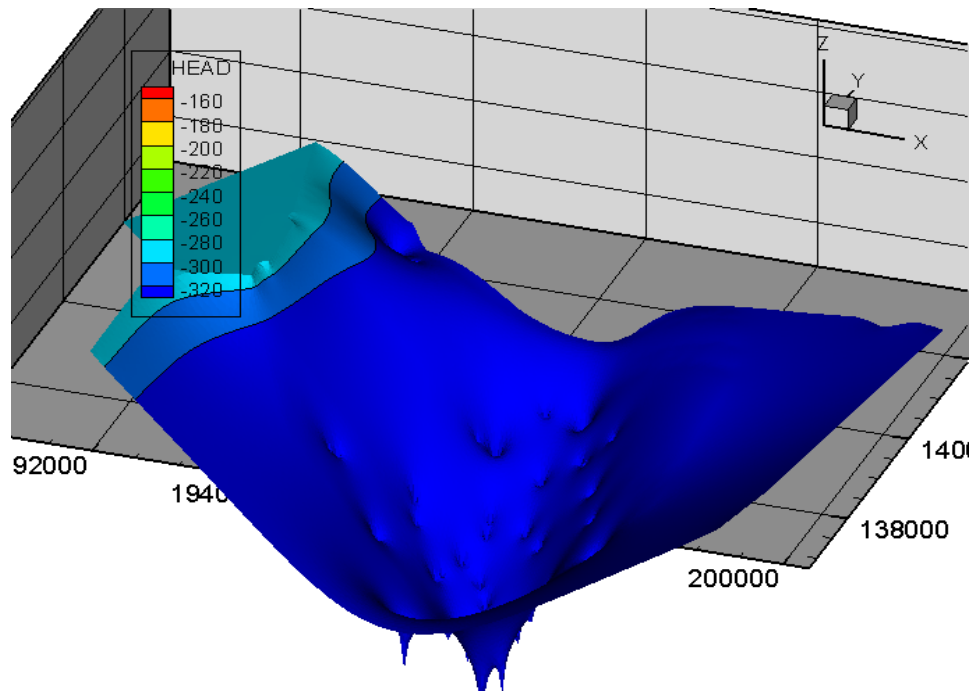


Fig. 69: Pumping effect on the groundwater table after the wet season of February

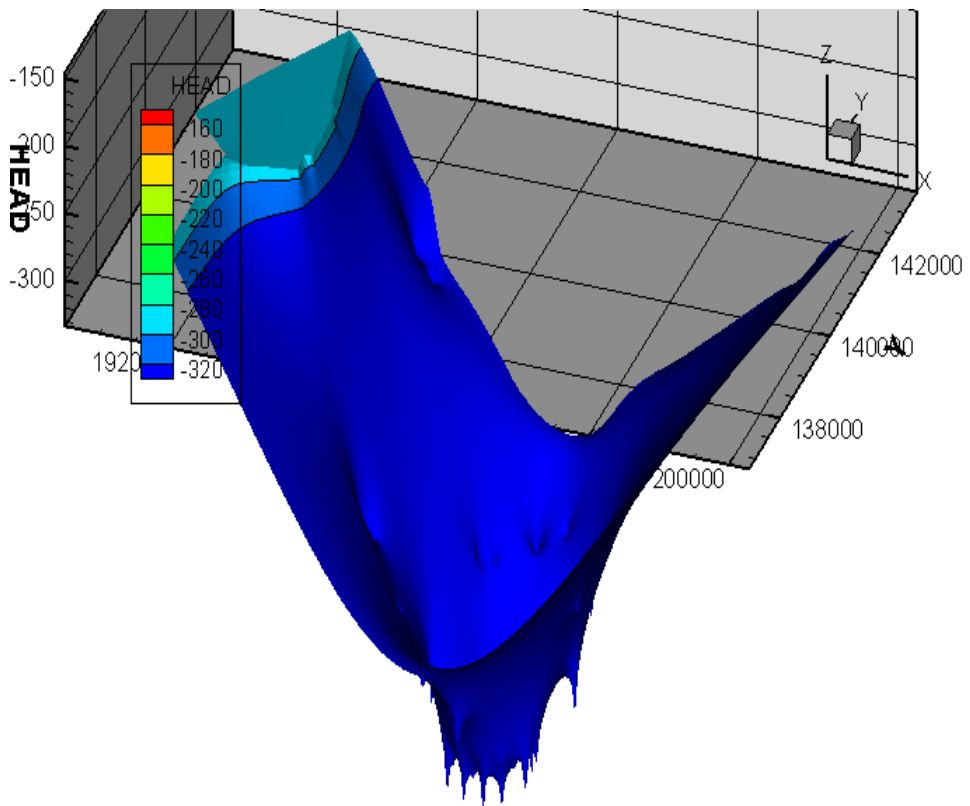


Fig. 70: Pumping effect on the groundwater table after the dry season of October

These assumed results under the previous mentioned model parameters show the effect of the seasonal water pumping on the water head of the shallow aquifer in Jericho, the water level dropped in the first agricultural season which come directly after the replenishment of the aquifer causes water level decreasing (Fig. 69). The pumping process in the second agricultural season which come directly after the dry season cause further decrement in the water head, as there was no replenishment after the first pumping time (Fig. 70).

This small application on the model (with its roughly calibrated parameters) visualized for a certain extend the effect of the major extensive pumping act at different times from the aquifer. However this model still subjected to further refining process to have clearer picture about the mixing rate from different recharge sources. Where further investigations of the hydraulic regime are necessary, in particular: the hydraulic functioning of wadis in feeding the system and the diffusive mode of recharge from the wadis to the groundwater table, and the local distributions of irrigation network, effective infiltration, evaporation from it still need to be calibrated taking into account surface water runoff (Beinhorn and Kolditz, 2005). The model depending on the above mentioned variable inputs and outputs should be calibrated and validated with the actual hydraulic situation in the study area.

Moreover, different expectation scenarios can be considered after refining this model to see the expected fluctuation in the water availability and demand depending on the future surrounding conditions. These scenarios can give a good idea to put forward a certain system for the pumping quota and water use.

A solute transport model also can be done using this primary conceptual model to visualize the spatial distribution of the saline and fresh water, and the mixing between them using a skimming model, by which different salinity measurement should be taken from a working pumping well in order to tracking the saline-fresh water interaction within the aquifer, where the salinity gradient is also fluctuated depending on many factors and conditions of recharge and abstraction rate.

Based on the concept of this model, as a model based on the groundwater movement through the porous media of the shallow layers (top 100-200m) with different lithological formations, an improved solute transport model can give more clearer picture about the rule of sedimentary rocks dissolution (the rock-water interaction) in the process of salinity. Such model can aid also in describing the

chemical reactions within the aquifer mainly the processes of mineralization and dissolution of minerals. It also can show the movement of different anthropogenic contaminants through the surface to the groundwater. By which, the susceptibility of the aquifer to different anthropogenic activities can be assessed.

CHAPTER 6: SUMMARY AND CONCLUSIONS

The high salinity in the shallow Pleistocene aquifer in the Jericho plain area is a function of 3 main contributing sources. The hydro-chemical and isotopic data appraise these contributions clearly. The hydrochemical data show: 1) the evolution of calcium chloride in the wells to the east which are relatively rich in Mg, strontium, Fe in parallel with low molar ratio with relation to chloride for most of the elements compared to sea water reflect a reverse softening and a mixing of brackish water. 2) The continuous increment in the molar ration of the major solutes to chloride, bearing the same ration from Lisan elution which confirms the mentioned in situ dissolution of rocks as an additional source of salinity. The increase of Mg, Ca and HCO_3 as well as most of the other elements in the eastern part of Jericho area due to the brine effect enhanced the process of mineralization in the eastern part of the aquifer. The high Mg input in the eastern part favored a process of calcite dolomitization. By which the calcium is elaborated in surplus amounts and forming Ca-Cl brackish water. 3) The anthropogenic effect from sewage and agriculture were clear influences in the wells that have low chloride content, but by no means low brackish water effect, this lower chloride with higher molar ratios, and high Br and nitrate suggest the input of different water that contains pollutants.

This water may result from agricultural back flow or sewage effluent. The lithological formation of the area has a two edge effect on the salinity increment in the area, one is the in situ weathering of the rock, the other is the structure of the formation which consists of gravel and marl from the highly trans-missive Samra layer with coarse gravel and high hydraulic conductivity, and the Lisan layer with fine silts and low hydraulic conductivity but with a highly fractured structure. Both serve as a good media for pollutant transmission and storage.

The isotopes analysis of (deuterium, nitrogen15, carbone13 and sulfur34) give a more clear picture about the possible sources of salinity, in addition, it confirms the results of hydrochemical data, and it helps in tracing the mode, the tracks and the source of salinity and pollutants in the groundwater within the Jericho area.

$\delta^{15}\text{N}_{\text{nitrate}}$ and $\delta^{18}\text{O}_{\text{nitrate}}$ values show that most of the groundwater samples from the wells and springs in Jericho area were mainly influenced by nitrate and derived from septic tanks. Sewage appeared to be the cause for increasing nitrate concentrations observed in most of the wells and springs in Jericho. The following factors highly

suggested manures as an additional source of nitrate in the groundwater, these are: the aerobic condition for most of the sampled shallow wells, the presence of animal farms especially in Wadi Qilt east and Ein Dyouk area, and the addition of the animal manure as a natural fertilizers directly to the land.

Less evidence of fertilizers nitrate was shown, but this could vary according to the seasonal application of the pesticides and its chemical composition. Long persistence of the nitrate within the groundwater reservoir for the dry season months (sampling time) gives a good chance for the beginning of slight denitrification process within the aquifer. $\delta^{15}\text{N}_{\text{nitrate}}$ and $\delta^{18}\text{O}_{\text{nitrate}}$ values in the northern wells have other sources of nitrate in addition to sewage, as the nitrate concentrations for these wells are low and exhibit high $\delta^{15}\text{N}_{\text{nitrate}}$ and $\delta^{18}\text{O}_{\text{nitrate}}$ signatures. This signature might reflect a mixing signature between chemical fertilizers and the residual nitrate from bacterial denitrification or from the sewage.

The isotopic signature of deuterium and $\delta^{18}\text{O}$ from water give the following indications: (1) In general there is no seasonal variation between dry and wet season except in deuterium in which the flushed water is enriched deuterium with due to ultrafiltration process. (2) Fitting the springs signatures with LMWL emphasize that the recharge area for the springs is different from those for the other wells in the lower plain with no further evaporation. (3) While most of the other wells show different infiltration zones through wadis, these wells which are often exposed to overexploitation, distributed around a calculated brackish water mixing line, reflect a salty water influence. (4) The other scattered depleted $\delta^{18}\text{O}$ signature can reflect less effect from brackish water with less chloride and salinity content, thus the susceptibility of these wells to anthropogenic contaminants was easier to indicate rather than those with highly saline content. The enriched $\delta^{18}\text{O}$ signatures for these wells with the low salinity suggest the effect of water irrigation backflow with heavier isotopic signatures. It was registered that many of the pumping wells are connected directly to fertilizer container in which pumped water is mixed with the chemicals and then applied directly to irrigate the farms. This in addition to highly boron, bromide and nitrate contents, which also suggests a sewage and manure influence from animal farms and septic tanks which are widely used in the area.

The raising of sulphate in groundwater in the Pleistocene aquifer in lower Jordan valley (Jericho area) mainly caused by disseminated and leached gypsum from Lisan and Samra layers that cover the area. There are two different sources or contribution

mechanisms for sulphate into the groundwater in the area, these are: (1) surface seepage leachate with the positive $\delta^{34}\text{S}_{\text{SULPHATE}}$ signatures of primary gypsum, and (2) upwelling brackish water which rise up under heavy abstraction (especially in the eastern wells), with the negative $\delta^{34}\text{S}_{\text{SULPHATE}}$ signatures, and highly sulphate contents.

The highly sulphate content in the groundwater from the eastern wells, in parallel with negative $\delta^{34}\text{S}_{\text{SULPHATE}}$ signature give also the signature of sulphate that originate from pyrite oxidation which is transported by up welling groundwater under heavy abstraction and oxidized in the aerobic environment in the upper layer. This result can also emphasize the assumption of Rosenthal and Möller (2006) (section 2.6.1), the signatures of deep brine source and the high Mg and Ca-chloride values may result from residual deep brine coincident on low depth. However, the signatures obtained in the Jericho area don't really go with other illustration described by them in section 2.6.1, which might be restricted to other area in the rift.

Two main contradictory inputs effect on the carbonate system and the water quality in the aquifer as a whole which also represent the two main end members of fresh and saline water. The first is the fresh carbonate rich water in the west, where the major fault systems, which bordering the Jericho plain area in the west, seem to play also a role in the water system feeding. The $\delta^{13}\text{C}$ data emphasize that there is a leakage from the calcareous water of the Upper Cretaceous aquifer, which feed the spring, to the shallow aquifer in the plain area. This leakage is clearer in the west and north area wells, where there is a mixing from this leaked fresh carbonate rich water with that water which feed the Pleistocene aquifer through the infiltration of the wadis run off. On the other hand, the brackish leachate from the wells to the east with high TDS including bicarbonate considered as the second end member that effect on the carbonate system. This brine water normally is of Cl-Na-Ca type and also rich by Mg and K as well as other elements. The presence of high carbonate and Mg input from the brackish water in the east creates a suitable environment for dolomitization of calcite. The anthropogenic influence in between play as an additive factor that effect on the carbon system in the aquifer system. This exacerbates to quietly differentiate the anthropogenic effect from the brackish effect from the east.

As overall result, the isotopic data as well as hydrochemical data appraise two main aspects:

1. The aspect of the recharge mechanism: as mentioned above the isotopes data of carbon, oxygen and deuterium emphasize a two recharge mechanisms for the Pleistocene aquifer system in Jericho plain area, by which one is the surface run off that feed the wells through the wadis, mainly Qilt and Nuwe'meh, and the second is that of the upper mountain aquifer leakage which enter the Pleistocene aquifer through the major fault system in the west of the plain. The water quality of some wells in the west as well as the isotopic signatures indicates such type of admixing between the two aquifer but obviously at certain limit. This finding of different sources mixing should be taken into account by planners and remediation specialist, the highly variation in water quality between the two aquifers put many questions about the possibility of the saline shallow aquifer remediation through inducing a type artificial recharge from the upper fresh aquifer or increasing the mixing rate between the two aquifers in a certain ways.
2. The aspect of salinity sources: the data shows that the high salinity in the shallow Pleistocene aquifer in Jericho plain area is mainly influenced by a slat leachate brackish water that mainly formed as a result of long contact with the salty rocks, or an old deep water that formed as the residual brines derived from evaporated Pliocene seawater and/or of brines resulting from solution of salts bodies in large depth, and is entrapped in the interstices of the sediments during the Pleistocene age. The presence of Mg and Ca-chloride rich water in the groundwater samples of the wells in the east of study area, is emphasize the same water type that described by Rosenthal and Möller (2006); Rosenthal (1988); Starinsky (1974), in the western shore of the Dead Sea, which reflect this residual old brine or a rich halite salts bodies (section 2.6.1). This water is coexisting deeply in a confined aquiclude chamber in the Lisan formation. This brackish water rising up under heavy abstraction due to pressure difference through conduits and vein in the Lisan formation. This assumption was approved by the low tritium units in the brackish groundwater samples in the eastern wells, as well as the depleted $\delta^{34}\text{S}_{\text{SULPHATE}}$ signatures. The exact age for this water as well as its sources can be investigated using $\delta^{14}\text{C}$ or $\delta^{81}\text{Kr}$. This problem should be taken into account by the planners as the main aspects that deteriorate the water quality in the shallow aquifer. This means that a lot of measurements and procedures should be adopted to prevent the evidences of interaction between this deep saline water and the upper fresh layers.

3. The aspect of pollution by sanitary systems and agriculture: the nitrate isotopes data approved that the main source of water deterioration by the anthropogenic pollution is the leakage from the septic tank. The sewage system in Jericho is not well developed; more conscious about the water disposing manners can help as well as the constructing of well sealed sewage network. The other anthropogenic pollution is that coming from agricultural residues. The processes of pesticides and fertilizers adoption in the agricultural lands should be monitored.

The GIS based model was constructed roughly as a basic conceptual model for the top 100-200 m layers in the shallow aquifer. This model can be considered as a primary basic flow model for further investigation or improvement, and still need more calibration and validation. However, some scenarios to test different recharge contribution and discharge events to and from the water system were adopted in the model. The model suggest by assumption different scenarios for the mode and mechanism of the contribution from the irrigation channels drained from sultan spring on the water table. It was noticed that the effective infiltration coefficient of about 2% from the irrigation channels has a noticeable effect on the groundwater level in the aquifer. This visualized hydrosystem data can also interpretate the presence of mixing between different recharge sources shown by the hydrochemistry and isotopes results. The other assumption adopted is that which appraising the effect of the two main annual heavy abstraction events on the groundwater level. The visualized results show the fluctuation in the water level between the two abstraction events where the water table is increased noticeably after that rain event which come directly after summer time. The model also appraises the effect of the well pumping on the water level especially this pumping in the period after the dry season in October. This results indeed reflect many big problems within the area. These problems are related mainly to water quantity which represented by the fluctuation in the groundwater level with respect to uncalculated recharge and discharge amount. The other problem is related to the quality, which represented by salinity raising and anthropogenic contaminant in this susceptible aquifer. It was noticed that the water quality become more deteriorated in the groundwater located further to the east of the study area where the formation become more finer and silty with more aquiclude like formations. The runoff water from the wadis has a relatively good quality and recharges by infiltration diffusively through the layers Lisan and Samra. On this way it dissolves salt minerals and evolves to a saline leachate. Moreover the heavy abstraction enhances the upwelling of salts

rich water confined in the deeper aquiclude formations formation to the upper fresh percolated water in the upper layers.

The above mentioned mechanisms of water salinisation can be faced by several remediation practices, organizing, and management tools, whether it must be adopted separately according to the groundwater quality and quantity for each well or collectively for the aquifer as a whole to achieve the higher efficient sustainable yield. This tools should also stand to special criteria's that taking into considerations both the sustainable water resources development and the special big water demands for this agricultural area. The main measurements that can be done in this regard as follow:

- The abstraction rates from each well should be calculated as a part of the aquifer as a whole depending on the amount of recharge for each year and the season of abstraction event.
- Storage dams or water retention structures on main wadis should be constructed.
- Feasibility and technical studies for artificial recharge of aquifers from seasonal runoff or treated wastewater for either seasonal storage or barrier for salt water intrusion especially in the eastern area.
- preventing the floodwaters from escaping to the Jordan River through efficient water exploitation.

There are a variety of options that can be adopted to manage salinity depending on the management objectives and the local biophysical environment. A combination of these options is needed to address salinity problems at both the farm and catchment's levels. Some land-use changes will be required at a catchment's scale and improvements may take a long time to generate outcomes, so in some cases living with and adapting to salinity will be unavoidable.

In addition to quantifying and identifying the sources of pollution and salinities that impaired groundwater qualities of the aquifer, which has already done within this study, it is also more necessary to adopt the following remediation steps:

1. Establishing a pollution potential source and load reduction targets necessary to achieve groundwater system restoration in this limited resources area.
2. Recommendations for continuous baseline and future water quality monitoring

programs to assess the environmental impacts to water quality changes.

3. Establishing a well designed and prepared sewage collection networks within the city, and dumping the widely used septic tanks.
4. Recommendations for designing and constructing water quality treatment facilities in the region, that dealing with the wastewater problem.
5. Recommendations for oversight and support of improved water quality modeling efforts in the area that consist of a number of tools for a better understanding of the salinity and pollution problems.
6. Recommendations for establishing and integrated remediation programs to achieve those targets in cooperation with related governmental and non-governmental institutes.
7. Raising the local environmental conscious in the communities of the region, through integrated environmental and related socioeconomic activities.
8. Recommendations for establishing an integrated best management practice in specific agricultural and urban areas where appropriate.
9. Expedite development of salinity based water quality criteria for different water aspects of use.

Moreover, further investigations are still needed to for a better qualifying the potential pollution using e.g. isotopic tracers to trace the water from irrigation run off and synthetic pesticides commonly used in the area. The Cl- isotope investigations could be an additional assisting tool to identify different sources of chloride which could be another good tracer to differentiate anthropogenic chloride from other natural sources.

Further modeling work in the area will be also an support, building different sorts of skimming and transient models which can provide more understanding for the saline water movement and fresh saline water interaction between water bodied in the aquifer. This can be combined with the suggested managements and remediation programs.

References:

- 1) ABDEEN, Z. & ABU-LIBDEH, H. (1993) Palestinian Population Handbook, Part 1. Jerusalem, the West Bank and Gaza Strip. Jerusalem: Planning and Research Centre Publications
- 2) ABED, A. M. (2000): Geology, Environment and Water of Jordan. Jordanian Geological Association Publications Amman, Jordan. 570 pp (in Arabic).
- 3) ABED RABBO, A., SCARPA, D.J., QANNAM, Z., ABDUL JABER, Q. and YOUNGER, P. (1999): Springs in the West Bank - water quality and chemistry. Palestinian Hydrology Group and Newcastle University, CMS Ltd., Palestine.
- 4) ALIEWI, A. S., MACKAY R., JAYYOUSI A., NASEREDDIN, K., MUSHTAHA, A. and YAQUBI, A. (2001) Numerical Simulation of the Movement of Saltwater under Skimming and Scavenger Pumping in the Pleistocene Aquifer of Gaza and Jericho Areas, Palestine. Transport in Porous Media Vol. 43, P.:195–212, 2001. Kluwer Academic Publishers, Netherlands.
- 5) ANDREW, I.J. (2000): Geology and geography of Jordan – a tourist's guide. (<http://www.andrewsi.freeserve.co.uk/jordan-geology.htm>, 06.02.2002).
- 6) ARKIN, Y. (1980): A survey of karst phenomena – western Judean mountains. Geological Survey of Israel, Rep. MM5/80, 30 p.
- 7) ARIJ (Applied Research Institute-Jerusalem): Water Resources. Chapter 8 in: The Status of the Environment in the West Bank. ARIJ, Jerusalem, 1997. pp.: 95-107.
- 8) ARIJ (Applied Research Institute-Jerusalem): Environmental Profile for the West Bank, Volume 2: Jericho District. ARIJ, Jerusalem, 1995.
- 9) ASCHROFT, G., Marsh, D. D., Evans, D. D. and Boersma L. (1962): Numerical method for solving the diffusion equation: 1. horizontal flow in semi-finite media soil. Science Society of America Proceedings, Vol.9, No.2, pp.97-156.
- 10) BANDEL, K. and Khoury, H. (1981): Lithostratigraphy of the Triassic in Jordan. Facies4, 1-26, Erlangen.
- 11) BARTOV, Y., ARKIN, Y., LEWY, Z. and MIMRAN, Y. (1981, reprinted 1988): Regional stratigraphy of Israel, A guide for geological mapping. Geological Survey of Israel-Ministry of Energy and Infrastructure, Jerusalem.

- 12) BAYER, H.-J., Hotzl, H., Jado, A. R., Roscher, B. & Voggenreiter, W. 1988. Sedimentary and structural evolution of the northwest Arabian Red Sea margin. *Tectonophysics*, 153, 137-152.
- 13) BEINHORN, M., GUTTMAN J. S., SAUTER M., TOLL M., KOLDITZ O., (2004). Groundwater modeling of the shallow aquifer in the Jericho area. In 5th Int Symposium on the Eastern Mediterranean Geology, Thessaloniki, Greece, pp. 1483-1486.
- 14) BEINHORN M and KOLDITZ O (2005): Overland Flow, theory and implementation, GeoSys – Preprint [2005-02], GeoSystems Research, Center for Applied Geosciences, University of Tübingen.
- 15) BEINHORN M and KOLDITZ O (2004): Object-oriented approach to preprocessing and process modeling in water resources, application to the Jericho area. In Proceedings of the 15th International Conference on Computational Methods in Water Resources (CMWR XV), Chapel Hill, NC, USA, Elsevier, pp. 1067-1077.
- 16) BEN-AVRAHAM, Z. 1992. Development of asymmetric basins along continental transform faults. *Tectonophysics*, 215, 209-220.
- 17) BRAUN, M. and HIRSCH, F. (1994): Mid Cretaceous (Albian-Cenomanian) carbonate platforms in Israel. *Cuadernos de Geologia Iberica*, 18: 59-81.
- 18) BURDON, D. (1959): Handbook of the Geology of Jordan; East of the Rift by A. M. Quennell. Govt. Hashemite Kingdom of Jordan, 82pp.
- 19) BÖTTCHER, J., STREBEL, O., VOERKELIUS, S. & SCHMIDT, H.-L. (1990) Using isotope fractionation of nitrate nitrogen and nitrate-oxygen for evaluation of microbial denitrification in a sandy aquifer. *J. Hydrol.* 114: 413-424.
- 20) CANTER LARRY W., 1996, Nitrate in Groundwater. Lewis Publishers, Inc., New York; (September 1996).
- 21) CARPENTER, A., 1978. Origin and chemical evolution of brines in sedimentary basins. *Oklahoma Geological Survey Circular* 39, 60±77.
- 22) CHEN C and KOLDITZ O (2005) A DEM based structural approach and TIN technology for terrain modeling, GeoSys – Preprint [2005-01], GeoSystems Research, Center for Applied Geosciences, University of Tübingen.
- 23) CHEN C, KHAYAT S and KOLDITZ O (2005): Development of a GIS based hydrosystem model for the Jericho area, Part 2: Structure model. GeoSys-Preprint [2005-4], GeoSystemsResearch, Center for Applied Geosciences, University of Tübingen, in preparation.
- 24) CUI CHEN, ALI SAWARIEH, THOMAS KALBACHER, MARTIN BEINHORN, WENMING WANG AND OLAF KOLDITZ (2004): A GIS

- based 3D Hydrosystem Model Application to the Zarqa Ma'in – Jiza areas in Central Jordan (accepted by Journal of Environmental Hydrology).
- 25) CLARK, I.D. and FRITZ, P. (1997) Environmental Isotopes in Hydrogeology: Lewis Publishers, New York, USA, 328pp.
 - 26) CLARK, I., FRITZ, P.: Nitrogen Cycling in Rural Watershed, Chapter 6 In: Environmental isotopes in hydrogeology. Lewis Publishers, Boca Raton, FL, 1997, pp.: 148-151.
 - 27) COOLEY, R.L., (1983) Some new procedures for numerical solution of variably saturated flow problems. Water Resour. Res., 19: 1271-1285.
 - 28) COPLEN, T.B., WILDMAN, J.D., AND CHEN, J., (1991). Improvements in the gaseous hydrogen-water equilibration technique for hydrogen isotope ratio analysis, *Analyt. Chem.*, 63:910-912.
 - 29) COPLEN, T.B. and HANSHAW, B.B., (1973): Ultrafiltration by a compacted clay membrane, I. Oxygen and hydrogen isotopic fractionation. *Geochim. Cosmochim. Acts*, 37, 2295-2310.
 - 30) CRAIG, H., (1963) The isotopic geochemistry of water and carbon in geothermal areas. In: E. Tongiorgi, (ED.), *Nuclear Geology on Geothermal Areas*, Spoleto, 1963. Consiglio Nazionale delle Ricerche, Laboratorio di Geologia Nucleare, Pisa: 17-53).
 - 31) CRAIG, H., (1961): Isotopic variation in meteoric waters. *Science* 133: 1702-1703.
 - 32) DREVER, J.I., (1997) *The Geochemistry of Natural Waters*, Prentice Hall Inc., 436p
 - 33) ELMUSA, SH.S. (1996): *Negotiation water: occupied Palestinian territories and the Palestinians*. Institute for Palestine Studies, USA.
 - 34) EI-NASER H.; SUBAH A., (2000): Using hydrochemistry and environmental isotopes to define the groundwater system of the Ain Maghara Spring, Jordan. *The Quarterly Journal of Engineering Geology and Hydrogeology*, Volume 33, Number 1, 1 January 2000, pp. 87-96(10).
 - 35) EXACT (1999): *Overview of Middle East Water Resources - Water Resources of Palestinian, Jordanian and Israeli Interest*. - compiled by U.S. Geological Survey for Executative Action Team, 44 p.; Washington
 - 36) EUROPEAN COMMISSION FIFTH RTD FRAMEWORK PROGRAMM, DEAD SEA BASIN, (2004): *Physiographic and Climate*. (Link:<http://www.deadseaproject.org/deadseaproject/DeadSeaProjectLink.htm>)

- 37) FARBER, E., VENGOSH, A., GAVRIELI, I., MARIE, A., BULLEN, T.D., MAYER, B., HOLZMAN, R., SEGAL, M., and SHAVIT, U. (2003) Hydrochemistry and Isotope Geochemistry of the Lower Jordan River: Constraints for the Origin and Mechanisms of Salinization. *Geochimica et Cosmochimica Acta*, Vol. 68, Issue 9, 1 May 2004, P.: 1989-2006.
- 38) FLEXER, A., YELLIN-DROR, A., KRONFELD, E., ROSENTHAL, E., BEN-AVRAHAM, Z., ARZSTEIN, PP., DAVIDSON, L., (2000): A Neogene salt body as the primary source of the salinity in Lake Kinneret. *Archiv Hydrobiol Spec Issue Adv Limnol* 55:69-85.
- 39) FLEXER, A., GILAT, A., HIRSCH, F., HONIGSTEIN, A.S., ROSENFELD, A., AND RUEFFER, T. (1989): Late Cretaceous evolution of the Judean Mountains as indicated by ostracods. *Terra Nova*, 1: 349-358.
- 40) FRIEDLI, H., LÖTSCHER, H. OESCHGER, U. SIEGENTHALER, AND B. STAUFFER. (1986). Ice core record of the $^{13}\text{C}/^{12}\text{C}$ ratio of atmospheric CO_2 in the past two centuries. *Nature* 324: 237-238.
- 41) FRITZ, P., AND FONTES, J. C., EDS: Handbook of Environmental Isotope Geochemistry, vol. 2B: The Terrestrial Environment, Elsevier Science, Amsterdam, pp. 361-425.
- 42) GASS, I. G. (1979): Evolutionary model for the Pan-African crystalline basement. In: Evolution and mineralization of the Arabian-Nubian Shield. *Bulletin of the Institute of Applied Geology, Jeddah*, 1, 11-20.
- 43) GAT, J.R. (1998): Modification of the isotopic composition of meteoric waters at the land-biosphere- atmosphere interface: In: Isotope Techniques in the Study of Environmental Change, IAEA, Vienna, Austria, 153-164.
- 44) GAT, J. and DANSGARD, W. (1972): "Stable isotope survey of the freshwater occurrences in Israel and the Northern Jordan Rift Valley." *Journal of Hydrology*, vol. 16 (177-212p.),
- 45) GAT, JR., MAYOR, E., TSUR, Y. (1969): The stable isotope composition of mineral waters in the Jordan Rift Valley. *J. Hydrol.* 7:334-352
- 46) GAVRIELI, I., STEIN, M., KOLODNY, Y., AND SPIRO, B. (1998): Sulfur Isotopes in Gypsum as indicator for Paleolimnological conditions of Lake Lisan, the Dead Sea Rift Valley. *Am. Geophys. U. Annul. Fall Meet.*, San Francisco, December, 1998, p. F521.
- 47) GAVRIELI, I., YECHIELI, Y., HALICZ, L., SPIRO, B., BEIN, A. AND EFRON, D. (2001): The sulfur system in anoxic subsurface brines and its implication on brine evolutionary pathways: The Ca-chloride brines in the Dead Sea area. *Earth Planet. Sci. Lett.* 186, 199-213.

- 48) GEOLOGICAL SURVEY OF ISRAEL (1999): Geological map of Israel- 1:200000, 4 sheets.
- 49) GEOLOGICAL SURVEY OF ISRAEL (1973): Geological map of Jericho- 1:50000, 2 sheets.
- 50) GARFUNKEL, Z., ZAK, I. AND FREUND R. (1981): Active faulting in the Dead Sea Rift. In: Freund R. and Garfunkel I. (ed.) The Dead Sea Rift. Tectonophysics V. 80. 1-26pp.
- 51) GOLANI, U., 1972. Groundwater resources in Jericho region. Tech. rep., Tahal Report HR/72/016 (in hebrew).
- 52) GUTTMAN, J. (2006): Geology and Hydrogeology of the Jordan Valley – Multi-lateral project, project 02WT9719 within the framework of the German-Israeli-Jordanian-Palestinian joint research program for the sustainable utilization of aquifer systems. (In progress).
- 53) GUTTMAN, J. (2000): Sub-project B - Hydrogeology of the Eastern Aquifer in the Judea Hills and Jordan Valley – Multi-lateral project, project 02WT9719 within the framework of the German-Israeli-Jordanian-Palestinian joint research program for the sustainable utilization of aquifer systems. Mekorot report no. 468. (unpublished).
- 54) GUTTMAN, J. and ZUKERMAN, CH. (1995). A model of the flow in the Eastern Basin of the Mountains of Judea and Samaria from the Far'ah to the Judean Desert. Water Planning for Israel, Inc (Tahal), Tel Aviv. (unpublished report).
- 55) GVIRTZMAN, H. (1994): Groundwater Allocation in Judea and Samaria, In: Water and Peace in the Middle East, Issac, J. and Shuval, H., Elsevier, Amsterdam.
- 56) GROPIUS, M.; KLINGBEIL, R. (1999): Modelling of Groundwater Flow Between the Cretaceous Mountain Aquifer Systems and the Jordan-Dead Sea Area. Diploma work, Eberhard-Karls University/ Tübingen.
- 57) HIRSCH, F. (1983): The geological map of Israel, 1:50,000, Sheet 11-III - Bet Guvrin. Explanatory notes. Geological Survey of Israel.
- 58) HOBLE, M & AL. (1993). Groundwater Resources of Northern Jordan - Vol. 3. Structural Features of the Main. Library of Water Authority of Jordan, Amman, Jordan.
- 59) HOEFS, J. (2004): Stable isotope geochemistry; 5th ed., Springer-Verlag, 2004. 244p.
- 60) HUSARY, S.; NAJJAR, T. and ELIEWI, A. (1995): Analysis of secondary source rainfall data from the northern West Bank. PHG, Jerusalem. (unpublished).
- 61) HÜNBER, H. 1986. Isotope effects of nitrogen in the soil and biosphere. In: P. Fritz and J. Ch. Fontes (eds.), Handbook of

- Environmental Geochemistry IA, Elsevier Science Publ., Amsterdam, New York: 361-426.
- 62) KAFRI, U., AND ARAD, A. (1979), Current subsurface intrusion of Mediterranean Sea water, a possible source of groundwater salinity in the Rift Valley system, Israel: *Journal of Hydrology*, v. 44, p. 267–287.
- 63) KALBACHER, T., WANG, W., MCDERMOTT, C., KOLDITZ, O., TANIGUCHI, T. (2003): Development and application of a CAD interface for fractured rock. *J Environmental Geology*, in print.
- 64) KALIN, R. (1996): Manual of mathematical model. Laboratory and Quality Dept. of Water Authority of Jordan. (Unpublished).
- 65) KASHAI, E.L., CROCKER, P.F. (1987). Structural geometry and evolution of the Dead Sea–Jordan rift system as deduced from new subsurface data. *Tectonophysics* 141: 33–60.
- 66) KENDAL, C., DOCTOR, D. (2004), Stable Isotope Application in Hydrologic Studies. In: Drever, J. I. (ed.): *Surface and groundwater, weathering and soils: 'Treatise on Geochemistry' V.5*, Elsevier Pergamon., Oxford, 2004, pp.: 319-364.
- 67) KENDALL, C., ARAVENA, R., (2000): Nitrate isotopes in groundwater systems. In: *Environmental tracers in subsurface hydrology*. Chapter 9. Cook, P. and Herczeg, A. L., Eds. Kluwer Academic Press, Dordrecht, 2000. pp.: 261-298.
- 68) KENDALL, C. (1998): Tracing nitrogen sources and cycling in catchments, chapter 16, In: Kendall C. and McDonnell, J. J., (ed.) *Isotope tracers in catchment hydrology*, Elsevier, Amsterdam, 1998, pp.: 519-576.
- 69) KENDALL, C., SKLASH, M.G., BULLEN, T.D. (1995). "Isotope Tracers of Water and Solute Sources in Catchments", In: *Solute Modelling in Catchment Systems*, John Wiley & Sons, New York, pp. 261- 303.
- 70) KHAYAT, S., HOETZL, H., GEYER, S. & ALI, W. (2005): Hydrochemical investigation of water from the Pleistocene wells and springs, Jericho area/ Palestine. *Hydrogeology Journal*, Springer Publisher. Online First, 26.Jan.2005.
- 71) KHAYAT, S., ALI, W., GEYER, S., AND HÖTZL, H. (2005): Development of a GIS based hydrosystem model for the Jericho area, Part 1: Data base. Technical report, Applied Geology, University of Karlsruhe (Unpublished).
- 72) KLEIN-BENDAVID O., SASS E., KATZ A. (2004): The evolution of marine evaporitic brines in inland.
- 73) KOLDITZ, O., AND KHAYAT, S. (2005): Development of a GIS based hydrosystem model for the Jericho area, Part 3: Groundwater model.

- GeoSys-Preprint [2005-5], GeoSystemsResearch, Center for Applied Geosciences, University of Tübingen, in preparation.
- 74) KOLDITZ, O., DE JONGE, J., BEINHORN, M., XIE, M., KALBACHER, T., WANG, W., BAUER, S., MCDERMOTT, C.I., CHEN, C., GRONEWOLD, J., BEYER, C., KEMMLER, D., WALSH, R., AND LEGEYDA, D. (2004), Open Source – Software Design Proposal. Technical Report, GeoSys –Preprint [2004-25], GeoSystemsResearch, Center for Applied Geosciences, University of Tübingen .
- 75) KOLDITZ, O., DE JONGE, J., BEINHORN, M., XIE M., KALBACHER, T., WANG, W., BAUER, S., MCDERMOTT CH., KAISER C.I., KOHLMEIER R., (2003), ROCKFLOW – Theory and User Manual, release 3.9. Technical Report, Groundwater Modeling Group, Center for Applied Geosciences, University of Tübingen & Institute of Fluid Mechanics, University of Hannover, 2003. GeoSys– Preprint, [2003-37], Center of Applied Geosciences, Geohydrology/Hydroinformatics, University of Tübingen.
- 76) KOLDITZ, O., HABBAR, A., KAISER, R., SCHULZE-RUHFUS, M. & THORENZ, C. (1998): ROCKFLOW - Theory and Users Manual. Release 3.2, Institut für Strömungsmechanik und Elektronisches Rechnen im Bauwesen, Universität Hannover, 1998.
- 77) KOMURA, I., AND IZAKI, K. (1971), Mechanism of mercuricchloride resistance in microorganisms. I. Vaporization of a mercury compound from mercuric chloride by multiple drug resistant strains of Escherichia coli. J. Biochem. (Tokyo) 70:885-893.
- 78) KRENKEL, E. (1924): Der Syrische Bogen. Mineral., 9: 274-281 and 10: 301-313.
- 79) LANDMANN, G., ABU QUDAIRA, G.M., SHAWABKEH, K. & WREDE, V., (2001): Geochemistry of Lisan Formation in Jordan and implications on palaeoclimate. The 7th Jordanian Geological Conference, Amman, Abstracts, 136.
- 80) LEGRAND, H.E. and STRINGFIELD, V.T. (1973): Karst hydrology – review. Journal of Hydrology, 20. North-Holland Publishing Company, Amsterdam: 97-120.
- 81) LIBISZEWSKI, S. (1995): Water disputes in the Jordan Basin Region and their role in the resolution of the Arab-Israeli conflict, ENCOP Occasional Paper No. 3. Center for Security Policy and conflict Research, Zurich; Swiss Peace Foundation Berne, Zurich. ISBN: 3-905641-36-4.
- 82) MARIE, A. AND VENGOSH, A. (2001) Sources of salinity in groundwater from Jericho area, Jordan valley. J. Groundwater. 39, 240-248.

- 83) MATSUI, E., (1980), A simple method using a disposable syringe to prepare samples for d18O measurements in water samples. *Analytica Chimica Acta* 120, 423–425.
- 84) MAZOR, E. (1997): *Chemical and isotopic groundwater hydrogeology, the applied approach*, 2nd Edition. Marcel Dekker, Inc., New York.
- 85) MILANOVIC, P.T. (1981): *Karst hydrogeology*. Water Resources Publications.
- 86) MILLENNIUM ENGINEERING GROUP -CH2M HILL / MONTGOMERY WATSON / ARABTECH JORDANEH (2000): *West Bank water resources, program 2 and Bethlehem 2000 project – Groundwater management modeling*.
- 87) MOOK WILLEM G., DE VRIES J. J., 2003, VOLUME I: Introduction - Theory, Methods, and Review. In: *Environmental Isotopes in the Hydrological Cycle Principles and Applications*. International Atomic Energy Agency, Vienna, Austria, 2004, pp.:89-120. [<http://www.iaea.org/programmes/ripc/ih/volumes/volumes.htm>]
- 88) NEEV, D., AND HALL, J. K., (1979), *Geophysical investigations in the Dead Sea: Sedimentary Geology*, v. 23, p. 209–238.
- 89) OSLO 2 ACCORDS (1995): Article 40 - Water and sewage, Tab. (unpublished)
- 90) PCBS - PALESTINIAN CENTRAL BUREAU OF STATISTICS (2002): *Small area populations, 1997-2010, Ramallah, Palestine*. (unpublished).
- 91) PETTIJOHN, F.J. (1957). *Sedimentary rocks*, 2nd Edition. Harper Brothers, New York: 718 p.
- 92) PHG-Palestinian Hydrology Group-Jerusalem, *Water Quality and Hydrogeology of the Eastern Aquifers Bordering the Jordan Valley-Jericho District*, technical report (1999).
- 93) PICARD, L. (1943): *Structure and evolution of Palestine with comparative notes on neighbouring countries*. Bull.Geol.Dept.Hebrew Univ.Jerusalem, 4, 1-143
- 94) PICARD, L. (1938): *The geology of new Jerusalem*. Bull. of the Geol. Dept Hebrew Univ. Jerusalem, 2, 1.
- 95) PWA - PALESTINIAN WATER AUTHORITY (2003): *Wells of the Jericho area and Jordan Rift Valley– Wells lithological profiles and groundwater data*. Palestinian Water Authority- Water Data Bank Section. Personal communication.
- 96) QANNAM, Z. and MERKEL, B. (2002): *Hydrogeology, hydrochemistry and contamination sources in Wadi Al Arroub driange basin, Palestine*. Freiburger Forschungshefte- Selected contribution to applied geology

- in the Jordan Rift Valley, C 494, Technische Universität Bergakademie Freiberg, Germany. ISBN: 3-86012-162-6: 111-123.
- 97) QUENNELL, A.M. (1956): Tectonics of the Dead Sea Rift. Proc. 20th. Int. Geol. Congress. Mexico, Ass. Deserv. Geol. Afrfricanos, 385-403.
- 98) QUENNELL, A.M. (1951): The geology and mineral resources of former Transjordan. Colon. Geol. Min. Resource. 2. 2.
- 99) REMSON, I., APPEL, C.A. AND WEBSTER, R.A. (1965): Groundwater model solved by digital computer. Journal of the hydraulics Division, American Society of Civil Engineers, Vol.91, No. HY3, pp 133-147.
- 100) ROFE and RAFFETY (1963): Jerusalem District water supply, Geological and Hydrological Report. Hashemite Kingdom of Jordan Central Water Authority. (unpublished).
- 101) ROSENTHAL E., AND FLEXER A., (2006): The Hydrochemical History of the Jordan Rift Valley– Multi-lateral project, project 02WT9719 within the framework of the German-Israeli-Jordanian-Palestinian joint research program for the sustainable utilization of aquifer systems. (In progress).
- 102) ROSENTHAL, E. (1988): Hydrochemistry of groundwater at unique outlets of the Bet- Shean-Harod multiple aquifer system. J Hydrol 97:75-87
- 103) ROSENTHAL, E., VENGOSH, A. (1994): Saline Groundwater in Israel: Ist on the Water Crisis in the Country. - Journal of Hydrology 156; (1994), p. 389-430; Amsterdam.
- 104) ROSENTHAL E., WEINBERGER G., KRONFELD J. (1999): Groundwater salinization caused by residual Neogene and Pliocene sea water – an example from the Judea Group aquifer, southern Israel. Groundwater 37: 261-270
- 105) ROTSTEIN, Y., BARTOV, Y., AND HOFSTETTER, A., (1991): Active compressional tectonics in the Jericho area, the Dead Sea Rift: Tectonophysics, v. 198, p. 239–259.
- 106) ROZANSKI, K., GRÖNING, M., (2004): Tritium assay in water samples using electrolytic enrichment and liquid scintillation spectrometry. TECDOC-1401, IAEA, pp. 195-217
- 107) SALAMEH, E. AND EL-NASER, H. (2000): Changes in the Dead Sea level and their impacts on the surrounding groundwater bodies. Acta Hydrochimica et Hydrobiologica 28, 24-33.
- 108) SALAMEH, E. (2002): Sources of water salinities in the Jordan Valley area/Jordan. Acta Hydrochimica Et Hydrobiologica vol. 29: 329-362.
- 109) SALAMEH, E. (1996): Water quality degradation in Jordan: impacts on environment, economy and future generating resource base.

- Friedrich Ebert Stiftungs, and Royal Society for Conservation of Nature, Amman, Jordan. 179pp.
- 110) SASS, E.; STARINSKY, A. (1979). Behaviour of strontium in subsurface calcium chloride brines: Southern Israel and Dead Sea rift valley. *Geochimica et Cosmochimica Acta*, vol. 43, Issue 6, pp.885-895.
- 111) SCHLUMBERGER, (2002): Oilfield glossary, 29.03.2002. (www.glossary.oilfield.slb.com/Display.cfm?Term=dolomitization).
- 112) SCHULMAN, N., (1959): The geology of the central Jordan Valley. *Bull. Res. Coun. Israel* 8G[2-3]: 63-90.
- 113) SCHWARZ, J. (1982): Water resources in Judea, Samaria and Gaza Strip; View on the present and the future, ed. by D. Elazar. American Enterprise Institute for Public Policy Res. Washington.
- 114) SHARMA, T. AND CLAYTON, R.N. (2000) Measurement of $\delta^{18}O/\delta^{16}O$ ratios of total oxygen of carbonates, *Geochimica et Cosmochimica Acta* 29(12), 1347-1353.
- 115) SHACHNAI, E. (1969): Lower Cretaceous stratigraphy of the Bet El (Ramallah) Mountain. *Israel Journal of Earth Sciences*, Vol. 18, No. 3-4: 169p.
- 116) SIEMANN, MG, SCHRAMM, M. (2002) Henry's and non-Henry's law behaviour of Br in simple marine systems. *Geochim Cosmochim Acta* 66:1387-1399.
- 117) SILVA, S.R., KENDALL, C., WILKINSON, D.H., ZIEGLER, A.C., CHANG, C.C.Y., AND AVANZINO, R.J.: A new method for collection of nitrate from fresh water and the analysis of nitrogen and oxygen isotope ratios. *J. Hydrol.* 228, pp.: 22-36 (2000).
- 118) SIMPSON, B., CARMI, I., 1983. The hydrology of the Jordan River (Israel): hydrographic and isotopic investigations. *J. Hydrol.* 62, 225±242.
- 119) STARINSKY, A. (1997): The evolution of brines along the Dead Sea Rift. In *The Dead Sea Rift as a Unique Global Site*. Proc. 13th meeting German Israeli Foundation for Scientific Research and Development, February 1997, Dead Sea, Israel.
- 120) STARINSKY, A. (1974): Relationships between Ca-chloride brines and sedimentary rocks in Israel. PhD thesis, Dept. of Geology, Hebrew University, Jerusalem
- 121) STOECKLIN, J. (1968). Salt deposits of the Middle East. In: R.B. Mattox [ed]. *International Conference of Saline Deposits, 1962*. *Geol. Soc Amer. Spec. Pap.* 88:157-181

- 122) STURM, C., RIBBE, L. and SCHWABE, C. (1996): Water resources management in the West Bank, Palestine - Final Report. ASA Program 1996. Carl Duisberg Gesellschaft e. V., Berlin. (<http://www.tt.fh-koeln.de/publi/westba97.pdf>, 02-04-2002).
- 123) TAYLOR, C.B., AND W. ROETHER, (1982): A uniform scale for reporting low-level tritium measurements in water, *Int. J. Appl. Radiat. Isot.*, 33, 377-382, 1982.
- 124) TEN BRINK, U.S., AND Z. BEN-AVRAHAM, (1999): The anatomy of a pull-apart basin: seismic reflection observations of the Dead Sea basin, *Tectonics*, v. 8, pp. 333-350, 1989.
- 125) TRACY, J.C., AND M.A. MARINO, (1987). Solute Movement Through Root soil Environment, *J. Irrig. and Drain. Engrg.*, ASCE, 115 (4), pp. 608-625.
- 126) TURI, B., 1986. Stable isotope geochemistry of travertine's. In: Fritz P., Fontes, J.C. (Eds.), *Handbook of Environmental Isotope Geochemistry*, Vol. 2, Elsevier, Amsterdam, pp.207±239.
- 127) VENGOSH, A. & E. ROSENTHAL, (1994): Saline groundwater in Israel: it's bearing on the water crisis in the country. *Journal of Hydrology* 156, 389-430.
- 128) VENGOSH, A., STARINSKY, A., KOLODNY, Y., CHIVAS, A. R., (1994). Boron isotope geochemistry of thermal springs from the northern Rift Valley, Israel. *J. Hydrol.* 162, 155±169.
- 129) VOGEL, J., AND EHHALT, C. (1963). The use of the carbon isotopes in groundwater studies. *Radioisotopes in Hydrology*, 383-395.
- 130) WENNRICH, R., (2005): The analytical methods, and detection limits for major and minor ions. Department of chemical analysis, UFZ Leipzig-Halle GmbH. [Personal communication].
- 131) WINTER, T.C., (1983). The Interaction of Lakes with Variably Saturated Porous Media, *Water Resour. Res.*, 19 (5), pp. 1203-1218.
- 132) WOLF, A.T. (1995): Hydro-politics along the Jordan River - scarce water and its impact on the Arab-Israeli conflict. United Nations University Press. The United Nations University. Tokyo, Japan: 383 p.
- 133) WOLFER, J. (1998): Hydrogeological Investigations along the Jerusalem-Jericho Transsect (Wadi el Qilt), Israel, West Bank. - Diploma Thesis, University of Karlsruhe.
- 134) WWS – WOODROW WILSON SCHOOL OF PUBLIC AND INTERNATIONAL AFFAIRS – PRINCETON UNIVERSITY (2002): Water rights in the Jordan Valley – Geography and water resources, WWS 401C. (www.wws.princeton.edu/~wws401c, 02-04-2002).

-
- 135)ZAK, I. (1963) Remarks on the stratigraphy and tectonics of the Triassic of Makhtesh Ramon. *Isr. J. Earth Sci.* 12:87-89.
- 136)ZIENKIEWICZ, O. C., MEYER, P., AND CHEUNG, Y. K. (1966): Solution of anisotropic seepage problems by finite elements. *Proceedings American Society of Civil Engineers*, Vol. 92 EMI, pp. 111-120.
- 137)ZIENKIEWICZ, O.C. (1971): *The finite element method in engineering science*, Mc Graw- Hill, London.

APENDIXES

Datenblatt : Palästina		hg UFZ-HDG Halle, wenn nicht anders angegeben, Hauptelemente mit IC gemessen!!										Ammonium (mg/l)					Spurenelemente
SampleID	Site	Well Code	K	Mg	Mg2+	Mg	Ca2+	Ca	Mn	Fe	NH4	B	Ba	Sr	Cr	As (AAS)	
J03-01	Arab Project6	19-14/066	82.6		213.7			186.1		0.0206	0.084	0.01	1.078	0.099		3.56	
J04-01	Arab Project6	19-14-66	78.3		198			168.1		-0.009	0.0333	0	1.023	0.1028	3.173	0.06	
J03-02	Arab Project6	19-14/067	104.1		220.8			167.3		-0.01	0.868	0	1.32	0.1534	2.843		
J04-02	Arab Project6	19-14/067	102.9		219.7			163.2		0.009	0.0447	0	1.313	0.1513	2.753	0.07	
J03-03	Arab Project7	19-14/073	79.6		164.6			128.3		-0.01	-0.05	0	0.973	0.2205	1.833		
J04-03	Arab Project7	19-14/073	75.1		158.9			123.9		0.009	0.0738	0.001	0.945	0.2113	1.729	0.05	
J03-04	Fahmi Nahas	19-13/048	15.38		69.9			91.5		-0.01	-0.05	0	0.2566	0.0651	2.003		
J04-04	Fahmi Nahas	19-13/048	14.68		66.4			89.8		0	0.0103	0	0.2666	0.0683	1.896	0.01	
J03-05	Fahmi Nahas	19-13/047	12.42		66.6			93.7		-0.01	-0.05	0.006	0.2671	0.0673	2.144		
J04-05	Fahmi Nahas	19-13/047	12.07		63.3			89.7		0	0	0.018	0.2633	0.0624	2.054	0.01	
J03-06	Sabiru Rantiz	19-13/006	7.95		93.5			173.4		-0.01	-0.05	0	0.3118	0.1269	3.553		
J04-06	Sabiru Rantiz	19-13/006	7.75		91.1			163		0	0	0.02	0.32	0.1242	3.415	0.01	
J03-07	Fahed Hishm	19-13/015	38.47		101.4			99.5		-0.01	0	0.002	0.476	0.0893	1.732		
J04-07	Fahed Hishm	19-13/015	37.34		101			103.9		0	0.1163	0.02	0.4659	0.0978	1.775	0.03	
J03-08	Zuhdi Hashwa	19-13/052	28.32		113.9			127.7		-0.01	-0.05	0.005	0.4956	0.0713	3.579		
J04-08	Zuhdi Hashwa	19-13/052	27.95		115.4			128		0	0.1531	0	0.527	0.0885	3.358	0.02	
J03-09	Salah Arouri	19-14/012	11.17		63.3			88.4		-0.01	-0.05	0.001	0.2083	0.054	1.887		
J04-09	Salah Arouri	19-14/012	10.86		60.2			87.7		-0.009	0.0188	0	0.2168	0.0592	1.814	0.01	
J03-10	Basil Husaini	19-13/020	17.01		73.4			92		0.2183	0.4107	0.007	0.4115	0.0838	1.607		
J04-10	Basil Husaini	19-13/020	14.82		63			82.8		-0.009	-0.01	0	0.3908	0.0732	1.366	0.01	
J03-11	Basil Husaini	19-13/018	9.63		52.2			87.7		-0.01	-0.05	0.004	0.216	0.0353	1.3		
J04-11	Basil Husaini	19-13/018	9.2		49.72			86.4		-0.009	-0.01	0	0.2262	0.0414	1.226	0.01	
J03-12	Ibrahim Daek	NW	39.52		130			131.7		-0.01	-0.05	0.008	0.734	0.126	2.259		
J04-12	Ibrahim Daek	IBRAIN DEK	39.32		127.3			126.7		-0.009	0.0303	0.169	0.746	0.1514	2.241	0.03	
J03-13	Iron Factory	19-13/26a	16.7		97.6			130		0.0218	-0.05	0.005	0.2302	0.3069	4.308		
J03-14	Ein Sultan	AC/061	2.503		30.08			79.1		-0.01	-0.05	0.005	0.0406	0.0301	0.1253		
J04-14	Ein Sultan	AC/61	2.678		27.88			83.9		-0.009	0.0328	0	0.0486	0.0334	0.1176	-0.005	
J03-15	Ein Dyouk	AC/060	2.471		29.81			81.5		-0.01	0.1126	0.015	0.0407	0.0342	0.1324		
J04-15	Ein Dyouk	AC/60	2.688		28.25			85.9		-0.009	0.0241	0.054	0.0467	0.0314	0.117	-0.005	
J03-16	Awni Hijazi	19-14/052	35.78		124.3			122		-0.01	-0.05	0.012	0.4954	0.1649	2.853		
J04-16	Awni Hijazi	19-14/052	34.12		117.3			115.6		0.049	0.3821	0.054	0.4702	0.1657	2.654	0.03	
J03-17	Saeed Aladee	19-14/062	24.18		109.9			140.7		-0.01	-0.05	0.016	0.295	0.079	1.19		
J04-17	Saeed Aladee	19-14/062	21.16		94.8			125.8	0	-0.009	-0.01	0.01	0.2717	0.0739	1.032	0.02	
J03-18	Mohammed N	19-14/038	19.42		102.1			128.1		-0.01	-0.05	0.031	0.294	0.1076	1.166		
J04-18	Mohammed N	19-14/38	19.04		97.5			140.1		0.0206	0.0591	0	0.3059	0.1054	1.116	0.02	
J03-19	Samed	19-14/26a	6.37		64.2			117.9		-0.01	-0.05	0.017	0.1239	0.0603	0.525		
J04-19	Samed	19-14/26a	5.56		58.5			116.9		-0.009	0.0117	0	0.1042	0.0641	0.4578	0.01	
J03-20	Arab Project6	19-13/069	79.6		140			116.7		-0.01	-0.05	0.017	0.818	0.16	1.961		
J04-20	Arab Project6	19-13/069	75		148.9			112.1		-0.009	0.0148	0	0.786	0.1561	1.809	0.05	
J03-21	Abdallah Arai	19-14/049	15.34		105.7			131.2		-0.01	0.1426	0.024	0.2927	0.1571	1.127		
J04-22	Awn Hijazi	19-14/37	47.14		157.4			157.2		-0.009	0.0185	0	0.595	0.1432	1.867	0.04	
J04-23	Saleem Nimr	19-13/49	50.1		76.2			71.9		-0.009	-0.01	0	0.519	0.126	1.126	0.03	
J04-24	Qasir Hisham	19-13/003	27.63		123.7			163.6		-0.009	0.0219	0	0.3349	0.0355	1.42	0.02	
J04-25	Bail Hussaini	19-13/22	42.26		135.6			133.7		-0.009	0.0223	0.01	0.648	0.1219	2.178	0.03	
J04-26	Mahmud Akra	19-13/50a	33.47		92.8			119.5		0.0428	0.4029	0.17	0.3775	0.1162	1.946	0.03	
J04-27	Bail Hussaini	19-13/21	36.26		118.2			117.4		-0.009	-0.01	0.03	0.586	0.1265	1.764	0.03	
J003-Z	Jericho Süd 1	Lisan	1334.5		145.4			4020		#WERT!	#WERT!	#WERT!	29.15	0.2565	39.5	0.03	
J003-I	Jericho Qilt 8	Lisan	166.3		754			2855		0.2005	#WERT!	5	5.2	1.139	183.4		
J003-X	Jericho Süd 1	Lisan	2770		836			3420		#WERT!	#WERT!	1	165.75	0.1595	58.6		
J003-P	Fertiliser cher	Fertilizer	151375		70.9			43.95		241.5	419.5	2	0.927	0.155	0.6725		
J004-Q	Lisan	Lisan	3.72		44.5			156		-0.01	-0.1		0.38	0.33	17.14		
J004-Z	Samara	Samara	1.28		4.66			18.2		-0.01	-0.1		0.06	0.02	0.1		
J004-Y	Samara	Samara	2.65		10.3			10.7		-0.01	-0.1		0.11	0.05	0.32		
J004-X	Lisan	Lisan	1.88		20.7			74.8		-0.01	-0.1		0.28	0.23	9.62		

Datenblatt : Palästina			Wasserproben											
schwarz=Eingte mg/l			IC : Anionen/Kationen (mg/l)											
	rot= Berechnu	Al	F-	Cl-	Br-	I	SO42-	NO3-	NO2-	C(HCO3) mg/L	C(CO3) mg/L	PO43-	P	Si
XXXXXXXXXX	XXXXXXXXXX	XXXXXXXXXX	XXXXXXXXXX	XXXXXXXXXX	XXXXXXXXXX	XXXXXXXXXX	XXXXXXXXXX	XXXXXXXXXX	XXXXXXXXXX	XXXXXXXXXX	XXXXXXXXXX	XXXXXXXXXX	XXXXXXXXXX	XXXXXXXXXX
SampleID	Site	Well Code	F	Cl	Br	I	SO4	NO3		HCO3	CO3	PO4	P	Si
J03-01	Arab Project6	19-14/066	-0.2	1423	15.7		300.9	29.69		439.2	0.474	0.035	0.01142105	8.8
J04-01	Arab Project6	19-14-66	-0.2	1405	11.5		285	38		409.31	0.939	0.01	0.00326316	8.51
J03-02	Arab Project6	19-14/067	-0.2	1638	14		183.4	38.86		366.61	0.358	0.043	0.01403158	8.36
J04-02	Arab Project6	19-14/067	-0.2	1725	13.9		221	51		405.04	0.566	0	0	7.94
J03-03	Arab Project7	19-14/073	-0.2	1000	7.6		95.9	40.41		405.65	0.358	0.016	0.00522105	7.97
J04-03	Arab Project7	19-14/073	-0.2	1014	7.1		111	48		386.13	0.352	0.01	0.00326316	7.56
J03-04	Fahmi Nahas	19-13/048	-0.2	238	2.5		70	41.67		347.7	0.362	0	0	7.3
J04-04	Fahmi Nahas	19-13/048	-0.2	240	1.6		82.7	61		317.81	0.316	0.05	0.01631579	6.89
J03-05	Fahmi Nahas	19-13/047	-0.2	225	2.2		77.2	43.73		355.02	0.384	0	0	7.96
J04-05	Fahmi Nahas	19-13/047	-0.2	228	1.2		82.2	71.5		322.69	0.28	0.05	0.01631579	7.45
J03-06	Sabiru Rantiz	19-13/006	-0.2	414	2.5		117.6	62		376.37	0.216	0.301	0.09822105	9.23
J04-06	Sabiru Rantiz	19-13/006	-0.2	452	2		153	100		342.21	0.266	0.01	0.00326316	8.8
J03-07	Fahed Hishm	19-13/015	-0.2	504	5.3		60.8	33.24		378.81	0.355	0.001	0.00032632	6.99
J04-07	Fahed Hishm	19-13/015	-0.2	513	4.5		62.1	50		337.33	0.341	0.3	0.09789474	6.77
J03-08	Zuhdi Hashwa	19-13/052	-0.2	536	4.1		166	46.55		369.05	0.404	0	0	7.43
J04-08	Zuhdi Hashwa	19-13/052	-0.2	556	3.4		194	79		349.53	0.351	0.05	0.01631579	7.14
J03-09	Salah Arouri	19-14/012	-0.2	187	1.9		59.2	40.54		417.85	0.383	0	0	7.74
J04-09	Salah Arouri	19-14/012	0.44	195	1.1		64.5	70		342.21	0.345	0.3	0.09789474	7.32
J03-10	Basil Husaini	19-13/020	-0.2	264	2.5		110.1	49.38		349.53	0.338	0.005	0.00163158	6.99
J04-10	Basil Husaini	19-13/020	0.44	243	1.6		120	65		317.2	0.452	0.06	0.01957895	6.2
J03-11	Basil Husaini	19-13/018	-0.2	162	2.2		58.6	29.08		304.39	0.311	0	0	7.05
J04-11	Basil Husaini	19-13/018	0.44	166	0.5		71.4	52		292.8	0.639	0.1	0.03263158	6.75
J03-12	Ibrahim Daek	NW	-0.2	750	6.2		167.7	29.68		376.37	0.312	0	0	6.98
J04-12	Ibrahim Daek	IBRAIN DEK	0.32	764	5.9		189	47		369.05	0.36	0.05	0.01631579	6.86
J03-13	Iron Factory	19-13/26a	-0.2	406	2.5		90	70.13		259.25	0.323	0	0	10.69
J03-14	Ein Sultan	AC/061	-0.2	34.4	1		17.2	42.46		295.24	0.622	0.095	0.031	4.757
J04-14	Ein Sultan	AC/61	0.2	48.7	0.5		24.1	48		266.57	0.381	0.165	0.05384211	4.43
J03-15	Ein Dyouk	AC/060	-0.2	34.9	0.5		16.7	29.07		287.31	0.229	0.097	0.03165263	4.785
J04-15	Ein Dyouk	AC/60	0.2	44.6	0.5		23.8	55		293.41	0.364	0.215	0.0701579	4.473
J03-16	Awni Hijazi	19-14/052	-0.2	745	7.2		72.1	34.07		380.03	0.242	0	0	8.17
J04-16	Awni Hijazi	19-14/052	-0.2	695	6.5		76.5	50		417.85	0.356	0.08	0.02610526	8.16
J03-17	Saeed Aladee	19-14/062	-0.2	656	8.7		40.6	5.18		364.17	0.226	0.088	0.02871579	6.87
J04-17	Saeed Aladee	19-14/062	0.29	566	5.6		43.5	20		393.45	0.29	0.2	0.06526316	6.36
J03-18	Mohammed N	19-14/038	-0.2	499	6.1		39.6	7.5		380.03	0.189	0	0	7.27
J04-18	Mohammed N	19-14/38	-0.2	527	6.2		44	10.5		403.21	0.287	0.06	0.01957895	6.87
J03-19	Samed	19-14/26a	-0.2	121	1.7		22.6	15.97		437.37	0.471	0	0	7.04
J04-19	Samed	19-14/26a	-0.2	130	0.9		20.9	41		412.97	0.37	0.03	0.00978947	6.48
J03-20	Arab Project6	19-13/069	-0.2	1041	10.9		103.8	24.51		418.46	0.399	0.012	0.00391579	7.85
J04-20	Arab Project6	19-13/069	-0.2	1054	11		109	43		415.41	0.371	0.012	0.00391579	7.39
J03-21	Abdallah Arai	19-14/049	-0.2	528	5.8		92.7	30.58		364.78	0.14	0.004	0.00130526	7.12
J04-22	Awn Hijazi	19-14/37	-0.2	916	8.4		117	49.5		383.69	0.275	0.01	0.00326316	8.22
J04-23	Saleem Nimr	19-13/49	-0.2	335	1.8		66.2	75		385.52	0.553	0.12	0.0391579	7.49
J04-24	Qasir Hisham	19-13/003	-0.2	890	11.9		52.6	23.5		349.53	0.341	0	0	9.31
J04-25	Bail Hussaini	19-13/22	-0.2	693	4.2		222	50		344.65	0.27	0.1	0.03263158	7.64
J04-26	Mahmud Akra	19-13/50a	-0.2	385	2		109	54		406.26	0.154	0.14	0.04568421	8.28
J04-27	Bail Hussaini	19-13/21	-0.2	722	5.7		172	95		349.53	0.404	0.023	0.00750526	7.11
J003-Z	Jericho Süd 1	Lisan	-0.2		#WERT!		5500	91				#WERT!	0.404	3.75
J003-I	Jericho Qilt 8	Lisan	-0.2		70.5		707.5	653				#WERT!	#WERT!	30.45
J003-X	Jericho Süd 1	Lisan	-0.2		77.5		24175	91				#WERT!	1.7235	6.945
J003-P	Fertiliser cher	Fertilizer	-0.2		#WERT!		1796.5	236000				250500	70875	8.53
J004-Q	Lisan	Lisan	1.7	882.66	6.21		20.19							10.8
J004-Z	Samara	Samara	0.48	2.46	0.14		10.4							4.28
J004-Y	Samara	Samara	0.93	94.91	0.63		18.27							3.96
J004-X	Lisan	Lisan	1.7	390.61	3.68		33.6							11.6

Datenblatt : Palästina																
		schwarz=Eind				Oxi										
		rot= Berechnu														
XXXXXXXXXX	XXXXXXXXXX	XXXXXXXXXX	XXXXXXXXXX	XXXXXXXXXX	XXXXXXXXXX	XXXXXXXXXX	XXXXXXXXXX	XXXXXXXXXX	XXXXXXXXXX	XXXXXXXXXX	XXXXXXXXXX	XXXXXXXXXX	XXXXXXXXXX	XXXXXXXXXX	XXXXXXXXXX	XXXXXXXXXX
SampleID	Site	Well Code	SiO2	CO2		18O	2H	corrected O18	Corr. D	13C(DIC)	18O(DIC)	34S(SO4)	18O(SO4)	34S(S-2)	N-15 (NO3)	O-18(NO3)
J03-01	Arab Project6	19-14/066	18.8571429	49.72		-5.39	-26.1	-5.25045234	-24.8459699	-9.56		-9.7	13.5		9.25	5.7
J04-01	Arab Project6	19-14-66	18.2357143	22		-5.4	-23.5	-5.28073594	-22.7122382	-9.3		-8.1	13.2			-3.3
J03-02	Arab Project6	19-14/067	17.9142857	46.64	-5.4	-5.29	-25.4	-5.16953433	-24.2736661	-9.1		-2.2	12.3		7.42	4.5
J04-02	Arab Project6	19-14/067	17.0142857	36.08		-5.28	-22.6	-5.16959367	-21.8728481	-9.6		-0.8	12			6.2
J03-03	Arab Project7	19-14/073	17.0785714	53.24	-5.28	-5.36	-26.7	-5.21245933	-25.3831252	-10.2		6	16.3		7.37	3.9
J04-03	Arab Project7	19-14/073	16.2	49.72		-5.39	-23.2	-5.26030983	-22.3388179	-10.2		6	17.8		7.1	4.5
J03-04	Fahmi Nahas	19-13/048	15.6428571	33	-5.39	-5.38	-26.2	-5.07342528	-23.7029171	-10.2		5.7	16.1		7.42	3.8
J04-04	Fahmi Nahas	19-13/048	14.7642857	31.68		-5.39	-23.6	-5.22580682	-22.4586899	-11.3		5.9	17.5		7.1	4.3
J03-05	Fahmi Nahas	19-13/047	17.0571429	32.12	-5.39	-5.39	-26	-5.07360199	-23.4062004	-10.7		6.9	16.3		6.94	3.8
J04-05	Fahmi Nahas	19-13/047	15.9642857	36.96		-5.41	-24	-5.24845511	-22.8730907	-10.7		6.9	17.2		6.6	3.8
J03-06	Sabiru Rantiz	19-13/006	19.7785714	69.08	-5.41	-5.5	-26.7	-5.23441427	-24.5122381	-10.5		3.5	16.8		9.29	2.3
J04-06	Sabiru Rantiz	19-13/006	18.8571429	46.2		-5.55	-25.9	-5.38754785	-24.7302478	-10.2		2.9	17.7		8.2	2.8
J03-07	Fahed Hishm	19-13/015	14.9785714	42.68	-5.55	-5.46	-26.3	-5.26826182	-24.6357731	-9.7		9.7	17.3		8.5	4.8
J04-07	Fahed Hishm	19-13/015	14.5071429	35.64		-5.44	-23.8	-5.2943918	-22.8108114	-10		10.4	18.8		7.5	4
J03-08	Zuhdi Hashw	19-13/052	15.9214286	36.08	-5.44	-5.44	-26.6	-5.22732556	-24.8609951	-9.84		-5.9	17.3		7.7	4.3
J04-08	Zuhdi Hashw	19-13/052	15.3	37.4		-5.44	-24.1	-5.28655603	-23.0728348	-9.4		-7	17.6		7.6	6
J03-09	Salah Arouri	19-14/012	16.5857143	44	-5.44	-5.5	-25.9	-5.13844728	-23.0084754	-10.6		4.6	16.9		8.47	4.3
J04-09	Salah Arouri	19-14/012	15.6857143	33.44		-5.51	-24.1	-5.34190729	-22.922612	-10.4		7.2	17.7		7.3	4.6
J03-10	Basil Husaini	19-13/020	14.9785714	34.76	-5.51	-5.27	-26.6	-4.98341386	-24.2048144	-9.3		3.6	16.8		6.89	3.4
J04-10	Basil Husaini	19-13/020	13.2857143	22.44		-5.28	-23.9	-5.13365575	-22.8864273	-10.8		4.5	18		6.8	3.9
J03-11	Basil Husaini	19-13/018	15.1071429	28.16	-5.28	-5.48	-27.7	-5.11731551	-24.6875768	-10.7		-1.3	17		8.29	5.2
J04-11	Basil Husaini	19-13/018	14.4642857	13.2		-5.44	-23.7	-5.27386453	-22.4868079	-11.3		-1.1	15.9		7.7	4.8
J03-12	Ibrahim Daek	NW	14.9571429	50.16	-5.44	-5.23	-26.4	-5.06174608	-24.9473417	-9.8		7.7	16.6		6.59	4.9
J04-12	Ibrahim Daek	IBRAIN DEK	14.7	42.24		-5.22	-23.4	-5.08778952	-22.5197872	-10.1		6.1	17.1		5.9	4.2
J03-13	Iron Factory	19-13/26a	22.9071429	21.56		-5.52	-27	-5.26626385	-25.0477606	-8.9		-5.1	3.3		9.64	5.2
J03-14	Ein Sultan	AC/061	10.1935714	12.76		-5.87	-28.1	-4.70182067	-18.3593402	-12.4		8.7	15		10.08	3.3
J04-14	Ein Sultan	AC/61	9.49285714	16.72		-5.96	-26.1	-5.76394463	-24.493606	-12.8		6.7	14.4		9.8	4
J03-15	Ein Dyouk	AC/060	10.2535714	32.12	-5.96	-5.87	-28.1	-4.71043933	-18.3429935	-12.7		6	9.9		10.48	3.9
J04-15	Ein Dyouk	AC/60	9.585	21.12		-5.96	-26.2	-5.76923048	-24.6333535	-13		7.8	9.9		10.1	3.9
J03-16	Awni Hijazi	19-14/052	17.5071429	66.44	-5.96	-5.5	-27.7	-5.3387881	-26.3239736	-10.2		12.5	14		9.99	4.9
J04-16	Awni Hijazi	19-14/052	17.4857143	54.12		-5.48	-24.8	-5.34801256	-23.92765	-10.6		11.8	15.5		8.9	4
J03-17	Saeed Aladee	19-14/062	14.7214286	63.36	-5.48	-5.54	-27.6	-5.36614783	-26.14332	-11.1		6.7	14.9		10.12	13.9
J04-17	Saeed Aladee	19-14/062	13.6285714	57.64		-5.55	-25.1	-5.40849132	-24.1213242	-12.5		5.7	16.2		12.7	10
J03-18	Mohammed N	19-14/038	15.5785714	81.4	-5.55	-5.54	-27.3	-5.32787279	-25.5916046	-11.6		5.9	12		2.99	14.7
J04-18	Mohammed N	19-14/38	14.7214286	60.72		-5.52	-25.7	-5.36748412	-24.6334926	-12.1		5.2	12.1			13
J03-19	Samed	19-14/26a	15.0857143	39.6	-5.52	-5.56	-27.8	-4.93916833	-22.8953837	-12.1		10	11.3		15.78	8.5
J04-19	Samed	19-14/26a	13.8857143	44.88		-5.52	-24.6	-5.31574368	-23.0844275	-12.8		9.9	10.8		11.3	6.4
J03-20	Arab Project6	19-13/069	16.8214286	51.04	-5.52	-5.54	-28.3	-5.41961856	-27.0936325	-9.57		3.8	13.9		10.9	7.3
J04-20	Arab Project6	19-13/069	15.8357143	54.56		-5.52	-23.6	-5.41186968	-22.8805482	-9.2		5.5	15.1		10.2	7.2
J03-21	Abdallah Arai	19-14/049	15.2571429	102.08		-5.54	-25.7	-5.33170781	-24.0210158	-11.9		9.5	12.7		8.14	3.4
J04-22	Awn Hijazi	19-14/37	17.6142857	61.16		-5.27	-22.8	-5.12744421	-21.8517433	-10.9		9.8	18.6		6.1	2.8
J04-23	Saleem Nimr	19-13/49	16.05	27.72		-5.51	-24.1	-5.38292131	-23.1912779	-9.7		10.9	17.8		8.1	4.1
J04-24	Qasir Hisham	19-13/003	19.95			-5.49	-24	-5.35640072	-23.0756809	-12.1		9.6	17.3		8.6	7.8
J04-25	Bail Hussaini	19-13/22	16.3714286			-5.27	-23.4	-5.11998011	-22.4022957	-10		-1.1	15.4		7.1	4.4
J04-26	Mahmud Akra	19-13/50a	17.7428571			-5.45	-23.9	-5.2894443	-22.76262	-7.4		-0.2	-3.8		7.9	5.1
J04-27	Bail Hussaini	19-13/21	15.2357143			-5.22	-23.1	-5.08819611	-22.2230034	-9.8		4.8	17.5		10.3	4.2
J003-Z	Jericho Süd 1	Lisan						#DIV/0!	#DIV/0!			13.1	16.34			
J003-I	Jericho Qilt 8	Lisan						#DIV/0!	#DIV/0!			12.1	15.17			
J003-X	Jericho Süd 1	Lisan						#DIV/0!	#DIV/0!			-5.1	11.89			
J003-P	Fertiliser cher	Fertilizer						#DIV/0!	#DIV/0!							
J004-Q	Lisan	Lisan										16.4	16.6			
J004-Z	Samara	Samara										6.9	1.4			
J004-Y	Samara	Samara										9.1	9.1			
J004-X	Lisan	Lisan										9.8	15.5			

